IRE Transactions

on ANTENNAS and PROPAGATION

Volume AP-4 JANUARY 1956 Number 1
Published Quarterly

TABLE OF CONTENTS

PUBLISHED BY THE
Professional Group on Antennas and Propagation

IRE TRANSACTIONS PGAP IS A QUARTERLY PUBLICATION DEVOTED TO EXPERIMENTAL AND THEORETICAL PAPERS ON ANTENNAS AND WIRELESS PROPAGATION OF ELECTROMAGNETIC WAVES

MANUSCRIPTS should be submitted to John B. Smyth, Editor, SRA, 3930 4th Avenue, San Diego 3, California. Manuscripts should be original typewritten copy, double spaced, plus one carbon copy. References should appear as footnotes and include author's name, title, journal, volume, initial and final page numbers, and date. Each paper must have an abstract of not more than 200 words. News items concerning PGAP members and group activities should be sent to the News Editor, Mr. H. A. Finke, Polytechnic Research and Development Company, 55 Johnson Street, Brooklyn, New York.

ILLUSTRATIONS should be submitted as follows: All line drawings (graphs, charts, block diagrams, cutaways, etc.) should be inked uniformly and ready for reproduction. If commercially printed grids are used in graph drawings, author should be sure printer's ink is of a color that will reproduce. All half-tone illustrations (photographs, wash, airbrush, or pencil renderings, etc.) should be clean and ready to reproduce. Photographs should be glossy prints. Call-outs or labels should be marked on a registered tissue overlay, not on the illustration itself. No illustration should be larger than 8 x 10 inches.

Copies can be purchased from
THE INSTITUTE OF RADIO ENGINEERS
1 East 79 St., New York 21, N.Y.

PRICE PER COPY: members of the Professional Group on Antennas and Propagation, $2.65; members of the IRE, $2.95; nonmembers, $7.95.

ANNUAL SUBSCRIPTION PRICE: IRE members, $8.50; Colleges and public libraries, $10.00; nonmembers, $17.00.

Entered as second-class matter, at the post office at Menasha, Wisconsin, under the act ot August 24, 1912. Acceptance for mailing at a special rate of postage is provided for in the act of February 28, 1925, embodied in Paragraph 4, Section 412, P. L. & R., authorized October 26, 1927.

news and views

PGAP News

Administrative Committee Responsibilities and Its Activities

H. G. Booker—*Vice-Chairman.*

R. L. Mattingly—*Secretary-Treasurer.* Also: Completing arrangements to distribute complimentary copies of TRANSACTIONS to appropriate foreign libraries; Public relations man responsible for publication of promotional information in other technical journals.

J. I. Bohnert—Actively promoting college and public library subscriptions now that fixed annual rate is established.

J. T. Bolljahn—Responsible for national technical symposia.

H. A. Finke—News and Views Editor.

R. A. Helliwell—Membership.

D. D. King—Promotion of local chapter organization and activity.

V. H. Rumsey—Propagation papers procurement.

George Sinclair—Papers review.

J. B. Smyth—TRANSACTIONS Editor.

R. C. Spencer—TRANSACTIONS—PROCEEDINGS liaison.

A. W. Straiton—Antennas paper procurement.

L. C. Van Atta—General.

H. W. Wells—Awards.

P. S. Carter, A. W. Waynick—Ex officio members.

PGAP now includes seven local chapters. A new local chapter at present is being organized in the Northern New Jersey Section by W. Sichak, Federal Telecommunication Laboratories, Nutley, N. J.

In addition to this, a large number of our membership is now helping us in various other activities:

Dr. S. A. Bowhill, Pennsylvania State University, is permanently assigned the responsibility of organizing the review of propagation papers. George Sinclair will continue to organize the review of antenna papers.

Arthur Dorne, Dorne & Margolin, is the PGAP representative on the 1956 National Convention Technical Program Committee.

S. M. King, I-T-E Circuit Breaker Co., is the PGAP representative on the Convention Record Committee.

S. Hershfield, G. L. Martin, and W. Sharpless, Bell Telephone Laboratories, are PGAP representatives on the organizing committees for the joint symposium on microwave techniques in Philadelphia next February.

General

The following letter written by D. C. Ports, Chairman of PGAP, to Dr. J. B. Smyth, Editor of our TRANSACTIONS, demonstrates a forward look that the membership should be pleased to note. The letter is quoted herewith:

"I feel that our PGAP TRANSACTIONS is well established and becoming recognized as the professional journal in our field of interest. Our membership is gradually increasing and the reaction from the papers published is quite gratifying. We will soon be including authors' biographies in the publication and there may well be other items of interest in addition to the present established departments. While we still have not established a satisfactory nonmember subscription rate, I feel that the library subscription problem is satisfactorily cleared up. Our promotional campaign for obtaining library subscriptions in this country is being organized and is about to get under way. We also have established an arrangement for distributing complimentary copies to appropriate foreign libraries and steps are being taken to get this started.

"It is time now to take stock of our situation and consider any additional steps that might be taken to further our cause so as to maintain a vital support to our profession and a service to the people in our field of interest.

"I would like to suggest that we consider the possibility and merits of changing to a bimonthly instead of a quarterly publication. There are both advantages and disadvantages to such a publication and by copies of this letter, I am asking for a discussion on the subject from the many people concerned. From the technical publication standpoint, it would appear that the available material would warrant an increased volume due to publication. In addition to the general material we have been publishing, there are also important areas of microwave optics, radio astronomy, information theory concept of antenna design; there will probably be a continuing series of new developments with respect to scatter mechanisms and applications, and perhaps several other more basic analyses. I would like to consider also, the value of republishing important technical papers of historical importance that are little known or unavailable to the great majority of our engineers. For example, a paper published in the *Proceedings of the Royal Institution of Great Britain*, Vol. 27, 1932, titled 'Radio Communications by Means of Very Short Electrical Waves' by Marchese Marconi, is of considerable interest both technically and historically, particularly at the present time with the renewed interest in beyond the horizon propagation. This paper is not too well known and copies are very difficult to obtain. It is also of historical interest that the number one paper in the first issue of the IRE PROCEEDINGS published in 1913 is a paper on radiation by Michael Pupin.

"Nontechnical information such as the News and Views would be more current and therefore of more interest and use to our subscribers, if the issues were released more frequently. It would also probably be much easier to maintain interest over a continued debate on some subject over a span of two months rather than three months. There may be other advantages that can be developed through a debate of the subject.

"Of the disadvantages, the increased editorial work load is probably the most obvious. In view of the increase in interest in the publication and the willingness of many people to help, this can probably be handled best by a panel of subeditors each in charge of specific areas of interest. The financial question must of course be faced, but this debate I will reserve for another round of correspondence.

"I am anxious to receive general comments and suggestions reg rding this matter."

Fringe Interest Groups

A Professional Groups Committee Meeting was held during the WESCON Show on August 25, 1955. The PGAP was represented by a number of people. Of the items that were reviewed by the Professional Groups Committee, one problem stands out of interest to the membership. This problem concerns the handling of fringe interest groups. From the notes below, Medical Electronics is carrying the ball for the moment, but quite a number of other groups, including our own, have the same problem and sooner or later will have to come to grips with it. Presented herewith are some excerpts from the Minutes of the Professional Groups Committee Meeting which best point up the problem:

"Dr. Zworykin pointed out the growing need for closer cooperation between the electronics and medical professions and stated that the electronics engineers need the help of the doctors in solving their problems. He feels this is a vital concern in this country and abroad. He advised that in Japan, an Institute of Medical Electronics has been formed and they have offered to cooperate with the PGME. Similar organizations are in the process of formation in France and Italy. Dr. Zworykin expressed concern that if the PGME is not in a position to offer special advantages to doctors, that the medical electronics activity will leave the IRE and form a new organization. Many top level people in the medical profession have expressed their interest in the PGME but are not interested in joining the IRE or in receiving the PROCEEDINGS."

"Mr. Podolsky called attention to the American Medical Association which has rigid rules for membership and advised that where a man wishes to belong to one of their subsidiary societies he must also belong to the mother society. He proposed that if it is desirable for the growth of the PGME to have the medical people take part in its activities and if these people are not willing to join the IRE, that the Group has the privilege of putting them on their mailing list to receive meeting notices and, if the Group can afford it, furnishing them with the Group publications."

"The Chairman expressed the hope that the Professional Groups would show so much vitality and strength that members of other organizations with an interest in electronics would feel that what they will get is worth the dollars involved and would want to affiliate with the Groups by becoming members of the IRE."

Membership Survey

Some of the Professional Groups are conducting surveys of their membership in an attempt to assess their areas of interest. The problem of best service to the membership can only be solved by an intimate knowledge of their needs. PGAP plans, in the near future, to conduct a poll of the Group along these lines: Fields of Interest; Type of Employment; Membership in Other Societies; Technical Preference; etc.

It is earnestly requested that full attention be given to this poll and that each member fill out the questionnaire that will be mailed to him so that the Administrative Committee can get a thorough evaluation of the Group's needs.

Symposium on Communication by Scatter Techniques

This symposium was sponsored by the IRE Professional Groups on Antennas and Propagation and Communications Systems, together with George Washington University. The symposium was held at George Wash-

Successful National Electronics Conference Held in Chicago Recently

A successful, well-attended panel discussion on radio astronomy, titled "Radio Astronomy Enlarges the Observable Universe," was held at the Conference. The general report was one of extreme satisfaction, attesting to the growing interest in the extension of radio techniques into the astronomical field. Participating in the panel discussion were (*left to right*): Dr. H. J. Ewen, Harvard University; Dr. R. C. Spencer, Air Force Cambridge Research Center; Dr. Lloyd Berkner, *Chairman*, Associated Industries, Inc.; Dr. Helen W. Dodson, McMath-Hulbert Observatory, University of Michigan; Dr. F. T. Haddock, Jr., Naval Research Laboratory.

ington University on November 14–15. The papers are listed below:

Propagation Mechanisms—Chairman, C. R. Burrows, Cornell University

"Auroral Propagation Mechanisms," *H. G. Booker*, Cornell University

"Tropospheric Scattering of Short Radio Waves Beyond Horizon," *J. H. Chisholm*, Lincoln Laboratory

"VHF Propagation by Ionospheric Scattering—A Survey of Experimental Results," *R. C. Kirby*, Central Radio Propagation Laboratory

"The Role of Meteors in Extended Range VHF Propagation," *O. G. Villard*, Stanford University

Communications Systems—Chairman, W. H. Radford, Massachusetts Institute of Technology

"Practical Considerations for Forward Scatter Applications," *J. R. McNitt*, United States Air Force

"Some Meteorological Effects on Scattered VHF Waves," *B. R. Bean*, Central Radio Propagation Laboratory

"Point to Point Radio Relay Via Scatter Methods of Tropospheric Propagation," *K. A. Norton*, Central Radio Propagation Laboratory

"A Simplified Diversity Communication System for Beyond-the-Horizon Links," *F. J. Altman*, Federal Telecommunication Laboratories

"Systems Engineering," *W. E. Morrow*, Lincoln Laboratory

System Components—Chairman, T. J. Carrol, Massachusetts Institute of Technology

"High Gain Antennas for VHF Scatter Propagation," *H. V. Cottony*, Central Radio Propagation Laboratory

"Transmitting Tubes for Scatter Communication," *T. Marino*, Varian Associates

"Power Amplifier Klystron for VHF Transmission," *Fred A. Speaks*, Eitel-McCullough

"Terminal Equipment for Scatter Communications," *J. Day*, Radio Engineering Laboratories, Inc.

"Implementation of Scatter Systems," *R. M. Ringoen*, Collins Radio Company

"System Parameters Using Tropospheric Scatter Propagation," *H. H. Beverage, E. A. LaPort and L. C. Simpson*, Radio Corporation of America

Propagation Results—Chairman, M. Katzin, Consultant

"The Scatter Theory and Results," *W. E. Gordon*, Cornell University

"Characteristics of Beyond-the-Horizon Radio Transmission," *K. A. Bullington*, Bell Telephone Laboratories

"Over-Water Scatter Propagation," *T. F. Rogers*, Air Force Cambridge Research Center

"Tropospheric Propagation, Montreal to Riverhead, Long Island," *G. S. Wickizer, D. G. Shipley and G. B. MacKimmie*, Radio Corporation of America

"Some Ionosphere Scatter Techniques," *D. A. Hedlund, L. C. Edwards and W. A. Whitcraft, Jr.*, Raytheon Manufacturing Company

Microwave Techniques Symposium

A Symposium on Microwave Techniques is planned to be held in Philadelphia, early next year. This program will be jointly sponsored by PGAP and the Professional Group on Microwave Theory and Techniques. Sandford Hershfield and William Sharpless are the PGAP members who are making the plans and arrange-

ments with the Microwave Theory and Techniques people. Our representatives, of course, report to Jack Balljahn who is responsible for all technical sessions of our Professional Group.

IRE National Convention

Work has already started on the program for the IRE National Convention. A. S. Dorne will represent the PGAP on the Technical Program Committee.

The PGAP would again like to have four technical sessions, one being of the panel discussion type. It should be pointed out that the problem of getting four technical sessions at the IRE National Convention is not a small one since each of the score of Professional Groups feels that they require a similar number and great wisdom is required in allocating the number of sessions to different groups.

There is some thought that in view of the fact that we co-sponsor a national technical session with URSI in April, we might emphasize papers presenting the applications, measurements, and more practical aspects of antenna and propagation engineering at the National Convention and encourage the presentation of the more theoretical type of paper at the April URSI meeting.

Chapter News

Los Angeles Chapter—The October meeting of the Los Angeles chapter of the PGAP was held on Tuesday, October 11, at the I.A.S. Building, 7660 Beverly Boulevard, with L. A. Kurtz of Hughes Research Laboratories, Antenna Development Section, as speaker. His subject was "Two-Dimensional Slot Array Antennas." Some radiation pattern deterioration effects were hypothesized as resulting from internal impedance mismatches rather than from mutual coupling between elements and a body of experimental evidence was presented to support the hypothesis. The meeting was preceded by a social hour and dinner, as usual, at the Encore Restaurant, 806 North La Cienga Boulevard.

General

The Transactions of the PGAP is trying to build up a Communications Section. This Section can serve a real need on the part of the subscribers by permitting short technical communications to appear quickly in the Transactions. Sections of this kind are generally read rather thoroughly by scientific people because experience indicates that a good fraction of the letters are quite timely. We earnestly request the membership to take advantage of this possibility and help build this Communications Section by offering short technical communications to your Editor, Dr. J. B. Smyth.

News and Views Department

The News and Views Department would like to encourage expansion of its scope by acquiring sub-editors in fields such as tropospheric and ionospheric propagation, high frequency and low frequency antennas, radio astronomy, etc. who might contribute readable, nonmathematical, short discussions on recent events in their fields. Should any one of our Group care to take on such responsibility as sub-editor in a given subfield of PGAP, your News and Views Editor would be pleased to hear from you.

Calendar of Events

Nov. 21–22, 1955: Aeronautical Communications Symposium, sponsored by the IRE Professional Group on Communications Systems, at the Hotel Utica, Utica, New York.

Feb. 2–3, 1956: Symposium on Microwave Theory and Techniques, University of Pennsylvania, Philadelphia, Pa.

March 19–22, 1956: IRE National Convention and Radio Engineering Show, Waldorf-Astoria Hotel and Kingsbridge Armory and Palace, New York, N. Y.

April 15–19, 1956: The 34th Annual Convention of the National Association of Radio and Television Broadcasters, Conrad Hilton Hotel, Chicago, Ill.

May 14–16, 1956: National Aeronautical and Navigational Electronics Conference, Dayton, Ohio.

Aug. 15–17, 1956: IRE/AIEE/IAS/ISA National Telemetering Conference, Statler Hotel, Los Angeles, Calif.

Aug. 21–25, 1956: WESCON.

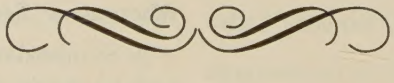

contributions

Exterior Electromagnetic Boundary Value Problems for Spheres and Cones*

L. L. BAILIN† AND SAMUEL SILVER‡

Summary—The problem of determining a harmonic time-varying electromagnetic field where the electric vector assumes prescribed values for its tangential components over given spherical or conical boundaries and which has proper radiation characteristics at infinity is considered by a procedure very much like that used in the theory of slots in waveguide walls. The technique used in solving this type of boundary value problem is to establish, by an application of the Lorentz Reciprocity Theorem, a Green's function which represents the electric and magnetic fields of a point generator (infinitesimal dipole) applied at an arbitrary position on the conducting surface where the fields satisfy homogeneous boundary conditions. The total fields for an arbitrary source are then obtained by superposition; *i.e.*, direct integration over the aperture.

Since detailed results for the case of a sphere have been obtained by many authors, we confine the details of the technique to the infinite cone. It is assumed that in each case the tangential components of the electric vector are given functions over the entire boundary surface. The results apply directly to the theory of radiating apertures in a perfectly conducting spherical wall or a cone, since the tangential components of the electric vector are different from zero only in the area of the aperture, where it is presumed they are known. The results are also applicable to scattering by conducting spheres and cones, since the tangential electric field components over the boundary surfaces are the negative of those of the incident field.

To illustrate the applicability and the limitations of the results, we shall present the formal solutions for arbitrarily shaped apertures on cones and apply them to the several types of delta slots which are usually discussed in connection with other radiating structures.

* Manuscript received by the PGAP, March 18, 1955; revised manuscript received September, 1955. Presented at URSI Meeting, Montreal, Canada, May, 1953. The work described in this paper was carried out through the sponsorship of the AF Cambridge Res. Lab., under Contract AF 19(604)-262-F-4.

† Microwave Lab., Hughes Aircraft Co., Culver City, Calif. Now at Elect. Engrg. Dept., University of Southern California.

‡ Div. of Elect. Engrg., Univ. of Calif., Berkeley, Calif., and Consultant, Microwave Laboratory, Hughes Aircraft Co., Culver City, Calif.

Introduction

THE PROBLEM of determining a harmonic time-varying electromagnetic field, the electric vector of which assumes prescribed values for its tangential components over given spherical or conical boundaries and which has proper radiation characteristics at infinity, is a basic one in many important practical problems concerning radiation and scattering in the radio-frequency region. Classic examples are the gap-excited spherical antenna,[1] biconical antenna,[2] and more recently the problem of scattering by a cone.[3]

The essence of the technique for solving the boundary value problem of this type is contained in Hansen's[4] development of spherical wave solutions to the vector wave equation. Stratton[5] gives a rather complete treatment of Hansen's theory. However, the delineation of the technique and its application to the general boundary value problem does not seem to be available in the literature. The applications in the antenna field seem to have been limited to cases possessing axial symmetry. In such cases, the field is determined by a single component and the method of solution is precisely the

[1] J. A. Stratton and L. J. Chu, "Steady-state solutions of electromagnetic field problems," *J. Appl. Phys.*, vol. 12, pp. 236–240; March, 1941.

[2] S. A. Shelkunoff, "Theory of antennas of arbitrary size and shape," PROC. IRE, vol. 29, p. 243; September, 1941.

[3] K. M. Siegel and H. A. Alperin, Rep. No. UMM-87, Willow Run Res. Ctr., Univ. of Mich.; January, 1952. Also L. B. Felson, Rep. No. R-362-54 PIB-296, Microwave Research Inst., Polytechnic Inst. of Brooklyn; February, 1954.

[4] W. W. Hansen, "A new type of expansion in radiation problems," *Phys. Rev.*, vol. 47, pp. 139–143; January, 1935.

[5] J. A. Stratton, "Electromagnetic Theory," McGraw-Hill Book Co., Inc., New York, N. Y.; first edition, ch. 7.

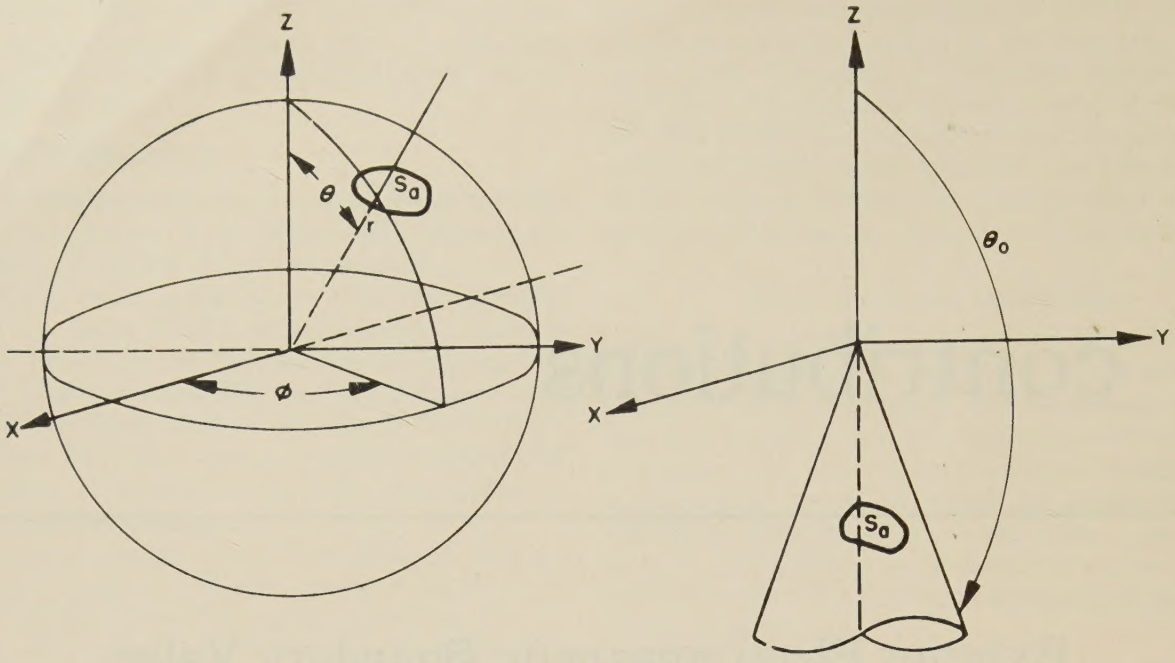

Fig. 1—Coordinate systems.

same as that for the Dirichlet or Neumann problems of potential theory. However, when the boundary values are of a more general type, the basic functions involved are orthogonal in a different sense and there are two general methods of formulating the problem. One way is to establish a Green's function which represents the electric and magnetic fields of a point generator (infinitesimal dipole) applied at an arbitrary position on a conducting surface where the fields satisfy homogeneous boundary conditions. In this case, the procedure is very much like that used in the theory of slots in waveguide walls.[6] A second way of formulating the exterior boundary value is to find the conventional Green's functions which represent the electric and magnetic fields of an oriented dipole source at an arbitrary point in space with homogeneous boundary conditions. The solution for arbitrary values to tangential E and H on the boundary can then be obtained by application of Green's theorem.

Although either technique can be applied, in the present paper only the first method will be used and formal solutions developed for the sphere and the infinite cone (Fig. 1). Since detailed results for the case of a sphere have been obtained by many authors, we shall confine the details of the technique to the infinite cone. It is assumed that in each case the tangential components of the electric vector, E_θ and E_ϕ in the case of the sphere, E_r and E_ϕ in the case of the cone, are given functions over the entire boundary surface. The results apply directly to the theory of radiating apertures in a conducting spherical or conical shell. On the assumption of perfect conductivity for the walls, the tangential components of the electric vector are different from zero over the boundary surface only in the area S_a of the aperture. If, in the case of the sphere, the area S_a is a narrow circumferential strip with uniform excitation around the strip, we have the boundary value problem of the gap-excited spherical antenna. The results are also applicable to scattering by conducting spheres and cones. In these cases, the tangential electric field components over the boundary surface are the negative of those of the incident field. When the primary field arises from a dipole source at a finite distance from the origin, we obtain the dyadic Green's function for the exterior problem.

Spherical Mode Functions

The general solution is synthesized by a superposition of appropriate sets of basic functions which are solutions of the source-free field equations in spherical coordinates. We shall use here the modal representations first developed by Mie[7] rather than the Hansen vector wave functions. There are three sets of basic functions as follows:

1) TEM-Modes: $E_r = H_r = 0$,

$$E_\theta = \frac{e^{\pm jkr}}{r \sin\theta} \qquad H_\phi = \pm \left(\frac{\epsilon}{\mu}\right)^{1/2} E_\theta;$$

$$k = 2\pi/\lambda. \tag{1}$$

The signs indicate the sense of the components in terms of the unit vectors $\bar{\imath}_r$, $\bar{\imath}_\theta$, $\bar{\imath}_\phi$ of the spherical coordinate system. We use $e^{j\omega t}$ as the time representation and correspondingly the outgoing wave is represented by e^{-jkr}.

[6] S. Silver, "Microwave Theory and Design," McGraw-Hill Book Co., Inc., New York, N. Y.; first edition, ch. 9.

[7] G. Mie, "Beiträge zur Optik trüber medien, speziell kolloidaler metallosungen," *Ann. Phys.*, pp. 25, 37; 1908 and P. Debye, "Der Lichtruch auf Kugeln von beliebigem Material," *Ann. Phys.*, pp. 30, 57; 1909.

2) $TM_{\nu m}$-Modes:

$$E_r = \frac{\partial^2}{\partial r^2}(r\Pi_{\nu m}) + k^2(r\Pi_{\nu m}) \qquad H_r = 0$$

$$E_\theta = \frac{1}{r}\frac{\partial^2}{\partial r\partial\theta}(r\Pi_{\nu m}) \qquad H_\theta = \frac{j\omega\epsilon}{r\sin\theta}\frac{\partial}{\partial\phi}(r\Pi_{\nu m})$$

$$E_\phi = \frac{1}{r\sin\theta}\frac{\partial^2}{\partial r\partial\phi}(r\Pi_{\nu m}) \qquad H_\phi = \frac{-j\omega\epsilon}{r}\frac{\partial}{\partial\theta}(r\pi_{\nu m}). \quad (2)$$

3) $TE_{\nu' m}$-Modes,

$$E_r = 0 \qquad H_r = \frac{\partial^2}{\partial r^2}(r\Pi_{\nu' m}{}^*) + k^2(r\Pi_{\nu' m}{}^*)$$

$$E_\theta = \frac{j\omega\mu}{r\sin\theta}\frac{\partial}{\partial\phi}(r\Pi_{\nu' m}{}^*) \qquad H_\theta = \frac{1}{r}\frac{\partial^2}{\partial r\partial\theta}(r\Pi_{\nu' m}{}^*)$$

$$E_\phi = \frac{j\omega\mu}{r}\frac{\partial}{\partial\theta}(r\Pi_{\nu' m}{}^*) \qquad H_\phi = \frac{1}{r\sin\theta}\frac{\partial^2}{\partial r\partial\phi}(r\Pi_{\nu' m}{}^*). \quad (3)$$

Here $\Pi_{\nu m}$ and $\Pi_{\nu' m}{}^*$ are determined by

$$\nabla^2\Pi + k^2\Pi = \nabla^2\Pi^* + k^2\Pi^* = 0, \quad (4)$$

the appropriate boundary conditions on conducting surfaces, and radiation condition at infinity.

The solutions to (4) have the form

$$\Pi_{\nu m_{\{o\}}^{\{e\}}} = \mathcal{Z}_\nu(kr)\,\mathcal{L}_\nu{}^m(\cos\theta)\begin{Bmatrix} A_{\nu m}\cos m\phi \\ B_{\nu m}\sin m\phi \end{Bmatrix} \quad (5)$$

where the designation e (even) and o (odd) refer to the $\cos m\phi$ and $\sin m\phi$ functions, $\mathcal{L}_\nu{}^m(\cos\theta)$ is a general solution of the association Legendre differential equation, and $\mathcal{Z}_\nu(kr)$ is the spherical function defined in terms of a general cylinder function $Z_{\nu+1/2}(kr)$ by

$$\mathcal{Z}_\nu(kr) = \left(\frac{\pi}{2kr}\right)^{1/2} Z_{\nu+1/2}(kr).$$

For outgoing waves, we use the spherical Hankel function of the second kind, $h_\nu{}^{(2)}(kr)$ with our choice of the time representation. Modes are designated as being even or odd according to whether they are developed from $\pi_{\nu m_e}$ or $\pi_{\nu m_o}$. Thus, form (5) it can be seen that each mode with the appropriate radial function for outgoing waves satisfies the radiation conditions[8]

$$\lim_{r\to\infty} r\left[(\bar{\imath}_r \times \overline{H}) + \left(\frac{\epsilon}{\mu}\right)^{1/2}\overline{E}\right] = 0$$

$$\lim_{r\to\infty} r\left[\overline{H} - \left(\frac{\epsilon}{\mu}\right)^{1/2}(\bar{\imath}_r \times \overline{E})\right] = 0 \quad (6)$$

which must be satisfied by solutions of the exterior problem.

The TEM mode field becomes infinite along the radii $\theta=0$ and $\theta=\pi$. It enters into the solution only when the physical structure; *e.g.*, a biconical antenna, is such as to exclude $\theta=0$ and $\theta=\pi$ from the region under consideration. In the problems dealt with in the following sections, either one or both of the two radii are within the region and the TEM mode is, therefore, excluded from the synthesis of the field.

The choice of the function $\mathcal{L}_\nu{}^m(\cos\theta)$ and the values of m and ν are governed by the physical structure involved and special boundary conditions which may be imposed on the modes over the surface of the structure. In the types of problems which are treated in this paper, where the physical domain is $0 \leqq \phi \leqq 2\pi$, m must be an integer to insure single-valuedness in ϕ. The TE and TM modes may have the same eigenvalues ν as in the case of the sphere, or different ones as in the case of the cone. In either case, the modes are orthogonal in the sense that there is no power flow between modes; that is,

$$\int_S (\overline{E}_{\nu m} \times \overline{H}_{\mu n})\cdot\bar{\imath}_r dS = 0 \text{ for } \nu \neq \mu \text{ or } m \neq n \quad (7)$$

the integral extending over a sphere or a segment of a sphere according to the type of physical structure involved. Appropriate normalization of functions can be introduced but it is not particularly necessary in present discussions. General representation for field is then

$$E_r = \sum_\nu\sum_m \frac{\nu(\nu+1)}{r}\mathcal{Z}_\nu(kr)\,\mathcal{L}_\nu{}^m(\cos\theta)[A_{\nu m}\cos m\phi + B_{\nu m}\sin m\phi]$$

$$E_\theta = \sum_\nu\sum_m \frac{1}{r}\frac{d}{dr}[r\mathcal{Z}_\nu]\frac{d\mathcal{L}_\nu{}^m}{d\theta}[A_{\nu m}\cos m\phi + B_{\nu m}\sin m\phi] + j\omega\mu\sum_{\nu'}\sum_m \frac{m}{\sin\theta}\mathcal{Z}_{\nu'}\mathcal{L}_{\nu'}{}^m[C_{\nu' m}\sin m\phi - D_{\nu' m}\cos m\phi]$$

$$E_\phi = \sum_\nu\sum_m \frac{-m}{r\sin\theta}\frac{d}{dr}[r\mathcal{Z}_\nu]\mathcal{L}_\nu{}^m[A_{\nu m}\sin m\phi - B_{\nu m}\cos m\phi] + j\omega\mu\sum_{\nu'}\sum_m \mathcal{Z}_\nu\frac{d\mathcal{L}_\nu{}^m}{d\theta}[C_{\nu' m}\cos m\phi + D_{\nu' m}\sin m\phi]$$

$$H_r = \sum_{\nu'}\sum_m \frac{\nu'(\nu'+1)}{r}\mathcal{Z}_{\nu'}(kr)\,\mathcal{L}_{\nu'}{}^m[C_{\nu' m}\cos n\phi + D_{\nu' m}\sin m\phi]$$

$$H_\theta = \sum_\nu\sum_m \frac{1}{r}\frac{d}{dr}[r\mathcal{Z}_{\nu'}]\frac{d\mathcal{L}_{\nu'}{}^m}{d\theta}[C_{\nu' m}\cos m\phi + D_{\nu' m}\sin m\phi] - j\omega\epsilon\sum_\nu\sum_m \frac{m}{\sin\theta}\mathcal{Z}_\nu\mathcal{L}_\nu{}^m[A_{\nu m}\sin m\phi - B_{\nu m}\cos m\phi]$$

$$H_\phi = \sum_{\nu'}\sum_m \frac{-m}{r\sin\theta}\frac{d}{dr}[r\mathcal{Z}_{\nu'}]\mathcal{L}_{\nu'}{}^m[C_{\nu' m}\sin m\phi - D_{\nu' m}\cos m\phi] - j\omega\epsilon\sum_\nu\sum_m \mathcal{Z}_\nu\frac{d\mathcal{L}_\nu{}^m}{d\theta}[A_{\nu m}\cos m\phi + B_{\nu m}\sin m\phi] \quad (8)$$

[8] Silver, *op. cit.*, p. 85.

where the summations are taken over the appropriate set of discrete eigenvalues. It is clear that the field can be determined readily if the boundary conditions consist of assigned values of $E_r(\theta, \phi)$ and $H_r(\theta, \phi)$ over a sphere completely enclosing the sources. It is necessary only to develop the assigned boundary values in a series of appropriate functions

$$\mathcal{L}_\nu^m(\cos\theta)\begin{Bmatrix}\cos m\phi\\ \sin m\phi\end{Bmatrix}.$$

However, the boundary conditions are rarely given in that form.

Boundary Value Problem of the Sphere

Let us now consider the problems of a sphere of radius a over which we have assigned the tangential components

$$E_\theta(a, \theta, \phi) = f_1(\theta, \phi) \quad E_\phi(a, \theta, \phi) = f_2(\theta, \phi). \tag{9}$$

In the case of the sphere, the function $\mathcal{L}_\nu^m(\cos\theta)$ is required to be finite at both $\theta = 0$ and $\theta = \pi$. The appropriate functions are, therefore, the associated Legendre polynomials $P_n^m(\cos\theta)$ and the eigenvalues ν are the integers $n = 0, 1, 2, \cdots$ for both the TE and TM modes. The field must also be required to have the sense of outgoing waves for all values of r, θ, ϕ; hence we use the radial functions $h_n^{(2)}(kr)$ throughout the representation for the field.

To determine the coefficients $A_{nm} \cdots D_{nm}$ we make use of the Lorentz reciprocity theorem: Given a region R bounded by a surface (or set of surfaces) S, and let $\overline{E}_1$, $\overline{H}_1$, and $\overline{E}_2$, $\overline{H}_2$ be any two source-free fields of the same frequency satisfying Maxwell's equations in R, then

$$\int_S (\overline{E}_1 \times \overline{H}_2)\cdot\bar{n}\,dS = \int_S (\overline{E}_2 \times \overline{H}_1)\cdot\bar{n}\,dS \tag{10}$$

where $\bar{n}$ is the outward normal to S. The region R in the present case is the infinite domain bounded by the sphere of radius a and the sphere at infinity. We take the field $\overline{E}_1$, $\overline{H}_1$, to be that corresponding to the given boundary values and for the field $\overline{E}_2$, $\overline{H}_2$ we use any one spherical mode. Since both fields satisfy the radiation conditions, (6), the surface integral in (10) over the infinite sphere vanishes and we are left with

$$\int_{sp} (\overline{E}_1 \times \overline{H}_2)\cdot\bar{\imath}_r dS = \int_{sp} (\overline{E}_2 \times \overline{H}_1)\cdot\bar{\imath}_r dS, \tag{11}$$

or

$$\int_{sp} (E_{\theta_1}H_{\phi_2} - E_{\phi_1}H_{\theta_2})dS = \int_{sp} (E_{\theta_2}H_{\phi_1} - E_{\phi_2}H_{\theta_1})dS. \tag{11a}$$

The given boundary values $f_1(\theta, \phi)$ and $f_2(\theta, \phi)$ obviously enter into the integral on the left-hand side. We use the series representations, (8), for H_{θ_1} and H_{ϕ_1} in the integral on the right-hand side. By taking $\overline{E}_2$, $\overline{H}_2$ to be successively a $\mathrm{TM}_{nme}, \cdots, \mathrm{TE}_{nmo}$ mode we obtain the unknown coefficients. Orthogonality between modes of different m values and different symmetries is directly evident. Orthogonality between modes of different n values and between TE and TM modes results from:

$$\int_0^\pi \left[P_{n'}^m(\cos\theta)\frac{dP_n^m}{d\theta}(\cos\theta) + P_n^m(\cos\theta)\frac{dP_{n'}^m}{d\theta}(\cos\theta)\right]d\theta = 0 \tag{12}$$

and

$$\int_0^\pi \left[\frac{dP_n^m(\cos\theta)}{d\theta}\frac{dP_{n'}^m(\cos\theta)}{d\theta} + \frac{m^2}{\sin^2\theta}P_n^m P_{n'}^m\right]\sin\theta\,d\theta = \begin{cases} 0 & \text{for } n \neq n' \\ \dfrac{2n(n+1)(n+m)!}{(2n+1)(n-m)!} & \text{for } n = n'. \end{cases} \tag{13}$$

The procedure is a straightforward one and leads directly to the coefficients:

$$A_{nm} = \frac{(2n+1)(n-m)!}{2n(n+1)(n+m)!}\frac{a}{\pi}\frac{\iint\left[f_1(\theta,\phi)\frac{dP_n^m}{d\theta}\cos m\phi - \frac{m}{\sin\theta}f_2(\theta,\phi)P_n^m\sin m\phi\right]\sin\theta\,d\theta d\phi}{\frac{d}{dr}\left[rh_n^{(2)}(kr)\right]_{r=a}}$$

$$B_{nm} = \frac{(2n+1)(n-m)!}{2n(n+1)(n+m)!}\frac{a}{\pi}\frac{\iint\left[f_1(\theta,\phi)\frac{dP_n^m}{d\theta}\sin m\phi + \frac{m}{\sin\theta}f_2(\theta,\phi)P_n^m\cos m\phi\right]\sin\theta\,d\theta d\phi}{\frac{d}{dr}\left[rh_n^{(2)}(kr)\right]_{r=a}}$$

$$C_{nm} = \frac{(2n+1)(n-m)!}{2n(n+1)(n+m)!}\frac{1}{\pi}\frac{\iint\left[\frac{m}{\sin\theta}f_1(\theta,\phi)P_n^m\sin m\phi + f_2(\theta,\phi)\frac{dP_n^m}{d\theta}\cos m\phi\right]\sin\theta\,d\theta d\phi}{j\omega\mu h_n^{(2)}(ka)}$$

$$D_{nm} = \frac{(2n+1)(n-m)!}{2n(n+1)(n+m)!}\frac{1}{\pi}\frac{\iint\left[\frac{m}{\sin\theta}f_1(\theta,\phi)P_n^m\cos m\phi - f_2(\theta,\phi)\frac{dP_n^m}{d\theta}\sin m\phi\right]\sin\theta\,d\theta d\phi}{-j\omega\mu h_n^{(2)}(ka)}. \tag{14}$$

Boundary Value Problem of the Infinite Cone-Spherical Mode Representation in the Incomplete Region

We consider now the radiation from an arbitrarily shaped aperture cut in an infinitely long, perfectly conducting right circular cone with exterior cone angle θ_0 (see Fig. 1). The technique that will be used in this problem will be essentially the same as that used in the previous section for the sphere except for one fundamental difference. In the case of the sphere, it was not necessary to introduce the concept of a point generator, since a single series was sufficient to represent the field over the surface and at infinity. However, for the infinite cone, special conditions must be imposed on the behavior of the fields in the neighborhood of the tip in addition to those at infinity. Thus, the boundary conditions at the tip and those at infinity cannot be met by a single series representation. It is, therefore, convenient to consider a point generator on the surface of the cone and to divide the exterior region into two parts. In one part, the series representation is designed to make energy at the tip finite; in the other, it is made to satisfy the radiation conditions. The two series representations can then be related by continuity across the hypothetical surface which divides the region. The fields of an arbitrary aperture may be found by integrating the fields due to the point generator over the physical dimensions of the aperture.

The axis of the cone serves as the z axis of our coordinate system and we choose the spherical coordinates, r, θ, ϕ, as most suited for developing the general solution, since the surface of the cone can be given as $\theta=\theta_0>\pi/2$. On the surface of the cone we have a slot of arbitrary shape bounded in the radial direction by r_1 and r_2 and, circumferentially, by the curves $\phi_1(r)$ and $\phi_2(r)$. The tangential electric field in the slot will, in general, have both r and ϕ components which we consider to be prescribed functions of $f_1(r, \phi)$ and $f_2(r, \phi)$. In view of the infinite conductivity of the wall, this represents a complete knowledge of the tangential electric field over the cone. Since the radiation conditions, (6), determine the form of the fields on the incomplete sphere at infinity, the fields are thus uniquely defined in the region exterior to the cone.

The solutions to Maxwell's equation in the region exterior to an infinite cone can be obtained from (2), (3), and (4). The θ dependence of (5), which is finite at $\theta=0$, is given by

$$\Pi_{\nu m\left\{\begin{smallmatrix}e\\o\end{smallmatrix}\right\}} = \mathcal{Z}_\nu(kr)P_\nu^m(\cos\theta)\left\{A_{\nu m}\cos m\phi + B_{\nu m}\sin m\phi\right\} \quad (15)$$

where the ν's are the non-integral eigenvalues defined such that tangential E vanishes at $\theta=\theta_0$. Thus from (2) and (3)

$$P_{\nu_i}^m(\cos\theta)\Big|_{\theta=\theta_0} = 0 \qquad \text{for the } TM \text{ set} \quad (16)$$

and

$$\frac{\partial P_{\nu_i'}^m(\cos\theta)}{\partial\theta}\Big|_{\theta=\theta_0} = 0 \qquad \text{for the } TE \text{ set.} \quad (17)$$

To determine the appropriate r dependence, we consider the region divided into two parts (see Fig. 2) such that in II $r>r_0$ and I $r<r_0$. Here r_0 is defined by the location of the point source at (r', θ_0, ϕ') such that $r_0<r'$.

To satisfy the radiation condition in region II, the r dependence of the fields must behave as an outgoing wave and, consequently,

$$\mathcal{Z}_\nu(kr) = h_\nu^{(2)}(kr). \quad (18)$$

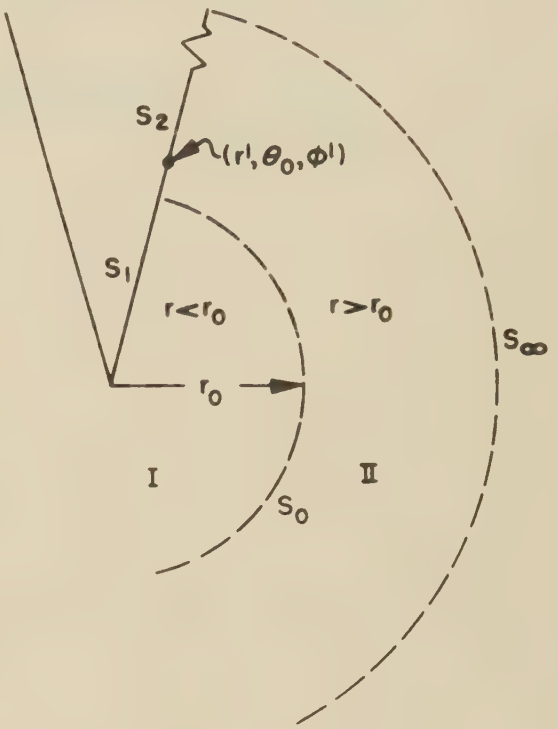

Fig. 2—Lorentz regions.

In region I, and therefore over S_0, the r dependence of the fields are determined by the functional behavior in the neighborhood of the tip. At the tip, the fields become singular, but the singularity must be integrable in such a way as to make the energy in the neighborhood of the tip finite. This restriction requires that the potential electric field behave as

$$\overline{E} \sim r^{\nu-1} \qquad \nu > 0 \quad (19)$$

which leads to potential functions II of the form

$$\Pi \sim r^\nu. \quad (20)$$

Thus, we seek solutions which behave as (20) for small r. In the neighborhood of the tip the two independent solutions of the spherical Bessel equation are $j_\nu(x)$ and $j_{-\nu}(x)$ and the component of the electric field behaves as

$$\lim_{x\to 0}\frac{j_\nu(x)}{x} \sim x^{\nu-1} \quad (21)$$

or

$$\lim_{x\to 0}\frac{j_{-\nu}(x)}{x} \sim x^{-\nu-1}.$$

Since the singularity described by the $j_{-\nu}(x)$ solution is of too high an order to satisfy the energy condition, the unknown fields in region I must be restricted to

$$\mathcal{Z}_\nu(kr) = j_\nu(kr). \tag{22}$$

Similar reasoning may be applied to Π^* and H. The general representation for the field is then given by inserting (15) with the appropriate r dependence, (18) or (22) into (8) as a superposition of basic waves with the summations taken over the infinite set of integral values m and the set i which denumerates the non-integral eigenvalues of (16) and (17).

To determine the unknown coefficients in (8) for a point generator, we apply the Lorentz Reciprocity Theorem described by (10) to region II. Thus, in component form for this region, (10) becomes

$$\int_{S_2}(E_{1r}H_{2\phi}-E_{1\phi}H_{2r})dS+\int_{S_0}-(E_{1\theta}H_{2\phi}-E_{1\phi}H_{2\theta})dS$$
$$+\int_{S_\infty}(E_{1\theta}H_{2\phi}-E_{1\phi}H_{2\theta})dS=\int_{S_2}(E_{2r}H_{1\phi}-E_{2\phi}H_{1r})dS$$
$$+\int_{S_0}-(E_{2\theta}H_{1\phi}-E_{2\phi}H_{1\theta})dS$$
$$+\int_{S_\infty}(E_{2\theta}H_{1\phi}-E_{2\phi}H_{1\theta})dS. \tag{23}$$

Now let $\overline{E}_1$, $\overline{H}_1$ be the actual field for which the expansion is formally given in (8) (see Fig. 2) and choose $\overline{E}_2$, $\overline{H}_2$ to be some one mode of unit coefficient. It can easily be shown that over S_∞

$$H_{2\phi} = +\left(\frac{\epsilon}{\mu}\right)^{1/2} E_{2\theta} \quad H_{2\theta} = -\left(\frac{\epsilon}{\mu}\right)^{1/2} E_{2\phi} \tag{24}$$

and

$$H_{1\phi} = \left(\frac{\epsilon}{\mu}\right)^{1/2} E_{1\theta} \qquad H_{1\theta} = -\left(\frac{\epsilon}{\mu}\right)^{1/2} E_{1\phi},$$

since both fields represent outgoing plane waves to order r^{-1}. Thus, (23) reduces

$$\int_{S_0}(E_{1\theta}H_{2\phi} - E_{1\phi}H_{2\theta})dS$$
$$-\int_{S_0}(E_{2\theta}H_{1\phi} - E_{2\phi}H_{1\theta})dS = K \tag{25}$$

where

$$K = \int_{S_2}(E_{1r}H_{2\phi} - E_{1\phi}H_{2r})dS$$

since the integrals over S_∞ cancel and the tangential components of $\overline{E}_2$ vanish over S_2.

To evaluate the integrals in (25) we consider two cases:

CASE 1 $\overline{E}_2$, $\overline{H}_2$ *is* $\mathrm{TM}_{m'\nu}$ mode even or odd

$$E_{2r} = \frac{\nu(\nu+1)}{r} h_\nu^{(2)}(kr) P_\nu^{m'}(\cos\theta) \begin{Bmatrix}\cos m'\phi\\ \sin m'\phi\end{Bmatrix}$$

$$E_{2\theta} = \frac{1}{r}\frac{d}{dr}\left[rh_\nu^{(2)}(kr)\right]\frac{dP_\nu^{m'}}{d\theta}\begin{Bmatrix}\cos m'\phi\\ \sin m'\phi\end{Bmatrix}$$

$$E_{2\phi} = (-m')\frac{1}{r}\frac{d}{dr}\left[rh_\nu^{(2)}(kr)\right]\frac{P_\nu^{m'}}{\sin\theta}\begin{Bmatrix}\sin m'\phi\\ -\cos m'\phi\end{Bmatrix}$$

$$H_{2r} = 0$$

$$H_{2\theta} = -j\omega\epsilon m' h_\nu^{(2)}(kr)\frac{P_\nu^{m'}}{\sin\theta}\begin{Bmatrix}\sin m'\phi\\ -\cos m'\phi\end{Bmatrix}$$

$$H_{2\phi} = -j\omega\epsilon h_\nu^{(2)}(kr)\frac{dP_\nu^{m'}}{d\theta}\begin{Bmatrix}\cos m'\phi\\ \sin m'\phi\end{Bmatrix}. \tag{26}$$

Inserting (26) and (8) into (25), the left-hand side will reduce as follows: first, it is easily shown (Appendix), that in this case the coefficients of C and D vanish. Second, due to the orthogonality in ϕ, only

$$\begin{Bmatrix}\cos m'\phi\\ \sin m'\phi\end{Bmatrix} \text{ combines with } \begin{Bmatrix}\cos m\phi\\ \sin m\phi\end{Bmatrix}$$

in the integration over ϕ from 0 to 2π, and that only for $m' = m$ since

$$\int_0^{2\pi}\begin{Bmatrix}\cos\\ \sin\end{Bmatrix}^2 m\phi d\phi = \pi(1 \pm \delta_{om}) \tag{27}$$

where

$$\delta_{om} = 0 \qquad m \neq 0$$
$$= 1. \qquad m = 0.$$

Thus, the left-hand side of (25) becomes

$$A_{m\nu_i}{}^{\mathrm{I}} j\omega\epsilon\left[(rj_{\nu_i})\frac{d}{dr}(rh_{\nu_i}^{(2)}) - rh_{\nu_i}^{(2)}\frac{d}{dr}(rj_{\nu_i})\right]\left[\pi(1+\delta_{om})\right]$$
$$\cdot\int_0^\theta\left[\frac{dP_{\nu_i}^m}{d\theta}\frac{dP_\nu^m}{d\theta} + \frac{m^2}{\sin^2\theta}P_{\nu_i}^m P_\nu^m\sin\theta\right]d\theta \tag{28}$$

where A^I is the unknown coefficient (A or B) in region I since S_0 was arbitrarily selected to be in this region. It is also shown in Appendix I that

$$\int_0^{\theta_0}\left[\frac{dP_{\nu_i}^m}{d\theta}\frac{dP_\nu^m}{d\theta} + \frac{m^2}{\sin^2\theta}P_{\nu_1}^m P_\nu^m\right]\sin\theta d\theta = 0$$

for $\nu \neq \nu_i$

$$= \nu_i(\nu_i+1)\int_0^{\theta_0}(P_{\nu_i}^m(\cos\theta)]^2\sin\theta d\theta \qquad \text{for } \nu = \nu_i$$

$$= \frac{\nu_i(\nu_i+1)}{2\nu_i+1}\sin\theta_0\frac{\partial P_{\nu_i}^m(\cos\theta)}{\partial\theta}\bigg|_{\theta=\theta_0}\frac{\partial P_\nu^m(\cos\theta)}{\partial\nu}\bigg|_{\substack{\theta=\theta_0\\ \nu=\nu_i}}. \tag{29}$$

Thus, (25) becomes

$$A_{m\nu_i}{}^{\mathrm{I}}(j\omega\epsilon)\left[rj_{\nu_i}\frac{d}{dr}(rh_{\nu_i}^{(2)}) - rh_{\nu_i}^{(2)}\frac{d}{dr}(rj_{\nu_i})\right]N = K \tag{30}$$

where

$$N = \pi(1+\delta_{om})\frac{\nu_i(\nu_i+1)}{2\nu_i+1}\sin\theta_0\frac{\partial P_{\nu_i}^m(\cos\theta)}{\partial\nu_i}\bigg|_{\theta=\theta_0}.$$

Eq. (27) can be further simplified by observing that the expression in the bracket is related to the Wronskian of $j_{\nu_i}(kr)$ and $h_{\nu_i}^{(2)}(kr)$ and therefore

$$\left[(r^2)\left\{j_{\nu_i}(kr)\frac{d}{dr}(h_{\nu_i}^{(2)}(kr)) - h_{\nu_i}^{(2)}(kr)\frac{d}{dr}j_{\nu_i}(kr)\right\}\right] = r^2 W(j_{\nu_i}, h_{\nu_i}^{(2)}) = \frac{-j}{k}. \quad (31)$$

Thus, (30) becomes

$$\left(\frac{\epsilon}{\mu}\right)^{1/2} A_{m\nu_i}^{\mathrm{I}} N = K. \quad (32)$$

Now applying the condition of continuity of fields across the hypothetical surface $r=r_0$, we have

$$A_{m\nu_i}^{\mathrm{II}} h_{\nu_i}^{(2)}(kr_0) = A_{m\nu_i}^{\mathrm{I}} j_{\nu_i}(kr)_0 \quad (33)$$

where A^{II} is the unknown coefficient (A or B) in region II. Thus, from (32) and (33) we obtain

$$A_{m\nu_i}^{\mathrm{I}} = \frac{K}{N}\left(\frac{\mu}{\epsilon}\right)^{1/2} \quad (34)$$

and

$$A_{m\nu_i}^{\mathrm{II}} = \frac{K}{N}\left(\frac{\mu}{\epsilon}\right)^{1/2}\frac{j_{\nu_i}(kr_0)}{h_{\nu_i}^{(2)}(kr_0)}. \quad (35)$$

The integral, K, may be readily evaluated for a point generator of TM waves located on the surface of a cone at r', θ_0, ϕ' since

$$E_{1r} = \frac{E_0\delta(r-r')\delta(\phi-\phi')}{r\sin\theta_0}, \quad (36)$$

where E_0 is the arbitrary amplitude of the generator, and

$$H_{2r} = 0.$$

Thus,

$$K_{e_0} = \int_S E_{1r}H_{2\phi}dS = \int_{r_0}^{\infty}\int_0^{2\pi}\frac{E_0\delta(r-r')\delta(\phi-\phi')}{r\sin\theta_0} - j\omega\epsilon h_{\nu_i}^{(2)}(kr)\left.\frac{dP_{\nu_i}^{m}}{d\theta}\right|_{\theta=\theta_0} \begin{Bmatrix}\cos m\phi\\ \sin m\phi\end{Bmatrix} r\sin\theta\, dr d\phi$$

$$= E_0\left[-j\omega\epsilon h_{\nu_i}^{(2)}(kr')\left.\frac{dP_{\nu_i}^{m}}{d\theta}\right|_{\theta=\theta_0}\begin{Bmatrix}\cos m\phi\\ \sin m\phi\end{Bmatrix}\right]. \quad (37)$$

If we now let $r_0 \to r'$, then (34) becomes

$$A_{m\nu_i}^{\mathrm{I}} = \frac{-jkE_0}{N}h_{\nu_i}^{(2)}(kr')\left.\frac{dP_{\nu_i}^{m}}{d\theta}\right|_{\theta=\theta_0}\begin{Bmatrix}\cos m\phi'\\ \sin m\phi'\end{Bmatrix} \quad (38)$$

and (35) reduces to

$$A_{m\nu_i}^{\mathrm{II}} = \frac{-jkE_0}{N}j_{\nu_i}(kr')\left.\frac{dP_{\nu_i}^{m}}{d\theta}\right|_{\theta=\theta_0}\begin{Bmatrix}\cos m\phi'\\ \sin m\phi'\end{Bmatrix}. \quad (39)$$

Combining the even and odd coefficients, (38) and (39), the total electric type potential function which is a superposition of the elementary functions of (5) can be written as

$$\Pi = \sum_{m=0}^{\infty}\sum_{i=1}^{\infty}\Pi_{\nu_i m} = \sum_{m=0}^{\infty}\sum_{i=1}^{\infty} \frac{-(jkE_0)(2\nu_i+1)P_{\nu_i}^{m}(\cos\theta)\cos m(\phi-\phi')}{\nu_i(\nu_i+1)(1+\delta_{om})\pi\sin\theta\left.\dfrac{\partial P_{\nu}^{m}}{\partial\nu}\right|_{\substack{\theta\to\theta_0\\ \nu=\nu_i}}} \times j_{\nu_i}(kr<)h_{\nu_i}^{(2)}(kr>) \quad (40)$$

where $r>$, $r<$ symbolizes the larger and smaller of the coordinates r, r', respectively. For an arbitrarily shaped source where $E_0 = f_1(r', \phi')$, (40) can be written

$$\Pi = \sum_{m=0}^{\infty}\sum_{i=1}^{\infty}\frac{(-jk)(2\nu_i+1)P_{\nu_i}^{m}(\cos\theta)}{\nu_i(\nu_i+1)(1+\delta_{om})\pi\sin\theta\left.\dfrac{\partial P^{m}}{\partial\nu}\right|_{\substack{\theta=\theta_0\\ \nu=\nu_i}}} \times\int_{r_1}^{r_2}\int_{\phi_1}^{\phi_2} f_1(r',\phi')\cos m(\phi-\phi')j_{\nu_i}(kr<) \cdot h_{\nu_i}^{(2)}(kr>)r'\sin\theta_0 dr' d\phi'. \quad (41)$$

All the field components may now be derived by applying the operators of (2).

CASE 2 E_2, H_2 is a $\mathrm{TE}_{m'\nu'}$ mode, even or odd

$$E_r = 0$$

$$E_\theta = j\omega\mu m h_{\nu'}^{(2)}(kr)\frac{P_{\nu'}^{m'}}{\sin\theta}\begin{Bmatrix}\sin m'\phi\\ -\cos m'\phi\end{Bmatrix}$$

$$E_\phi = j\omega\mu h_{\nu'}^{(2)}(kr)\frac{dP_{\nu'}^{m'}}{d\theta}\begin{Bmatrix}\cos m'\phi\\ \sin m'\phi\end{Bmatrix}$$

$$H_r = \frac{\nu'(\nu'+1)}{r}h_{\nu'}^{(2)}P_{\nu'}^{m'}\begin{Bmatrix}\cos m'\phi\\ \sin m'\phi\end{Bmatrix}$$

$$H_\theta = \frac{1}{r}\frac{d}{dr}[rh_{\nu'}^{(2)}]\frac{dP_{\nu'}^{m'}}{d\theta}\begin{Bmatrix}\cos m'\phi\\ \sin m'\phi\end{Bmatrix}$$

$$H_\phi = -m'\frac{1}{r}\frac{d}{dr}[rh_{\nu'}^{(2)}]\frac{P_{\nu'}^{m}}{\sin\theta}\begin{Bmatrix}\sin m'\phi\\ -\cos m'\phi\end{Bmatrix}. \quad (42)$$

If we insert (42) and (8) into (25), then the left hand will reduce as follows: As in Case 1, it can be shown (Appendix I) that all coefficients of A and B vanish and that, due to the orthogonality in ϕ, given by (27), we need only consider the terms where $m'=m$. Thus, for this case, (25) reduces to

$$-\left(\frac{\mu}{\epsilon}\right)^{1/2}N'C_{m\nu}^{\mathrm{I}} = K' \quad (43)$$

where

$$N' = -\pi(1+\delta_{om})\frac{\nu_i'(\nu_i'+1)}{2\nu_i'+1}\sin\theta_0 P_{\nu_i}^{m}(\cos\theta_0)\left.\frac{\partial^2 P_{\nu_i'}^{m}}{\partial\theta\partial\nu}\right|_{\substack{\theta=\theta_0\\ \nu=\nu_i}}$$

and C^{I} is unknown coefficient (C or D) in region I. If we again invoke continuity condition at $r=r_0$, then

$$C_{m\nu_i'}^{\mathrm{II}} h_{\nu_i'}^{(2)}(kr)_0 = C_{m\nu_i'}^{\mathrm{I}} j_{\nu_i}(kr_0). \quad (44)$$

Thus, from (43) and (44) simultaneously, we obtain

$$C_{m\nu_i'}^{\mathrm{I}} = \frac{-K'}{N'}\left(\frac{\epsilon}{\mu}\right)^{1/2} \tag{45}$$

and

$$C_{m\nu_i'}^{\mathrm{II}} = -\frac{K'}{N'}\left(\frac{\epsilon}{\mu}\right)^{1/2} \frac{j_{\nu_i}(kr_0)}{h_{\nu_i}^{(2)}(kr_0)}. \tag{46}$$

The integral K' may be readily evaluated for a point generator of TE waves located on the surface of a cone at r', θ_0, ϕ' since

$$E_{1\phi} = \frac{E_0'\delta(r-r')\delta(\phi-\phi')}{r\sin\theta_0} \tag{47}$$

and

$$E_{1r} = 0$$

where E'_0 is the arbitrary amplitude of the generator. Thus,

$$E_{\substack{e\\o}} = \int_S E_{1\phi}H_{2r}dS = -\int_{r_0}^{\infty}\int_0^{2\pi} \frac{E_0'\delta(r-r')\delta(\phi-\phi')}{r\sin\theta_0} \times\left[\frac{\nu_i'(\nu_i'+1)}{r} h_{\nu_i'}^{(2)}(kr)P_{\nu_i'}^{m}(\cos\theta_0) \cdot\begin{Bmatrix}\cos m\phi\\ \sin m\phi\end{Bmatrix}\right] r\sin\theta_0\, drd\phi$$

$$-E_0'\left[\frac{\nu_i'(\nu_i'+1)}{r'} h_{\nu_i'}^{(2)}(kr)P_{\nu_i'}^{m}(\cos\theta_0) \cdot\begin{Bmatrix}\cos m\phi\\ \sin m\phi\end{Bmatrix}\right]. \tag{48}$$

Again we let $r_0\to r'$ and (45) and (46) become

$$C_{m\nu_i'}^{\mathrm{I}} = \frac{E_0'\left(\frac{\epsilon}{\mu}\right)^{1/2}}{N'}\left[\frac{\nu_i'(\nu_i'+1)}{r'} P_{\nu_i'}^{m}(\cos\theta_0) \cdot\begin{Bmatrix}\cos m\phi'\\ \sin m\phi'\end{Bmatrix} h_{\nu'}^{(2)}(kr')\right] \tag{49}$$

and

$$C_{m\nu_i'}^{\mathrm{II}} = \frac{E_0'\left(\frac{\epsilon}{\mu}\right)^{1/2}}{N'}\left[\frac{\nu_i'(\nu_i'+1)}{r'} P_{\nu_i'}^{m}(\cos\theta_0) \cdot\begin{Bmatrix}\cos m\phi'\\ \sin m\phi'\end{Bmatrix} j_{\nu_i}(kr')\right]. \tag{50}$$

Combining (49) and (50) and the even and odd coefficients, the total magnetic type potential function which is a superposition of the elementary functions of (5) can be given as

$$\Pi^* = \sum_{m=0}^{\infty}\sum_{i=1}^{\infty}\Pi_{\nu_i'm}^* = \sum_{m=0}^{\infty}\sum_{i=1}^{\infty} \frac{2(\nu_{i'}+1)\left(\frac{\epsilon}{\mu}\right)^{1/2}\frac{E_0'}{r'}\cos m(\phi-\phi')P_{\nu_i'}^{m}(\cos\theta)}{-\pi(1+\delta_{om})\sin\theta_0\left.\frac{\partial^2 P_\nu^m}{\partial\theta\partial\nu}\right|_{\substack{\theta=\theta_0\\ \nu=\nu_i'}}} \times j_{\nu_i'}(kr<)h_{\nu_i'}^{(2)}(kr)>). \tag{51}$$

For an arbitrarily shaped source where $E_0^1 = f_2(r', \phi')$

$$\Pi^* = \sum_{m=0}^{\infty}\sum_{i=1}^{\infty} \frac{(2\nu_i'+1)\left(\frac{\epsilon}{\mu}\right)^{1/2}P_{\nu_i'}^{m}(\cos\theta)}{-\pi(1+\delta_{om})\sin\theta_0\left.\frac{\partial^2 P_\nu^m}{\partial\theta\partial\nu}\right|_{\substack{\theta=\theta_0\\ \nu=\nu_i'}}} \times\int_{r_1}^{r_2}\int_{\phi_1}^{\phi_2}\frac{f_2(r',\phi')}{r'}\cos m(\phi-\phi')j_{\nu_i}(kr<)h_{\nu_i}^{(2)}(kr>)r'\sin\theta_0 drd\phi', \tag{52}$$

and the various field components may be derived by applying the operators of (3).

Illustrative Examples of Slots on Cones

To illustrate the applicability and the limitations of the results, we shall present briefly the formal solutions to several types of delta slots which are usually discussed in connection with other radiating structures.

A) *Circumferential Slot* [see Fig. 3(a)]

We consider first a uniformly excited circumferential slot. The slot runs around the cone in the ϕ direction and has a height $2w$ which is very much smaller than the circumference at the position of the slot. If the slot is centered about $r=a$ and $\phi=0$, then, for convenience, we shall take $r_1=a-w$ and $r_2=a+w$ and $\phi_1(r) = -\phi$, $\phi_2(r) = +\phi_0$, where $\phi_0=\pi$. The tangential electric field in the slot has only an r component and is independent of ϕ; thus, at $\theta=\theta_0$

$$\begin{aligned} f_1(r',\phi') &= E_0 \quad \text{for } |r'-a| \leqq w\\ &= 0 \quad \text{for } |r'-a| > w\\ f_2(r',\phi') &= 0 \quad \text{for } all\ r'. \end{aligned}$$

The integrals in (52) vanish and those in (41) become

$$\Pi = \sum_{m=0}^{\infty}\sum_{i=1}^{\infty} \frac{(-ik)(2\nu_i+1)(aV_0)P_{\nu_i}^{m}i_{\nu_i}(kr<)h_{\nu_i}^{(2)}(kr>)}{\nu_i(\nu_i+1)(1+\delta_{om})\pi\left.\frac{\partial P_\nu^m}{\partial\nu}\right|_{\substack{\theta=\theta_0\\ \nu=\nu_i}}} \cdot\left[\frac{2\cos m\phi\sin m\phi_0}{m}\right] \tag{53}$$

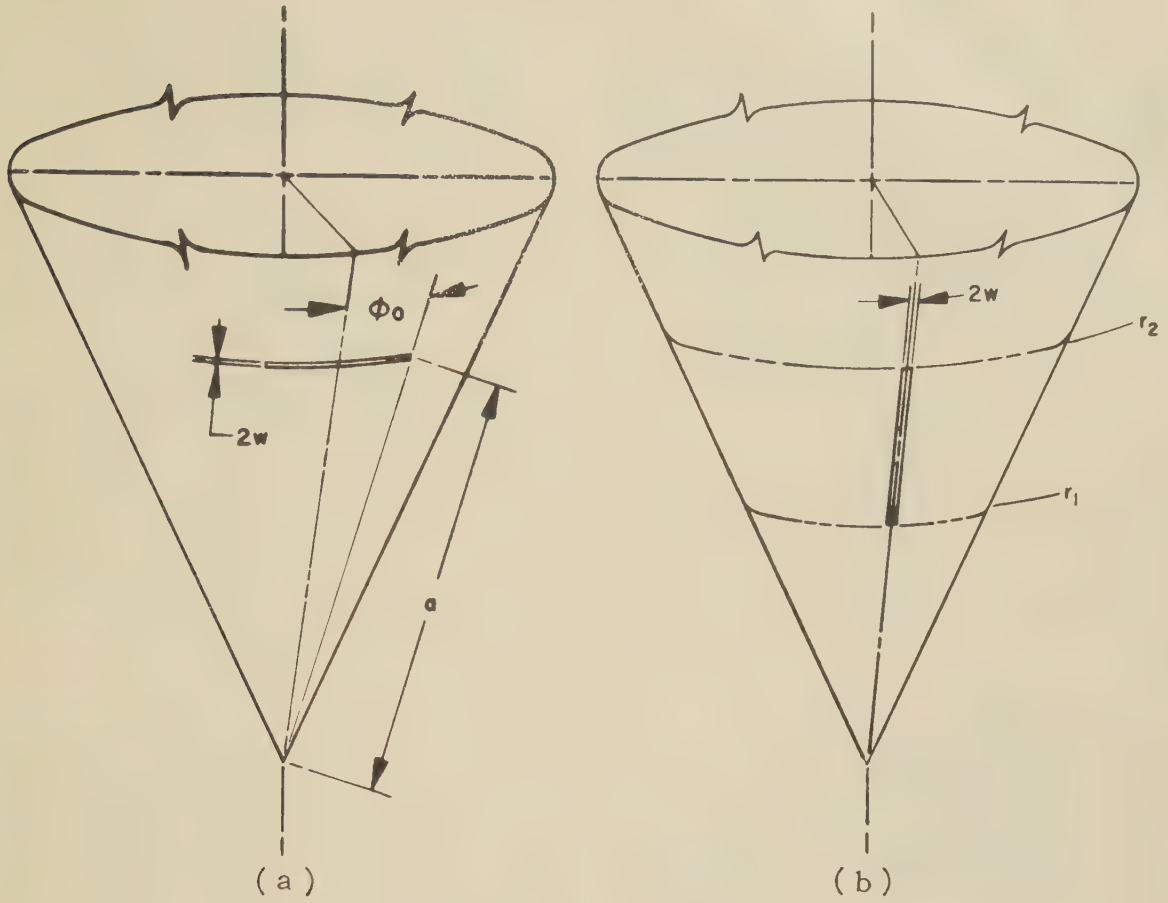

Fig. 3—Slot coordinates.

where the voltage across the slot is defined to be $V_0 = 2E_0W$. Thus, a superposition of the TM modes is appropriate only for the fields from this type of slot.

For a uniformly excited, axially symmetric circumferential slot which runs completely around the cone, $\phi_0 = \pi$, (41) reduces to

$$\Pi = \sum_{i=0}^{\infty} \frac{(jkaV_0)(2\nu_i+1)P_{\nu_i}(\cos\theta)}{\nu_i(\nu_i+1)\left.\frac{\partial P_\nu}{\partial \nu}\right|_{\substack{\theta=\theta_0\\ \nu=\nu_i}}} j_{\nu_i}(ha_<)h_{\nu_i}^{(2)}(kr_>) \quad (54)$$

which is proportional to the $m=0$ term of (53).

If the excitation is not uniform around the axially symmetric slot but is such that

$$\begin{aligned} f_1(r', \phi') &= E_0 \cos n\phi' && |r'-a| \leqq w \\ &= 0 && |r'-a| \geqq w \end{aligned}$$

where $n = 1, 2, 3, 4, \cdots$, then

$$\Pi = \sum_{i=1}^{\infty} \frac{(-jkaV_0)(2\nu_i+1)}{\nu_i(\nu_i+1)} \cdot \frac{P_{\nu_i}^{n}(\cos\theta) j_{\nu_i}(ka_<)h_{\nu_i}^{(2)}(kr_>)\cos n\phi}{\left.\frac{\partial P_\nu^{n}}{\partial \nu}\right|_{\substack{\theta=\theta_0\\ \nu=\nu_i}}}, \quad (55)$$

which is proportional to $m=n$ term of series in (53).

Next we shall consider a thin circumferential slot defined by $|r'-a| \leqq w$, $|\phi'| \leqq \phi_0$ with the following distribution across its surface

$$\begin{aligned} f_1(r', \phi') &= E_0 \cos\frac{\pi\phi'}{2\phi_0} && \text{for} \quad |\phi'| \leqq \phi_0 \\ &= 0 && \text{for} \quad |\phi'| > \phi_0, \end{aligned}$$

where ϕ_0 is the half angle of the slot. The frequency of source is so chosen that slot is a half-wavelength long; *i.e.*, $2\phi_0\alpha \sin\theta_0 = \lambda/2$ or $\phi_0 = \pi/2\ ka \sin\theta_0$. Since

$$\int_{-\phi_0}^{\phi_0} \cos\left[(ka\sin\theta_0)\phi'\right]\cos m(\phi-\phi')d\phi' = \frac{\cos m\phi \cos\left(\frac{m\pi}{2ka\sin\theta_0}\right)}{(ka\sin\theta_0)^2 - m^2}, \quad (56)$$

then

$$\Pi = \sum_{m=0}^{\infty}\sum_{i=1}^{\infty} \frac{(-jkaV_0)(2\nu_i+1)}{(1+\delta_{om})\pi[\nu_i(\nu_i+1)]} \frac{P_{\nu_i}^{m}(\cos\theta)}{\left.\frac{\partial P_{\nu_i}^{m}(\cos\theta)}{\partial\nu}\right|_{\substack{\theta=\theta_0\\ \nu=\nu_i}}} \cdot j_{\nu_i}(ka_<)h_{\nu_i}^{(2)}(kr_>) \times \frac{\cos m\phi \cos\left(m\frac{\pi}{2ka\sin\theta_0}\right)}{(ka\sin\theta_0)^2 - m^2} \quad (57)$$

which is proportional term by term to (53).

B. Longitudinal Slot [see Fig. 3(b)]

For the case of a narrow slot, parallel to the generator of the cone, assume that the electric field has only a uniform E_ϕ component or

$$f_1(r', 0') = 0 \quad \text{and} \quad f_2(r', \phi) = E_0'.$$

If the width $2w$ of the slot is very much smaller than the circumference of the cone at its center, and the length, $r_2 - r_1$, is such as to permit the sides to be approximated by constant values of ϕ', then the integrals in (41) vanish and those in (52) become

$$\Pi^* = \sum_{m=0}^{\infty} \sum_{i=1}^{\infty} \frac{(2\nu_i' + 1)\left(\frac{\epsilon}{\mu}\right)^{1/2} P_{\nu_i'}{}^m(\cos\theta) V_0' \cos m\phi}{-\pi(1 + \delta_{om}) \sin\theta_0 \left.\frac{\partial^2 P_\nu{}^m}{\partial\theta\partial\nu}\right|_{\substack{\theta=\theta_0 \\ \nu=\nu_i'}}} \cdot \int_{r_1}^{r_2} j_{\nu_i'}(kr<) h_{\nu_i'}{}^{(2)}(kr>) dr' \tag{58}$$

where $V'_0 = 2wE'_0$. Due to the nature of the functions involved and the fact that a longitudinal slot cannot be conveniently described by the coordinate system on the surface of a cone, no further simplification seems possible.

Numerical Results

The computation of the field patterns of the radiation from the slots mentioned above is severely limited by the difficulty of obtaining the non-integral eigenvalues defined by (16). However, excellent progress has been made recently by the National Bureau of Standards at the Institute for Numerical Analysis in overcoming this difficulty. They have obtained, with the aid of SWAC (high-speed digital computer), the eigenvalues of (16), the corresponding eigenfunctions, and the normalizing integrals of (30) for the following cases: $m = 0$, 1, 2, and $i = 1(1)30$. Thus, numerical results may be obtained for the slot described in case $A(2)$ and for $n = 1$, 2, of case $A(3)$, or the first three terms in the synthesis of a half-wavelength delta slot.

Computations have been made for the far field patterns of the uniformly excited, axially symmetric slot (case $A2$) for a 30° cone angle ($\theta_0 = 165°$). Although this slot is not a very practical radiation device, it is the first term in the synthesis of a more useful radiator, the half-wavelength slot. Thus, if we consider the far field where $r \gg a$ and

$$h_{\nu_i}{}^{(2)}(kr) = \frac{e^{-jkr}}{kr} e^{j(\nu_i+1)\pi/2}, \tag{59}$$

(54) becomes

$$\Pi = kaV_0 \left(\frac{e^{-jkr}}{kr}\right)\left(\frac{\pi}{2ka}\right)^{1/2} \cdot \sum_{i=1}^{\infty} \frac{(2\nu_i + 1) P_{\nu_i}(\cos\theta)}{\nu_i(\nu_i + 1) \left.\frac{\partial P_\nu(\cos\theta)}{\partial\nu}\right|_{\substack{\theta=\theta_0 \\ \nu=\nu_i}}} e^{j(\nu_i\pi/2)} J_{\nu_i+1/2}(ka), \tag{60}$$

and from (2) the dominant terms of the far field components are

$$E_\theta = \left(\frac{\mu}{\epsilon}\right)^{1/2} H_\phi = A \sum_{i=1}^{\infty} \frac{(2\nu_i + 1)\frac{\partial(P_{\nu_i})}{\partial\theta}}{\nu_i(\nu_i + 1) \left.\frac{\partial P_{\nu_i}}{\partial\nu_i}\right|_{\theta=\theta_0}} \cdot J_{\nu_i+1/2}(ka) e^{j\nu_i(\pi/2)} \tag{61}$$

where

$$A = -jkaV_0 \left(\frac{\pi}{2ka}\right)^{1/2} \frac{e^{-jkr}}{r}.$$

An examination of the terms in the series given by (61) points out another numerical difficulty which is encountered when the position of the slot denoted by a is many wavelengths from the tip of the cone. Under these circumstances the series in (61) do not converge until the order of the Bessel function, $(\nu_i + 1/2)$, exceeds the argument, ka. Thus, for $a = 25\lambda$ or $ka = 50\pi$, we must sum 165 terms to obtain convergence, since

$$\nu_i \to \left(\frac{12}{11}(i) - \frac{17}{22}\right)$$

for large i.[9]

Although the I.N.A. results provided us with the eignevalues and sufficient data to compute the derivatives of the Legendre functions shown in (58) in the range where they are most difficult to compute, $i = 1$ to 30, it was still necessary to evaluate these functions for $i = 31$ to 165. The eigenvalues in the latter range were computed from expressions derived by Pal.[10] The derivatives were obtained from two terms of the asymptotic series for the Legendre functions given by Hobson.[11] The computation of the Bessel functions, $J_{\nu_i+1/2}(ka)$, also offered difficulty since there is no single formula for all values of i. The following formulas were used in the calculations of $J_{\nu_i+1/2}(50\pi)$:

1) For $i = 1$ to 30; the usual Hankel asymptotic series.[12]
2) For $i = 31$ to /110; the asymptotic expansions of Debye.[13]
3) For $i = 111$ to 143; the asymptotic expansions of Langer.[14]
4) For $i = 144$; the asymptotic expansion of Langer.[15]
5) For $i = 145$ to 165; the asymptotic expansion of Langer.[16]

[9] H. M. Macdonald, *Proc. Math. Soc.*, London, Eng. 1, vol. 31, 1900.
[10] B. Pal, *Bull. Calcutta Math. Soc.*, vol. 9, pp. 85–95; 1917–1918.
[11] E. W. Hobson, "Spherical and Ellipsoidal Harmonics," Cambridge University Press, Cambridge, Eng., p. 302; 1931.
[12] G. N. Watson, "A Treatise on the Theory of Bessel Functions," second edition, p. 199.
[13] *Ibid.*, p. 244.
[14] R. E. Langer, *Trans. Am. Math. Soc.*, vol. 34, p. 60; 1932.
[15] *Ibid.*, p. 63.
[16] *Ibid.*, p. 61.

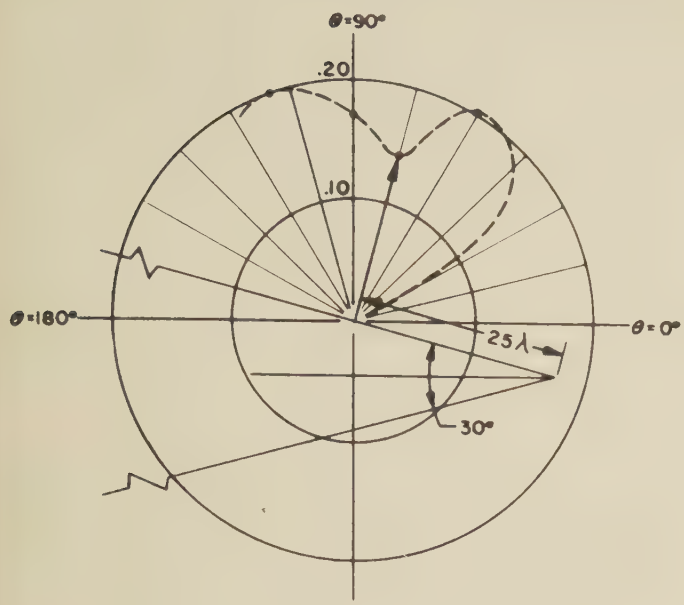

Fig. 4—Axially symmetric circumferential slot.

Checks on the validity of each expansion in its doubtful region were made by overlapping cases 1 and 2, 2 and 3, 3 and 4, and 4 and 5. The magnitudes of the normalized field components which result from the summation given in (58) are shown in Fig. 4. Due to the tedious nature of this summation, calculations were made at $\theta = 60°$, 75°, 90°, 105° and, of course, $\theta = 0$. As ka becomes small, the number of terms necessary for the convergence of the series becomes small: *i.e.*, for $ka \leqq 5\pi$, only 25 terms are necessary. The number of terms given by the I.N.A. results for the θ dependence are sufficient. The Bessel functions for arguments of $ka \leqq 5\pi$ were computed directly from the usual power series expansion.[17] The fields given by (58) for $ka = 5\pi$, 3π, and π at approximately 10° intervals in θ are shown in Fig. 5.

Appendix

To derive the orthogonality condition for the incomplete θ region as shown in (29), we follow the procedure given by Smythe.[18] Let $P_\nu^m(x) = y$ and $P_{\nu'}^m(x) = y'$ be two solutions of Legendre associated differential equation such that

$$P_\nu^m(x_0) = P_{\nu'}^m(x_0) = 0. \tag{62}$$

Thus, we have

$$(1 - x^2)\frac{d^2y}{dx^2} - 2x\frac{dy}{dx} + \left[\nu(\nu + 1) - \frac{m^2}{1 - x^2}\right]y = 0 \tag{63}$$

and

$$(1 - x^2)\frac{d^2y'}{dx^2} - 2x\frac{dy'}{dx} + \left[\nu'(\nu' + 1) - \frac{m^2}{1 - x^2}\right]y' = 0.$$

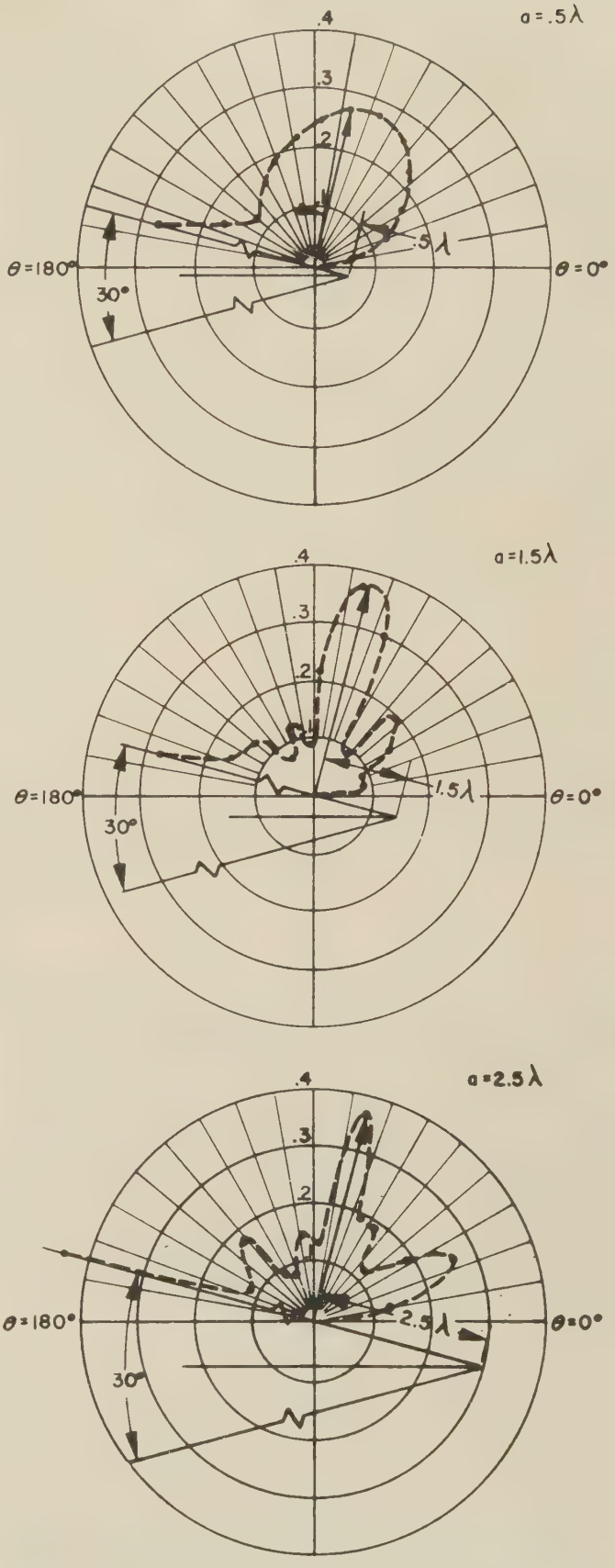

Fig. 5—Axially symmetric circumferential slot.

Multiplying the first by y' and the second by y and adding, we obtain

[17] Watson, *op. cit.*, p. 15.
[18] W. R. Smythe, "Static and Dynamic Electricity," McGraw-Hill Book Co., New York, N. Y., second edition, p. 156. Also Appendix D of Rep. No. UMM-87 of reference 3.

$$\frac{d}{dx}\left[(1-x^2)\left(y'\frac{dy}{dx}+y\frac{dy'}{dx}\right)\right]-2(1-x^2)\frac{dy}{dx}\frac{dy'}{dx}$$
$$+[\nu'(\nu'+1)+\nu(\nu+1)]yy'-2m^2\frac{yy'}{1-x^2}=0. \quad (64)$$

Integrating both sides of (3) from x_0 to 1, and we get

$$\int_{x_0}^{1}\left[(1-x^2)\frac{dP_{\nu'}{}^m}{dx}\frac{dP_\nu{}^m}{dx}+\frac{m^2P_{\nu'}{}^mP_\nu{}^m}{1-x^2}\right]dx$$
$$=\left[\frac{\nu'(\nu'+1)+\nu(\nu+1)}{\nu}\right]\int_{x_0}^{1}P_{\nu'}{}^mP_\nu{}^m dx. \quad (65)$$

From the results of footnote 18, the right side of (4) vanishes if $\nu'\neq\nu$. Thus if $\nu'=\nu$, the left side of (4) becomes

$$\int_{x_0}^{1}\left[(1-x^2)\left(\frac{dP_\nu{}^m}{dx}\right)^2+\frac{m^2}{1-x^2}(P_\nu{}^m)^2\right]dx$$
$$=\frac{-\nu(\nu+1)}{2\nu+1}(1-x_0{}^2)\left[\frac{\partial P_\nu{}^m}{\partial\nu}\frac{\partial P_\nu{}^m}{\partial x}\right]_{x=x_0} \quad (66)$$

for $P_\nu{}^m(x_0)=0$ and

$$\int_{x_0}^{1}\left[(1-x^2)\left(\frac{dP_\nu{}^m}{dx}\right)^2+\frac{m^2}{1-x^2}(P_\nu{}^m)^2\right]dx$$
$$=\frac{\nu(\nu+1)(1-x_0{}^2)}{2\nu+1}\left[\frac{\partial^2P_\nu{}^m}{\partial x\partial\nu}\right]_{x=x_0}P_\nu{}^m(x_0) \quad (67)$$

for

$$\left.\frac{dP_\nu{}^m(x)}{dx}\right|_{x=x_0}=0.$$

Acknowledgment

The authors wish to thank Dr. E. C. Yowell and La Verne E. Rickard of the Institute of Numerical Analysis for the eigenvalues upon which the calculations are based and Annabelle Cordova and the numerical computation group at Hughes Aircraft Company for their computing services.

Analysis of a Terminated-Waveguide Slot Antenna by an Equivalent Circuit Method*

L. B. FELSEN†

Summary—**The pattern in a half-space of a slot in the wall of a waveguide is a function of the terminating impedance. The description of the far fields in such a configuration is simplified considerably by the adoption of a network viewpoint, whereby the half-space is represented approximately by two (or more) spherical transmission lines, the feeding waveguide by a single uniform transmission line, and the slot by a coupling network which is directly analogous to that for a hybrid junction. For a given waveguide termination, the spherical mode voltages are computed by a simple network calculation, and the gain pattern is obtained by modal synthesis. The slot equivalent circuit parameters are obtained readily by simple measurements or from available theoretical formulas. Described in detail both theoretically and experimentally is a symmetric rectangular slot cut in either the broad or narrow face of a rectangular waveguide.**

I. Introduction

THE TERMINATED-WAVEGUIDE slot antenna consists of a slot cut in the wall of a waveguide terminated in a known impedance. The slot field and therefore the gain pattern of this configuration is a function of the waveguide termination and may change markedly for different impedance values. Since the determination of the slot field is usually an extremely difficult task, it is desirable to employ a technique which enables one to find the radiated field without a *detailed* knowledge of the slot field. If the slot radiates into a half-space; *i.e.*, the slot is contained in an "infinite" baffle, the radiated fields are analyzed very conveniently in terms of spherical transmission line theory.[1] For many small aperture configurations, a single spherical transmission line suffices to represent approximately the far fields radiated from a slot excited with symmetric and antisymmetric incident electric fields, respectively, so that the half-space is represented approximately by two spherical transmission lines, and the slot is viewed as a network coupling the waveguide with the half-space region. If the equivalent circuit parameters of the slot are known, the far spherical mode voltages and currents for a given waveguide

* Manuscript received by the PGAP, February 20, 1955; revised manuscript received September 26, 1955. The contents of this paper were presented at the IRE National Convention in New York, N. Y., in March, 1954.

† Polytechnic Inst. of Brooklyn, Brooklyn 1, N. Y.

[1] L. B. Felsen and N. Marcuvitz, "Slot coupling of rectangular and spherical waveguides," *J. Appl. Phys.*, vol. 24, pp. 755–770; June, 1953.

excitation and termination may be computed by simple network calculations, and the radiated fields determined directly by modal synthesis.

The specific configurations considered here are symmetric rectangular E plane and H plane slots radiating from the broad or narrow face of rectangular waveguide. The electromagnetic field analysis for these configurations has been carried out elsewhere[2] on the assumption that propagation in the half-space region is characterized by two propagating spherical modes.[3,4] The coupling properties of the slot are represented by a lossless four terminal-pair equivalent network whose parameters, at suitable reference planes, may be expressed approximately in terms of those of the lossy two terminal-pair equivalent circuit for the radiating slot when considered as a dissipative element in the rectangular waveguide. The parameters for the latter network are determined either theoretically from a variational calculation[5] or from direct measurement in the feeding guide. From a knowledge of the slot equivalent circuit parameters the pattern of the slot with a given termination is computed from a simple network calculation and subsequent modal synthesis as shown in Section B of the following part.

For large slots two spherical modes are no longer adequate to characterize propagation in the half-space region, and additional modes are required. The rigorous treatment of these other modes implies the addition of a corresponding number of terminal pairs to the equivalent network which, though readily formulated, is no longer evaluated as simply as above. An approximation procedure employed in this case is described in Section C of the next Part. The complete procedure for computing the patterns of both E plane and H plane slots is summarized in *stepwise form* in Part V.

II. E Plane Slot

A) The Coupling Slot Equivalent Circuit Parameters

1) *Four Terminal-Pair Equivalent Network;* The E plane slot configuration is shown in Fig. 1, where the rectangular waveguide is assumed to propagate only the dominant (H_{10}) mode. If the slot is excited by two waves having identical electric field components E at the symmetric, "far" terminal planes T_1 and T_2 (Fig. 2), a magnetic wall ($H_{\text{tangential}}=0$) exists at the $z=0$ plane; the corresponding slot field is shown approximately in Fig. 3(a). For convenience, planes T_1

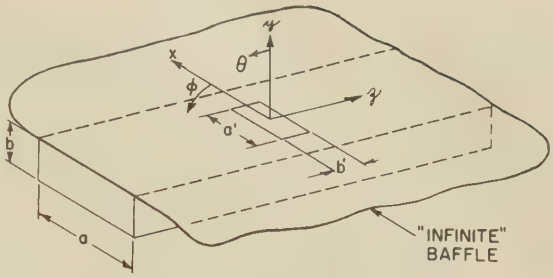

Fig. 1—Slot structure and orientation of coordinates for E plane slot.

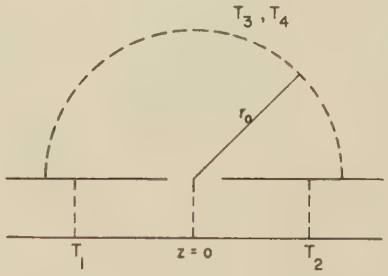

Fig. 2—E plane slot structure (side view) and terminal plane locations.

and T_2 are chosen a "large" integral number of guide wavelengths away from the symmetry plane. It is seen from the symmetry of the slot field configuration that the fields radiated into the half-space region resemble those due to a radiating electric dipole placed perpendicularly to the infinite plane at the slot center

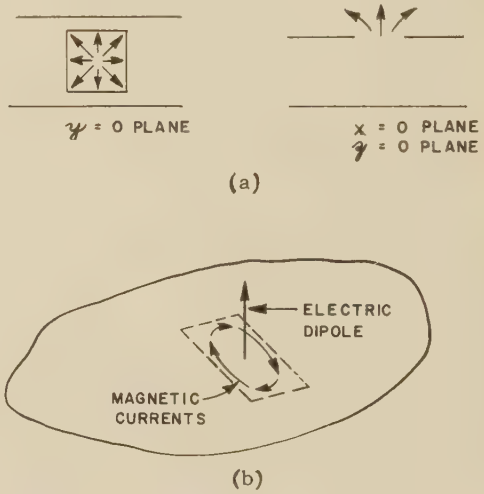

Fig. 3—Symmetrically excited slot (E plane); (a) slot electric field, (b) equivalent source.

as in Fig. 3(b). For anti-symmetric electric field excitation of the slot an electric wall ($E_{\text{tangential}}=0$) exists at the $z=0$ plane; the approximate form of the slot field is shown in Fig. 4(a). The radiated field behaves essentially like the field of a magnetic dipole lying in the slot plane and directed perpendicular to the electric field

[2] L. B. Felsen, "Analysis of a terminated-waveguide slot antenna by an equivalent circuit method," Microwave Res. Inst., Polytechnic Instit. of Brooklyn, Rep. R-400-54, PIB-333; September, 1954.

[3] M. Toran, "Spherical mode representation of far fields," M.E.E. Thesis, Polytechnic Inst. of Brooklyn; June, 1953.

[4] Felsen and Marcuvitz, *op. cit.*, Sec. III.

[5] A. A. Oliner, *et al.*, "Equivalent circuits for slots in rectangular waveguide," Microwave Res. Inst., Polytechnic Inst. of Brooklyn; August, 1951. Sections on E plane radiating slots. Material on H plane slots is in preparation.

lines shown in Fig. 4(b). The electric and magnetic dipole modes suffice to adequately represent the far fields radiated by a symmetrically and anti-symmetrically excited small slot, respectively.[3,4]

Since the slot, for a given waveguide termination, can be represented as a superposition of symmetric and anti-symmetric field excitations, propagation in the half-space region may be approximated in terms of the two above-mentioned basic, independent, propagating modes. To derive the parameters of the equivalent circuit for the slot, the electric and magnetic fields on each side of the slot are represented in terms of a complete set of vector modes, whose amplitude coefficients (for each mode) satisfy transmission line equations and can be interpreted as transmission line voltages and currents. The relationship between the mode voltages and currents at the "far" terminal planes shown in Fig. 2 is expressed in terms of an equivalent network for the slot.[2]

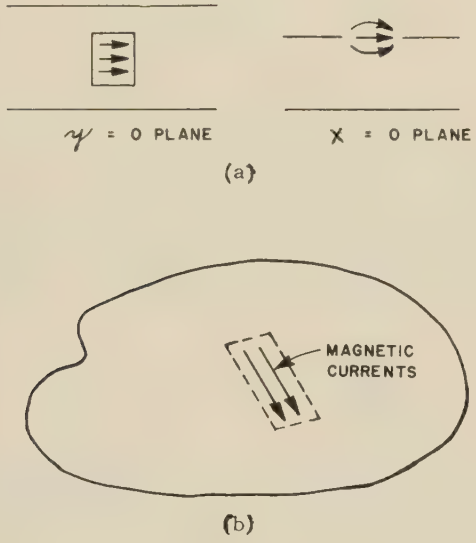

Fig. 4—Anti-symmetrically excited slot (E plane); (a) slot electric field, (b) equivalent source.

Let V_3, I_3 denote the spherical E (vertical electric dipole) mode voltage and current at the far terminal plane T_3, and V_4, I_4 the spherical H (tangential magnetic dipole) mode voltage and current at the far terminal plane T_4; then the equivalent circuit for the slot structure in Fig. 2 is that shown schematically in Fig. 5. The network terminal pairs T_3 and T_4 in Fig. 5 have been chosen to coincide at the single hemispheric terminal surface (T_3, T_4) in Fig. 2. The uniform transmission lines are characterized by the dominant (rectangular guide) mode propagation constant κ and the characteristic admittance Y. Since the spherical transmission lines are situated in a "far" region, their characteristics become identical with those of uniform transmission lines in free space, except that r is still the propagation direction;[6] thus, their propagation constants and characteristic admittances are equal to the free-space values k and $\eta=(\epsilon/\mu)^{1/2}$, respectively. Since the physical structure is nondissipative and all major propagating modes have been explicitly considered, the equivalent circuit is approximately reactive.

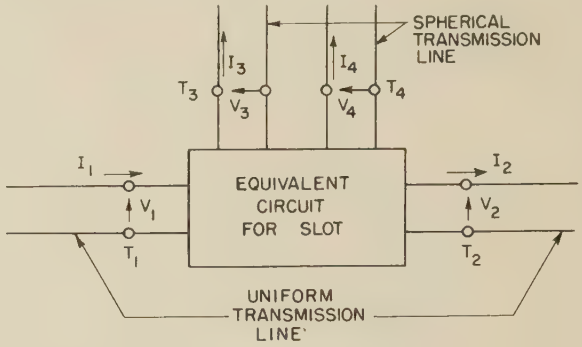

Fig. 5—Network equivalent of slot structure.

In view of the symmetry of the configuration about the $z=0$ plane, the far fields satisfy certain symmetry requirements. Expressed in terms of voltage-current relations on the equivalent network the symmetry requirements are the following: 1) symmetric voltage (anti-symmetric current) excitation at ports T_1 and T_2 excites only port T_3 (Fig. 3); 2) anti-symmetric voltage (symmetric current) excitation at ports T_1 and T_2 excites only port T_4 (Fig. 4); 3) when identical terminations are placed at ports T_1 and T_2, excitation at port T_4 does not couple to T_3, and vice versa. Thus the structure behaves like a hybrid junction. It can be shown from field-theoretic considerations[2] that the half

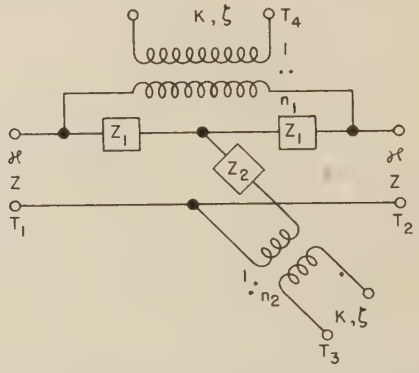

Fig. 6—Approximate network representation.

structures resulting from open and short circuit bisection at the symmetry plane are approximately series and shunt, respectively, provided that $r_0=(q+1/4)\lambda$, where q is a large integer and λ is the free-space wavelength. Thus, the over-all approximate equivalent circuit is that given in Fig. 6.

[6] Felsen and Marcuvitz, *op. cit.*, Eqs. (2.14).

2) *Relationship with the Two-Terminal Pair Equivalent Circuit for the Slot;* When the slot radiates into an empty half-space region, impedances equal to the characteristic impedance $\zeta(=\sqrt{\mu/\epsilon}=1/\eta)$ of free space are connected to terminal pairs T_3 and T_4 of the equivalent circuit in Fig. 6 to yield a bridged Tee network, which may alternatively be expressed as the admittance Pi circuit in Fig. 7. (A Pi circuit rather than a

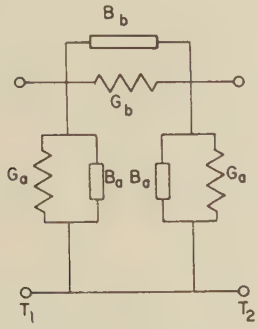

Fig. 7—Two terminal-pair Pi network for radiating slot.

Tee circuit is chosen since a narrow slot (b' small) behaves like a series network so that the shunt admittances are very small.) The equivalent four terminal-pair circuit for the slot is approximately lossless; *i.e.*, the elements Z_1 and Z_2 are pure reactances, and n_1 and n_2 are real. Since both circuits contain four independent elements it is possible to express the parameter values of one in terms of those of the other. One obtains (letting $Z_{1,2}=jX_{1,2}$):

$$n_2^2 = \frac{\zeta}{Z}\frac{2}{R_a'},$$

$$n_1^2 = \frac{Z}{\zeta}\frac{2}{G_a' + 2G_b'},$$

$$\frac{-1}{X_1'} = B_a' + 2B_b',$$

$$X_2' = \tfrac{1}{2}(X_a' - X_1'), \qquad (1)$$

where

$$\zeta/Z = \lambda/\lambda_g, \qquad \lambda_g = \text{guide wavelength},$$

$$R_a' = \frac{G_a'}{G_a'^2 + B_a'^2}, \quad X_a' = -\frac{B_a'}{G_a'^2 + B_a'^2}, \qquad (2)$$

and the primes on the impedance (admittance) parameters denote normalization with respect to the characteristic impedance Z (admittance Y) of the rectangular waveguide. The algebraic sign of n_1 and n_2 can be determined from a field analysis. The circuit in Fig. 7 represents the radiating slot when viewed as a lossy transmission structure in the waveguide; its equivalent circuit elements can be measured readily by any of the techniques applicable to the measurement of dissipative microwave fourpoles. Thus, it is possible to determine the parameters of the four-terminal pair network coupling the waveguide and half-space regions from *simple* measurements carried out entirely *within* the waveguide, without the need of special terminations in the half-space region. Variational expressions for the circuit elements in Figs. 6 and 7 have been obtained;[2] explicit formulas for the latter are available.[5]

B) Computation of the Pattern

Consider an incident wave at terminal plane T_1 in the rectangular waveguide (see Fig. 2), with specified terminations at terminal planes T_2, T_3, T_4. Although we consider here only radiation into an empty half-space region, other terminations which do not generate additional modes can be treated as well. Such terminations comprise hemispheric shells of uniform composition centered about the slot so that the problems of radiation into a hemispheric cavity, or through one or more dielectric shells are readily solved. The input impedance of such configurations at terminals T_3 and T_4 is determined from spherical transmission line theory which, in this "far" range, reduces to ordinary uniform transmission line manipulations.[7,8] With a specified excitation at terminal pair T_1 and specified terminations at terminal pairs T_2, T_3, and T_4 in Fig. 6, the currents I_3 and I_4 flowing into terminals T_3 and T_4, respectively, are computed by ordinary network methods. The resulting network configuration is shown in Fig. 8, where Z_i^T represents the termination at the ith terminal pair.

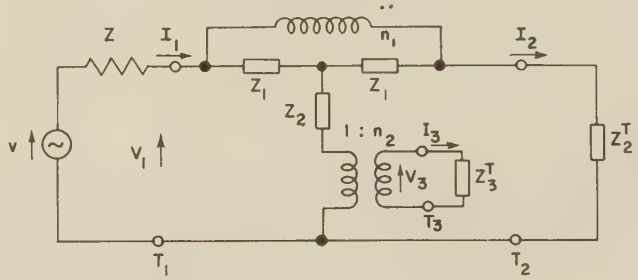

Fig. 8—Final network problem.

Assuming a matched power source, the strength of the equivalent generator v is equal to 2 V_{inc}, where V_{inc} is the known amplitude of the incident wave. The determination of the voltages and currents at the terminals of the network completes the problem of modal analysis.

[7] N. Marcuvitz, "Waveguide Handbook," McGraw-Hill Book Co., New York, N. Y., Secs. 1.8 and 2.8; 1951.

[8] L. B. Felsen, "Spherical transmission line theory," Rep. R-253-51, PIB-194, Microwave Res. Inst., Polytechnic Inst. of Brooklyn, Sec. II-B; January, 1952.

The far fields radiated into the half space are computed directly by modal synthesis. Since only two modes are assumed to propagate, one obtains the following approximate far magnetic field representation:[9]

$$rH(r) \approx I_3(r)h_3(\theta, \Phi) + I_4(r)h_4(\theta, \Phi). \quad (3)$$

The mode functions in (3) are transverse to r; their detailed evaluation depends on the choice of coordinate orientation in the half space. If the y axis in Fig. 1 is chosen as the polar axis of the spherical coordinate system, the electric dipole mode function is given by[10]

$$h_3(\theta, \Phi) \equiv h_{01e}'(\theta, \Phi) = \sqrt{\frac{3}{4\pi}} \sin\theta \, \Phi_0, \quad (4)$$

while the magnetic dipole mode function is

$$h_4(\theta, \Phi) \equiv h_{11e}''(\theta, \Phi) = \sqrt{\frac{3}{4\pi}} (\theta_0 \cos\theta \cos\Phi - \Phi_0 \sin\Phi). \quad (5)$$

The single and double primes on the mode functions denote E and H mode quantities, respectively, while θ_0 and Φ_0 are unit vectors in the θ and Φ directions. The Φ coordinate is measured in the $y=0$ plane from the positive x axis. The far mode current $I_3(r)$ is related to its value at the terminal plane r_0 by

$$I_3(r) = I_3[\cos k(r - r_0) - j\eta Z_3^T \sin k(r - r_0)], \quad r > r_0. \quad (6)$$

A similar expression applies to $I_4(r)$.

If the slot radiates into an empty half-space region, the values of $Z_{3,4}^T$ become equal to $\zeta = 1/\eta$, and (6) yields a traveling wave. For this case, the far field becomes:

$$rH(r) \approx \left\{e^{-jk(r-r_0)} \sqrt{\frac{3}{4\pi}} v\right\} \left(\frac{I_4}{v}\right) \cdot \left[\theta_0 \cos\theta \cos\Phi + \Phi_0 \left(\frac{I_3}{I_4} \sin\theta - \sin\Phi\right)\right]. \quad (7)$$

The manner in which (7) is written permits a convenient identification of the terms. For any fixed load Z_2^T, the magnitude of the factors outside the square brackets is constant so that the gain pattern is given by the magnitude of the expression in the square brackets. If the power level relative to the incident wave is required as well, the magnitude of (I_4/v) must be computed; this is readily accomplished in terms of the network in Fig. 8. The magnitude of the expression inside the braces depends only on the strength of the generator and is of no interest. Thus, the pattern function of the slot is the following:

$$G \approx |[\ ]|^2 \approx \cos^2\theta \cos^2\Phi + \sin^2\Phi + \left|\frac{I_3}{I_4}\right|^2 \sin^2\theta - 2\sin\theta \sin\Phi \operatorname{Re}\left(\frac{I_3}{I_4}\right), \quad (8)$$

where Re denotes "the real part of." G is proportional to the squared magnitude of the far field.

As mentioned above the ratios (I_3/I_4) and (I_4/v) are computed directly from the network shown in Fig. 8. However, for the purpose of a discussion in the next part it is convenient to express (I_3/I_4) for a given waveguide termination in terms of properly superposed symmetric and anti-symmetric voltage excitations of the slot. Let

$$V_1 = V_a + V_s, \qquad I_1 = I_a + I_s,$$
$$V_2 = V_s - V_a, \qquad I_2 = I_a - I_s, \quad (9)$$

where V_a, I_a, and V_s, I_s, are anti-symmetric and symmetric voltage and current excitations, respectively. With regard to the Pi circuit in Fig. 7 it is seen that the bisection admittances are the following:

$$\frac{I_s}{V_s} = Y_a, \quad \frac{I_a}{V_a} = Y_a + 2Y_b, \quad Y_{a,b} = G_{a,b} + jB_{a,b}, \quad (10)$$

and one finds:

$$\frac{V_a}{V_s} = \frac{1 + Z_2'^T Y_a'}{1 + Z_2'^T (Y_a' + 2Y_b')}, \quad Z_2'^T = \frac{V_2}{ZI_2}. \quad (11)$$

Eq. (11) expresses the dependence of the equivalent symmetric and antisymmetric excitations on the terminating impedance. Upon applying symmetric and anti-symmetric excitations to the circuit in Fig. 6 (with terminations at T_3 and T_4) one obtains the following relationship:

$$\frac{I_3}{I_4} = \frac{n_1}{n_2} \frac{Y_a'\zeta}{Z} \frac{V_s}{V_a}. \quad (12)$$

Thus, the ratio (I_3/I_4) appearing in (12) is a measure of the ratio of the symmetric and anti-symmetric voltage excitations and therefore of the induced symmetric and anti-symmetric slot fields.

A slot of the type shown in Fig. 1 is principally a series slot (especially when b' is small) so that the value of Y_a' is usually small. Thus, the value of (I_3/I_4) given in (11–12) is generally small so that the gain pattern as expressed by (8) is essentially that of a magnetic dipole. However, for large values of $Z_2'^T$, the ratio (I_3/I_4) can become appreciable and corresponding distortion of the magnetic dipole pattern is to be expected. This distorting effect is particularly noticeable if $Z_2'^T$ is chosen as a large reactance, as is verified by the experimental measurements (see Part IV).

[9] Felsen and Marcuvitz, *op. cit.*, Eq. (3.7).

[10] L. B. Felsen, "A spherical transmission line approach to the calculation of radiation conductances," Microwave Res. Inst., Polytechnic Inst. of Brooklyn, Rep. R-281-52, PIB-220, pp. 16–17; October, 1952.

Since Y_a' is usually a small parameter (masked out by the larger parameter Y_b'), its experimental determination is often inaccurate. Therefore, it is usually desirable to compute R_a' required for the evaluation of n_2 from an approximate theoretical formula which has been obtained previously:[11]

$$R_a' \approx \frac{\pi^3 abb'^2}{3\lambda\lambda_g^3} \frac{(1-\alpha^2)^2}{\cos^2\frac{\pi\alpha}{2}} \cdot \frac{1}{I_1^2\left(\frac{\pi b'}{\lambda_g}\right)\left[1-\left(\frac{\alpha\pi}{ka}\right)^2\right]^2}(D^2+E^2), \quad (13)$$

where $\alpha = a^1/a$, a and b are the dimensions of the waveguide, a' and b' are the slot dimensions, λ_g is the guide wavelength, and $k = 2\pi/\lambda$.

$$D = 1 - .5\alpha^2 - .05(1 - .25\alpha^2)\left(\frac{kb'}{2}\right)^2 - .024(4 - 3\alpha^2)\left(\frac{ka'}{\pi}\right)^2,$$

$$E = \sqrt{\frac{15}{4}}\left[.2\alpha^2 - (.017 + .0012\alpha^2)\left(\frac{kb'}{2}\right)^2 + (.031 - .033\alpha^2)\left(\frac{ka'}{\pi}\right)^2\right], \quad (14)$$

C) Modifications for Larger Slots Radiating into a Half-Space

The theory developed in the preceding sections is based on the assumption that two spherical modes suffice to adequately represent the far fields in the half-space region. For larger slots, the two-mode approximation may no longer be accurate so that additional modes are required. Each additional mode adds another pair of terminals to the equivalent circuit. To avoid the complications inherent in the evaluation of the rigorously formulated equivalent circuit parameters, we resort to an approximation procedure.

It was seen in the preceding section (12) that the ratio (I_3/I_4) is a measure of the ratio of the intensities of the symmetric and anti-symmetric slot fields. In the treatment of larger slots it is assumed that the ratio of the dominant (symmetric and anti-symmetric) mode currents (I_3/I_4) is still given approximately by (12). However, the fields radiated by the constituent slot fields are now represented in more detail. For a narrow slot (a' large; see Fig. 1), the constituent slot fields and their equivalent magnetic currents are pictured approximately in Figs. 3(b) and 4(b). The anti-symmetrically excited slot still produces the tangential magnetic dipole mode (H_{11}) as the dominant mode. Although the larger extent of the source requires additional modes for a more detailed description (the higher modes are: H_{mn}, m odd, n odd; E_{mn}, m odd, n even),[10] the dominant mode alone may be retained for a first-order description. However, the induced magnetic currents for the symmetrically excited slot are no longer approximately circular as for a small slot (circular magnetic currents excite the vertical electric dipole mode (E_{01}) as the dominant mode). Instead they may be characterized by dipoles directed oppositely in pairs [see Fig. 3(b)] which excite two significant modes: E_{01} and H_{22}.[10] Thus, a more realistic description includes both the E_{01} and H_{22} modes for the representation of the fields radiated by the symmetrically excited slot.

Upon taking into account three propagating modes as described above, the following approximate far field representation is obtained:

$$r\boldsymbol{H}(r) \approx I_4(r)\left\{\boldsymbol{h}_4(\theta,\Phi) + \frac{I_3(r)}{I_4(r)} \cdot \left[\boldsymbol{h}_3(\theta,\Phi) + \frac{I_{22}''(r)}{I_3(r)}\boldsymbol{h}_{22}''(\theta,\Phi)\right]\right\}. \quad (15)$$

If it is assumed that the ratio $I_3/I_4 = I_3(r)/I_4(r)$ is still given by (12), (15) differs from (7) only in that the factor multiplying (I_3/I_4) represents a more detailed description of the radiation from the symmetrically excited slot. On that basis, the ratio $I_{22}''(r)/I_3(r)$ can be computed approximately by assuming an appropriate symmetric constituent slot field. A calculation of this type has been carried out previously for the purpose of determining the value of the parameter R_a [see Fig. 7(b)] which is a function of the real power radiated by the symmetrically excited slot. It was found that (note: $I_3 \equiv I_{01}' = \eta V_{01}'$; $I_{22}'' = \eta V_{22}''$):[12]

$$\frac{I_{22}''(r)}{I_3(r)} = \frac{V_{22}''(r)}{V_3(r)} = \frac{I_{22}''}{I_3} \approx \frac{E}{D}, \quad (16)$$

where D and E are given in (14). It is seen that for small slots (a' and $b' \to 0$), the ratio in (16) vanishes so that (15) goes over into (7).

The H_{22} vector mode function is given by:[10]

$$h_{22}''(\theta,\Phi) \approx h_{220}''(\theta,\Phi) = -\frac{1}{2}\sqrt{\frac{5}{\pi}}\left(\theta_0 \frac{1}{2}\sin 2\theta \sin 2\Phi + \Phi_0 \sin\theta \cos 2\Phi\right). \quad (17)$$

Thus, the gain pattern function becomes:

[11] Felsen, *ibid.*, Eq. (65).

[12] *Ibid.*, Eqs. (59) and (62).

$$G \approx \cos^2\theta\cos^2\Phi - \sqrt{\frac{5}{3}}\frac{I_{22}''}{I_3}$$
$$\cdot \mathrm{Re}\left(\frac{I_3}{I_4}\right)\sin 2\theta \sin 2\Phi \cos\theta\cos\Phi$$
$$+\frac{5}{12}\left(\frac{I_{22}''}{I_3}\right)^2\left|\frac{I_3}{I_4}\right|^2 \sin^2 2\theta \sin^2 2\Phi + \sin^2\Phi$$
$$-2\mathrm{Re}\left(\frac{I_3}{I_4}\right)\sin\Phi\left(\sin\theta - \sqrt{\frac{5}{3}}\frac{I_{22}''}{I_3}\sin\theta\cos 2\Phi\right)$$
$$+\left|\frac{I_3}{I_4}\right|^2\left(\sin\theta - \sqrt{\frac{5}{3}}\frac{I_{22}''}{I_3}\sin\theta\cos 2\Phi\right)^2. \qquad (18)$$

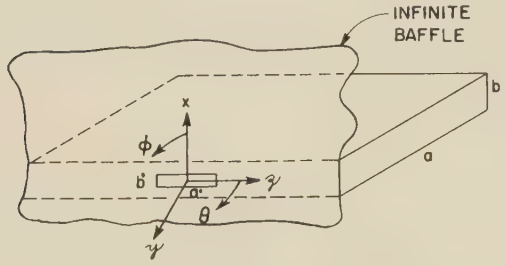

Fig. 9—Physical structure and choice of coordinates (H plane slot).

III. H Plane Slot

A) Derivation of the Coupling Slot Equivalent Circuit Parameters

The physical configuration in this case is shown in Fig. 9. A rectangular slot of dimensions $a' \times b'$ is located symmetrically in the narrow face of a rectangular waveguide ("zero thickness" wall) and radiates into a half-space region. The field analysis proceeds as for the E plane slot except for a difference in the two dominant modes which describe the behavior of the far fields.

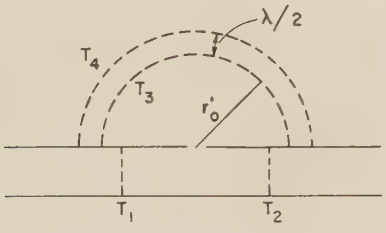

Fig. 10—Location of terminal planes (H plane slot).

The approximate constituent slot fields induced by symmetric and anti-symmetric electric field excitation of the slot at terminal planes T_1 and T_2 in Fig. 10 are shown in Figs. 11 and 12; the dominant modes excited in the half-space by these magnetic current distributions are H_{01} (magnetic dipole mode) and H_{02} (axial magnetic quadrupole mode), respectively, if the z axis in Fig. 9 is chosen as the polar axis of the spherical coordinate system. The reference planes T_3 and T_4 in Fig. 10 have been chosen so as to make the field formulation in this problem identical with that for the E plane slot and thus permit directly the utilization of the equivalent circuit derived in Section II. Moreover, the subscripts 3 and 4 refer, as in the E plane case, to the modes excited by symmetric and anti-symmetric elec-

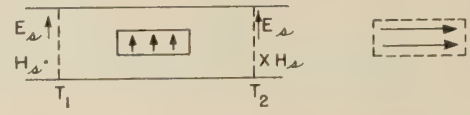

Fig. 11—Symmetrically excited slot (H plane).

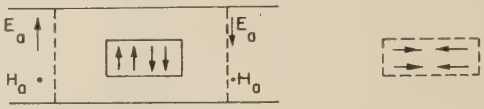

Fig. 12—Anti-symmetrically excited slot (H plane).

tric field excitation of the slot, respectively. It is to be noted in this connection that the magnetic dipole mode now carries the subscript 3 while for the E plane slot it carried the subscript 4. If the terminal plane T_3 is located at a radius

$$r_0' = m\lambda, \qquad m = \text{large integer}, \qquad (19)$$

the theoretical analysis proceeds exactly as in the E plane case, and the approximate equivalent circuit is that shown in Fig. 6. In relating the parameters of the (lossless) four terminal-pair equivalent circuit to those of the two terminal-pair network obtained when the

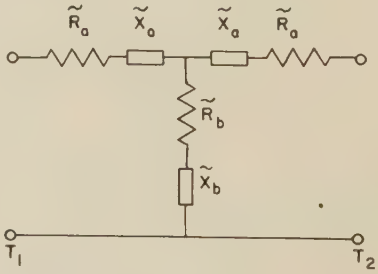

Fig. 13—Two terminal-pair Tee network for H plane radiating slot.

slot is viewed as a lossy (radiating) structure in the rectangular waveguide, it is convenient to use not the Pi network shown in Fig. 7 but the Tee network shown in Fig. 13, since the H plane slot is essentially shunt so that the series impedances of the Tee are small. (The $\sim$ serve to designate H plane slot quantities.) The network parameters in Figs. 6 and 13 are related as follows:

$$\tilde{n}_2^2 = \frac{2\lambda/\lambda_g}{\tilde{R}_a' + 2\tilde{R}_b'},$$
$$\tilde{n}_1^2 = \frac{2\lambda_g/\lambda}{\tilde{G}_a'},$$
$$\tilde{X}_1' = \frac{-1}{\tilde{B}_a'}, \qquad (20)$$
$$\tilde{X}_2' = \frac{1}{2}\left(\tilde{X}_a' + 2\tilde{X}_b' + \frac{1}{\tilde{B}_a'}\right),$$
$$\tilde{G}_a' = \frac{\tilde{R}_a'}{\tilde{R}_a'^2 + \tilde{X}_a'^2}, \qquad \tilde{B}_a' = -\frac{\tilde{X}_a'}{\tilde{R}_a'^2 + \tilde{X}_a'^2}. \qquad (21)$$

The primes denote normalization with respect to the characteristic impedance (admittance) of the rectangular waveguide. The two terminal-pair equivalent circuit parameters for the slot are readily determined from measurements within the rectangular waveguide. A theoretical evaluation of these parameters via a variational procedure is also available.[5]

B) Computation of the Pattern

As for the E plane slot, the network in Fig. 8 is employed to calculate the mode currents I_3 and I_4 appropriate to the H plane slot radiating into the empty half-space region (provided that all parameters are replaced by their $\sim$ values). The far radiated magnetic field is given approximately by:

$$\boldsymbol{rH}(\boldsymbol{r}) \approx I_3 e^{-jk(r-r_0')}\left(\boldsymbol{h}_3(\theta, \Phi) - \frac{I_4}{I_3}\boldsymbol{h}_4(\theta, \Phi)\right), \qquad (22)$$

where in this case

$$\boldsymbol{h}_3(\theta, \Phi) \equiv \boldsymbol{h}_{01}''(\theta, \Phi) = \boldsymbol{\theta}_0\sqrt{\frac{3}{4\pi}}\sin\theta, \qquad (23)$$

$$\boldsymbol{h}_4(\theta, \Phi) \equiv \boldsymbol{h}_{02}''(\theta, \Phi) = \boldsymbol{\theta}_0\frac{3}{4}\sqrt{\frac{5}{3\pi}}\sin 2\theta. \qquad (24)$$

Since the z axis in Fig. 9 has been chosen as the polar axis of the spherical coordinate system the mode functions $\boldsymbol{h}_{01}''$ and $\boldsymbol{h}_{02}''$, characteristic of magnetic dipoles directed along the z axis, are independent of the Φ coordinate which is measured in the xy plane. This azimuthal symmetry about the dipole axis, directly evident from (23), is obscured in (5) because of the different choice of coordinates in the E plane slot problem. One also notes the duality between the axial electric and magnetic dipole mode functions in (4) and (23), respectively.

Upon substituting (23) and (24) into (22) and taking the square of the magnitude of the result, one obtains, for small slots:

$$|\boldsymbol{rH}|^2 \approx \left(\frac{3}{4\pi}|v|^2\right)\left|\frac{I_3}{v}\right|^2\tilde{G}, \qquad (25)$$

$$\tilde{G} = \sin^2\theta + \frac{5}{4}\left|\frac{I_4}{I_3}\right|^2\sin^2 2\theta - \sqrt{5}\,\mathrm{Re}\left(\frac{I_4}{I_3}\right)\sin\theta\sin 2\theta. \qquad (26)$$

By considerations analogous to those employed in Part II, Section B, it is readily found that

$$\frac{I_4}{I_3} = \frac{\tilde{n}_2}{\tilde{n}_1}\frac{\lambda_g}{\lambda}\tilde{Z}_a'\frac{(\tilde{Z}_a' + 2\tilde{Z}_b') + Z_2'^T}{\tilde{Z}_a' + Z_2'^T}. \qquad (27)$$

Since the H plane slot shown in Fig. 9 is essentially a shunt slot at centerline reference planes, $\tilde{Z}_a'$ is usually a small quantity. Therefore, (I_4/I_3) is usually small and the pattern in (26) is essentially that of a magnetic dipole in the slot plane. However, for very small values of $Z_2'^T$, the ratio (I_4/I_3) may be appreciable and the quadrupole pattern becomes more pronounced (see Part IV). Since $\tilde{Z}_a'$ is usually small and its experimental determination often inaccurate, it is again appropriate to employ an approximate theoretical formula for $\tilde{G}_a'$ which has been obtained previously:[13]

$$\tilde{G}_a' \approx \frac{16\pi^3}{15}\frac{ab}{\lambda\lambda_g}\frac{[1 - (a'/\lambda_g)^2]^2}{(a'/a)^2\sin^2(\pi a'/\lambda_g)}\left(\frac{a'}{\lambda}\right)^4 \cdot\left[1 - \left(\frac{\pi^2 - 6}{14}\right)\left(\frac{a'}{\lambda}\right)^2 - \frac{1}{21}\left(\frac{\pi b'}{\lambda}\right)^2\right]^2. \qquad (28)$$

For longer slots commonly used in practice, the increased slot length is expected to effect principally the radiation pattern due to the current distribution in Fig. 11. The next mode excited by this distribution is H_{03}.[14] The radiated field due to the three modes under consideration is given by:

$$\boldsymbol{rH}(\boldsymbol{r}) \approx I_3(r)\left[\boldsymbol{h}_3(\theta, \Phi) + \frac{I_{03}''(r)}{I_3(r)}\boldsymbol{h}_{03}''(\theta, \Phi) + \frac{I_4(r)}{I_3(r)}\boldsymbol{h}_4(\theta, \Phi)\right]. \qquad (29)$$

As in the E plane case we now make the simplifying assumption that (I_4/I_3) in (29) is still given by (27). The ratio of (I_{03}''/I_3) for an assumed cosine field in the slot has been calculated previously.[15] Upon substituting the values for the vector mode functions and for (I_{03}''/I_3) into (29) one obtains the following gain pattern function:

$$\tilde{G} = F^2\sin^2\theta - \sqrt{5}\,\mathrm{Re}\left(\frac{I_4}{I_3}\right)F\sin\theta\sin 2\theta + \frac{5}{4}\left|\frac{I_4}{I_3}\right|^2\sin^2 2\theta, \qquad (30)$$

[13] *Ibid.*, Eq. (80).
[14] Felsen and Marcuvitz, *op. cit.*, Section III.
[15] *Ibid.*, Eqs. (3.10).

where

$$F = 1 - \frac{1}{2}\left(\cos^2\theta - \frac{1}{5}\right)\left(\frac{a'}{\lambda}\right)^2 \left[\frac{(\pi^2 - 8) - \frac{\pi^2}{6}\left(\frac{b'}{a'}\right)^2}{1 - \frac{2}{5}\left(\frac{a'}{\lambda}\right)^2\left[\left(\frac{\pi^2}{4} - 2\right) + \frac{\pi^2}{6}\left(\frac{b'}{a'}\right)^2\right]}\right]. \quad (31)$$

IV. Experimental Verification

To test the validity of the various approximations made in the preceding analysis, gain pattern measurements at $\lambda = 3.2$ cm were carried out in an anechoic chamber on several E plane and H plane slots terminated in a variable reactive load (variable short circuit). The slots were fitted into a $2\frac{1}{2}$ foot square copper sheet (intended to simulate an "infinite" baffle) which could be rotated through an angle of 180 degrees, and a stationary rectangular horn served as a pickup. Slot dimensions were chosen large enough so that an appreciable amount of power was radiated for the entire range of reactive waveguide terminations. For the two E plane slots employed, relative dimensions and measured two-terminal pair equivalent circuit parameters were the following ($a = 0.900''$, $b = 0.400''$ throughout):

Slot I:

$$a'/\lambda = .714, \quad b'/\lambda = .318$$
$$G_b' = .980, \quad B_b' = .694$$
$$R_a' = 1.30, \quad X_a' = 7.78 \quad (32)$$

Slot II:

$$a'/\lambda = .510, \quad b'/\lambda = .324$$
$$G_b' = .816, \quad B_b' = .123$$
$$R_a' = .730, \quad X_a' = 6.26 \quad (33)$$

The values for R_a' are not experimental but computed from (13). With the network parameters as given by (32) and (33), the ratio of (I_3/I_4) is computed from (11, 12) with n_1 and n_2 given in (1), and $Z_2'^T = j \tan\varphi$, $\varphi = 2\pi l/\lambda_g$, appropriate to a perfect short-circuit located a distance l from the terminal plane T_2. The ratio (I_{22}''/I_3) is calculated from (16), and the gain pattern is then obtained from (18). The calculations were carried out for the two mutually perpendicular planes $\Phi = 0$, π, and $\Phi = \pm\pi/2$, in which measurements were taken.

Graphs of the measured and calculated gain patterns for slot I are shown in Fig. 14 for various short-circuit locations, φ. The plots are carried out over an intensity range from 0 db to -10 db, where the maximum level in any particular pattern is taken as the 0 db point. In view of the weak power source employed, readings could not be taken below the -10 db level for most of the patterns considered. It is seen that the theoretical curves predict the essential pattern behavior quite well over the entire range of short-circuit settings. In the critical region $\varphi \approx 90°$ where the pattern is critically affected by small changes in φ, the computed pattern leads the experimental pattern by approximately 5° in φ; *i.e.*, the theoretical pattern at $\varphi = 90°$, for example, represents rather closely measured pattern at $\varphi = 95°$ etc.

The relative power levels of the various gain patterns were also computed on the assumption of a matched generator as in Fig. 8. This entails the determination of (I_4/v), [see (7)], with v taken as constant. The computed and measured maximum power levels for various gain patterns showed similar variations, but differed in actual magnitude by a maximum of 2 db in the critical region $\varphi \approx 90°$.

The agreement between computed and measured gain patterns for slot II in (33) was similar to that obtained for slot I. Since the patterns for the two slots are almost alike the comparison between theory and experiment is not given for slot II.

Gain pattern measurements were also carried out on an H plane slot with relative dimensions $a'/\lambda = .714$, $b'/\lambda = .202$ (see Fig. 9). As for the E plane slot, a variable short-circuit was employed to yield a series of reactive waveguide terminations. Patterns measured in the $x = 0$ plane are plotted in Fig. 15 (page 26), and are compared with patterns calculated from (30). It is seen again that reasonable agreement prevails throughout but is poorest in the critical region where the output impedance is very small; *i.e.*, $\tan\varphi \approx 0$. In this region, the calculated pattern appears to lag the measured pattern by about 5° in φ. The patterns in the $z = 0$ plane (Fig. 11) were also measured but are not plotted here since they agreed with the theoretically predicted (Φ independent) constant value.

Measurements were also taken on several smaller slots and yielded patterns analogous to those shown in Figs. 14 and 15. A complete check with the theory was not possible for those slots since the power level of the patterns in the critical region was too small to be measured with the equipment employed in the experiments.

V. Stepwise Procedure for Calculating Patterns

A) E plane Slot

1) Obtain the equivalent circuit parameters in Fig. 7 either from measurement or from theory.[5]
2) Compute (n_1/n_2) from (1), and (I_3/I_4) from (11, 12), for the specified output terminating impedance $Z_2'^T$ (all primes indicate normalized parameters). *Note:* A theoretical expression for R_a' given in (13) is appropriate when the measured values of Y_a' are not reliable.
3) Compute the gain pattern for a small slot from (8). If the a' dimension of the slot is large, the modified expression (18) is employed, with (I_{22}''/I_3) computed from (16).

B) H plane Slot

1) Obtain the equivalent circuit parameters in Fig. 13 from measurement.

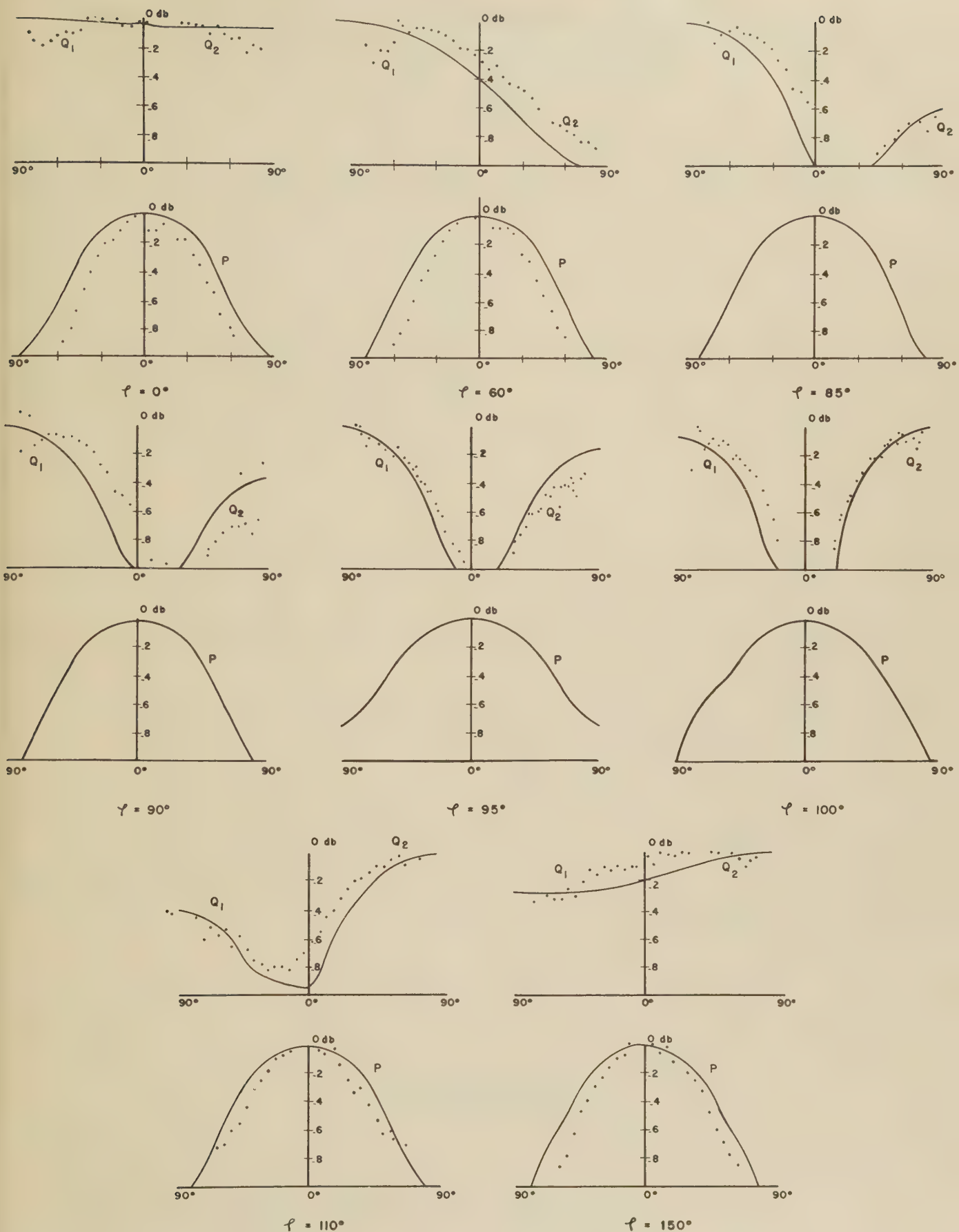

Fig. 14—*E* plane slot radiation patterns (relative power plots). ϕ = electrical length in degrees from slot symmetry plane to short circuit termination; Q_1 = pattern in $\Phi = -\pi/2$ plane; Q_2 = pattern in $\Phi = +\pi/2$ plane; P = pattern in $\Phi = 0$, π plane; · = experimental points; – = theoretical curve. Each graph extends over a power range from 0 to −10 db.

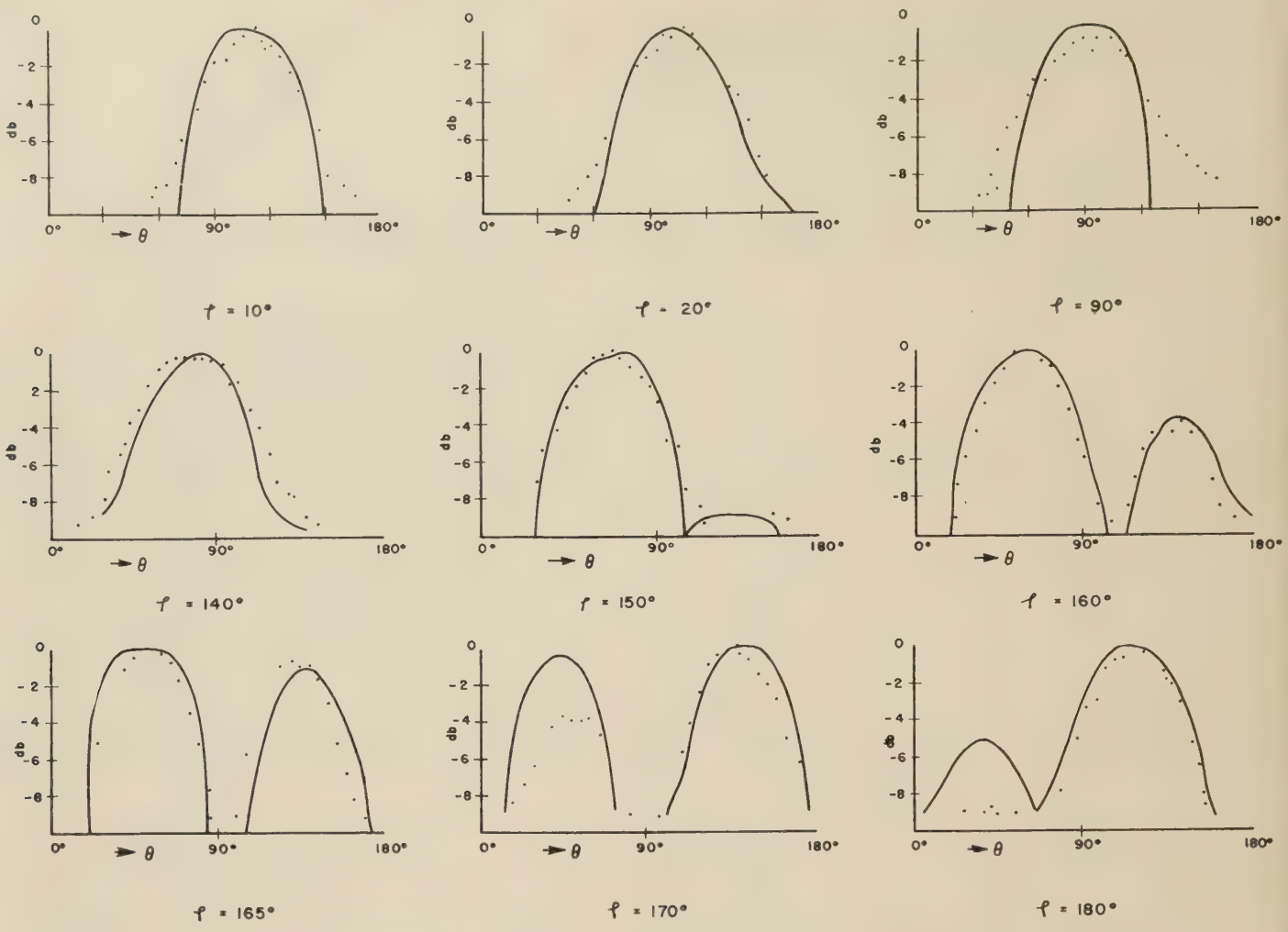

Fig. 15—H plane slot radiation patterns. ϕ = electrical length in degrees from slot symmetry plane to short circuit termination; · = experimental points; – = theoretical curve. Each graph extends over a power range from 0 to −10 db.

2) Compute $(\tilde{n}_2/\tilde{n}_1)$ from (20), and (I_4/I_3) from (27(, for a specified output terminating impedance $Z_2'^T$. *Note:* A theoretical expression for $\tilde{G}_a'$ given in (28) is appropriate when the measured values of $\tilde{Z}_a'$ are not reliable.
3) Compute the gain pattern for a small slot from (26). If the a' dimension of the slot is large, the modified expression (30) is employed.

Acknowledgment

The research described in this report was carried out under Contract No. AF-19(604)-890 sponsored by the Air Force Cambridge Research Center.

The author gratefully acknowledges the assistance of Mr. Stanley Schneider in the experimental phase of this project.

An Experimental Study of the Disk-Loaded Folded Monopole*

E. W. SEELEY†

Summary—Data is presented to show the reduction in size and increase in radiation resistance and bandwidth of the disk-loaded folded monopole as compared with a disk-loaded monopole of the same electrical length. The ratio of diameters of the folded part to the diameter of the driven part was varied for one series of impedance measurements and the axial spacing between the driven part and folded part was varied for another series. The resonant radiation resistance and resonant length may be varied almost independently. The radiation resistance depends upon the ratio of diameter of the folded part to the diameter of the driven part, and the resonant length depends upon axial spacing. The radiation resistance multiplication factor relative to a disk-loaded monopole of the same electrical length is approximately the same as the multiplication factor of a folded dipole relative to a dipole. The disk-loaded folded monopole has a greater bandwidth than an unloaded monopole of the same wavelength-to-diameter ratio. Where the effective diameter[1] of the folded antenna is $\sqrt{2D_dS}$, its radiation pattern is essentially that of an unloaded monopole.

RAYMOND and Webb[2] show the extent to which radiation resistance and resonant length are reduced by disk loading a monopole. Guertler[3] has shown that the radiation resistance of a dipole can be increased considerably by folding. Disk loading and folding may be combined to produce a short, broadband antenna with high radiation resistance. Curves are presented that may be used to design the disk-loaded folded monopole for specific applications. Only the second resonance characteristics of this antenna are presented.

Impedance measurements were made on the disk-loaded folded monopole shown in Fig. 1, at frequencies from 200 mc to 300 mc, using a ground screen fifty feet in diameter. Two physical parameters, D_f/D_d and S, were varied for several sets of impedance vs frequency. Figs. 2 and 3 (next page) show effect of varying D_f/D_d and S upon second resonance and upon radiation resistance. Disk-loaded folded monopole does not resonate in the vicinity of its second natural frequency when $D_f/D_d>7$ and $S=2.5$ inches, as its self impedance is predominately inductive. One general rule emerged from these measurements: vary the axial spacing to change resonant frequency and vary D_f/D_d to change radiation resistance.

The ratio of the radiation resistances of the disk-loaded folded monopole and the disk-load monopole of equal length is shown in Fig. 4. The dashed curve is a plot of Guertler's equation for the ratio of resonant resistances of folded to unfolded dipoles.[4]

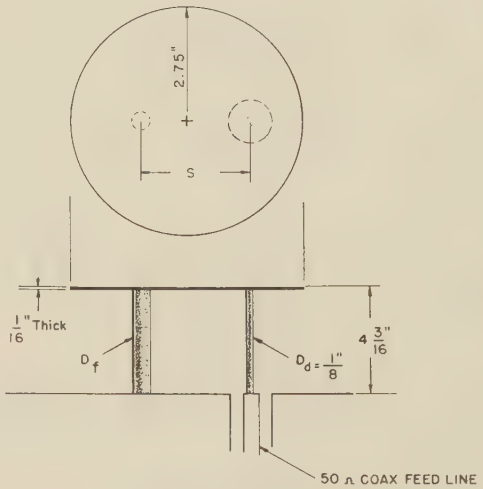

Fig. 1—Disk-loaded folded monopole.

The disk-loaded folded monopole has a greater bandwidth than an unloaded dipole of the same wavelength to-diameter ratio. Fig. 5 shows the vswr for $D_f/D_d=1$ and $S=2.5$ inches when antenna was fed with a 50Ω line and generator. Dashed line indicates vswr for which antenna accepts 50 per cent of power from a 50Ω line.

As reported by Hill,[5] the radiation pattern of the disk-loaded folded monopole is essentially that of an unloaded monopole.

Conclusion

The disk-loaded folded monopole has more desirable characteristics than the disk-loaded monopole or the unloaded monopole. The resonant radiation resistance may be varied over a wide range by changing D_f/D_d without the aid of a matching network. The resonant length is two and a half times shorter than a monopole with the same wavelength-to-diameter ratio. The bandwidth is greater than that of a comparable monopole and many times greater than a disk-loaded monopole the same length and the bandwidth increases with D_f/D_d. The disk-loaded folded monopole is a small electromagnetic radiator whose electrical characteristics have not been deteriorated by shortening and loading. On the contrary, its electrical characteristics improved.

* Manuscript received by the PGAP, May 23, 1955; revised manuscript received August 19, 1955.

† Naval Ordnance Lab., Corona, Calif.

[1] S. A. Schelkunoff, "Antennas, Theory and Practice," John Wiley and Sons Inc., New York; 1952.

[2] R. C. Raymond and W. Webb, "Radiation resistance of loaded antennas," *J. Appl. Phys.*, vol. 20, pp. 328–330; April, 1949.

[3] R. Guertler, "Impedance transformation in folded dipoles," PROC. IRE, vol. 38, pp. 1042–1047; September, 1950.

[4] R. Guertler, *ibid.*

[5] E. G. Hill, "VHF antenna for trains," *Electronics*, vol. 19, pp. 134–136; November, 1946.

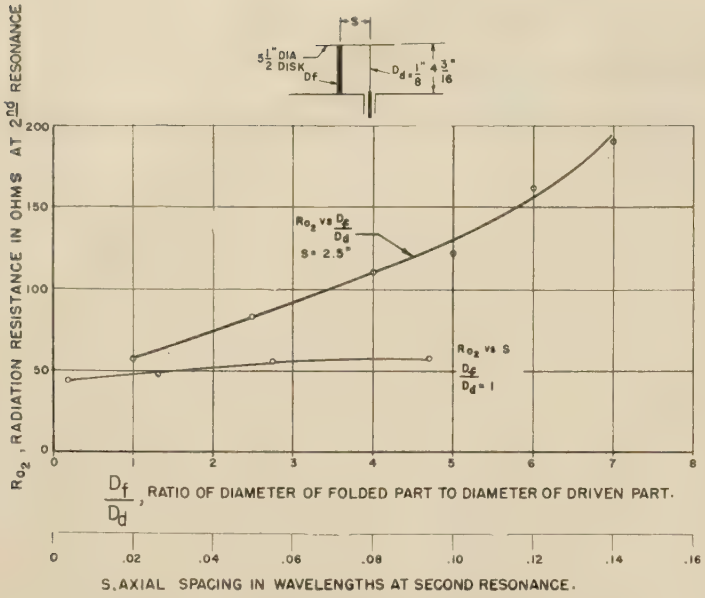

Fig. 2—Variation in radiation resistance at second resonance with changes in D_f/D_d ratio and changes in axial spacing.

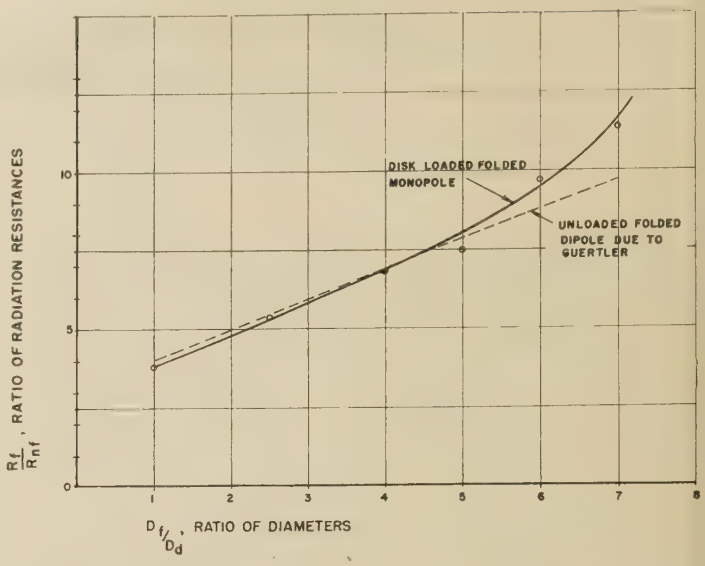

Fig. 4—Increase in radiation resistance due to folding a disk-loaded monopole as the D_f/D_d ratio is increased.

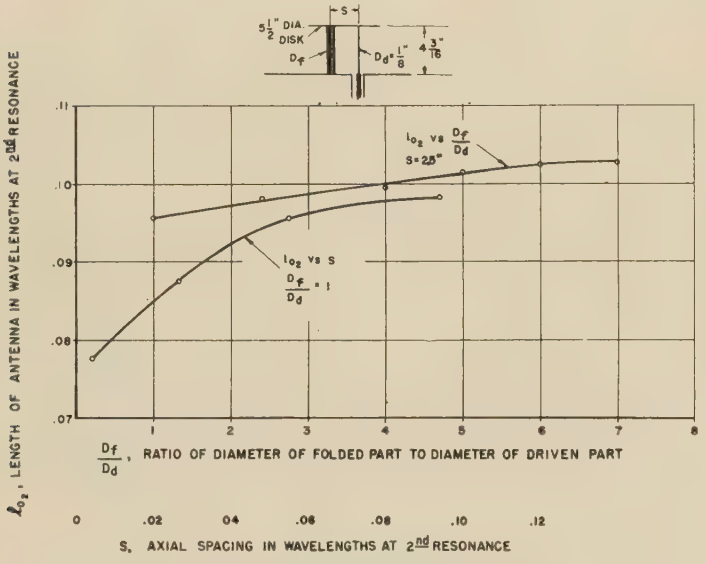

Fig. 3—Variations in antenna electrical length with changes in D_f/D_d ratio and changes in axial spacing.

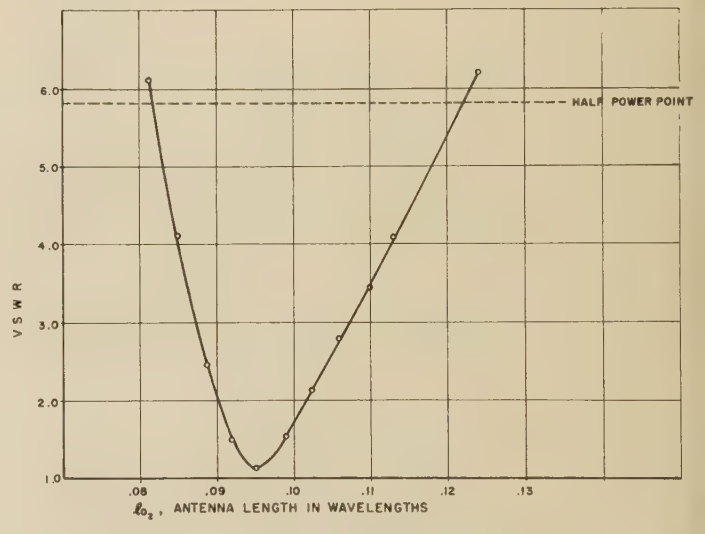

Fig. 5—Variations in vswr with changes in antenna length for $D_f/D_d = 1$ and $S = 2.5$ inches.

Some Data for the Design of Electromagnetic Horns*

E. H. BRAUN†

Summary—**Using an idea recently suggested by the author,[1] a table is presented from which the gain of all electromagnetic horns may be calculated with substantially the same accuracy obtainable using the gain formula.**

The exact parameters of an optimum horn are given, and a simple procedure for the design of optimum horns with a specified gain and other desirable properties is described.

RECENTLY the author described a method for extending the range and improving the accuracy of published curves for the gain of electromagnetic horns.[1] It has been found, however, that the curves which are available still leave something to be desired in the way of either accuracy or range, or both. Actually, the above method makes it unnecessary to plot a family of curves for various slant heights; only one curve is required to calculate the gain of all horns. Such a curve has recently been accurately computed by machine for l_E and $l_H = 50\lambda$, and gain figures obtained from it agree with those calculated from the formula within about 0.01 db. Such a curve obviates the necessity for ever using the formula.

Rather than reproduce this curve on a scale large enough to be read conveniently, it is felt that for publication purposes it would be simpler to present a table listing gain vs (adjusted) aperture dimensions (Tables I and II on the next page). Linear interpolation of the aperture dimension will result in negligible error.

The tables are used as indicated below.

For Pyramidal Horns

Let the H-plane and E-plane aperture dimensions and slant heights of the horn (*in wavelengths*) be a, b, l_H, and l_E, respectively. (See Fig. 1.)

1) Calculate

$$A = a\sqrt{\frac{50}{l_H}} \qquad B = b\sqrt{\frac{50}{l_E}}.$$

2) Look up G_H and G_E in the tables for these particular values of A and B, respectively.

3) Calculate

$$g = \frac{G_E G_H}{\frac{32}{\pi}\sqrt{\frac{50}{l_H}}\sqrt{\frac{50}{l_E}}} = \frac{G_E G_H}{10.1859\sqrt{\frac{50}{l_H}}\sqrt{\frac{50}{l_E}}}.$$

This is the actual gain of the horn.

If the values of either A or B or both come out smaller than 2, then simply substitute $(32/\pi)A$ and/or $(32/\pi)B$ for G_H and/or G_E, respectively, in the formula for g.

The gain of sectoral horns is obtained in a similar way.

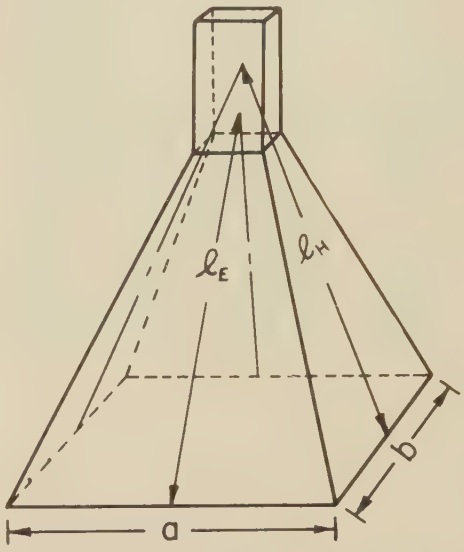

Fig. 1—Physical dimensions for calculating the gain.

For H-plane Sectoral Horns

1) Calculate

$$A = a\sqrt{\frac{50}{l_H}}.$$

2) Look up G_H in the H-plane table for this value of A.

3) Calculate

$$g = b\frac{G_H}{\sqrt{\frac{50}{l_H}}}.$$

This is the actual gain of the horn.

For E-plane Sectoral Horns

1) Calculate

$$B = b\sqrt{\frac{50}{l_E}}.$$

2) Look up G_E in the E-plane table for this value of B.

3) Calculate

$$g = a\frac{G_E}{\sqrt{\frac{50}{l_E}}}.$$

This is the actual gain of the horn.

* Manuscript received by the PGAP, August 2, 1955.

† Microwave Antennas and Components Branch, Electronics Div., Naval Research Lab., Washington 25, D. C.

[1] E. H. Braun, "Gain of electromagnetic horns," PROC. IRE, vol. 41, pp. 109–115; January, 1953.

TABLE I

G_H AS A FUNCTION OF H-PLANE APERTURE DIMENSION "A"

A	G_H	A	G_H	A	G_H	A	G_H	A	G_H	A	G_H	A	G_H
2.0	20.370	4.6	46.635	7.2	71.291	9.8	90.633	12.4	99.019	15.0	92.591	17.6	75.416
2.1	21.387	4.7	47.628	7.3	72.164	9.9	91.195	12.5	99.052	15.1	92.066	17.7	74.701
2.2	22.402	4.8	48.619	7.4	73.031	10.0	91.740	12.6	99.062	15.2	91.528	17.8	73.991
2.3	23.422	4.9	49.609	7.5	73.889	10.1	92.270	12.7	99.051	15.3	90.972	17.9	73.282
2.4	24.439	5.0	50.595	7.6	74.739	10.2	92.781	12.8	99.012	15.4	90.400	18.0	72.581
2.5	25.452	5.1	51.578	7.7	75.580	10.3	93.274	12.9	98.953	15.5	89.822	18.1	71.886
2.6	26.471	5.2	52.559	7.8	76.413	10.4	93.751	13.0	98.871	15.6	89.214	18.2	71.199
2.7	27.488	5.3	53.536	7.9	77.236	10.5	94.208	13.1	98.763	15.7	88.601	18.3	70.516
2.8	28.501	5.4	54.512	8.0	78.049	10.6	94.646	13.2	98.638	15.8	87.976	18.4	69.847
2.9	29.518	5.5	55.475	8.1	78.854	10.7	95.067	13.3	98.486	15.9	87.337	18.5	69.183
3.0	30.532	5.6	56.449	8.2	79.644	10.8	95.470	13.4	98.309	16.0	86.688	18.6	68.534
3.1	31.545	5.7	57.418	8.3	80.427	10.9	95.848	13.5	98.114	16.1	86.026	18.7	67.891
3.2	32.560	5.8	58.377	8.4	81.196	11.0	96.207	13.6	97.894	16.2	85.355	18.8	67.262
3.3	33.573	5.9	59.334	8.5	81.956	11.1	96.547	13.7	97.654	16.3	84.677	18.9	66.643
3.4	34.579	6.0	60.286	8.6	82.703	11.2	96.869	13.8	97.387	16.4	83.990	19.0	66.038
3.5	35.595	6.1	61.232	8.7	83.440	11.3	97.168	13.9	97.101	16.5	83.319	19.1	65.447
3.6	36.605	6.2	62.176	8.8	84.164	11.4	97.446	14.0	96.793	16.6	82.594	19.2	64.871
3.7	37.612	6.3	63.115	8.9	84.875	11.5	97.702	14.1	96.464	16.7	81.888	19.3	64.305
3.8	38.622	6.4	64.046	9.0	85.567	11.6	97.938	14.2	96.113	16.8	81.179	19.4	63.758
3.9	39.629	6.5	64.975	9.1	86.250	11.7	98.149	14.3	95.740	16.9	80.461	19.5	63.222
4.0	40.633	6.6	65.896	9.2	86.923	11.8	98.342	14.4	95.348	17.0	79.742	19.6	62.703
4.1	41.637	6.7	66.810	9.3	87.579	11.9	98.510	14.5	94.936	17.1	79.023	19.7	62.201
4.2	42.645	6.8	67.720	9.4	88.221	12.0	98.658	14.6	94.504	17.2	78.301	19.8	61.714
4.3	43.639	6.9	68.623	9.5	88.844	12.1	98.783	14.7	94.054	17.3	77.578	19.9	61.243
4.4	44.641	7.0	69.518	9.6	89.460	12.2	98.882	14.8	93.586	17.4	76.854	20.0	60.788
4.5	45.639	7.1	70.407	9.7	90.053	12.3	98.965	14.9	93.095	17.5	76.134		

TABLE II

G_E AS A FUNCTION OF E-PLANE APERTURE DIMENSION "B"

B	G_E	B	G_E	B	G_E	B	G_E	B	G_E	B	G_E	B	G_E
2.0	20.362	4.6	46.397	7.2	69.123	9.8	81.301	12.4	73.784	15.0	46.499	17.6	19.910
2.1	21.381	4.7	47.362	7.3	69.847	9.9	81.426	12.5	73.041	15.1	45.268	17.7	19.316
2.2	22.395	4.8	48.326	7.4	70.555	10.0	81.518	12.6	72.265	15.2	44.040	17.8	18.767
2.3	23.410	4.9	49.283	7.5	71.248	10.1	81.581	12.7	71.459	15.3	42.813	17.9	18.264
2.4	24.425	5.0	50.233	7.6	71.923	10.2	81.611	12.8	70.621	15.4	41.593	18.0	17.805
2.5	25.440	5.1	51.181	7.7	72.586	10.3	81.609	12.9	69.753	15.5	40.379	18.1	17.395
2.6	26.456	5.2	52.123	7.8	73.219	10.4	81.575	13.0	68.856	15.6	39.174	18.2	17.030
2.7	27.472	5.3	53.057	7.9	73.841	10.5	81.510	13.1	67.931	15.7	37.982	18.3	16.714
2.8	28.481	5.4	53.985	8.0	74.441	10.6	81.408	13.2	66.980	15.8	36.801	18.4	16.445
2.9	29.490	5.5	54.908	8.1	75.025	10.7	81.277	13.3	66.001	15.9	35.636	18.5	16.223
3.0	30.503	5.6	55.821	8.2	75.585	10.8	81.110	13.4	64.997	16.0	34.488	18.6	16.048
3.1	31.511	5.7	56.728	8.3	76.127	10.9	80.909	13.5	63.969	16.1	33.359	18.7	15.921
3.2	32.518	5.8	57.626	8.4	76.645	11.0	80.676	13.6	62.917	16.2	32.250	18.8	15.839
3.3	33.527	5.9	58.517	8.5	77.142	11.1	80.405	13.7	61.844	16.3	31.164	18.9	15.804
3.4	34.530	6.0	59.401	8.6	77.616	11.2	80.104	13.8	60.748	16.4	30.104	19.0	15.814
3.5	35.534	6.1	60.272	8.7	78.065	11.3	79.765	13.9	59.635	16.5	29.069	19.1	15.870
3.6	36.534	6.2	61.134	8.8	78.492	11.4	79.393	14.0	58.501	16.6	28.063	19.2	15.967
3.7	37.531	6.3	61.987	8.9	78.892	11.5	78.987	14.1	57.351	16.7	27.086	19.3	16.108
3.8	38.530	6.4	62.828	9.0	79.269	11.6	78.545	14.2	56.188	16.8	26.142	19.4	16.289
3.9	39.524	6.5	63.659	9.1	79.619	11.7	78.068	14.3	55.008	16.9	25.232	19.5	16.521
4.0	40.515	6.6	64.477	9.2	79.944	11.8	77.559	14.4	53.816	17.0	24.355	19.6	16.769
4.1	41.504	6.7	65.285	9.3	80.240	11.9	77.014	14.5	52.614	17.1	23.515	19.7	17.064
4.2	42.490	6.8	66.080	9.4	80.510	12.0	76.435	14.6	51.402	17.2	22.713	19.8	17.394
4.3	43.472	6.9	66.862	9.5	80.752	12.1	75.822	14.7	50.183	17.3	21.951	18.9	17.755
4.4	44.450	7.0	67.630	9.6	80.964	12.2	75.176	14.8	48.959	17.4	21.228	20.0	18.147
4.5	45.425	7.1	68.385	9.7	81.146	12.3	74.497	14.9	47.731	17.5	20.548		

The following is a procedure for designing a horn having these four properties:

1) It is an optimum[2] horn.
2) It has approximately equal (half-power) E- and H-plane beamwidths.
3) It has a specified gain g.
4) It fits whatever waveguide is chosen in a simple butt joint.

[2] An optimum horn has aperture dimensions chosen to give maximum gain when the slant height is held fixed.

The exact dimensions fulfilling the first three conditions are (in wavelengths):[3]

$$a = 0.468\sqrt{g}$$

$$b = 0.346\sqrt{g}$$

$$l_E = 0.0576\ g$$

$$l_H = 0.0689\ g$$

where a and b, and l_H and l_E, are the H-plane and E-

[3] All dimensions in this paper are in wavelengths.

plane aperture dimensions and slant heights, respectively, all I.D. (See Fig. 1.)

However, if it is desired to have all sides of the horn meet the waveguide in a common plane, at least one dimension, say l_H, must be altered somewhat from the optimum value. This results in a horn having a gain which differs by a few tenths of a db from the original desired value. Hence two procedures are given, depending on whether or not the designer is willing to accept the few tenths of a db difference. In any case it should be emphasized that exact value of gain of final horn, as computed from Schelkunoff's curves, will be known. This theoretical gain should in turn be within about $\frac{1}{2}$ db of true gain, and in most cases, considerably closer.

Procedure (A): (Designer willing to accept small difference in gain)

1) Calculate

$$a = 0.468\sqrt{g}$$

$$b = 0.346\sqrt{g}$$

$$l_E = 0.0576g$$

$$l_H = \frac{a}{a - w_H}\sqrt{\left[l_E^2 - \left(\frac{b}{2}\right)^2\right]\left[\frac{b - w_E}{b}\right]^2 + \left(\frac{a - w_H}{2}\right)^2};$$

w_H and w_E are the H-plane and E-plane guide widths, respectively, both I.D. and in wavelengths.

2) Calculate gain of this horn using above method. Its gain will differ only slightly from original desired gain, and it will fit the waveguide accurately.

Procedure (B): (Designer desiring closer approximation to original gain)

1) Calculate

$$\bar{a} = 0.468\sqrt{g}$$

$$\bar{b} = 0.346\sqrt{g}$$

$$\bar{l}_E = 0.0576\ g$$

$$\bar{l}_H = \frac{\dfrac{\bar{b} - w_E}{\bar{b}}}{\dfrac{\bar{a} - w_H}{\bar{a}}}\bar{l}_E.$$

2) Compute the gain of this horn as above. Call this gain g_1.

3) Calculate

$$a = 0.468\sqrt{\frac{g^2}{g_1}}$$

$$b = 0.346\sqrt{\frac{g^2}{g_1}}$$

$$l_E = 0.0576\frac{g^2}{g_1}$$

$$l_H = \frac{a}{a - w_H}\sqrt{\left[l_E^2 - \left(\frac{b}{2}\right)^2\right]\left[\frac{b - w_E}{b}\right]^2 + \left(\frac{a - w_H}{2}\right)^2}.$$

4) Calculate the gain of this horn, which will now be extremely close to the original desired gain, and will fit the waveguide accurately.

Measured Performance of Matched Dielectric Lenses*

E. M. T. JONES, T. MORITA, AND S. B. COHN†

***Summary*—Two microwave lenses whose surfaces have been matched respectively by embedded capacitive walls and by simulated quarter-wave transformers were built and compared experimentally to an unmatched lens of identical aperture and focal length. At the design frequency, the matched lenses exhibited reductions in side-lobe level of 14 and 10 db with respect to the unmatched lens, and increases in over-all gain of 0.35 and 0.1 db. The input vswr of the feed horn was reduced from 1.6 for the unmatched case to 1.02 and 1.05 for the matched cases. The bandwidth of good performance for the two lenses ranged from 16 per cent to at least 44 per cent.**

Introduction

THE PERFORMANCE of dielectric lenses as microwave focusing elements is seriously degraded unless reflections at the air, dielectric interfaces are cancelled. In a previous paper[1] a technique for cancelling surface reflections by means of reactive walls embedded within the dielectric was described. Surface reflections may also be cancelled by placing simulated quarter-wave transforming sections on the surface of the lens, as discussed by Morita and Cohn.[2] The theoretical design information for these matching techniques was determined for plane dielectric, air interfaces having plane waves incident upon them with arbitrary angles of incidence and polarization. Verification of the theory was originally obtained by waveguide measurements on small samples.

In order to study experimentally the effectiveness of these matching techniques as applied to curved surfaces,

* Manuscript received by the PGAP, July 18, 1955. The work reported in this paper was made possible through support extended by the U. S. Signal Corps.

† Stanford Research Inst., Stanford, Calif.

[1] E. M. T. Jones and S. B. Cohn, "Surface matching of dielectric lenses," *Jour. Appl. Phys.*, vol. 26, pp. 452–457; April, 1955.

[2] T. Morita and S. B. Cohn, "Microwave lens matching by simulated quarter-wave transformers," TRANS. IRE, vol. AP-3, this issue.

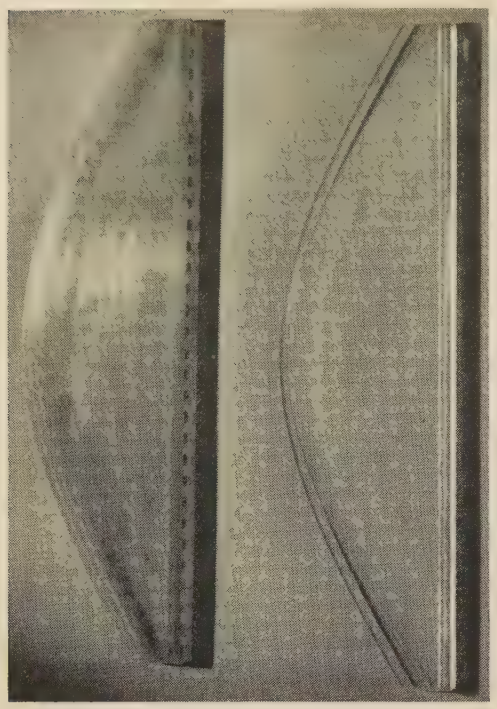

Fig. 1—Photograph of two matched dielectric lenses. The lens on the left is matched with capacitive walls while that on the right is matched with simulated quarter-wave transformers.

three dielectric lenses were built to operate at X-band frequencies. These lenses were designed to mount in the 12-inch aperture of an H-plane sectoral horn and to focus the cylindrical phase front of a wave propagating in the horn to a plane phase front at the mouth of the horn. Photographs of the two matched lenses are shown in Fig. 1. The lens matched with capacitive walls is shown at the left, while the lens matched with quarter-wave transformers is shown at the right. A photograph of the disassembled H-plane horn is shown in Fig. 2,

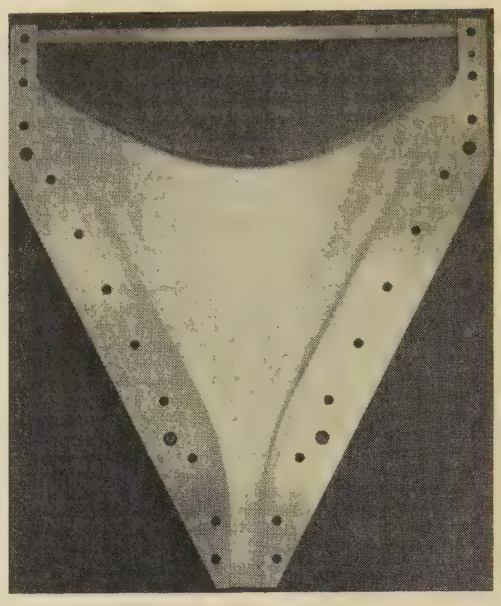

Fig. 2—Disassembled H plane test horn with the unmatched lens in place.

with the unmatched lens in place. The rounded corners of the H-plane horn provide a low-reflection transition between the horn and feeding waveguide. A flared E-plane horn added in tandem with the H-plane horn provides a good match between the exit aperture of the H-plane horn and free space.

Experimental Results

The radiation patterns of Fig. 3 taken at the design frequency of 9.40 rmc show the substantial reduction in side-lobe level obtained with the matched lenses. This improvement in side-lobe suppression is attributed to the fact that multiple reflections within the lens, and particularly between the curved surface of the lens and the walls of the H plane horn, are very small. Over

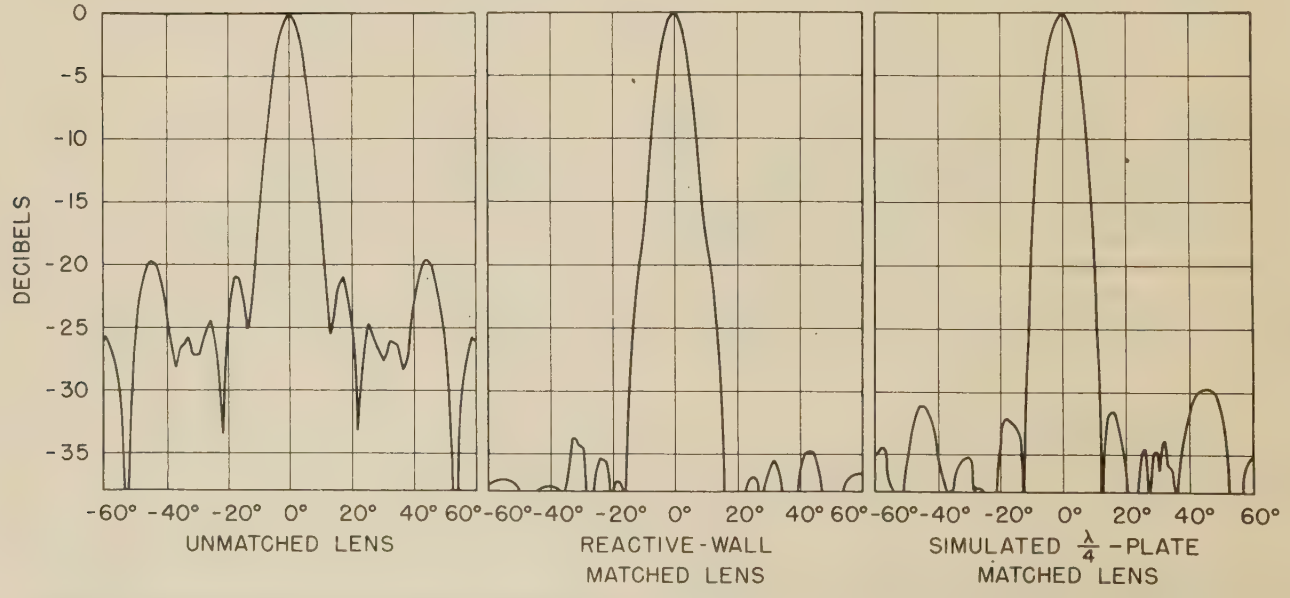

Fig. 3—Radiation patterns of an unmatched dielectric lens and two matched dielectric lenses. Patterns taken at 9.40 kmc, the design frequency of the matched lenses.

a 16 per cent frequency band, the side-lobe level of the lens matched with the capacitive wall never exceeds −27 db. On the other hand, the side-lobe level of the lens matched with the quarter-wave transformer is never greater than −25 db from at least 8.46 kmc to 12.22 kmc.

The vswr at the input to the *H* plane horn with no lens in place is less than 1.05 from at least 8.46 kmc to 12.22 kmc. However, with the unmatched lens in place, it varies from 1.34 to 1.89 over the same frequency range. The input vswr with the reactive-wall matched lens in place is 1.02 at the design frequency and less than 1.20 over a 16 per cent frequency band. The input vswr of the quarter-wave-transformer matched lens is 1.05 at the design frequency and less than 1.26 from at least 8.46 kmc to 12.22 kmc.

Power gain measurements on these lenses show that at the design frequency the power gain of the quarter-wave-transformer matched lens and capacitive-wall matched lens increases by about 0.1 and 0.35 db respectively over that of the unmatched lens. The improvement in gain of the capacitive-wall matched lens is nearly that expected theoretically.

Design Details

The outer dimensions of the polystyrene lenses (refractive index 1.59) used in these experiments are: width 12 inches, thickness 3.5 inches and height 0.400 inch. The focal length of the lenses is 9.0 inches and the outer contour of the curved surface is hyperbolic.

The spacing of the capacitive wall inside the lens surface and the disk diameters were determined from the data of Jones and Cohn.[1] Because the capacitive wall was composed of a square array of disks rather than the hexagonal one assumed,[1] the disk diameters were increased by the factor $(2/\sqrt{3})^{1/3}=1.047$ which may be shown theoretically to be the factor necessary to compensate for this change in geometry. The center-to-center spacing of the disks is 0.400 inch. On the flat side of the lens the disks have a diameter of 0.221 inch and are embedded 0.283 inch. On the curved side of the lens the disk diameters vary from 0.221 inch at the center to 0.277 inch at the edges, while their spacing from the lens surface at the center is 0.283 inch and 0.325 inch at the edges. The disks were formed by spraying Metaplast 18-S silver paint through an appropriate mask on a lens cut to the proper contour. A layer of polystyrene glued over the disks increased the lens size to its proper dimensions.

The dimensions of the simulated quarter-wave transforming sections were determined from the data of Morita and Cohn.[2] On the flat surface of the lens the depth of the corrugation is 0.196 inch while the tongue thickness is 0.231 inch. On the curved surface the depth of the corrugation varies from 0.196 inch at the center to 0.479 inch at the edges, while the thickness of the tongue varies from 0.231 inch at the center to 0.179 inch at the edges.

Conclusions

The results of the measurements on the matched dielectric lenses show that either reactive walls or simulated quarter-wave transformers can greatly improve the performance of microwave dielectric lenses.

Microwave Lens Matching by Simulated Quarter-Wave Transformers*

T. MORITA† and S. B. COHN†

Summary—**The reflections from the surface of a dielectric lens may be cancelled by a quarter-wavelength layer of refractive index intermediate between that of air and the lens medium. The possibility of simulating a quarter-wave matching section by perturbing the boundary of the lens is described in this paper. Some of the configurations considered are corrugated surfaces, arrays of dielectric cylinders, and arrays of holes in the dielectric surface. In each case, a match may be obtained at a given frequency and angle of incidence by the proper adjustment of the depth of the perturbation, and of one other parameter such as the width of a groove.**

* Manuscript received by the PGAP, July 18, 1955; revised manuscript received October 1, 1955.

† Stanford Research Inst., Stanford, Calif.

Introduction

REFLECTIONS from the surfaces of a dielectric lens usually cause a decrease in the gain of the antenna system due to increases in side-lobe level and input standing-wave ratio. By the use of a reactive wall inside the surface of the lens, Jones and Cohn have shown that it is possible to cancel these surface reflections.[1] This paper considers an alternative method for cancelling these surface reflections that

[1] E. M. T. Jones and S. B. Cohn, "Surface matching of dielectric lenses," *J. Appl. Phys.*, vol. 26, pp. 452–457; April, 1955.

utilizes a quarter-wavelength layer of refractive index lying between one and n, where n is the refractive index of the lens medium. For normal incidence, the required value is exactly $\sqrt{n}$, while for oblique incidence the dependence is more complex. Because of the unavailability of a satisfactory low-loss dielectric with correct refractive index, the quarter-wavelength matching layer has been simulated by perturbing the shape of the dielectric boundary.[2-4]

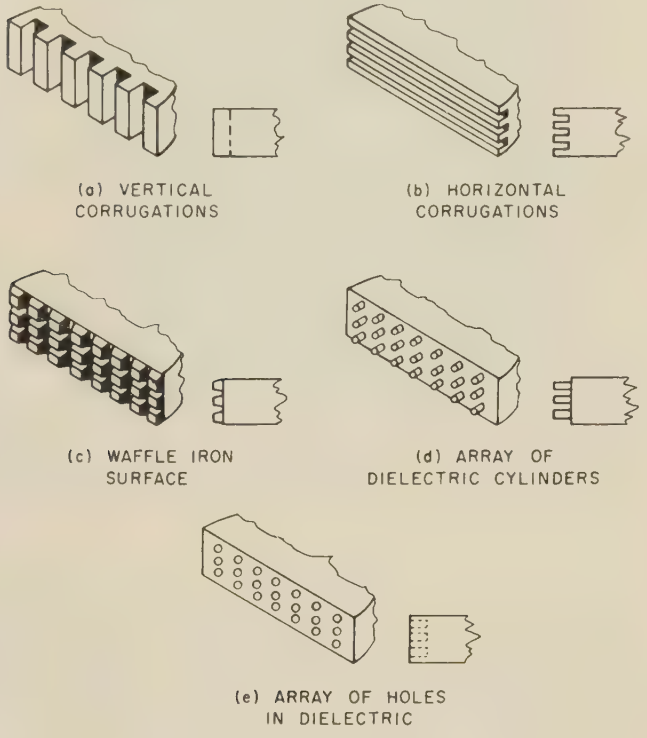

Fig. 1—Simulated quarter-wave matching transformer for lens surface.

Fig. 1 shows the configurations that are considered in this paper. Formulas for the dimensional parameters of these perturbed surfaces are given, and in each case a match may be obtained at the desired frequency and angle of incidence by the proper adjustment of the depth of the perturbation and of one other parameter, such as the width of a groove. An experimental investigation of these matching sheets was carried out in order to determine importance of approximations in the theoretical analysis. Measurements reported here were made in waveguide, while in a companion paper measurements on an actual microwave lens are reported.[5]

In the following analysis of the various matching sections, the mks system is used throughout. The characteristics of the matching sections are determined initially for a section of infinite depth, and it is assumed that the propagation constant and characteristic impedance thus obtained are valid for the quarter-wave sheet. All discontinuity effects at each boundary, other than the abrupt change in characteristic impedance, are neglected. The analysis is divided into the two cases of perpendicular and parallel polarization with respect to the plane of incidence.

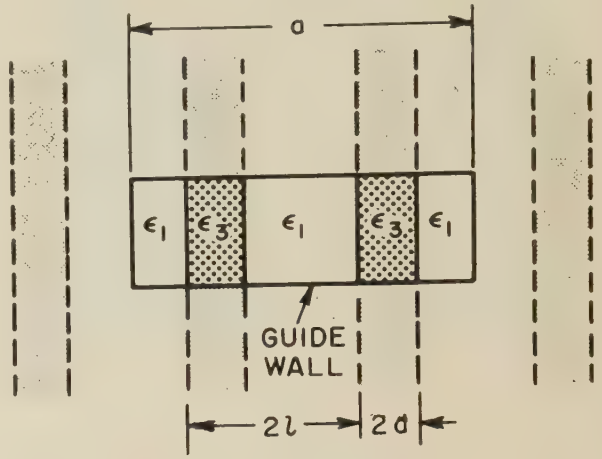

Fig. 2—Infinite medium formed by images in guide wall.

Analysis of Perturbed Surfaces—Perpendicular Polarization

Vertical Corrugations

1) General Case: Consider the vertically corrugated surface of Fig. 2 inside a waveguide. The images in the conducting wall form an infinite sheet of vertical corrugations of width $2d$ separated by a distance $a/2-2d$. The behavior of this structure inside the guide is equivalent to a TE wave incident on the infinite sheet at an angle $\theta_1=\sin^{-1}(\lambda_1/2a)$, where $\lambda_1=\lambda_0/(\epsilon_1)^{1/2}$, $\lambda_0=$free space wavelength, and $\epsilon_1=$relative dielectric constant of the first medium. In the dielectric region, the angle of transmission is given by $\theta_3=\sin^{-1}(\lambda_3/2a)$, where $\lambda_3=\lambda_0/(\epsilon_3)^{1/2}$ and ϵ_3 is the relative dielectric constant of the dielectric medium. In order to prevent the infinite sheet of corrugations from exciting waves in directions other than θ_3, it is necessary that the center-to-center spacing $2l$ be such that a higher-order grating effect is not possible. The spacing is hence restricted by the relation $2l\leqq\lambda_3/(1+|\sin\theta_3|)$. For polystyrene $\epsilon_3=2.55$, and thus at least $1\frac{1}{2}$ corrugations must be present in the guide section, if analogy to the infinite sheet is to apply.

The equation for the propagation constant in the corrugated region may be derived for the general case of n corrugations inside the guide by the application of transmission-line filter theory.[6] Consider the half-section formed by dielectric and air slabs shown in Fig. 3(b). Here $2d$ is the width of a single corrugation and

[2] D. W. Fry and G. K. Goward, "Aerials for Centimeter Wavelengths," Cambridge University Press, Cambridge, 1950; pp. 152–154.

[3] A. G. Fox, U. S. Patent 2,432,093 filed March 30, 1943.

[4] R. H. Garnham, "Some methods of preventing the reflection of electromagnetic waves at the boundary between dielectrics," T. R.E. Technical Note No. 131; August, 1951.

[5] E. M. T. Jones, T. Morita, and S. B. Cohn, "Experimental performance of matched dielectric lenses," Trans. IRE, vol. AP-3, this issue.

[6] Radio Research Laboratory Staff, "Very High Frequency Techniques," McGraw-Hill Book Co., Inc., New York, N. Y., vol. 2; 1947; see S. B. Cohn, "Principles of transmission line filter design," ch. 26.

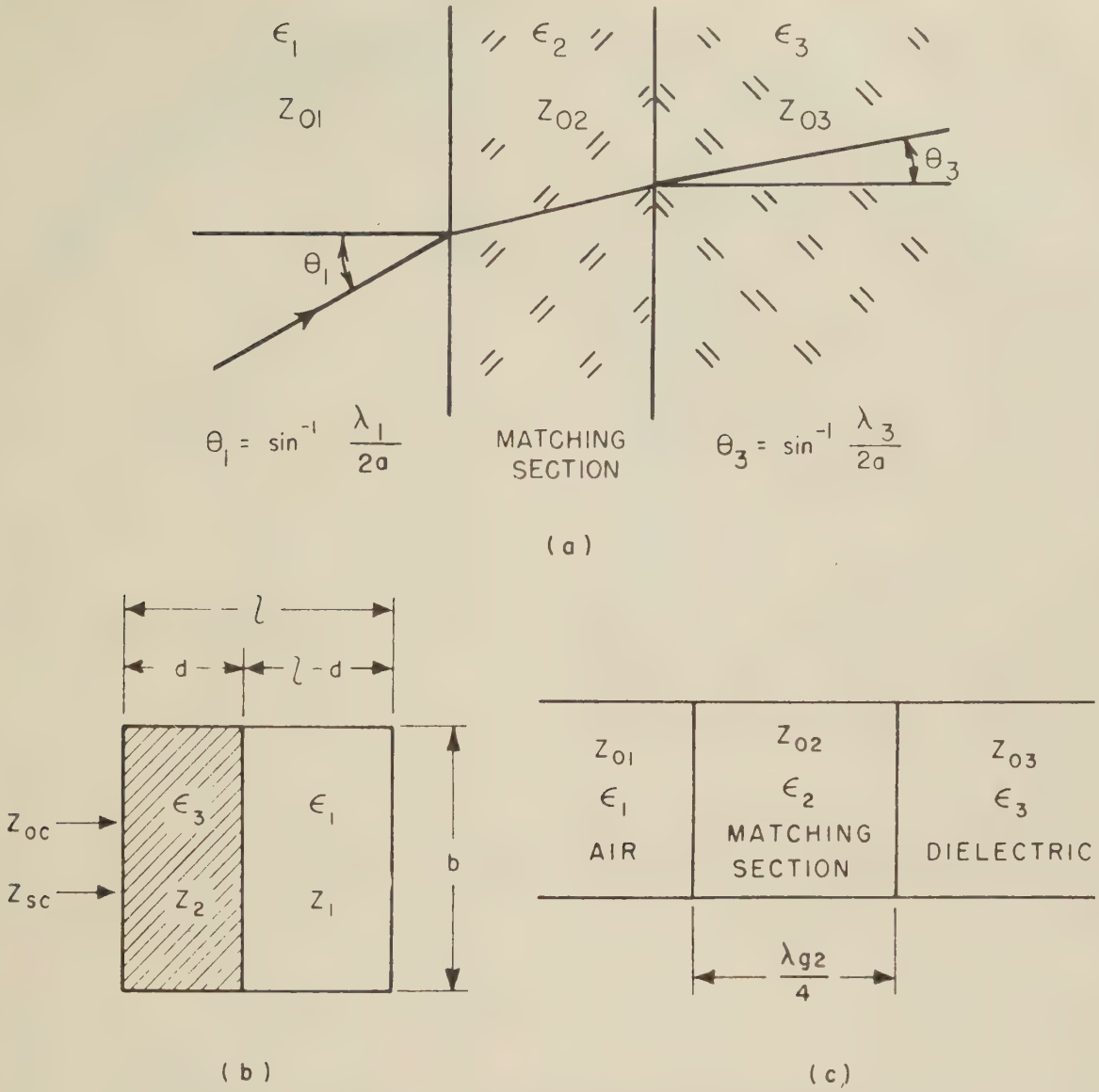

Fig. 3—(a) Angle of incidence and transmission, (b) Half-section for dielectric slab medium, and (c) Equivalent transmission-line representation.

$2(l-d)$ the width of the air space. Let n half-sections be contained in the guide cross section and assume the TE_{q0} mode to be incident on the corrugated boundary. Then the integers n and q may be chosen to give the angle of incidence $\theta_1=\sin^{-1}(q\lambda_1/2nl)$ arbitrarily close to any desired value. In terms of filter-theory terminology and assuming the direction of propagation in the dielectric-slab medium to be transverse to the axis of the waveguide, the image transfer constant Θ is equal to $\alpha+j\beta$, where α is the total attenuation in nepers per half-section and β is the total phase shift in radians per half-section. In the waveguide, a standing wave must exist in the transverse direction perpendicular to the dielectric interface[7,8], and the total phase shift in the transverse direction is $q\pi$ radians for the TE_{q0} mode.

[7] N. H. Frank, Rad. Lab. Rep. No. T-9; 1942.
[8] C. G. Montgomery, R. H. Dicke, and E. M. Purcell, "Principles of Microwave Circuits," Rad. Lab. Ser., McGraw-Hill Book Co., Inc., New York, N. Y., vol. 8, pp. 385–398; 1948.

Thus for the lossless-dielectric case $\Theta=j\beta=jq\pi/n$. The image transfer constant may be derived from the short-circuit and open-circuit impedances Z_{sc} and Z_{oc} as follows

$$\tanh\Theta=(Z_{sc}/Z_{oc})^{1/2} \tag{1}$$

with

$$Z_{sc}=jZ_2\tan\left[K_2d+\tan^{-1}\left\{\frac{Z_1}{Z_2}\tan K_1(l-d)\right\}\right].$$

$$Z_{oc}=jZ_2\tan\left[K_2d-\tan^{-1}\left\{\frac{Z_1}{Z_2}\cot K_1(l-d)\right\}\right].$$

Here Z_1 and Z_2 are the characteristic impedances of the air and dielectric slabs for transverse propagation, and K_1 and K_2 are the respective propagation constants. For any TE mode $Z_1/Z_2=K_2/K_1$. Thus the following transcendental equation is obtained

$$\left(j \tan \frac{q\pi}{n}\right)^2 = \frac{\tan\left[BR + \tan^{-1}\frac{B}{A}\tan(A - AR)\right]}{\tan\left[BR - \tan^{-1}\frac{B}{A}\cot(A - AR)\right]} \quad (2)$$

where $A = K_1 l$, $B = K_2 l$, and $R = d/l$. R is desired ratio of dielectric width to total width of half-section.

The requirement that the corrugated section behave as a quarter-wave matching transformer makes it possible to derive relationships for the transverse propagation constants K_1 and K_2 in terms of the angle of incidence and the relative dielectric constant ϵ_3 of the medium to be matched. To do this, consider the equivalent transmission-line representation of Fig. 3(c) for propagation along the guide axis. The characteristic impedances Z_{01} and Z_{03} are given by

$$Z_{01} = \eta/(\epsilon_1 - p^2)^{1/2} \qquad Z_{03} = \eta/(\epsilon_3 - p^2)^{1/2}$$

where $p = (\epsilon_1)^{1/2} \sin \theta_1$ and η = intrinsic impedance of free space. The matching section must have a characteristic impedance Z_{02} whose value is the geometric mean of the two guides. Since the guide wavelength is inversely proportional to the characteristic impedance, the desired guide-wavelength in the matching section is given by

$$\lambda_{g2} = \lambda_0/[(\epsilon_1 - p^2)(\epsilon_3 - p^2)]^{1/4}. \quad (3)$$

The transverse propagation constants K_1 and K_2 in the matching section may be shown quite readily to be

$$K_1 = \frac{2\pi}{\lambda_0}\left[\epsilon_1 - \left\{(\epsilon_1 - p^2)(\epsilon_3 - p^2)\right\}^{1/2}\right]^{1/2} \quad (4)$$

and

$$K_2 = \frac{2\pi}{\lambda_0}\left[\epsilon_3 - \left\{(\epsilon_1 - p^2)(\epsilon_3 - p^2)\right\}^{1/2}\right]^{1/2}. \quad (5)$$

Applying (4) and (5), one may solve (2) for R, the desired ratio of dielectric to total width for the half-section. This has been done for $\epsilon_1 = 1$ and $\epsilon_3 = 2.55$ (polystyrene) for various angles of incidence with l/λ as a parameter and is plotted in Fig. 4. The depth of corrugation required for each angle of incidence is $\lambda_{g2}/4$, which may be computed from (3). This quantity is plotted in Fig. 5. These design curves are directly applicable for matching the surface of a polystyrene lens for a wave of perpendicular polarization and any angle of incidence. The only approximation in the analysis and in Figs. 4 and 5 is the neglect of discontinuity effects at the interfaces other than the changes in characteristic impedance. Measurements have shown this approximation not to be serious.

2) Static Limit: Of importance is the special case where $l/\lambda \to 0$, since this will serve as a guide in interpreting the result of the static analysis to be discussed in a later section for a more complicated structure. As $l/\lambda \to 0$ the approximations $\tan x \to x$, $\cot x \to 1/x$, and $\tan^{-1}(1/x) \to \pi/2 - x$ can be made in (2). Upon applying (4) and (5), the desired expression for R as $l/\lambda \to 0$ is given by

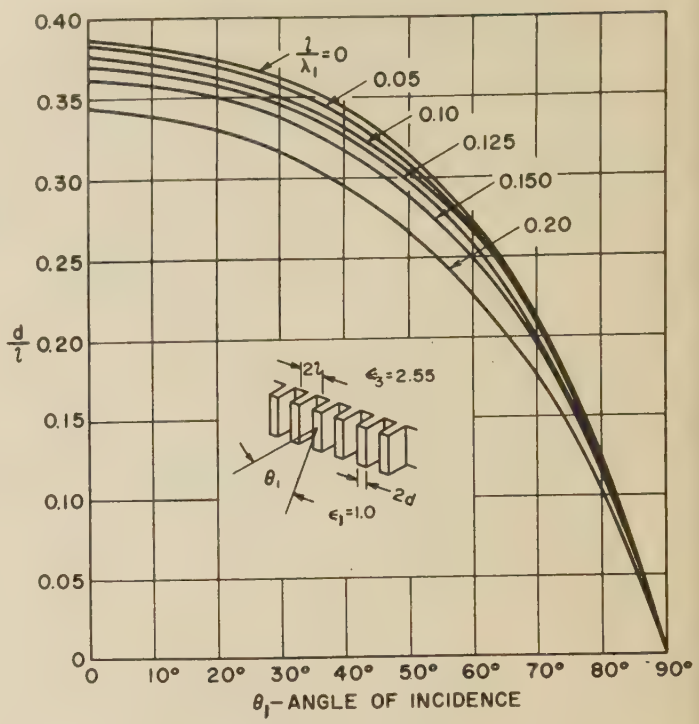

Fig. 4—Matching with vertical corrugations—perpendicular polarization.

$$R = \frac{p^2 - \epsilon_1 + [(\epsilon_1 - p^2)(\epsilon_3 - p^2)]^{1/2}}{[\epsilon_3 - \epsilon_1]}. \quad (6)$$

This result may also be obtained by considering the static capacitance formed by the half-section and solving for the effective dielectric constant. Referring to Fig. 4, the amount of dielectric required for the static case ($l/\lambda_1 \to 0$) is seen to be always greater than for the case of finite wavelength.

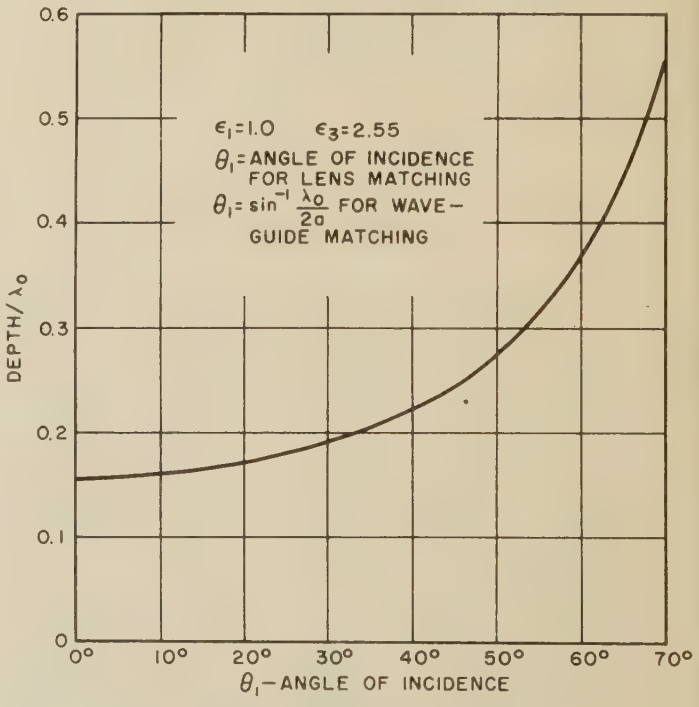

Fig. 5—Depth of corrugations for quarter-wave matching section.

3) Application to Waveguide Matching TE_{10} Mode: The general equation for vertical corrugations (2) is directly applicable to the case of waveguide matching in the transition from a guide filled with dielectric constant ϵ_1 to a guide with dielectric ϵ_3. Fig. 6 is a plot of d/l vs $\theta_1 = \sin^{-1}(\lambda_0/2a)$ with n the number of half-sections as a parameter. The depth of corrugation is given as before by Fig. 5. For a given configuration, as the frequency is increased K_1 becomes imaginary, and hence the energy begins to concentrate in the dielectric part until at a sufficiently high frequency the energy concentration is almost completely in the dielectric.[8] Since the higher-order modes will have begun to propagate before then, this is of no consequence. The case of one dielectric slab centered in the cross section ($n=2$, $q=1$)[9] is identical to the case which has been analyzed by others.[7,8,10–13]

As an indication of the number of corrugations required in the guide cross section before the static analysis is valid, Fig. 7 is a plot of d/l vs n for $p^2=0.5$. For $n=20$ (10 corrugations), d/l is within 0.6 per cent of the static value.

Horizontal Corrugations

The analysis of horizontal corrugations [Fig. 1(b)] may be made by the application of transmission-line filter theory assuming vertical propagation in the waveguide. The equivalent filter half-section is represented by Fig. 3(b), if the figure is considered to be rotated by 90 degrees. The mode is of the TM type for the assumed direction of propagation. Thus $Z_1/Z_2 = \epsilon_3 K_1/\epsilon_1 K_2$. Furthermore, the total image phase shift β of the structure is equal to zero. Hence the following transcendental equation for $R=d/l$ is obtained for perpendicular polarization.

$$\frac{B}{\epsilon_3}\tan BR = -\frac{A}{\epsilon_1}\tan(A - AR) \qquad (7)$$

where $A=K_1 l$ and $B=K_2 l$.

For this case a difficulty in applying the quarter-wave matching concept occurs, since a constant characteristic impedance does not exist in the waveguide

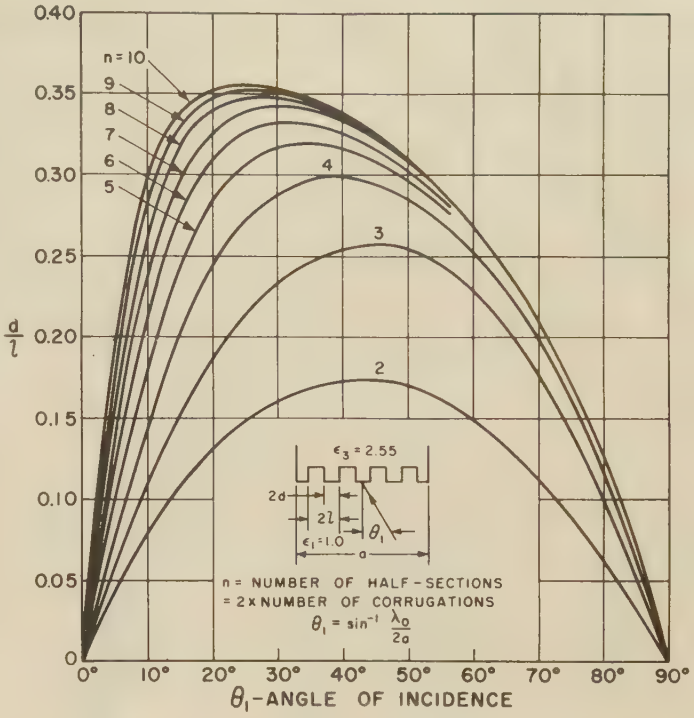

Fig. 6—Vertical corrugations—waveguide matching, TE_{10} mode.

cross section. By making the approximation that the dielectric-slab-medium characteristic impedance is the same as that for the TE mode in a uniform dielectric that would yield the same phase velocity, the following equations for the transverse propagation constants are obtained:

$$K_1 = \frac{2\pi}{\lambda_0}\left[\epsilon_1 - p^2 - \left\{(\epsilon_1 - p^2)(\epsilon_3 - p^2)\right\}^{1/2}\right]^{1/2} \qquad (8)$$

$$K_2 = \frac{2\pi}{\lambda_0}\left[\epsilon_3 - p^2 - \left\{(\epsilon_1 - p^2)(\epsilon_3 - p^2)\right\}^{1/2}\right]^{1/2}. \qquad (9)$$

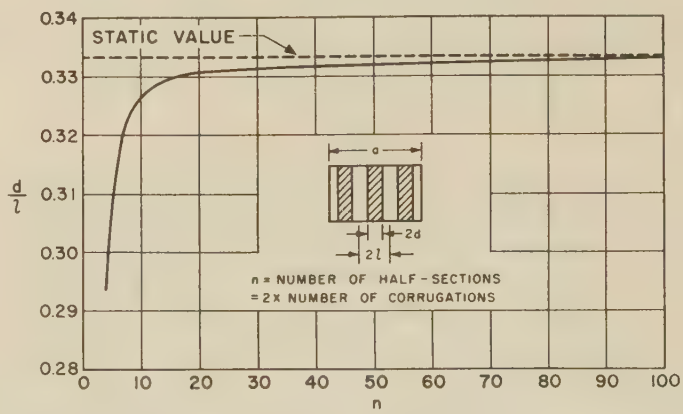

Fig. 7—Dependence on number of half-sections for waveguide matching, $\lambda_0/2a=0.707$.

The transcendental equation, (7), has been solved for R with $\epsilon_1=1$ and $\epsilon_3=2.55$, and the results are plotted in Fig. 8 as a function of the angle of incidence with l/λ as parameter. The plot of Fig. 5 gives the corrugation depth for horizontal as well as vertical corrugations.

[9] The case of $n=2$ and $q=1$ is a special one, since it requires the basic half-section to be at its cutoff, where its image impedances are zero and infinity. Although (2) applies correctly to one dielectric slab centered in a waveguide cross section, it does not apply to the case of two half-slabs on each side of the cross section. For the latter case, a correct formula may be obtained by computing Z_{sc} and Z_{oc} from the right in Fig. 3(b), instead of from the left. However, for all other values of n (with $q=1$), (2) gives the correct result for either possible arrangement of half-sections in a rectangular waveguide propagating the fundamental mode.

[10] L. Pincherle, "Electromagnetic waves in a metal tube filled longitudinally with two dielectrics," *Phys. Rev.*, vol. 66, pp. 118–130; September 1–15, 1944.

[11] N. Marcuvitz, "Waveguide Handbook," Rad. Lab. Ser., McGraw-Hill Book Co., Inc., New York, N. Y., vol. 10, pp. 391–393; 1951.

[12] J. Van Bladel and T. J. Higgins, "Cut-off frequency in two dielectric layered rectangular waveguides," *J. Appl. Phys.*, vol. 22, pp. 329–333; March, 1951.

[13] R. B. Adler, "Properties of guided waves on inhomogeneous cylindrical structures," M.I.T. Res. Lab. Electr., Tech. Rep. No. 102; May 27, 1949.

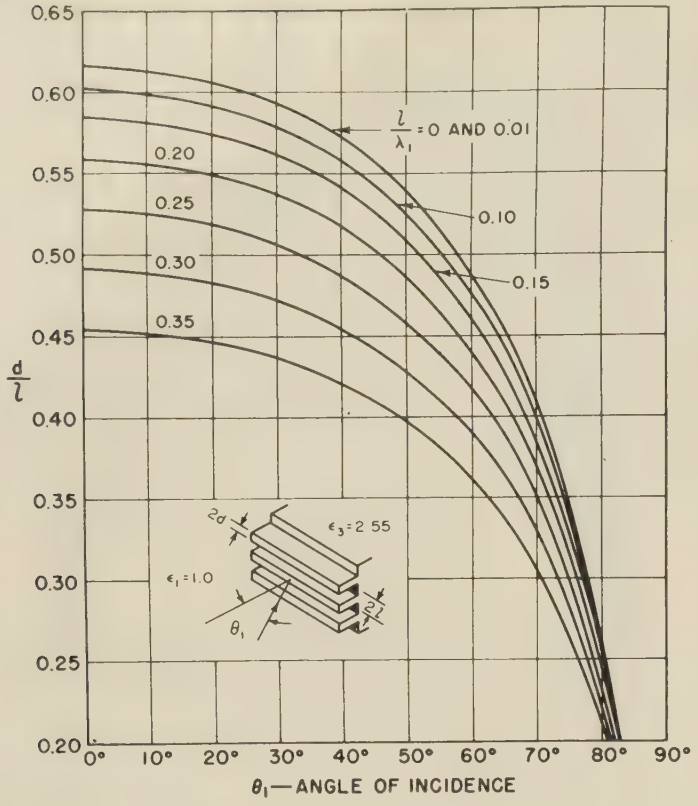

Fig. 8—Matching with horizontal corrugations—perpendicular polarization.

Array of Dielectric Cylinders

A rigorous solution for the array of dielectric cylinders of Fig. 1(d) is beyond the present scope of analysis. However, an approximate method, which has been used previously for artificial dielectric media, is applicable.[14,15] By obtaining the electric dipole moment of a dielectric cylinder in a static electric field normal to the axis of the cylinder, the polarization P and hence the effective dielectric constant of an array of dielectric cylinders may be obtained. The ratio of dielectric area to total area for the matching layer is then given by

$$R_{cyl} = \frac{(\epsilon_3 + \epsilon_1)\left[p^2 - \epsilon_1 + \left\{(\epsilon_1 - p^2)(\epsilon_3 - p^2)\right\}^{1/2}\right]}{2\epsilon_1(\epsilon_3 - \epsilon_1)} \quad (10)$$

where perpendicular polarization is assumed, and $\theta_1 = \sin^{-1}(p/\epsilon_1^{1/2})$ is the angle of incidence. Fig. 9 is the plot of R_{cyl} as a function of the angle of incidence for $\epsilon_1 = 1$ and $\epsilon_3 = 2.55$. The curve of Fig. 5 for the depth of corrugation is also applicable for this case.

To match an air, polystyrene surface, (10) predicts area occupied by dielectric should be 68 per cent at normal incidence. Since this violates assumption of small diameter compared to spacing, and since rather narrow clearance would be required, case of array of cylindrical holes in a dielectric medium is next considered.

[14] W. E. Kock, "Metallic delay lenses," *Bell Syst. Tech. Jour.*, vol. 27, pp. 58–82; January, 1948.

[15] S. B. Cohn, "The electric and magentic constants of metallic delay media," *Jour. Appl. Phys.*, vol. 22, pp. 628–634; May, 1951.

Array of Holes in a Dielectric Medium

The geometric configuration of the holes in the dielectric medium of Fig. 1(e) is identical to that of the array of dielectric cylinders. Hence the solution obtained for the latter is applicable to the former if the relative dielectric constant ϵ_3 of the cylinder is replaced by ϵ_1, while the medium ϵ_1 is replaced by ϵ_3. Thus the ratio of the area occupied by the air cylinder to total area is, for perpendicular polarization,

$$R_{hole} = \frac{(\epsilon_3 + \epsilon_1)\left[\epsilon_3 - p^2 - \left\{(\epsilon_1 - p^2)(\epsilon_3 - p^2)\right\}^{1/2}\right]}{2\epsilon_3(\epsilon_3 - \epsilon_1)} \quad (11)$$

where $\theta_1 = \sin^{-1}(p/\epsilon_1^{1/2})$ is the angle of incidence, as above. This is shown plotted in Fig. 9 as a function of angle of incidence. Fig. 5 gives hole depth for matching.

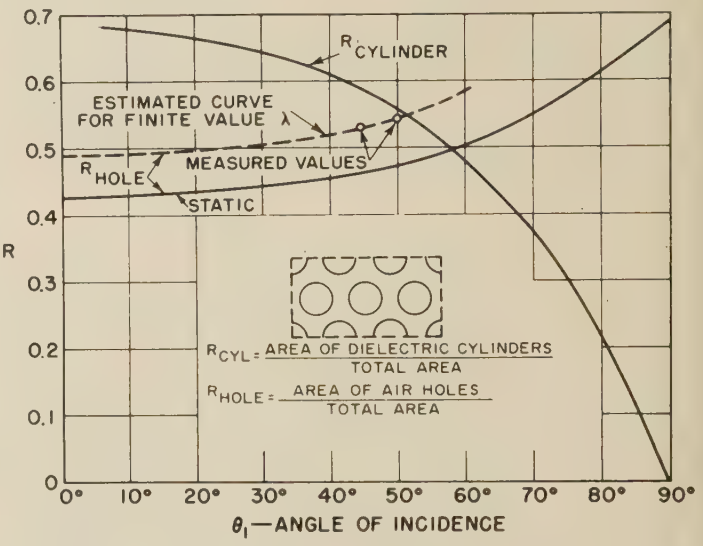

Fig. 9—Matching with array of dielectric cylinders and array of holes—air to polystyrene matching.

Measured Results—Perpendicular Polarization

Fig. 10 is a photograph of typical matching sections that have been tested inside a waveguide. The polystyrene insert was slotted so that a probe could be inserted to measure the standing-wave ratio in the dielectric-filled guide, with the air guide terminated in its characteristic impedance. From the design curves presented previously, the air, dielectric transition can be matched at a given angle of incidence in the waveguide and related to the case of an electromagnetic wave incident at the same angle on an infinite matching sheet in free space. Fig. 11 shows typical measured results for the case of two vertical corrugations inside the waveguide with angles of incidence equal to 41.1, 44.4, and 52.1°. In each case a match is obtained at the design frequency with vswr less than 1.02. Vswr's less than 1.02 have also been obtained for the case of horizontal corrugations, indicating that the assumption concerning the characteristic impedance in the matching section is valid.

For the case of the hole-type structure, only the static analysis of the last section is available. Since the solu-

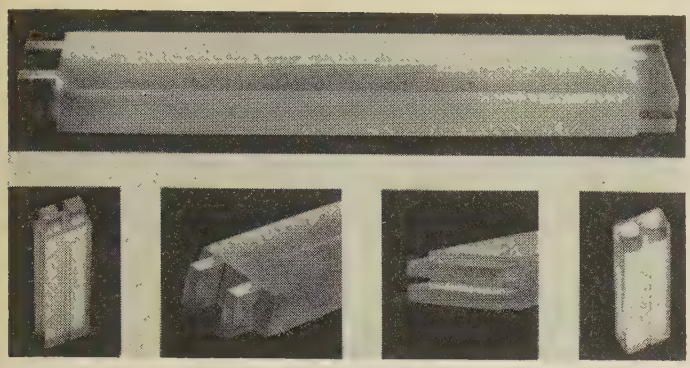

Fig. 10—Photograph of perturbed surfaces.

tions for horizontal and vertical corrugations for $l/\lambda \to 0$ give values of dielectric area roughly 10 per cent greater than that for typical finite wavelengths, one may expect the static analysis of (11) to give values of R_{hole} smaller than that required for perfect match. In fact, experimental results show that by increasing the value of R obtained from (11) by 15 per cent, a vswr less than 1.10 is obtained. The curve for this is shown dotted in Fig. 9.

No theoretical analysis is available for the waffle-iron surface of Fig. 1(c), but the design of this structure may be based on the relative area of dielectric in the other matched structures treated previously. The experimental result for a waffle-iron structure simulated by two square projections from a dielectric insert filling a waveguide indicates that by taking a dielectric area approximately 12 per cent less than that predicted for horizontal corrugations, a reasonable match is obtained.

Analysis of Perturbed Surfaces—Parallel Polarization

The analyses presented above have been for the case of a perpendicularly polarized incident wave. The case of parallel polarization may be analyzed in a similar manner by considering TM wave propagation in a parallel-plane transmission line of height b.[16] The design formulas are tabulated below for the two cases.

Vertical Corrugations

Angle of Incidence:

$$\theta_1 = \sin^{-1}(q\lambda_1/2b)$$

where q = number of half-period variations of the TM mode between the plates of spacing b.

Guide Wavelength:

$$\lambda_{g2} = \lambda_0 \frac{2\left[(\epsilon_1 - p^2)(\epsilon_3 - p^2)\right]^{1/4}}{(\epsilon_1\epsilon_3)^{1/2} + \left[\epsilon_1\epsilon_3 - 4p^2\left\{(\epsilon_1 - p^2)(\epsilon_3 - p^2)\right\}^{1/2}\right]^{1/2}} \quad (12)$$

Transcendental Equation:

$$\tan BR + \frac{B}{A}(A - AR) = 0 \quad (13)$$

[16] R. W. Klopfenstein, "Low frequency waves on transmission lines of composite section," Trans. IRE, vol. AP-2, pp. 103–109; July, 1954.

with $A = K_1 l$, $B = K_2 l$, $R = d/l$; where l = width of half-section, d = width of dielectric in half-section.

$$K_1^2 = \left(j\frac{2\pi}{\lambda_{g2}}\right)^2 + \left(\frac{2\pi\epsilon_1^{1/2}}{\lambda_0}\right)^2 - \left(\frac{q\pi}{b}\right)^2 \quad (14)$$

$$K_2^2 = \left(j\frac{2\pi}{\lambda_{g2}}\right)^2 + \left(\frac{2\pi\epsilon_3^{1/2}}{\lambda_0}\right)^2 - \left(\frac{q\pi}{b}\right)^2 \quad (15)$$

Horizontal Corrugations

Angle of Incidence:

$$\theta_1 = \sin^{-1} q\lambda_1/2nl$$

where q is the order of the TM mode, and n is an integer chosen with q to obtain θ_1 arbitrarily close to any desired angle of incidence.

CASE	f_0	θ_1	λ_0	$\frac{d}{l}$	$\frac{l}{\lambda_0}$	DEPTH/λ_0
A	4.8 kMc	41.1°	6.25 cm	0.298	0.1905	0.239
B	4.5 kMc	44.4°	6.67 cm	0.295	0.1782	0.247
C	4.0 kMc	52.1°	7.5 cm	0.280	0.158	0.271

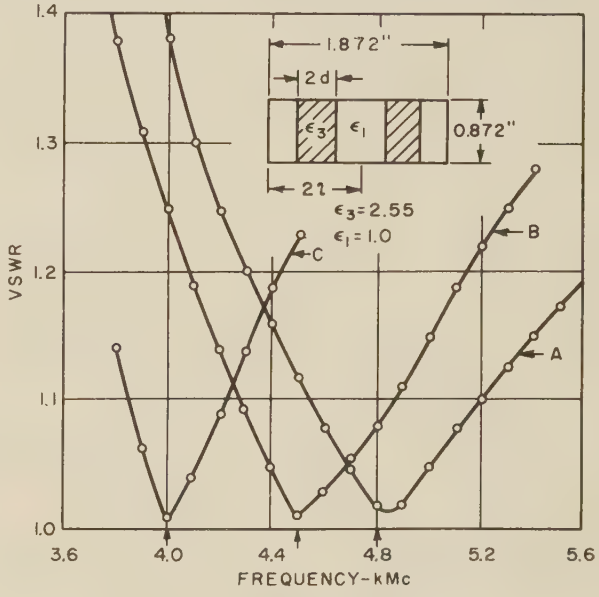

Fig. 11—Measured data for two vertical corrugations.

Transcendental equation:

$$\left(j\tan\frac{q\pi}{n}\right)^2 = \frac{\tan\left\{BR + \tan^{-1}\frac{\epsilon_3 A}{\epsilon_1 B}\tan(A - AR)\right\}}{\tan\left\{BR - \tan^{-1}\frac{\epsilon_3 A}{\epsilon_1 B}\cot(A - AR)\right\}}$$

with $A = K_1 l$, $B = K_2 l$, $R = d/l$, l = height of half-section and d = height of dielectric in half-section. The depth of corrugation is obtained from guide wavelength of (12), while transverse propagation coefficients K_1 and K_2 are the same as (14) and (15) with $(q\pi/b)^2$ omitted.

Acknowledgment

The work reported in this paper was supported by the Signal Corps under Contract No. DA 36-039 SC-52595.

A Mechanically Simple Foster Scanner*

R. C. HONEY† AND E. M. T. JONES†

Summary—**This paper describes the design, construction, and testing of a Foster scanner that is much simpler to build than the conventional Foster scanner. The simplifications result from the use of a choke groove and a solid barrier to replace the conventional inter-leaving finger barriers. The choke groove and solid barrier are very simple to construct, give excellent electrical performance, and permit very high scan rates. A scanner has been built and tested at 35 kmc, where the tolerance problems are very severe, and found to perform extremely well over at least a 10 per cent frequency bandwidth.**

Introduction

THE FOSTER SCANNER is a mechanical scanning antenna permitting relatively high scanning rates. In its various forms it utilizes a rapidly rotating cone located inside a conical stator to vary periodically the angle of the radiated beam with respect to the fixed exit aperture. In the construction of the conventional Foster scanner, interleaving fingers are used to direct the energy around the parallel-plate transmission line formed by the space between the rotor and the stator. For good electrical performance it is necessary that the clearance between the interleaving fingers be very small.

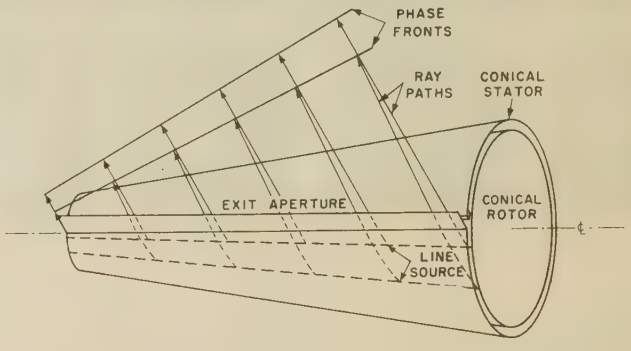

Fig. 1—Sketch showing how rotation of the rotor causes scanning of the beam emerging from the exit aperture on the stator.

Description of Scanner

The manner in which rotation of the conical rotor causes the radiated beam to scan is illustrated in Fig. 1. Here the paths of typical rays traveling between the line source in the rotor and the exit aperture on the stator are shown as dashed lines for two different rotor positions. The paths of the rays outside the exit aperture are shown as solid lines.

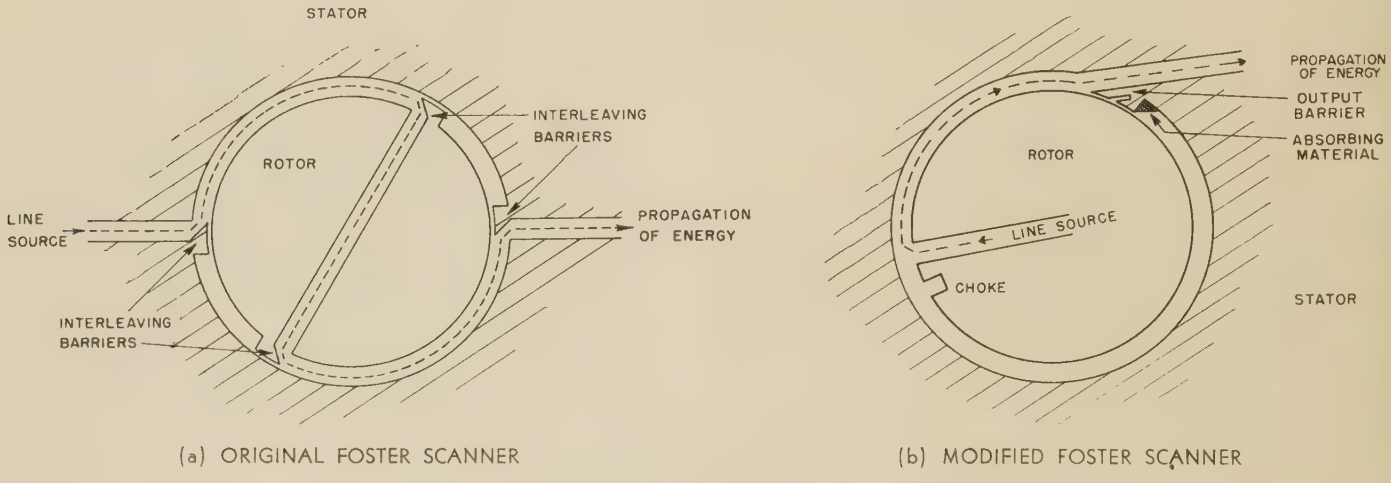

Fig. 2—Cross sections through the cones of two forms of the Foster scanner.

The form of the scanner described here does not have this mechanical limitation because it uses a choke groove and a solid barrier instead of interleaving fingers to direct the energy around the rotor. This form of the scanner is easy to construct, gives excellent electrical performance, and permits high scanning speeds.

The usual form of the antenna, as originated by J. F. Foster,[1] is shown in cross section in Fig. 2(a). Four sets of serrated, interleaving barriers, are used to direct energy along proper paths. Mechanical problems involved in construction of such a scanner are quite severe.

The configuration of Fig. 2(b) avoids the necessity for machining the multitudes of fine teeth in four sets of

* Manuscript received by the PGAP, April 8, 1955; revised manuscript received August 29, 1955. The work described in this paper was performed at Stanford Res. Inst. on Signal Corps Contracts Nos. DA 36-039-sc-5503 and DA 36-039-sc-52595.

† Stanford Research Inst., Menlo Park, Calif.

[1] D. W. Fry and F. K. Goward, "Aerials for Centimetre Wavelengths," Cambridge University Press, Cambridge, England, p. 131; 1950.

barriers. Two sets of barriers are eliminated by enclosing the line source within the rotor, and feeding it through a standard rotary joint. One of the remaining barriers is replaced by a choke, and the last barrier is made solid rather than serrated. Because the performance of a choke is sensitive to the angle of incidence of the radiation, a choke barrier will operate most satisfactorily at a location where this angle of incidence is constant. It is important to note that the geometry of the conical transmission region is such that the location adjacent to the line source is the only one that satisfies this condition. The use of chokes to replace the serrated barrier was mentioned by Fry and Goward;[1] however, it is believed that the scanner described here is the first to successfully embody these ideas. Additional advantages accrue from the adoption of the form of Fig. 2(b):

1) Increased scanning rates may be obtained because the rotor need not be weakened by being split entirely in two. Furthermore, by using a linear, slotted waveguide array instead of a pillbox as used in this scanner, the cone need not be split at all. These factors are partially offset by the fact that the form of scanner shown in Fig. 2(a) provides two scans per revolution, while that of Fig. 2(b) provides only one.
2) As will be explained later, both the solid barrier and the choke junctions may be simply and accurately designed using data on barrier and choke reflections measured in standard waveguide with conventional techniques.

Physical Design

It may be shown that the effective path lengths involved in the propagation of energy between curved surfaces such as those used in the Foster scanner can be very accurately determined (if the spacing is less than one-third wavelength and radius of curvature greater than one wavelength) by measuring distances on a single curved sheet lying midway between the two surfaces. If this sheet is then developed onto a flat plane, the ray paths or phase fronts become straight lines. In Fig. 3 the line-source aperture becomes a radius on the developed surface, and during a scan cycle sweeps through a total angle ϕ, the angle of the developed cone. On the developed surface, energy radiates in straight lines from the source and at a constant angle from it at all times in the scan cycle. Assuming zero switching time in the scan cycle, the maximum scan angle is equal to ϕ, which is geometrically related to the angle θ of the undeveloped cone by

$$\sin\frac{\theta}{2} = \frac{\phi}{2\pi}.$$

Fig. 4 illustrates one of the limitations on the maximum scan angle of the Foster scanner when the beamwidth must remain constant over the scanning cycle. When

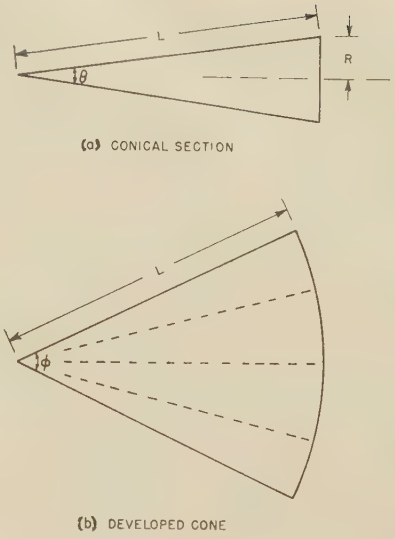

Fig. 3—Notation for developing conical surface.

the radiation from the line source is normal to the source [Fig. 4(a)], the length L' of the cone required to prevent any obstruction of the effective aperture, L, is given by

$$L' = L + (L + r)(\sec\phi - 1),$$

where the radius r is related to the diameter D of the small end of the rotor by $\phi r = \pi D$. If, however, the energy radiates at an angle of $\phi/2$ from the normal to the line source [Fig. 4(b)], (this condition is henceforth referred to as "canted" radiation), the length L'' of the required cone is given by:

$$L'' = L + (L + r)\left(\sec\frac{\phi}{2} - 1\right).$$

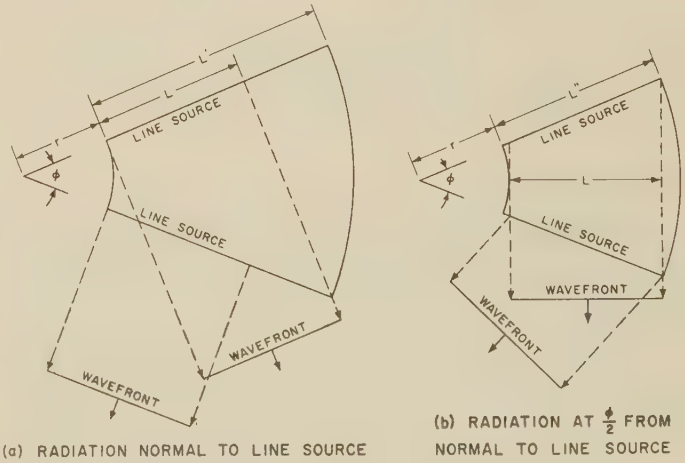

Fig. 4—Ray paths on developed surface at the two ends of the scanning cycle.

For the scanner actually built ($\phi = 50.1$ degrees) the increase in cone length required for normal radiation would have amounted to 73 per cent of the effective aperture length; whereas by using canted radiation the increase in required cone length over the effective aperture length is only 14 per cent.

Canting the radiation in this way reduces the range of incident angles over which the solid barrier junction must operate to only half that required for normal radiation. As explained later, this means that the equivalent fractional frequency bandwidth over which such a junction must operate for a constant angle of incidence is reduced from $(1-\cos\phi)$ for normal radiation to $[1-\cos(\phi/2)]$ for canted radiation.

Furthermore, the width of the output horn, if it is to face a direction midway between the two extreme scan angles, can be much smaller for canted radiation than for normal radiation. Referring to Fig. 4, the minimum horn width required is $L'/\cos(\phi/2)$ for normal radiation, and only L'' for canted radiation.

For reasons discussed in the following section, a parabolic pillbox has been selected as the line source within the rotor, and several additional advantages of canted radiation result from this choice:

1) The size of the conical rotor necessary to contain the parabola is much smaller.
2) The interaction between the feedhorn and the parabolic reflecting surface is appreciably less.
3) The increase in side lobes due to scattering from the feedhorn is less than that for normal radiation since the feedhorn is shifted from the point of maximum illumination.

Electrical Design

Line Source

From a mechanical standpoint, a non-resonant slotted-waveguide array would be the best type of line source to incorporate within the rotor. However, the design and construction of such an array for 35 kmc would be a rather extensive project and it was felt that this was unnecessary merely to test the basic design of this new scanner. Therefore, a single-layer parabolic pillbox was chosen as the line source.

Waveguide Chokes

As shown in Fig. 2(b), it is necessary that all the energy leaving the line source pass without reflection into the parallel-plate region formed between the rotor and stator, and that no energy leak past the choke groove in the rotor. The design of the choke groove in the scanner is rigorously equivalent to the design of a series choke in waveguide, while the design of the reflectionless transition between the line source and the parallel-plate region is rigorously equivalent to the design of a unity-coupling-factor series T-junction in waveguide. To convert the waveguide dimensions to the parallel-plate dimensions, it is only necessary to multiply the waveguide dimensions by $\lambda \sec(\phi/2)/\lambda_g$; where λ_g is the guide wavelength, λ is the free space wavelength in the parallel-plate region and $\phi/2$ is the angle at which energy is incident on the junction measured with respect to the junction normal (see Fig. 4).

The analysis of series junctions by Allanson, Cooper and Cowling[2] was used to design the chokes since it predicted the measured rejection frequencies within a small fraction of 1 per cent in most cases. A slight deviation from the theoretical curve was noted for the small choke depths used at the higher frequencies. This is due to the failure of the theory to account for the proximity of the shorting end-plate of the choke section to the local fields at the junction, since measurements on three-quarter-wavelength-deep chokes at these frequencies agree almost exactly with the theoretical predictions. The measured values of maximum attenuation past the one-quarter and three-quarter-wavelength chokes were not appreciably different.

Unity-Coupling-Factor Series T-Junctions

A unity-coupling-factor series T-junction is a lossless three terminal waveguide T-junction that has the property of transmitting all the signal incident on the series arm to one of the through arms if a perfect short circuit is suitably placed in the other through arm.

The analysis of the series T-junctions[2] is not applicable to the design of unity-coupling-factor T-junctions because the results are only tabulated for the case where the height c of the series arm is equal to the height b of the through arms. However, it has been found that the data for the case where $c>b$ (quoted by L. G. H. Huxley[3] who reproduces a curve due to MacFarlane), based on the theory of Frank and Chu,[4] gave the best results in designing these junctions. The dimensions of the junctions designed by this theory agree with those determined experimentally within 0.4 per cent.

Unity-Coupling-Factor Junctions Combined With Waveguide Chokes

It has been found in the two previous sections that at one frequency a well-constructed waveguide choke will behave as an almost perfect short circuit, and at one frequency a T-junction for $c>b$ will have perfect transmission between arms 1 and 2 (see Fig. 5) with a short circuit appropriately placed in arm 3. It should be possible, then, to combine the choke and the T-junction so that at one frequency essentially perfect transmission will occur between arms 1 and 2, and practically no power will be transmitted through into arm 3. Such a junction was built with $3\lambda_g/4$ spacing between the reference planes in the two junctions and its behavior was exactly as predicted. Measurements of the junction parameters as functions of frequency are shown in Fig. 5.

[2] J. T. Allanson, R. Cooper, and T. G. Cowling, "The theory and experimental behavior of right-angled junctions in rectangular-section wave guides," *J. Inst. Elect. Engrs.*, vol. 93, pp. 177–187; May, 1946.

[3] L. G. H. Huxley, "A Survey of the Principles and Practice of Wave Guides," The MacMillan Co., New York, N. Y., p. 170; 1947.

[4] N. J. Frank and L. J. Chu, "T-junctions in rectangular waveguide," M.I.T. Rad. Lab. Reps. 179 and 180; July, 1942.

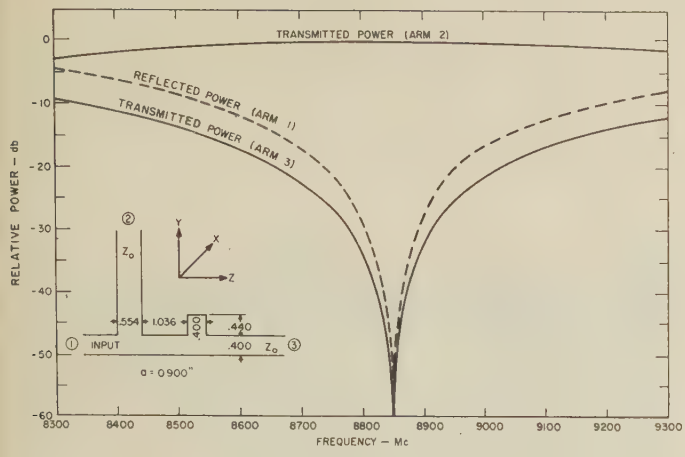

Fig. 5—Experimental performance of junction with three-quarter guide-wavelength spacing.

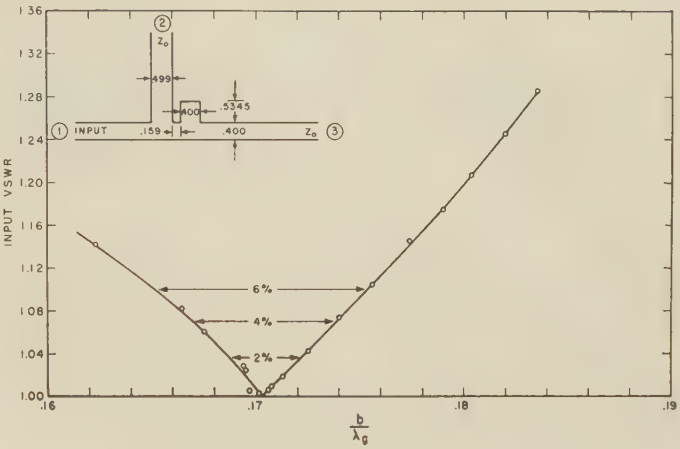

Fig. 7—Input voltage standing wave ratio vs b/λ_g for completed junction.

Greater bandwidth may be achieved by using $\lambda_g/4$ spacing between the reference planes of the choke and the T-junction. However, with this closer spacing the higher order fields of the two junctions intermingle and modify the performance of the structure requiring empirical adjustment of the width c of the T-junction to obtain a unity coupling factor.

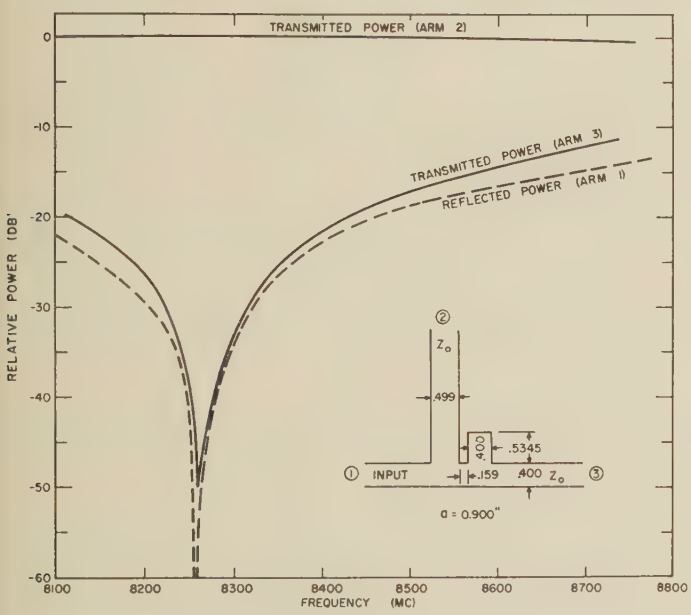

Fig. 6—Experimental performance of junction with one-quarter guide-wavelength spacing.

In Fig. 6 the measured values of transmitted and reflected power out of the various arms of such a quarter-wave spaced choke and T-junction are plotted as functions of frequency. The input vswr is plotted vs b/λ_g in Fig. 7, since the spread on the b/λ_g scale is directly proportional to the frequency bandwidth for the same junction scaled for use between parallel planes. It can be seen that the junction has a 6 per cent bandwidth for an input vswr less than 1.10. Incidentally, any power transmitted into arm 3 can be dissipated in absorbing material placed around the circumference of the stator at each end of the cone and along the back side of the solid barrier junction, and will not contribute to the side lobes or otherwise interfere with the radiation pattern. The actual power lost by this means, even at the extremes of the 6 per cent bandwidth, is less than 0.4 per cent or 0.02 db.

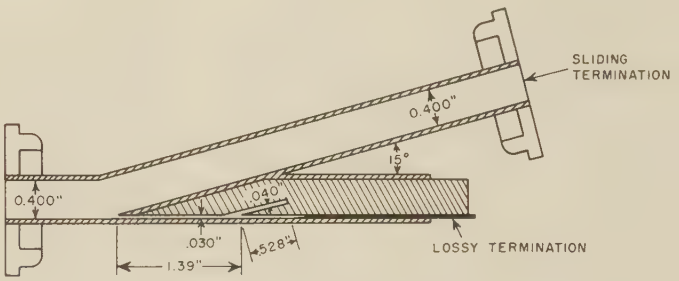

Fig. 8—Cross section of solid barrier junction scaled to x-band waveguide.

Barrier Junction

The design of the solid barrier junction of Fig. 2(b) was largely empirical, and, as with the choke junction, was carried out in waveguide. The completed assembly shown in Fig. 8 was tested and found to have a vswr <1.04 over the applicable frequency range. The only point in the scan cycle where reflections from this junction will cause input impedance variations occurs when the energy is normally incident on the junction, but this is sufficiently low for the design shown (vswr <1.01) to be undetectable in the final scanner.

Output Horn

The output horn was designed with a double flare in order to keep the reflections from each change in flare angle as low as possible and approximately equal, without making the horn too long. In the construction of the actual horn, the bends were made round rather than sharp to further reduce the reflection coefficients.

Construction

A complete scanning antenna based on the design information described above has been built and tested. Some of the basic design data for the scanner are listed in Table I.

TABLE I

Dimensions of the Experimental Foster Scanner

Vertex angle of conical rotor	=16 in.
Diameter of large end of rotor	=11.530 in.
Diameter of small end of rotor	= 2.243 in.
Axial length of rotor	=33.04 in.
Gap between rotor and stator	= 0.0636 in
Maximum clearance between rotor and solid-barrier junction	= 0.006 in.
Focal length of parabolic pillbox	= 6.2 in.
Width of parabolic pillbox	= 0.0794 in.
Depth of choke groove	= 0.0850 in.
Width of choke groove	= 0.0636 in.
Spacing of choke groove from pillbox	= 0.0253 in.
Design frequency	=34.9 kmc (8.6 mm)
Maximum scan angle (zero switching time)	=50.10 in.

The stator was too large to be turned in one piece on available lathes, and was therefore cast in three sections. The castings, made by the Aluminum Company of America, were of stress-relieved 356-T51 aluminum alloy, to minimize the distortion of the stator when the output aperture was cut through along one side.

The rotor, of 356-T6 aluminum alloy, was cast in two identical halves. The parabolic pillbox was milled into one flat aluminum plate, and screwed to one rotor section with flush-head aluminum screws. Another flat plate was similarly screwed to the other rotor section and the two sections securely bolted together, sandwiching the pillbox between them. The feed for the pillbox, consisting of a slot in the broad side of standard K_a-band waveguide, was inset in an aluminum clip designed to keep the rotor from expanding at high speeds. The reinforcing clip increases the obstruction across the aperture and alters the primary feed pattern; however, preliminary tests of the rotor alone indicated that the 2- or 3-db resultant increase in side-lobe level to about -18 db was not too serious for the present tests.

The rotor was not balanced for the initial electrical tests; however, approximate calculations indicated that a speed of 500 rpm would cause a spread of the two rotor sections of less than 0.001 inch which should not appreciably affect the electrical performance.[5] It is felt that speeds as high as 3,600 rpm could be attained if the two rotor sections were bonded together with nonreflecting supports, such as have been developed for use in conventional Foster scanners.[6] If, as mentioned before, a slotted waveguide were used as the line source, even greater speeds would be possible.

[5] Leonard Hatkin of SCEL informed the authors that the Signal Corps later balanced this rotor and spun it at 1,000 rpm with no spreading of the rotor halves being detected.

[6] Such supports have been developed by W. C. Wilkinson of RCA and by W. Rotman of AF Cambridge Research Center.

Electrical Tests

The complete scanning antenna is shown in Fig. 9. A large number of radiation patterns were recorded for many angular positions of the rotor at the design frequency and at frequencies ± 5 and -10 per cent from the design frequency. A set of patterns obtained at the design frequency are reproduced in Fig. 10. The most significant points noted in these patterns and in other patterns not shown are:

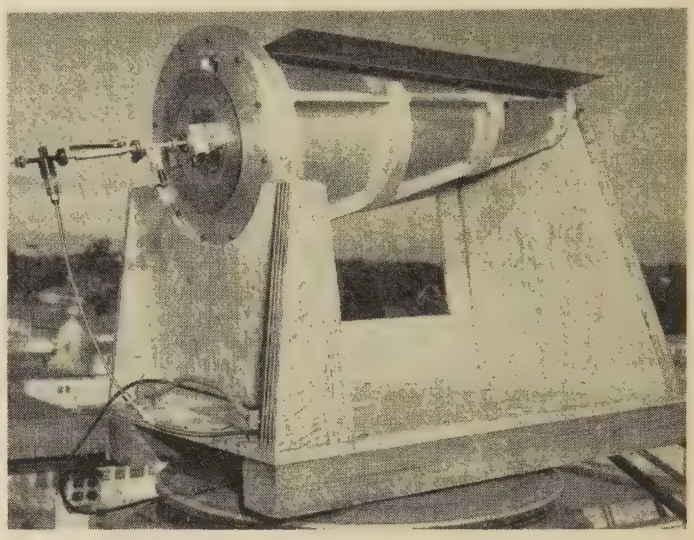

Fig. 9—Complete Foster scanner on the antenna pattern range.

1) At the design frequency, the main beam and the minor lobe structure remain virtually unchanged throughout the entire scan cycle and are very similar to those of the rotor alone. In other words, the scanning action does not alter the radiation pattern of the line source to any appreciable extent.
2) The patterns at frequencies ± 5 per cent from the design frequency are nearly as good as those at the design frequency.
3) At a frequency 10 per cent below the design frequency, significant pattern perturbations are observed, which are due to multiple reflections between choke junction and solid barrier.

At all frequencies tested, the angle of scan was a linear function of the rotor angle within the error of the measurements (0.1 degree).

A series of measurements were also made of the amplitude of the main beam as a function of the rotor angle, or azimuth scan angle, for same frequencies employed in pattern measurements. Fig. 11 (p. 46) shows how the amplitude decays uniformly with scan angle at the design frequency. At ± 5 per cent from the design frequency the behavior is very similar but when the frequency is 10 per cent below the design frequency the amplitude is an erratic function of scan angle. The

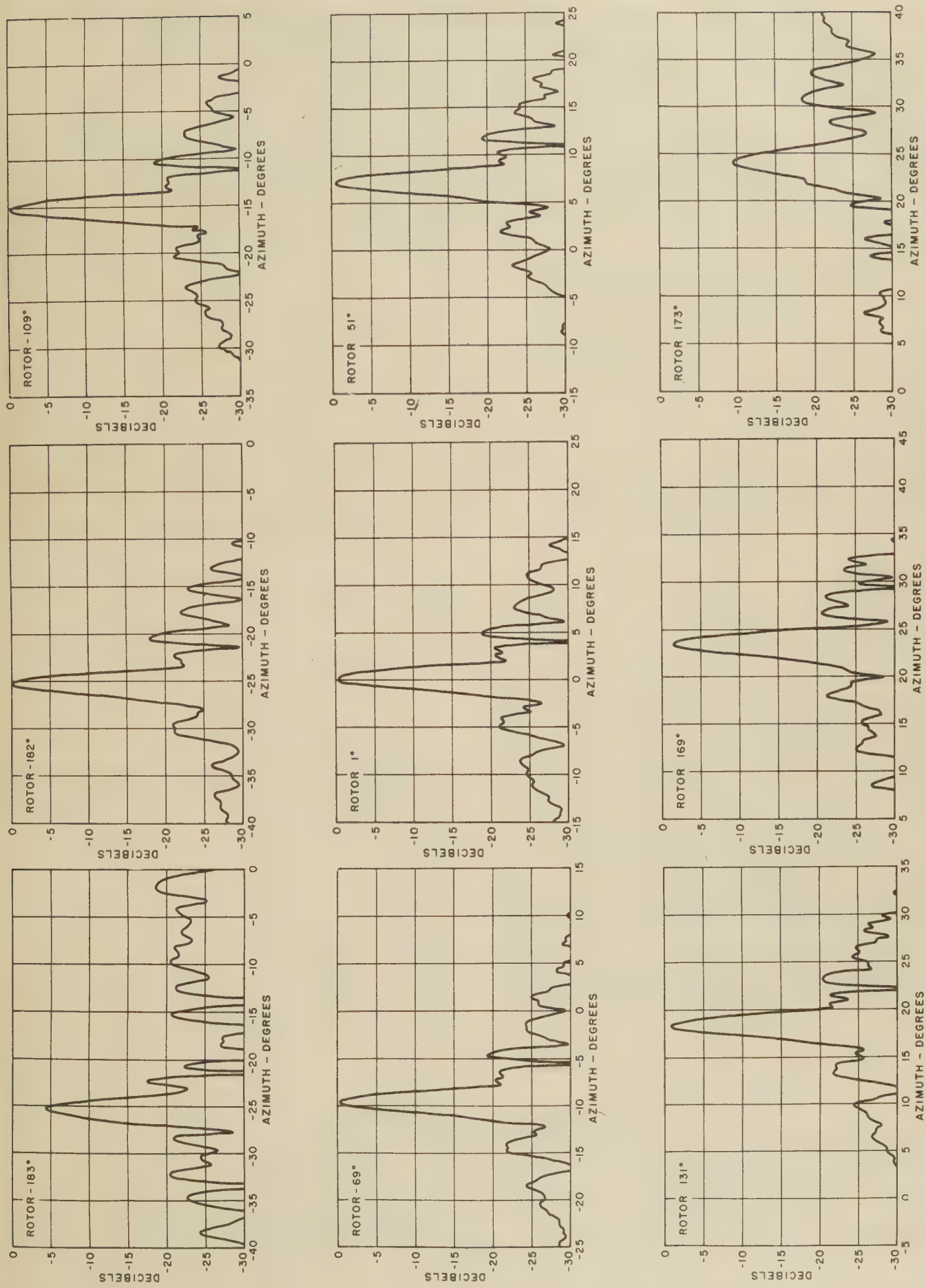

Fig. 10—Radiation patterns of Foster scanner at design frequency—34.9 kmc.

gradual slope observed in the amplitude through the scan cycle is due entirely to the attenuation that occurs as the energy propagates through greater and greater lengths in the conical transmission line between the rotor and the stator. For the frequencies, spacings, and aluminum alloys employed here, the theoretical change in amplitude from one end of the scan cycle to the other is approximately three-quarters of a decibel, and the theoretical curve is superimposed on Fig. 11.

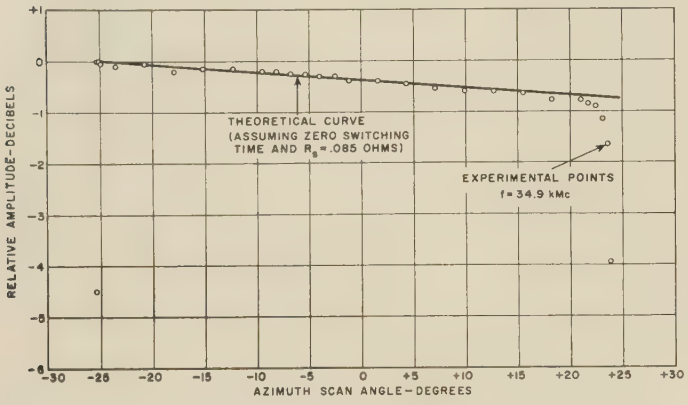

Fig. 11—Relative maximum amplitude as a function of azimuth scan angle.

It is seen from the figure that a total scan angle of 47° is obtained at the center frequency with virtually no change in the radiation characteristics aside from the gradual change in amplitude due to dissipation in the rotor and the stator. In order to calculate the gain approximately, the scanner was connected as a transmitter and the rotor turned until the radiation from the scanner was normal to the output horn and the field along the horn was measured with a very small probe. The results are shown in Fig. 12. Also included on the figure are directive gains[7] obtained for the *H*-plane by numerical integration of the measured curve assuming constant phase distribution over the indicated portions of the aperture. The directive gain in the *E*-plane was calculated from Schelkunoff's gain curves.[8] The lowest computed directive gain of 32.8 db, is undoubtedly closest to the actual gain since in the regions outside the boundaries shown, the phase must be going through large and rapid changes, and contributing little if anything to the over-all gain.

The measured gain, obtained by comparison with a horn whose gain can be calculated from Schelkunoff's analysis, was 30.7 ± 0.5 db. Since there is approximately 0.4 db attenuation in the waveguide feeding the parabolic line source, 0.4 db attenuation within the pillbox, and 0.5 db spill-over loss from the pillbox, the directive gain of the antenna is approximately 32 ± 0.5 db. In view of the uncertainties involved in these calculations,

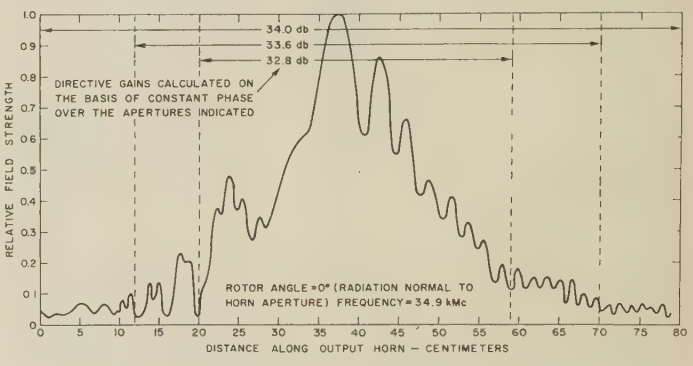

Fig. 12—Measured amplitude distribution along the output horn of the Foster scanner.

this figure agrees well with that computed from the amplitude distribution. It may be concluded therefore that this Foster scanner operates in the manner predicted, without the occurrence of any unusual losses or other abnormalities in performance.

Conclusion

The modification of the Foster scanner described in this paper has been found to perform extremely well. The experimental tests have demonstrated that the principle of using choke joints to direct the energy around the conical rotor is sound. The choke joints have also been shown to have important advantages over the conventional interleaving-finger barriers.

Acknowledgment

The authors wish to acknowledge the assistance of Howard P. Wurtz, Jr., who worked out the mechanical design for the experimental Foster scanner, and of Robert B. McPherson who constructed the scanner.

[7] S. Silver, "Microwave Antenna Theory and Design," McGraw-Hill Book Co., Inc., New York, N. Y., pp. 177–179; 1949.

[8] S. A. Schelkunoff and H. T. Friis, "Antennas, Theory and Practice," J. Wiley & Sons, Inc., New York, N. Y., pp. 523–529; 1952.

Surface Currents Excited by an Infinite Slot on Half-Planes and Ribbons*

J. R. WAIT† AND M. O'GRADY‡

Summary—**The distribution of surface current density on a perfectly conducting half-plane excited by an infinite axial slot is determined. The slot is assumed to be of small width and it is excited throughout its length by a uniform transverse voltage. It is shown that the surface currents which flow toward the edge of the half-plane are somewhat smaller than they would be if they were on an infinite plane. For sake of comparison the surface currents of an infinite axial slot on a thin elliptic cylinder or ribbon are also examined**

Introduction

IN THE theoretical study of slot antennas little attention has been paid to the near fields. Since the slots are cut usually in metal surfaces, which can be represented or approximated by circular cylinders, elliptic cylinders, or wedges, it is of interest to examine the surface currents that are excited by the slot. In these cases it is not permissible to make any of the usual far field approximations[1,2] and the analysis becomes very difficult, in general. However, if slot is assumed to be of infinite length and parallel to axis of cylinders or wedge edge, resulting expressions for surface currents are in a form suitable for computation.

It is the purpose of this paper to examine the surface currents excited by an axial slot on a wedge of vanishing thickness or half-plane and also for the axial slot on a thin elliptic cylinder or ribbon. These cases are illustrated in Fig. 1. It whould be mentioned that Papas and King[3] have studied the currents on an infinite circular cylinder excited by an axial slot.

Slot on Half-Plane or Thin Wedge

Expressions were given previously[4] for the fields of a line source of magnetic current parallel to the edge of a semi-infinite, infinitesimally thin, and perfectly conducting wedge or half-plane. When the source is allowed to coincide with the surface of one side of the half-plane the magnetic current is equivalent to an axial slot excited by a uniform voltage V throughout its length. Choosing a cylindrical coordinate system (ρ, ϕ, z) coaxial with edge of half-plane, slot is located at $\rho=\rho_0$ on upper side, $\phi=0$, of half-plane. Resulting magnetic field which has only an axial component is then given by

$$H_z=\frac{-\epsilon\omega V}{4}\sum_{m=0,1,2,3\cdots}^{\infty} H_{m/2}^{(2)}(k\rho_0)J_{m/2}(k\rho)\epsilon_m\cos(m\phi/2) \quad (1)$$

for $\rho<\rho_0$ and

$$H_z=\frac{-\epsilon\omega V}{4}\sum_{m=0,1,2,3\cdots}^{\infty} J_{m/2}(k\rho_0)H_{m/2}^{(2)}(k\rho)\epsilon_m\cos(m\phi/2) \quad (2)$$

for $\rho>\rho_0$ where $\epsilon_0=1$, $\epsilon_m=2$ for $m\neq 0$, ϵ is the dielectric constant of free space, $k=2\pi/$free space wavelength, and ω is the angular frequency. $J_{m/2}(x)$ is the Bessel function of the first type of order $m/2$ and argument x, and $H_{m/2}^{(2)}(x)$ is the Hankel function of the second kind of order $m/2$ and argument x.

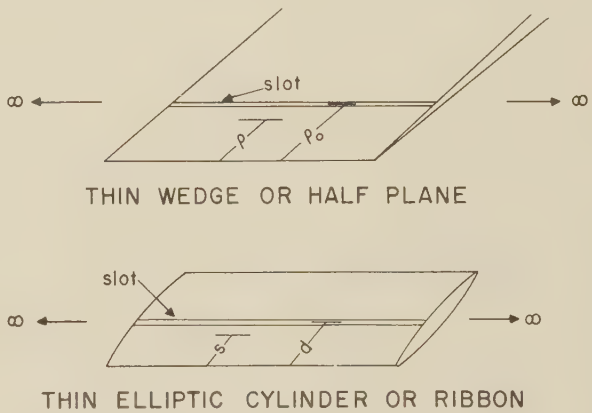

Fig. 1—Illustrations of an axial slot cut on one side of half-planes and ribbons.

Current density in amp per meter on half-plane is now numerically equal to tangential magnetic field and it flows in the ρ direction. But for purposes of computation and presentation, it is convenient to introduce a dimensionless current parameter defined by

$$I_U = (\epsilon\omega V)^{-1}[H_z]_{\phi=0} \quad (3)$$

for the upper side and

$$I_L = (\epsilon\omega V)^{-1}[H_z]_{\phi=2\pi} \quad (4)$$

for the lower side.

Noting that the even terms in the summation can be summed by employing a well-known addition formula[5] for integral order Bessel functions, it follows that

* Manuscript received by the PGAP, April 22, 1955; revised manuscript received August 1, 1955.

† Central Radio Propagation Laboratory, Boulder, Colo.
‡ Radio Physics Lab., Defense Research Board, Ottawa, Canada.

[1] S. Silver and W. K. Saunders, "Field produced by an arbitrary slot on a circular cylinder," *J. Appl. Phys.*, vol. 21, pp. 153–158; January, 1950.

[2] J. R. Wait and S. Kahana, "Radiation from a slot on a cylindrically tipped wedge," *Can. J. Phys.*, vol. 31, pp. 714–722; November, 1954.

[3] C. H. Papas and R. King, "Currents on the surface of a infinite cylinder excited by an axial slot," *Quart. Appl. Math.*, vol. 7, pp. 175–182; April, 1949.

[4] J. R. Wait, "Radiation from a line source adjacent to a conducting half-plane," *J. Appl. Phys.*, vol. 24, pp. 1528–1529; December, 1953. The problem can also be solved using a Wiener-Hopf technique, for example, see R. F. Harrington, "Current element parallel to a conducting half-plane," *J. Appl. Phys.*, vol. 24, pp. 547–551; June, 1953. The problem has also been discussed in detail by C. T. Tai, "Radiation From Apertures in a Half-Plane Sheet," Technical Report No. 45, Stanford Research Institute, June, 1954.

[5] G. N. Watson, "Theory of Bessel Functions," Cambridge University Press, Cambridge, 1944; p. 361.

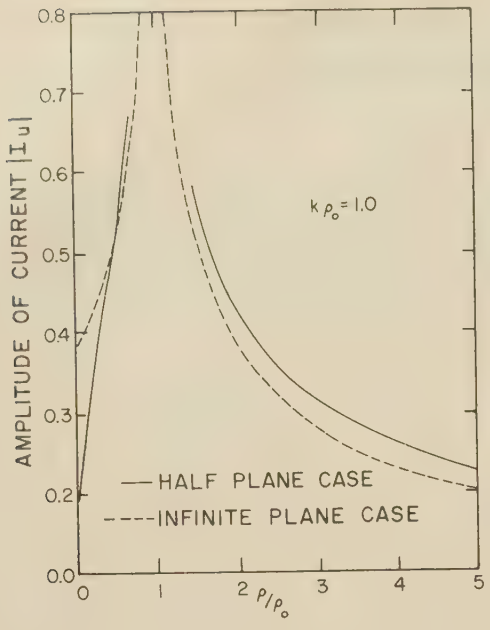

(a)

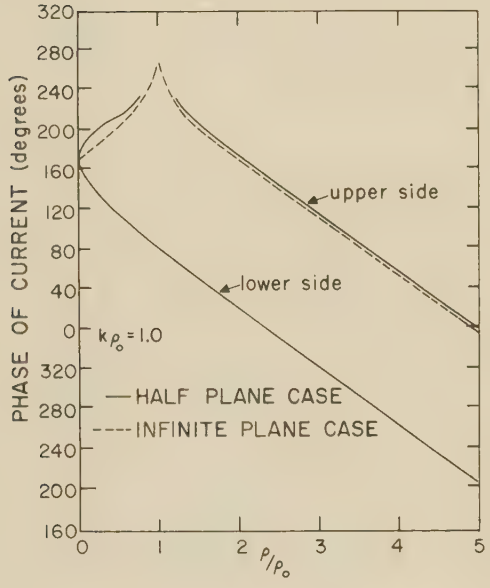

(b)

Fig 2—(a) The amplitude of the current density on the half-plane for $k\rho_0 = 1.0$. (b) The phase of the current density on the half-plane for $k\rho_0 = 1.0$.

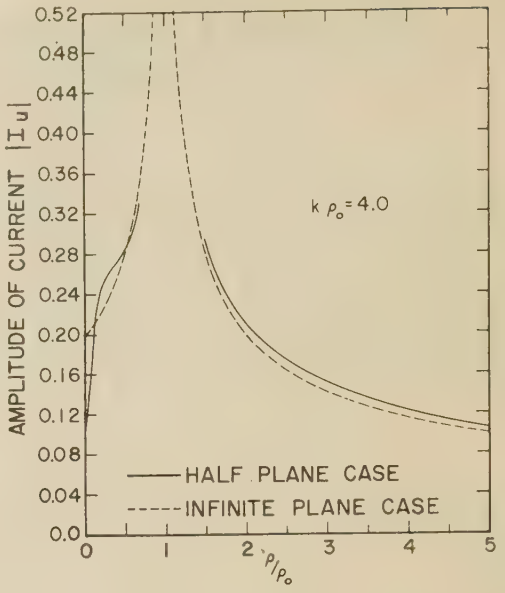

(a)

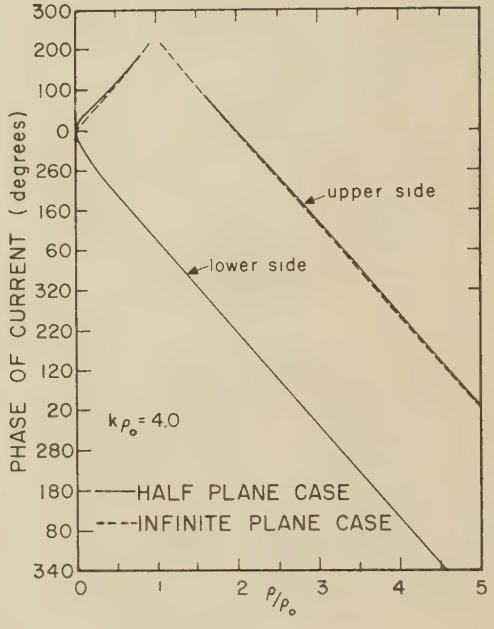

(b)

Fig. 3—(a) The amplitude of the current density on the half-plane for $k\rho_0 = 4.0$. (b) The phase of the current density on the half-plane for $k\rho_0 = 4.0$.

$$I_U = -H_0^{(2)}[k(\rho_0 - \rho)]/4 + P(\rho_0, \rho)$$
$$I_L = -H_0^{(2)}[k(\rho_0 - \rho)]/4 - P(\rho_0, \rho) \qquad (5)$$

for $\rho < \rho_0$ and

$$I_U = -H_0^{(2)}[k(\rho - \rho_0)]/4 + P(\rho, \rho_0)$$
$$I_L = -H_0^{(2)}[k(\rho - \rho_0)]/4 - P(\rho, \rho_0) \qquad (6)$$

for $\rho > \rho_0$. The summation term $P(\rho_0, \rho)$ involving half order Bessel functions is given by

$$P(\rho_0, \rho) = \frac{1}{2} \sum_{m=1,3,5\cdots}^{\infty} H_{m/2}^{(2)}(k\rho_0) J_{m/2}(k\rho)$$
$$= \sum_{m=1,3,5\cdots}^{\infty} [J_{m/2}(k\rho_0) + i(-1)^{(m-1)/2} J_{-m/2}(k\rho_0)] J_{m/2}(k\rho). \qquad (7)$$

The expression for $P(\rho, \rho_0)$ is identical in form to the above when ρ is interchanged with ρ_0.

If the edge of the half-plane was infinitely remote from the slot the expressions for I_U would correspond identically to the normalized current density I_U^{∞} for a thin slot on an infinitely extensive conducting plane. It is easy to show that for this case[6]

$$I_U^{\infty} = -H_0^{(2)}[k|\rho_0 - \rho|]/2. \qquad (8)$$

Numerical computations have been carried out for the amplitude and phase of I_U and I_L utilizing available

[6] N. A. Begovich, "Slot radiators," Proc. IRE, vol. 37; pp. 803–806; July, 1950.

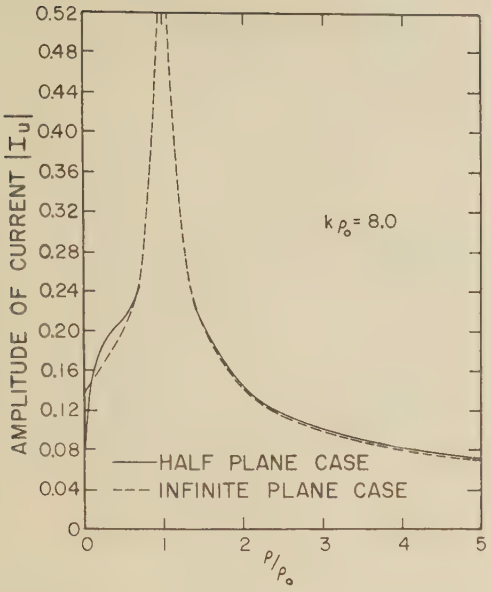

(a)

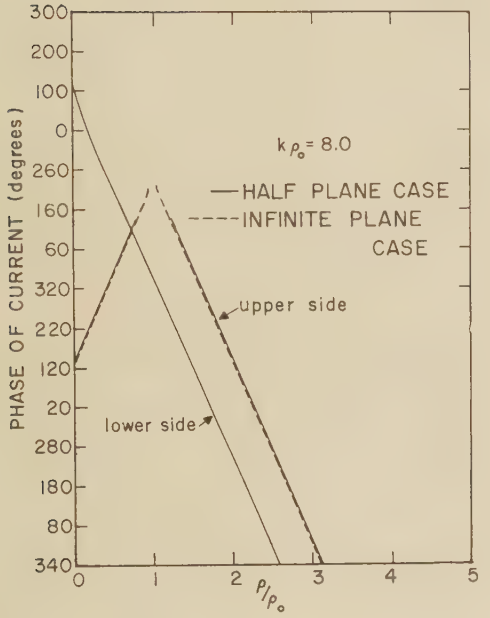

(b)

Fig. 4—(a) The amplitude of the current density on the half-plane for $k\rho_0 = 8.0$. (b) The phase of the current density on the half-plane for $k\rho_0 = 8.0$.

tables of the half-order Bessel functions of positive and negative order. The results are plotted in Figs. 2 to 5 where the abscissas are ρ/ρ_0 and the $k\rho_0$ values chosen were 1, 4, and 8. The amplitude and phase of I_U^∞ are shown for comparison in Figs. 2 to 4. The similarity between I_U and I_U^∞ is striking. It is noted that the current density is disturbed by the presence of the edge in a consistent manner. In all cases the ratio I_U/I_U^∞ approaches 1/2 as ρ tends to zero. This is in accord with the fact that the summation term $P(\rho_0, \rho)$ approaches zero as ρ tends to zero. The ripples in the curve of $|I_U|$ for ρ between 0 and ρ_0 can be interpreted as a sort of standing wave pattern resulting from the interference of the wave partially reflected from the edge with the direct excitation from the slot.

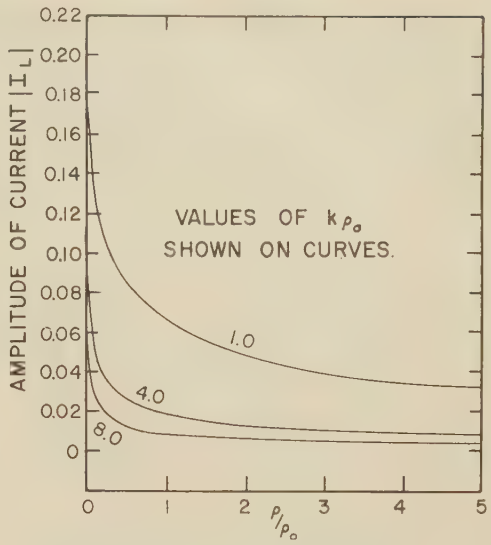

Fig. 5—The amplitude of the current density on the lower side of the half-plane for various values of $k\rho_0$.

The amplitude of the density on the lower side of the sheet is seen from the curves in Fig. 5 to decrease monotonically with distance ρ from the edge. As seen in Figs. 2 to 4 the phase is almost a linear function of ρ. It is worthwhile to note that I_U and I_L are continuous at the edge.

Slot on Ribbon or Thin Elliptic Cylinder

When the slot is cut on a thin conducting ribbon of infinite length the excited surface currents can be studied by representing the ribbon by an elliptic cylinder of infinite length with a vanishing minor axis. Employing the general results given in a previous analysis[7] it is possible to write down a rigorous expression for the tangential magnetic or surface currents for an arbitrary slot with any specified distribution or electric field. Unfortunately, the infinite integrals appearing inside the summation of Mathieu functions are not easy to evaluate for finite slots in the near field. For the case of the thin axial slot of infinite length, however, with a uniform voltage distribution V, the troublesome infinite integrals disappear. Consequently the magnetic field H_z in terms of elliptic cylinder coordinates (u, v, z) for a slot located at $v = v_0$ on the elliptic cylinder $u = u_0$ with semi-focal distance d is given by

$$H_z = i\epsilon\omega V \cdot \sum_{m=0}^{\infty} \frac{Se_m(kd, v_0)Se_m(kd, v)He_m^{(2)}(kd, u_0)}{N_m^{e,o}(kd)\left[\partial He_m^{(2)}(kd, u)/\partial u\right]_{u=u_0}} \quad (9)$$

where Se_m and So_m are the even and odd angular Mathieu functions, He_m and Ho_m are the even and odd radial Mathieu functions of the fourth kind and N_m^e and N_m^o are the appropriate normalization factors.[8] Double suffix e, o in (9) is to indicate summation is over both even and odd Mathieu functions. Again, current

[7] J. R. Wait, "Field produced by an arbitrary slot on an elliptic cylinder," *J. Appl. Phys.*, vol. 36, pp. 458–463; May, 1955.

[8] J. A. Stratton, "Electromagnetic Theory," McGraw-Hill Book Co., Inc., New York, N. Y., 1951; p. 375.

density on surface of elliptic cylinder is numerically equal to tangential magnetic field H_z at $u = u_0$.

To effect the transition to a thin ribbon, u_0 is set equal to zero. The simplification will be made also that the slot is located centrally on the upper side of the ribbon, so that (9) can now be simplified by making use of the following identities:[9]

$$H_0^{(2)}(kd \mid \cos v \mid)$$

$$= 4 \sum_{m=0}^{\infty} \frac{Se_m(kd, v) Se_m(kd, \pi/2)}{N_m^e(kd)} Je_m(kd, 0) He_m^{(2)}(kd, 0) \quad (10)$$

and

$$[\partial He_m^{(2)}(kd, u)/\partial u]_{u=0} = -i/Je_m(kd, 0) \quad (11)$$

where Je_m is radial Mathieu function of the first kind. Tangential magnetic field H_{zt} on ribbon is then given by

$$H_{zt} = -\frac{\epsilon\omega V}{4} \left\{ H_0^{(2)}[kd \mid \cos v \mid] - i4 \sum_{m=0}^{\infty} \frac{So_m(kd, v) So_m(kd, \pi/2) Ho_m^{(2)}(kd, o)^{u_0=0}}{N_m^0(kd) [\partial Ho_m^{(2)}(hd, u_0)/\partial u_0]} \right\} \quad (12)$$

and the normalized current densities on the upper and lower sides of the ribbon are given by

$$I_U = (\epsilon\omega V)^{-1} H_{zt} \text{ for } 0 \leqq v \leqq \pi \quad (13)$$

and

$$I_L = (\epsilon\omega V)^{-1} H_{zt} \text{ for } 0 \geqq v \geqq -\pi, \quad (14)$$

respectively.

Employing tabulated values of the Mathieu functions, numerical results can be obtained from (12) although, the convergence of the series is poor. As an example, the amplitude and phase of I_U and I_L are plotted in Fig. 6 for $kd = 4$ as a function of s/d where s is measured from the edge of the ribbon of width $2d$ (*i.e.*, $s/d = 1 = p \mid \cos v \mid$). For comparison half-plane results for $k\rho_0 = 4$ are shown in Fig. 6 along with infinite plane results.

The similarity between the current density near the edge of the ribbon and that near the edge of a half-plane is most striking. Apparently, the behavior of the surface current between a slot and an edge is mainly determined by their distance of separation. The surface current on the lower side of the ribbon is however, quite different from that of the half-plane. No doubt the oscillating nature of the curve of I_L shown in Fig. 6 for the ribbon results from interference between the waves coming from the two edges of the ribbon.[10,11]

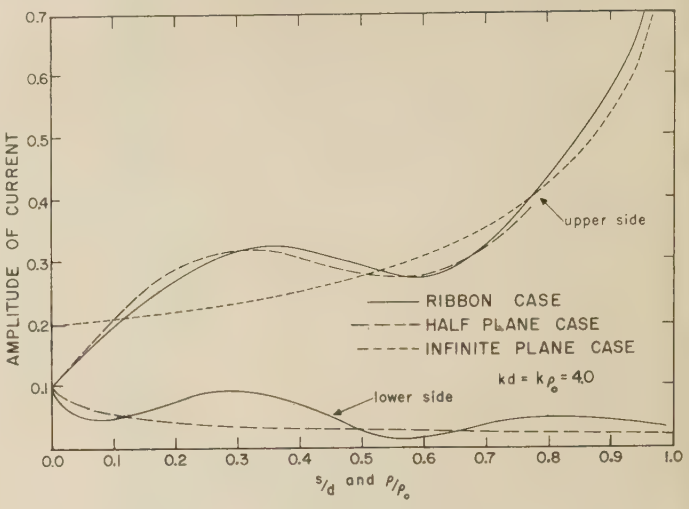

(a)

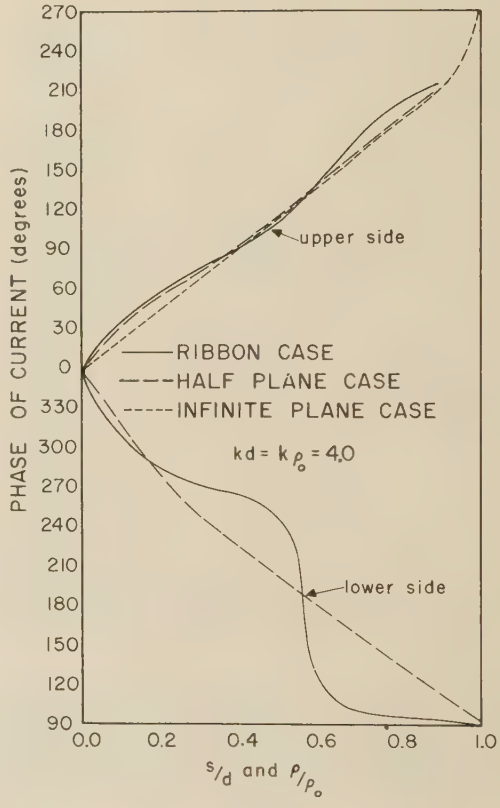

(b)

Fig. 6—(a) The amplitude of the current on the ribbon with the results for the half-plane shown for comparison. (b) The phase of the current on the ribbon with the results for the half-plane shown for comparison.

Conclusion

While the results of this analysis are confined to an infinite slot on a half-plane, and to ribbons that are infinite in axial direction, it is believed they show, in a qualitative way, effect of an edge which is parallel to a slot. It would be interesting to extend this analysis to an axial half-wave slot on a half-plane or ribbon.

[9] P. M. Morse and H. Feshbach, "Methods of Theoretical Physics," McGraw-Hill Book Co., Inc., N. Y., N. Y., 1953; vol. 2, p. 1421.

[10] J. R. Wait and R. E. Walpole, "Calculated radiation characteristics of slots cut in metal sheets, Pt. I," vol. 33, pp. 211–227, May, 1955; and Pt. II, vol. 34, March, 1956 (in press).

[11] D. C. Frood and J. R. Wait, "An experimental investigation of slot radiators in metal plates," *Proc. I.E.E.*, Pt. B, vol. 103, January, 1956 (in press).

Radar Back-Scattering Cross Sections for Nonspherical Targets*

P. N. MATHUR† AND E. A. MUELLER†

Summary—**Studies were made of the scattering of electromagnetic waves from nonspherical targets by making exact determination of the nose-on radar back-scattering cross sections of conducting prolate spheroids of various sizes and shapes. Curves are given for the back-scattered cross sections as a function of dimensionless size and shape parameters for prolate spheroids. The results are compared with the Rayleigh-Gans first order approximation and Stevenson's third-order approximation, and the range of applicability of these approximations is evaluated.**

Introduction

EXACT SOLUTIONS of the scattering of electromagnetic waves by nonspherical particles have been obtained only in a few cases. Contributions to this problem were made by Herzfeld [1] and Möglich [2] who attacked the problem by methods of exact analyses. Their solutions are, however, formal ones and a great deal of work is required to reduce them to calculable forms. Schultz [3] obtained an exact solution for the special case of a conducting prolate spheroid at nose-on incidence. Even for this case the calculations are quite involved and tedious. Siegel, Gere, Marx, and Sleator [4] have made a radar scattering study from this solution for a thin prolate spheroid (axis ratio 10:1).

Gans [5] and Rayleigh [6] obtained first-order solutions on the assumption that the characteristic dimensions of the scatterers are very small compared to the wavelength of the incident radiation. This limitation on size is a serious one, and the results, while reasonable and useful, are of uncertain accuracy in detail. More recently, Stevenson [7] has extended these solutions to third-order terms. With the exception of the range of validity of this higher order approximation, his solution is quite general.

The purpose of the present investigation was: to study the effect of size and shape of the target on radar echo, and to determine the range of applicability of the Rayleigh-Gans and Stevenson approximations by evaluating these solutions against an exact solution.

A brief outline of the formulas used and the results obtained are described in the following sections.

Theory

Basic Definitions

Since most radar applications are based upon the transmission of short pulses of electromagnetic energy and reception of echo pulses from a distant target, it is desirable to express the returned signal power in terms of radar system parameters, the range to the target, and quantities that depend upon the nature of the scatterer. Establishment of a radar equation relating these factors leads to the concept of back-scattering cross section. Back-scattering cross section, σ, may be defined as the area intercepting that amount of power which, when scattered isotropically, produces an echo at the transmitter equal to that observed from the target. Mathematically,

$$\sigma = \frac{4\pi R^2 (S_s^R)_{\theta=0}}{S_i^Z} \tag{1}$$

where $(S_s^R)_{\theta=0}$ is the radial component of the Poynting vector of the scattered wave in the backward direction ($\theta=0$), S_i^Z is the magnitude of the Poynting vector of the incident beam (incident direction $\theta=\pi$), and R represents a large radial distance from the scatterer to the point where $(S_s^R)_{\theta=0}$ is evaluated.

It is convenient to normalize this cross section by the approximate geometric cross section, σ_G, obtained from geometrical optics.

$$\sigma_G = \pi R_1 \cdot R_2 \tag{2}$$

where R_1 and R_2 are the two principal radii of curvature at the point of reflection. For nose-on incidence of the beam upon a prolate spheroid, the geometric cross section is

$$\sigma_G = b^4/a^2$$

where b and a are the semiminor and semimajor axes respectively. The size of the prolate may be conveniently defined by the dimensionless parameter, α, which is defined as

$$\alpha = ka$$

where $k = 2\pi/\lambda$ is the wave number, and λ is the wavelength of the incident field.

Results and Conclusions

The values of the radar back-scattering cross section computed from three different theories are presented in Figs. 1–3, as a function of the dimensionless parameter α. These figures show three different shapes of conducting prolate spheroids (axis ratios b/a) characterized by the values $b/a = 0.4167$, 0.5528, 0.639.

Fig. 4 shows the comparison of the approximate solutions with the exact values obtained from Schultz's solution. The effect of the shape of the prolate spheroidal target on radar echo is shown in Fig. 5 by a comparison

* Manuscript received by the PGAP, April 28, 1955; revised manuscript received September 6, 1955.

† Illinois State Water Survey, Urbana, Ill.

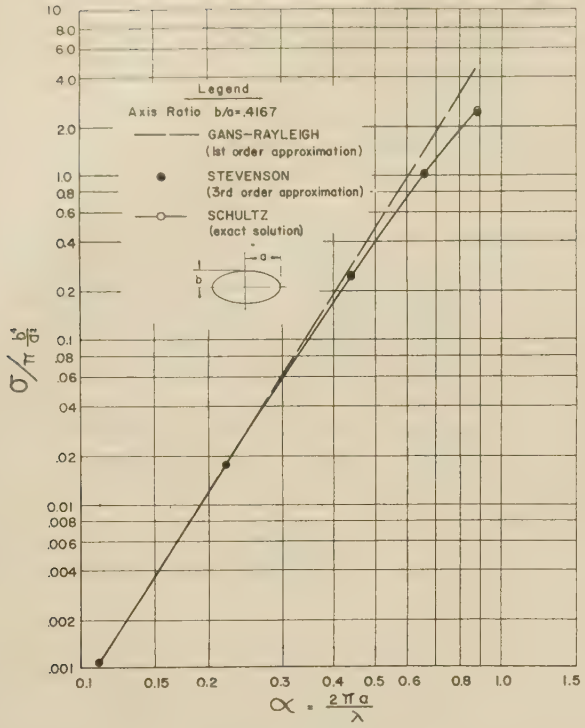

Fig. 1—Comparisons of back-scattering cross sections as computed from Schultz, Stevenson, and Gans for axis ratio of 0.4167.

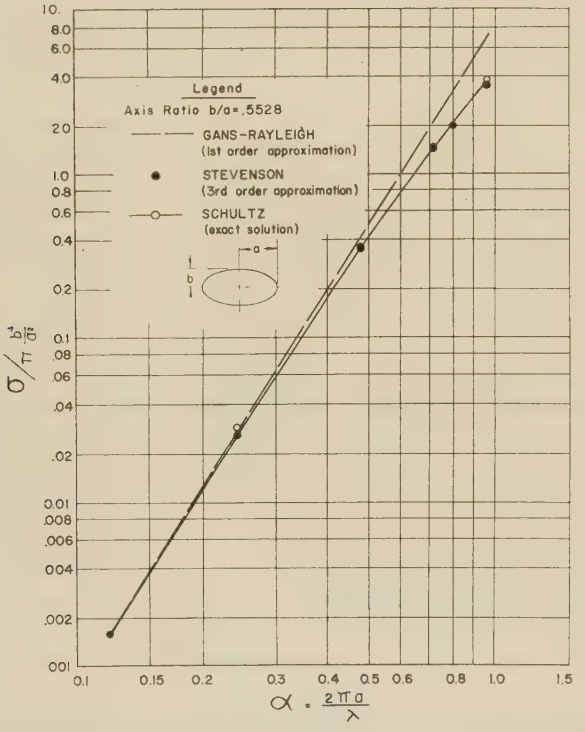

Fig. 2—Comparison of back-scattering cross sections as computed from Schultz, Stevenson, and Gans for axis ratio of 0.5528.

with the back-scattering cross section of spheres having the same volume. The curves in Fig. 5 are extrapolated to an axis ratio $b/a = 0.2$ [see 4].

The results indicate a substantial decrease in the values of the radar back-scattering cross sections as the shape of the equivolumetric scatters vary from spher-

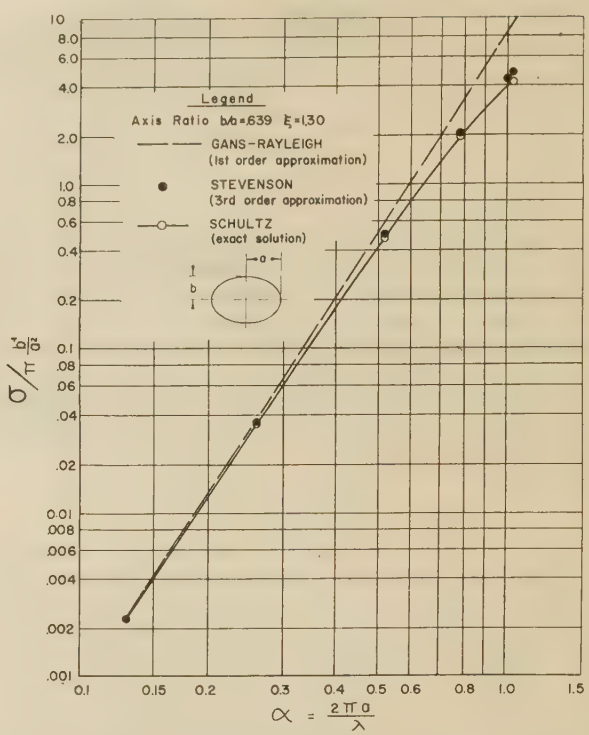

Fig. 3—Comparisons of back-scattering cross sections as computed from Schultz, Stevenson, and Gans for axis ratio of 0.639.

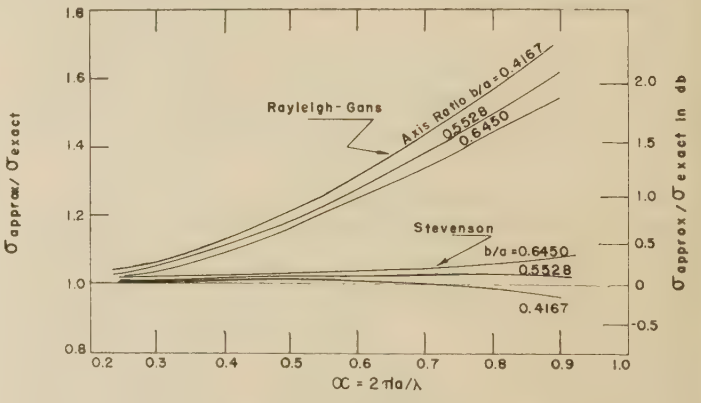

Fig. 4—Ratio of approximate back-scattering to actual back-scattering for conducting prolates.

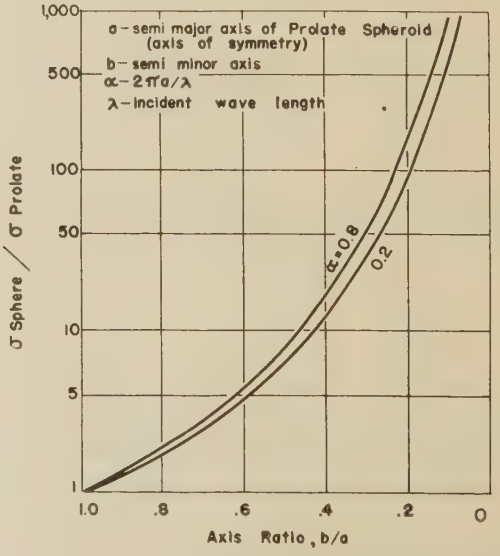

Fig. 5—Comparison of back-scattering cross section of a spheroid to the back-scattering cross section of an equivolumetric sphere.

ical to thin prolate spheroidal shapes. For a prolate of axis ratio $b/a=0.8$, $\alpha=0.8$, the ratio σ sphere/σ prolate is about 1/2 and decreases to a value of approximately 1/200 for a prolate spheroid of axis ratio $b/a=0.2$, $\alpha=0.8$.

Figs. 1–3 suggest that the Rayleigh-Gans first order solution is not adequate in the size range $\alpha>0.3$. However, Stevenson's third order solution yields results nearly identical with the exact values in the size range $\alpha<1.0$.

Acknowledgment

The investigation was conducted under the supervision of G. E. Stout, head of the Meteorology Subdivision, State Water Survey Division.

The authors wish to acknowledge the assistance of D. M. Sen and Ruth Cipelle in computations and checking of the numerical work.

Bibliography

[1] K. F. Herzfeld, "Uber die Beugung von elektro-magnetischen Wellen an gestreckten, Vollkommen leitenden Rotation-sellipsoiden." *Wiener Berichte Wien Akademi der Wissenschaften*, Vol. 120 (1911), p. 1587.
[2] Möglich, F., "Beugungserscheiinungen an Körpern von Ellipsoidischer Gestalt." *Annalen der Physik*, Vol. 83 (1927), pp. 609–000.
[3] Schultz, F. V. *Scattering by a Prolate Spheroid.* Engrg. Res. Inst. Univ. of Mich., Rept. UMM-42, March, 1950.
[4] Siegel, K. M., Gere, B. H., Marx, I., and Sleator, F. B., *The Numerical Determination of Radar Cross-Section of a Prolate Spheroid.* Engrg. Res. Inst., Univ. of Mich. Rep. UMM-126, October, 1953.
[5] Gans, R., "Uber die Form ultramikroskopischer Goldteilchen." *Annalen der Physik*, Vol. 37 (1912), pp. 881–900.
[6] Lord Rayleigh, "On the incidence of aerial and electric waves upon small obstacles," *The Philosophical Magazine*, Vol. 44, (1897), p. 28.
[7] Stevenson, A. F., "Electromagnetic Scattering by an Ellipsoid in the Third Approximation." *Journal of Applied Physics*, Vol. 24, (September, 1953), pp. 1143–1151.
[8] Mathur, P. N., and Mueller, E. A., *Radar Back-Scattering Cross Sections from Non-Spherical Raindrops.* Ill. State Water Survey, Urbana, Ill., Rep. of Investigation No. 28, 1955.
[9] Stratton, J. A., and others, *Elliptic Cylinder and Spheroidal Wave Functions.* New York, John Wiley & Sons, Inc., 1941.

An Experimental Investigation of Cavity-Mounted Helical Antennas*

A. BYSTROM, Jr.†, and D. G. BERNTSEN†

***Summary*—This paper presents the results of an experimental investigation which led to the development of cavity-mounted helical antennas for airborne applications. The effects on patterns and impedance of various antenna parameters, such as number of turns, cavity size and shape, helix pitch angle, and conductor size, were investigated.**

Methods of feeding the helix which produce an input impedance near 50 ohms, without external compensation, throughout the axial mode frequency range are discussed. Some of the types of cavity-mounted helices developed and typical performance data are described.

Introduction

IN RECENT years the need for broadband elliptically-polarized antennas which can be flush mounted on high-speed aircraft has increased. The helix inherently fulfills the broadband, elliptical polarization requirements and, in addition, is mechanically simple and relatively small in terms of wavelengths. While helices mounted on a ground plane have been often discussed in the literature,[1] it has been necessary to investigate and develop cavity-mounted helices to satisfy the flush-mounting requirement.

* Manuscript received by the PGAP, January 21, 1955; revised manuscript received September 8, 1955.
† Boeing Airplane Company, Seattle, Wash.
[1] While the references are too numerous to list completely, very thorough discussions of helix characteristics are given by J. D. Kraus, "Antennas," McGraw-Hill Book Co., Inc., 1950; ch. 7, and "The helical antenna," Proc. IRE, vol. 27, pp. 263–272; March, 1949.

Basic Helix Types

Each of the three fundamentally different types of helices studied by other investigators[2] with the helices mounted on a ground plane—the tapered helix, the small end-loaded helix, and the uniform or cylindrical helix—has proved useful for cavity applications requiring performance characteristics similar to those of the ground plane mounted helix. The tapered helix shown in Fig. 1(a) is, in its present design, normally used as a broadband receiving antenna where bandwidths exceed an octave and some beam tilt away from the helix axis can be tolerated. The small, end-loaded helix shown in Fig. 1(b) was developed for use in the lower frequency ranges where physical size was an important consideration and some deterioration in electrical characteristics was acceptable. A typical cavity-mounted cylindrical helix, shown in Fig. 1(c), was designed for optimum performance with a minimum of compromises and generally provides the best performance in most applications.

The cavity-mounted cylindrical helix has an input impedance near 50 ohms and a broad, single-lobed

[2] In addition to the literature already cited, tapered, and small, end-loaded helices are discussed in detail in P. W. Springer, "End-loaded and expanding helices as broadband circularly polarized radiators," *Proc. Natl. Electr. Conf.*, vol. 5, pp. 161–171; 1949, and J. S. Chatterjee, "Radiation field of a conical helix," *J. Appl. Phys.*, vol. 24, pp. 550–559; May, 1951.

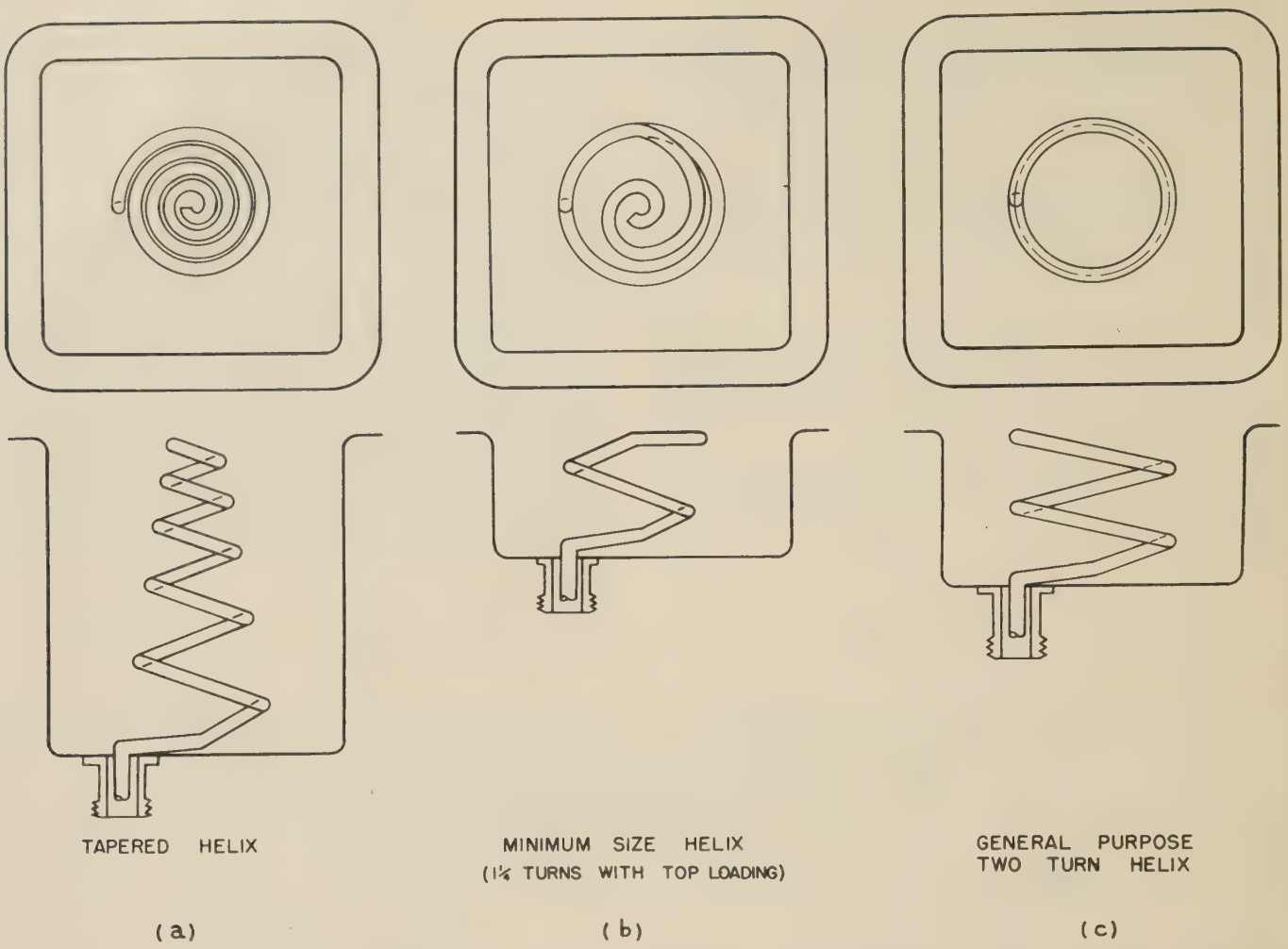

Fig. 1—Three types of cavity-mounted helical antennas.

radiation pattern, approximately circular in both cross section and polarization, with an axis that coincides with the helix axis. With the helix circumference equal to one wavelength at the center of the band, a bandwidth of nearly an octave is obtained. Since the cylindrical helix is generally the most useful, this paper is concerned primarily with this helix type.

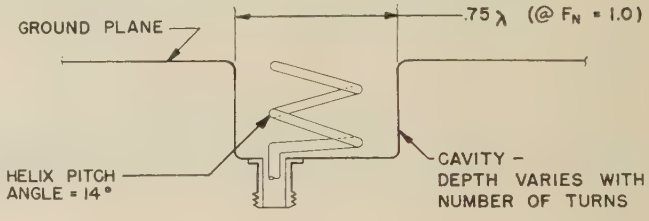

Effect of Helix and Cavity Parameter Variations

Data shown in Fig. 2 illustrates[3] the effect of the number of helix turns on the pattern half-power beamwidths with the helix coils mounted in square cavities. In general, except for the spread of points at the low end of the band, largely due to pattern shaping, the half-power beamwidths are independent of the number of helix turns used. Other data indicate similar results for axial ratio and impedance with helix coils of 2 to 6 turns. (Axial ratio as used here is defined as the ratio of the major axis to the minor axis of the polarization

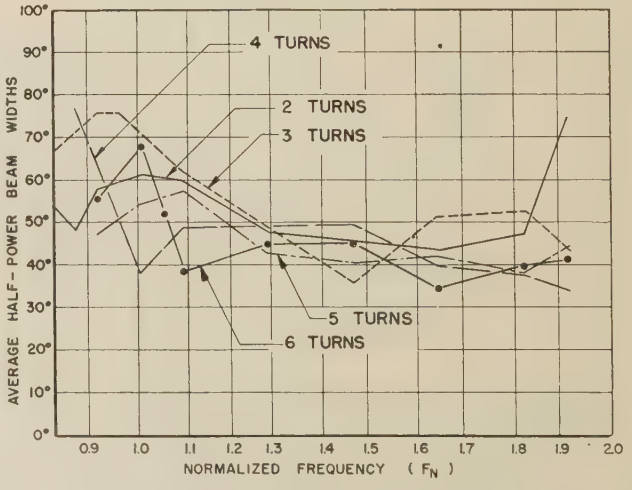

Fig. 2—Effect of number of helix turns on half-power beamwidths.

[3] When normalizing frequency for illustrations, the frequency at which $Fn=1$ was taken is either at the low end of what was considered to be the useful band of the antenna, or at the low end of the band for which the unit was being developed.

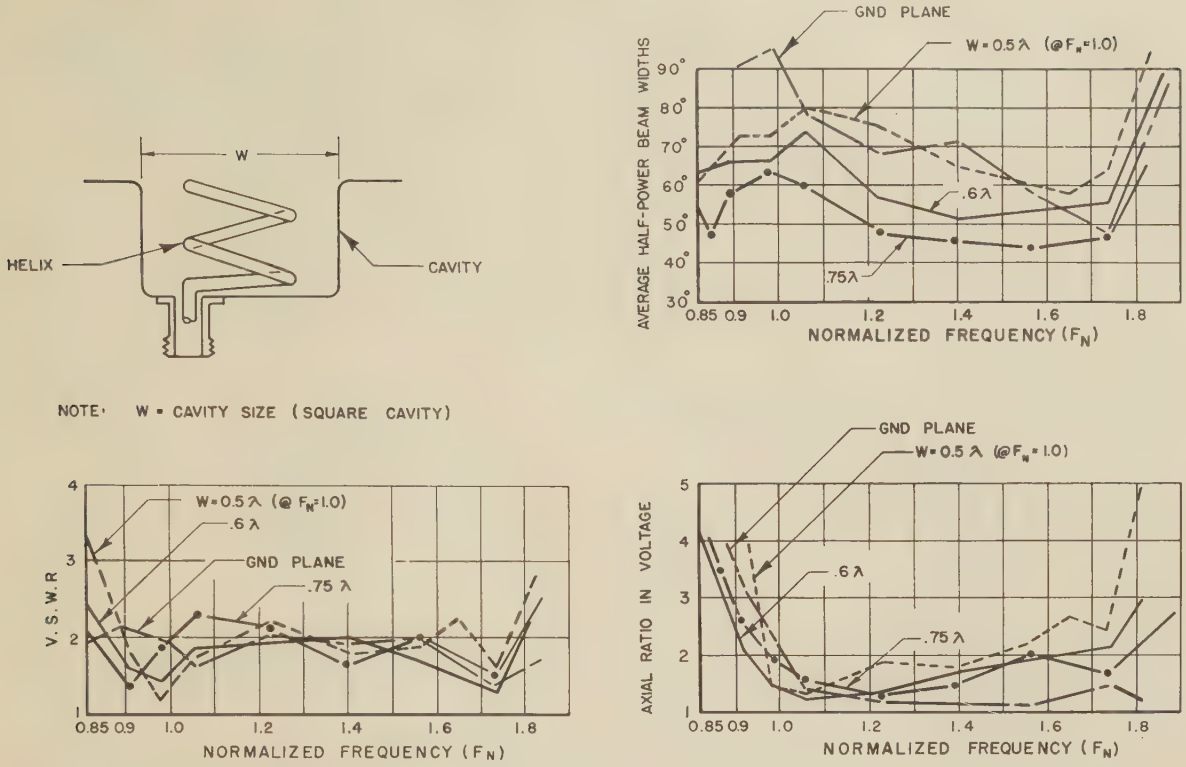

Fig. 3—Effect of cavity size on patterns, axial ratio, and vswr (two-turn helix).

ellipse measured on the helix axis.) While no particular improvement in performance resulted from using a helix with more than 2 turns, both pattern and impedance characteristics became less desirable as the number of turns was decreased below 2.

Cavity size was an important pattern determining parameter as can be seen in Fig. 3 where beamwidth, vswr and axial ratio are shown for various size cavities. As expected, the half-power beamwidths tend to be narrower for the larger cavity sizes. Also the beamwidths measured and those estimated on the basis of uniformly illuminated apertures[4] are in approximate agreement for both square and round cavity shapes. Axial ratios measured are generally higher than those for the helix mounted on a ground plane, but this effect could be reduced by proper choice of other parameters. While helix pitch angles between 10 degrees and 20 degrees were examined, 12 degree and 14 degree angles were used in most of the parameter studies. A pitch angle of 12 degrees was found to provide a minimum helix height without sacrificing performance characteristics.

For a given physical helix diameter, a usable bandwidth of nearly an octave is obtained when the helix circumference is equal to one wavelength at the center of the band, as in most cases illustrated here. In applications where the required bandwidth is considerably less than an octave, the helix diameter can be chosen so that the portion of the usable bandwidth which best satisfies pattern requirements is utilized.

Helix conductor diameters approximately equal to 1/15 of the mean helix coil diameter appear to be near optimum for lowest axial ratios, although this is not critical. The choice of conductor diameter for use in a particular antenna design usually is a compromise between allowable axial ratio and other considerations, such as impedance, efficiency, power level, and mechanical design.

Effects due to the existence of dielectrics in the antenna cavity were also investigated. It was found that the dielectric support structures used within the helix coil did not alter pattern and impedance characteristics appreciably, but dielectrics in the cavity outside the helix coil affected both patterns and impedance although, in certain cases, this effect could be used to advantage.

The vswr and the axial ratio, for example, can be reduced by proper choice of radome materials and dimensions. In this case, the use of a radome cover provides a convenient form of impedance and pattern compensation of the aperture discontinuities. How well this effect can be utilized depends, of course, on other antenna parameters as well as the type and thickness of radome which can be used.

Methods Used to Feed the Helix

The point at which the helix is excited as well as the slope of the helix conductor in the vicinity of this feed point were found to be very important in determining

[4] S. Silver, "Microwave antenna theory and design," M.I.T. Rad. Lab. Ser., vol. 12, ch. 6, McGraw-Hill Book Co., Inc., New York, N. Y.; 1949.

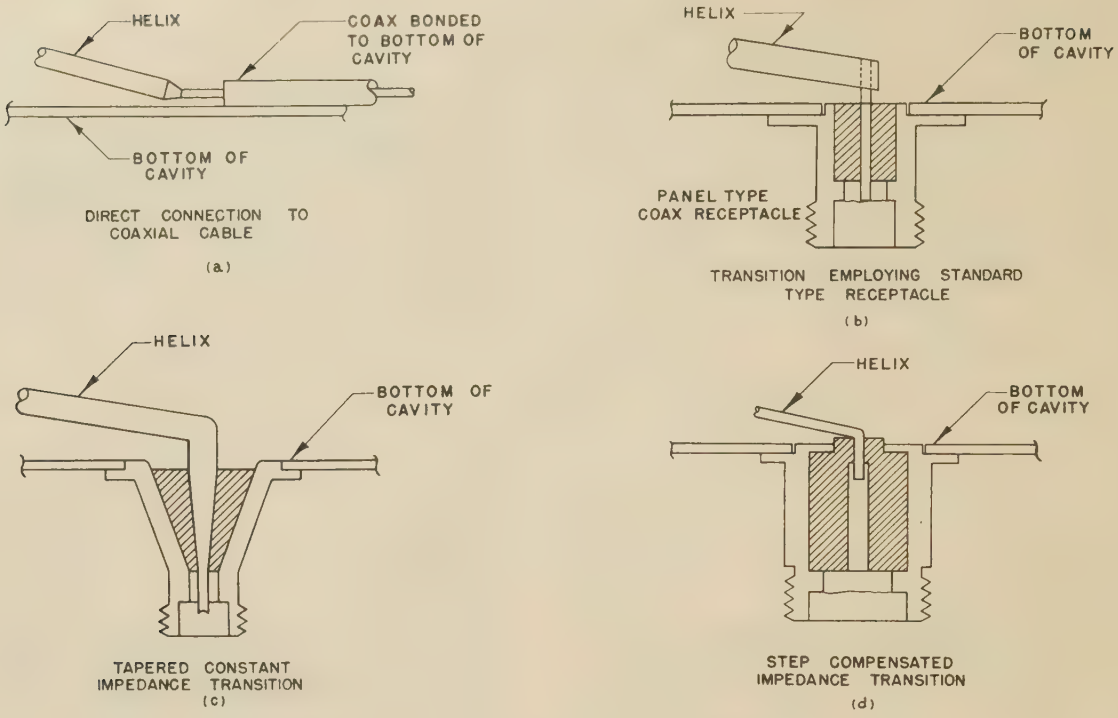

Fig. 4—Various types of coax to helix transitions.

the input impedances obtained. Impedance and pattern studies have shown that more uniform axial ratio and impedance characteristics could be obtained by feeding the helix on the perimeter rather than radially from the center of the helix. In addition, the helix conductor slope was reduced for the first one-quarter turn to form a conductor over a gound plane transmission line transformer with the change from transmission line to radiator being a gradual one. While pitch angles between 2 degrees and 6 degrees were used for this portion of the helix, the optimum pitch angle depends upon the particular antenna design and choice of other parameters.

Detail design of the transition from coax to helix used in the perimeter-type feed is governed by electrical and mechanical requirements as well as production costs. Several types of transitions from coax to helix are shown in Fig. 4. A direct connection to the coax, as shown in Fig. 4(a), has been used where space limitations prevent the use of a connector on the bottom of the cavity. A very simple transition, suitable for receiving antennas, is shown in Fig. 4(b) where a panel mounting receptacle is attached directly to the helix. The constant impedance and step-compensated transitions shown in Fig. 4(c) and 4(d) provide the best impedance match to 50 ohms and are suitable for use at the same power levels as the connector and cable series for which they are designed. When the smaller connector types are used with low frequency helices, the constant impedance transition is used to minimize the discontinuity between the helix conductor and the small center pin of the connector. The step-compensated design provides an optimum broadband impedance match for high frequency helices used with the larger connector types where the helix conductor and the connector center pin are approximately the same size.

Typical Performance Data

Fig. 5 illustrates the electrical characteristics of a typical two-turn cavity-mounted helical antenna. The aperture used in this unit was .6λ square at $Fn=1$ and was not covered with a radome.

While pattern beamwidth and axial ratio bandwidths are dependent upon exact performance requirements, the antenna shown here is considered to have a useful bandwidth of 1.7:1 with half-power beamwidths between 80 degrees and 50 degrees, on-axis axial ratios below 4 db, and negligible pattern tilt. This example does not illustrate the best results obtained; however, improved performance usually results in slightly reduced bandwidths in the order of 1.6:1 or 1.5:1.

Impedance bandwidths are determined by the allowable vswr requirements and also by the type of coax to helix transition used. Smith Chart impedance plots for antennas with two types of transitions are shown in Fig. 6. If an impedance compensated transition is used, a very good impedance match to 50 ohms can be obtained without excessive difficulty, as shown in Fig. 6(a). This particular antenna had vswr values generally below 1.2:1 over nearly a 1.6:1 bandwidth. Fig. 6(b) shows that the tapered, constant impedance

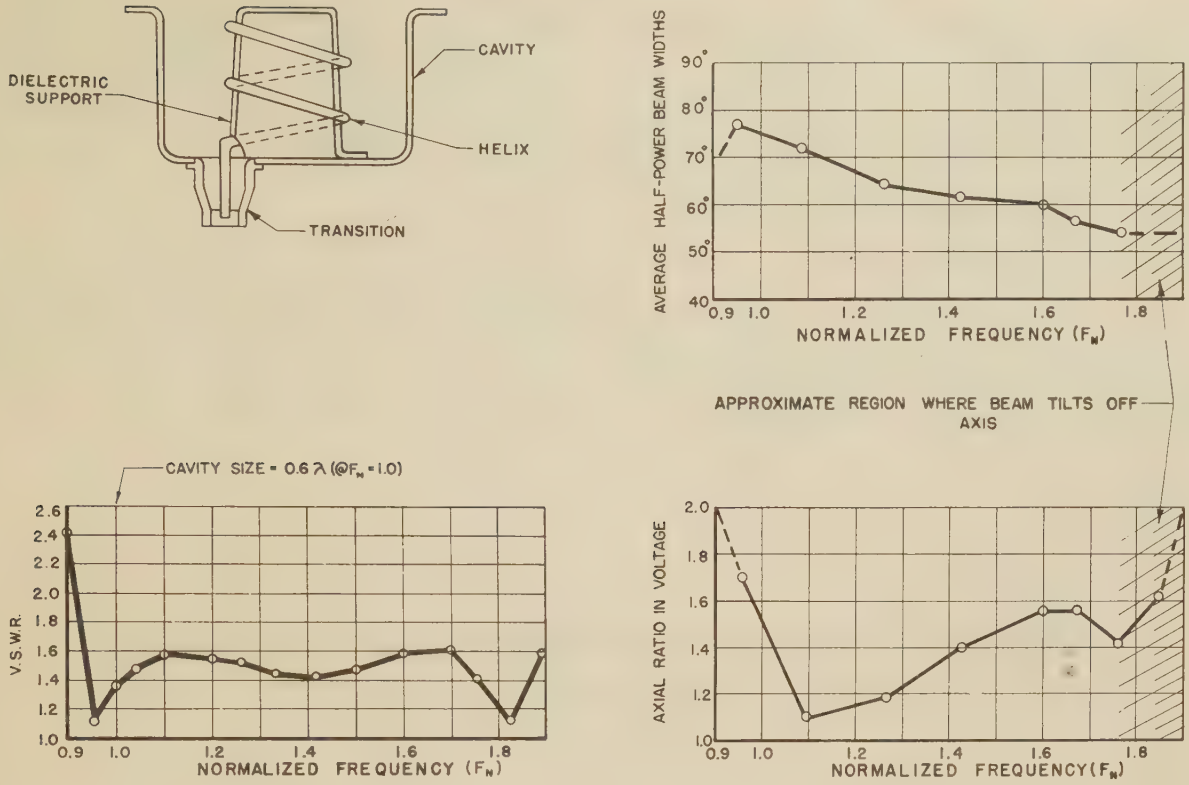

Fig. 5—A typical two-turn cavity mounted helical antenna and its performance characteristics.

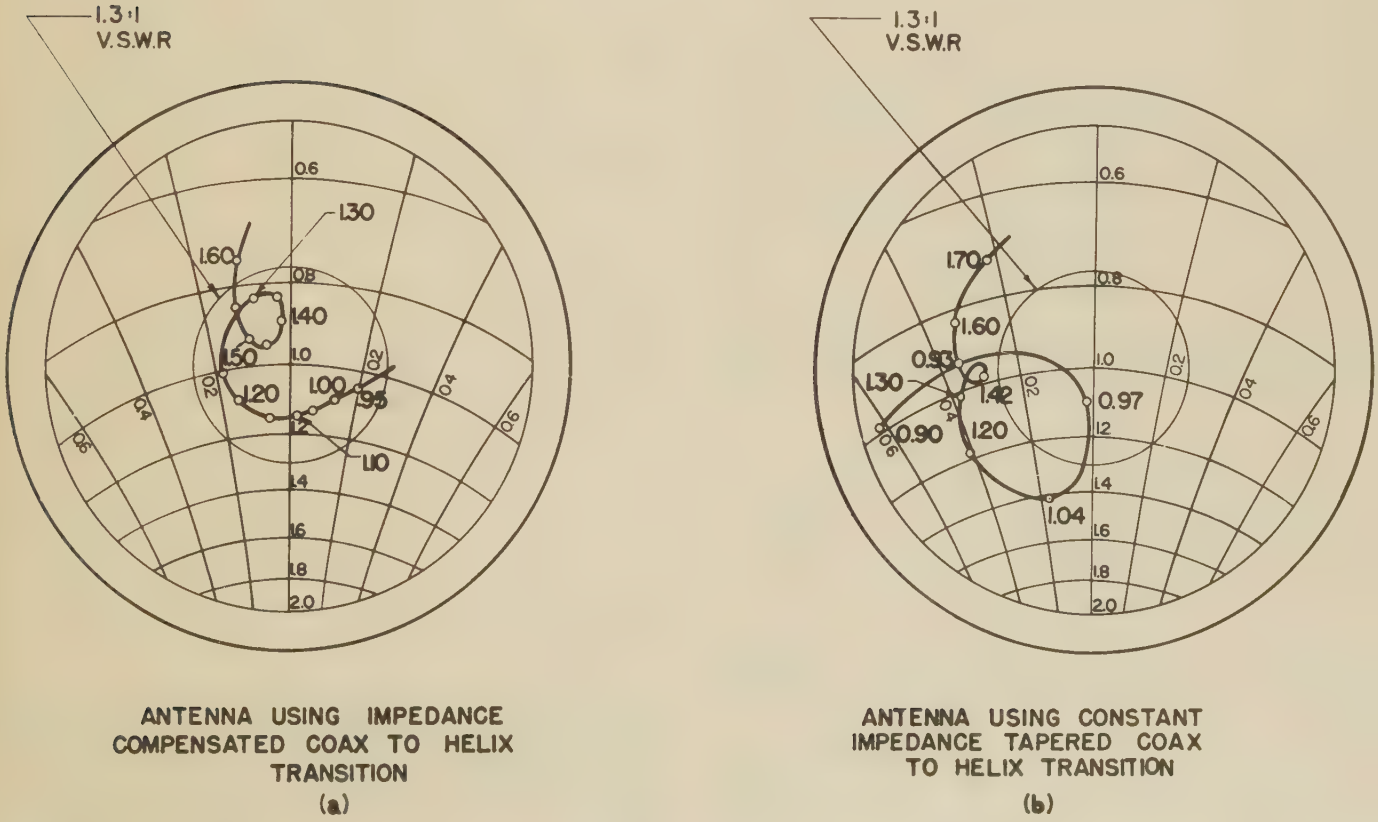

ANTENNA USING IMPEDANCE COMPENSATED COAX TO HELIX TRANSITION
(a)

ANTENNA USING CONSTANT IMPEDANCE TAPERED COAX TO HELIX TRANSITION
(b)

Fig. 6—Typical Smith Chart impedance plots for two-turn cavity mounted helical antennas. Numbers on Smith Charts are normalized frequency (F_N) cavity size 0.6λ (square) @ $F_N = 1.0$.

transition provides a reasonable match to 50 ohms without any special impedance compensation.

High altitude and rf power tests have shown the two-turn cavity mounted helix to be well suited to transmitting applications. The maximum voltage gradient measured on the helix conductor did not exceed the gradient in 50 ohm air-filled coaxial line with a center conductor equivalent to the helix conductor.

Conclusion

The cavity mounted helical antenna can be a useful addition to the antenna field in applications requiring relatively small, broadband, elliptically-polarized antennas which can be flush mounted on high speed aircraft. The antenna design lends itself to scaling for operation in a wide choice of frequency bands and applications ranging from simple receiving to high-powered transmitting antennas.

Acknowledgment

The authors wish to acknowledge the included work of J. D. Kelly, T. G. Dalby, and other members of the antenna laboratory at the Boeing Airplane Company, as well as the interest and guidance of F. W. Bushman in the preparation of this paper.

Radiation Patterns of Unsymmetrically Fed Prolate Spheroidal Antennas*

H. A. MYERS†

Summary—**This paper describes the radiation pattern of the unsymmetrically-fed prolate spheroidal transmitting antenna. Maxwell's equations are solved in prolate spheroidal coordinates subject to the boundary conditions. The prolate spheroidal functions are expressed in the form of power series and Laurent series. Radiation patterns have been obtained for antennas of three different lengths up to about one wavelength long, for length/thickness ratios of about 5/1, 10/1, 22/1, and 316/1, and for nine unsymmetrical gap locations as well as for the symmetrically-fed cases. It was found that the two most important factors affecting the radiation pattern of a fairly thin antenna were the location of the gap and the electrical length. For antennas less than a half wavelength long, the pattern was the usual symmetrical figure eight and was essentially independent of the location of the gap (except for magnitude changes due to the different gap impedances). For antennas two-thirds to three-quarters of a wavelength long the figure eight patterns could be "bent" in the direction of the longer element, and for antennas one wavelength long or longer minor lobes began to appear.**

Introduction

THE PROBLEM of the forced oscillations of a prolate spheroid was first considered by Page and Adams,[1] who treated the case of the thin spheroid driven by a plane wave whose electric field was parallel to the major axis. This would correspond to the case of the receiving antenna with its gap or feed point shorted out. Some of the ideas used here in constructing radial spheroidal functions were first presented by Page and Adams.

Chu and Stratton[2] attacked the case of the center-fed prolate spheroidal transmitting antenna by different methods and obtained curves from which the impedance at the gap can be estimated. The basic electromagnetic theory used in this paper follows the analysis of Chu and Stratton as elaborated by Schelkunoff.[3]

R. M. Ryder[4] extended the work of Page and Adams by investigating the behavior of the harmonics due to forced oscillations by perturbation methods. In a second and third paper, Page[5] treated the more general vector wave equation and extended his previous results for the thin receiving antenna.

The problem of determining the current distribution and impedance of an unsymmetrically driven cylindrical antenna was formulated by Ronold King,[6] who made use of an integral equation which he solved by the method of successive approximations to obtain general expressions for the current and impedance. He was able to find a simple approximate expression for the impedance of the unsymmetrically driven antenna involving a series combination of the known impedances of symmetrically driven antennas. The impedance and current distribution for a cylindrical antenna of length $3\lambda/4$

* Manuscript received by PGAP, May 9, 1955; revised manuscript received September 8, 1955.

This paper is an extract from a Ph.D. thesis submitted at Michigan State College. The work was done under a U. S. Signal Corps Contract.

† Electronics Div., The Rand Corp., Santa Monica, Calif.

[1] L. Page and N. I. Adams, "The electrical oscillations of a prolate spheroid, I," *Phys. Rev.*, vol. 53, pp. 819–831; May 15, 1938.

[2] L. J. Chu and J. A. Stratton, "Forced oscillations of a prolate spheroid," *J. Appl. Phys.*, vol. 12, pp. 241–248; March, 1941.

[3] S. A. Schelkunoff, "Advanced Antenna Theory," John Wiley and Sons, New York, pp. 111–125; 1952.

[4] R. M. Ryder, "The electrical oscillations of a perfectly conducting prolate spheroid," *J. Appl. Phys.*, vol. 13, pp. 327–343; May, 1942.

[5] L. Page, "The electrical oscillations of a prolate spheroid, II and III," *Phys. Rev.*, vol. 65, pp. 98–117; February 1 and 15, 1944.

[6] Ronold King, "Asymmetrically driven antennas and the sleeve dipole," Technical Report No. 93 for Office of Naval Research, Cruft Lab., Harvard; 1949.

driven $\lambda/4$ from one end were evaluated and the broadband properties were discussed.

The theory and tables of prolate spheroidal functions were first published by Stratton, Morse, Chu, and Hutner,[7] hereafter referred to as Stratton *et al.* The equations they solved were more general than the Maxwell equations in spheroidal coordinates in that they include the latter as a special case. This work was extended by Spence[8] and most recently by Hatcher.[9] Many of the values for the norms and the radial functions used in this paper were taken from the tables worked out by Spence and Hatcher.

The particular problem studied in this paper is the unsymmetrically-fed prolate spheroidal transmitting antenna. Radiation patterns have been obtained for antennas of three different lengths up to about one wavelength long, for length/thickness ratios of about 5/1, 10/1, 22/1, and 316/1, and for nine unsymmetrical gap locations as well as for the symmetrically-fed cases.

The prolate spheroidal configuration was chosen for the following reasons. The integral equations for the cylindrical antenna are very complicated and a large amount of computing is required to find even a first approximation to the solution. Moreover, the approximation involved in replacing the cylinder by the spheroid is probably better than the approximations one must use in solving the integral equation.[10] In addition, prolate spheroids are good approximations to the bodies of missiles and so have a physical counterpart in their own right. The problem of end effects which enters the cylindrical antenna and is of considerable importance is eliminated by going to the prolate spheroid. Also, by eliminating these end effects, more attention can be given to the unsymmetrical effects and the spheroidal functions themselves.

Analysis

The prolate spheroidal coordinate system is shown in Fig. 1. The radial and angular variables are taken as u, v, and ϕ, and the development of Maxwell's equations follows that of Schelkunoff's.[11] Thus the equations to be solved are:

$$(u^2 - 1)\frac{d^2U}{du^2} + (c^2u^2 - k)U = 0 \tag{1}$$

and

$$(1 - v^2)\frac{d^2V}{dv^2} + (k - c^2v^2)V = 0, \tag{2}$$

subject to the boundary conditions

$$U_k(u) \sim \epsilon^{-icu} \text{ as } u \to \infty, \tag{3}$$

and

$$V_k(\pm 1) = 0. \tag{4}$$

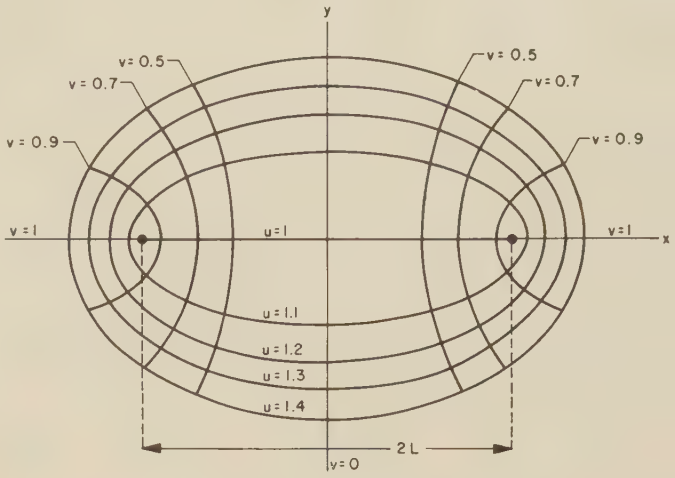

Fig. 1—The prolate spheroidal coordinate system.

The auxiliary wave function A which can be made to satisfy the boundary conditions on the surface of the spheroid by the proper choice of values for the a_ν is, after Schelkunoff,

$$A = \sum_{\nu=0}^{\infty} a_\nu U_{k\nu}(u)V_{k\nu}(v). \tag{5}$$

If the gap or feed point is small compared with the length of the antenna and the applied field is assumed to be concentrated in the gap, the expression for the a_ν is[12]

$$a_\nu = \frac{\beta L V_{k\nu}(v_0)}{i\eta N_\nu U_{k\nu}'(u_0)} V^a, \tag{6}$$

where $\beta = 2\pi/\lambda$, L is the semifocal distance, v_0 is the value of the angular variable at the center of the gap, V^a is the magnitude of the voltage applied at the gap, $i = \sqrt{-1}$, η is the impedance of free space, $U_{k\nu}'(u_0)$ is the derivative of the radial function evaluated at $u = u_0$ (the value of the radial variable at the surface of the antenna), and N_ν is the normalizing factor (norm)[13]

$$N_\nu = \int_{-1}^{1} (1 - v^2)^{-1} V_{k\nu}^2(v)dv. \tag{7}$$

Further analysis[14] indicates that larger gap widths and different methods of feeding the antenna yield only slightly different values for the a_ν; the effect of these variations is negligible insofar as the radiation patterns are concerned.

[7] J. A. Stratton, P. M. Morse, L. J. Chu, R. A. Hutner, "Elliptic Cylinder and Spheroidal Wave Functions," John Wiley and Sons, New York; 1941.

[8] R. D. Spence, "The scattering of sound from prolate spheroids," Final Report, Office of Naval Research, NONR-02400; 1951.

[9] E. C. Hatcher, Jr., "Radiation of a point dipole located at the tip of a prolate spheroid," *J. Appl. Phys.*, vol. 25, pp. 1250–1253; October, 1954.

[10] R. M. Ryder, "The electrical oscillations of a perfectly conducting prolate spheroid," *J. Appl. Phys.*, vol. 13, p. 327; May, 1942.

[11] S. A. Schelkunoff, "Advanced Antenna Theory," John Wiley and Sons, New York, p. 111; 1952.

[12] *Ibid.*, p. 116.

[13] *Ibid.*, p. 115.

[14] H. A. Myers, "The unsymmetrically fed prolate spheroidal antenna," Ph.D. thesis, Michigan State College, 1954.

The solution of (2) was taken in the form of a power series:

$$V_k(v) = \sum_{n=0,1}^{\infty}{}' c_n v^n. \tag{8}$$

The c_n satisfy the following recursion formula:

$$-(n+2)(n+1)c_{n+2} + [n(n-1) - k]c_n + c^2 c_{n-2} = 0, \tag{9}$$

where $c = \beta L$, and the prime on the summation indicates that the sum is taken over the c's with even subscripts if n starts with zero, and over the odd subscripts if n starts with one. The values of the separation constant k_r used in this paper were taken from the eleven place tables recently computed by the Bureau of Standards.

The solution of the radial (1) can be expressed in many ways. One expression for $U_k(u)$ which satisfies the boundary condition, (3), is

$$U_k(u) = \epsilon^{-icu} \sum_{n=0}^{\infty} a_n (iu)^{-n}, \qquad a_0 = 1. \tag{10}$$

The argument in the power series was taken as (iu) so that the a_n would all be real. Substitution of this expression in (1) leads to the recursion formula for the a_n:

$$2c(n+1)a_{n+1} + [(n+1)n + c^2 - k]a_n + 2c(n-1)a_{n-1} + (n-1)(n-2)a_{n-2} = 0. \tag{11}$$

McCrea and Newing[15] have proven the existence of series solutions satisfying the boundary conditions for the generalized spheroidal wave equation, and therefore (10) can converge and represent $U_k(u)$ for $|u| \geqq 1$. Computations indicated that the series did, in fact, converge if and only if $k = k_r$, where k_r is one of the eigenvalues of the differential equation.

For thin antennas it is necessary to evaluate the radial functions $U_k(u)$ for values of u_0 in the neighborhood of one, and this is just the region for which the convergence of (10) is very slow. One form of $U_k(u)$ which does converge rapidly was taken as

$$U_k(u) = U^{(1)} + U^{(2)} \tag{12}$$

where

$$U^{(1)} = \sum_{n=0}^{\infty} b_n (u^{2-1})^{n+1} \tag{13}$$

and

$$U^{(2)} = U^{(1)} \ln (u^2 - 1) + \sum_{n=0}^{\infty} d_n (u^2 - 1)^n. \tag{14}$$

[15] W. H. McCrea, and R. A. Newing, "Boundary conditions for the wave equation," *Proc., London Math. Soc.*, vol. 37, pp. 520–534; 1934.

Unfortunately, this expression for $U_k(u)$ cannot be conveniently expanded in powers of u in order to correlate it with (10), which satisfies the boundary condition at infinity.

Still another expression for $U_k(u)$ is the Laurent series

$$U_k(u) = \sum_{n=-\infty}^{+\infty} f_n u^n. \tag{15}$$

The series of terms with positive exponents converges rapidly in the neighborhood of $u = 1$, but the series of terms with negative exponents converges too slowly for computational purposes. However, this difficulty was avoided by picking the series with negative exponents out of the $U^{(1)} \ln(u^2 - 1)$ term of (14). Thus

$$\ln (u^2 - 1) = \ln \frac{(u-1)}{(u+1)} + 2 \ln (u+1) \tag{16}$$

and

$$\ln \frac{(u-1)}{(u+1)}$$

can be expanded in powers of u with negative exponents. Following this line of reasoning, the complete expression for $U_k(u)$ for $k_0, k_2, k_4, \cdots$ can be written as

$$U_k(u) = A \sum_{n=0}^{\infty}{}' c_n u^n + \sum_{n=1}^{\infty}{}' c_n u^n + B\left(\sum_{n=0}^{\infty}{}' c_n u^n \ln \frac{u-1}{u+1} + 2 \sum_{n=1}^{\infty}{}' D_n u^n \right). \tag{17}$$

The first term in (17) is actually $V_k(v)$, as can be seen from (8); c_0 is taken as unity, for convenience. The constants $A, c_1, c_3, c_5, \cdots, B$, and $D_1, D_3, D_5, \cdots$ are obtained and checked by comparing coefficients of like powers of u in (17) and (10).

To obtain the derivative of the radial function $U_k'(u)$, it is only necessary to differentiate each term in (17). Since the constants have already been determined, only the derived series need be summed again because of the factor of n that was introduced by the differentiation.

The radial functions for the k's with odd subscripts are computed in exactly the same way, the only difference being that the summation over the odd powers in the previous case are now taken over the even powers, and *vice-versa*. Thus, for k_1, k_3, k_5, etc.,

$$U(u) = A \sum_{n=1}^{\infty}{}' c_n u^n + \sum_{n=0}^{\infty}{}' c_n u^n + B\left(\sum_{n=1}^{\infty}{}' c_n u^n \ln \frac{u-1}{u+1} + 2 \sum_{n=0}^{\infty}{}' D_n u^n \right). \tag{18}$$

In this case, c_1 is taken as unity, and the constants $A, c_0, c_2, c_4, \cdots, B$, and $D_0, D_2, D_4, \cdots$ are obtained in the same manner as before.

Finally, if a sufficient number of significant figures have been retained in the computation of the radial function and its derivative, a good check on the accuracy of $U_k(u)$ and $U_k'(u)$ can be obtained by the use of the Wronskian. If one writes

$$U_k(u) = U_1 + U_2 \tag{19}$$

where U_1 is the real part and U_2 is the imaginary part, including the i, substitution of U_1 and U_2 into (1), multiplying the first by U_2 and the second by U_1, and subtracting the two resulting equations leads to

$$U_2U_1'' - U_1U_2'' = 0, \tag{20}$$

or, equivalently,

$$U_1'U_2 - U_1U_2' = C, \tag{21}$$

where C is a constant that can be determined from the behavior of the radial function at infinity. Thus, as u approaches infinity

$$U_1 \sim \cos(cu), \qquad U_2 \sim -i \sin(cu)$$
$$U_1' \sim -c \sin(cu), \qquad U_2' \sim -ic \cos(cu),$$

and therefore

$$U_1'U_2 - U_1U_2' = ic, \tag{22}$$

which is the simple condition that the calculated values of the radial functions and their derivatives must satisfy.

Radiation Patterns

Once the spheroidal functions have been evaluated, it is a simple matter to compute the coefficients a_r in (6) and then the auxiliary wave function A of (5). From Schelkunoff[16] the expression for H_θ is

$$H_\phi = \frac{1}{L}\left[(u^2 - 1)(1 - v^2)\right]^{-1/2}A. \tag{23}$$

The mean intensity of energy flow in the far zone is

$$S = \frac{\eta}{2} H_\phi \tilde{H}_\phi. \quad \tilde{H}_\phi \text{ is the complex conjugate of } H_\phi. \tag{24}$$

For convenience in computation, $2r^2\eta S'$ was actually plotted, and so to obtain a numerical value for the radiation intensity for a particular antenna in a given direction, one must divide the plotted value by $240\pi r^2$ (for free space), where r is the distance from the center of the spheroid, and multiply by the voltage at the gap squared, since the applied voltage was taken as unity for these patterns. The units for S will then be in watts per square meter.

As can be seen from the curves, the radiation patterns vary with the width of the antenna, the electrical length, and the location of the gap. For the thicker antennas the derivatives of the radial functions are not as large, other parameters held constant, and so the higher order a_r, are somewhat larger, and therefore the unsymmetrical effects are slightly greater. This effect is most easily seen for the case $c=2$, in which the radiation patterns are plotted for three rather widely varying L/D ratios—10/1 ($u_0=1.005$), 22/1 ($u_0=1.001$), and 316/1 ($u_0=1.00001$). Fig. 2 shows the relative shapes of the antennas. Fig. 3 shows the gap locations.

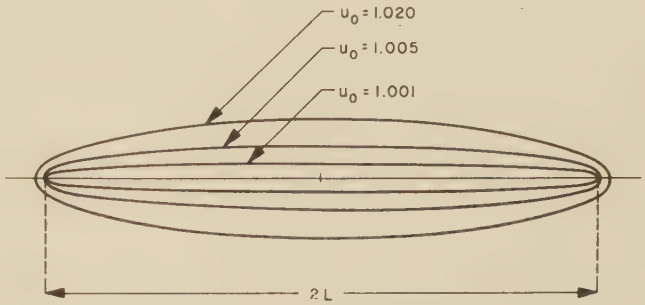

Fig. 2—Prolate spheroids.

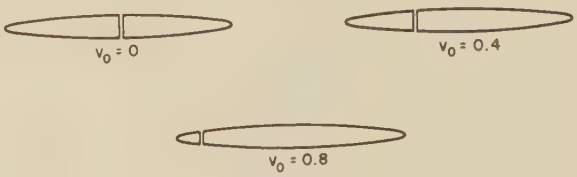

Fig. 3—Gap locations ($\mu_0=1.005$).

As the antennas become longer electrically, the unsymmetrical effects are more pronounced. Thus, for $c=1$[17] (Fig. 4) the unsymmetrical effect is negligible for almost any gap location, whereas for $c=2$ (Fig. 5) it becomes quite noticeable, and for $c=3$ (Fig. 6, p. 64) it is very pronounced, with small lobes also occurring for the unsymmetrical feeds. For a further investigation the most interesting cases would occur between $c=2$ and $c=3$ in that for certain gap locations these cases would produce the most unsymmetrical patterns with negligible spurious lobes. These patterns could be obtained relatively easily, because convergence of series for A, (5), is very good in the far zone.

The location of the gap, of course, contributes greatly to the asymmetry of the radiation pattern. The size of the radiation pattern is an indication of the impedance at the gap, because the same voltage was assumed in every case. Thus, for locations near one end of the antenna the impedance is higher, and therefore the current and the radiated power are lower.

[16] Schelkunoff, *op. cit.*, p. 113.

[17] c is defined such that the interfocal length is $c\lambda/\pi$. The distance of the gap from the center is V_0L, where L is the semifocal distance.

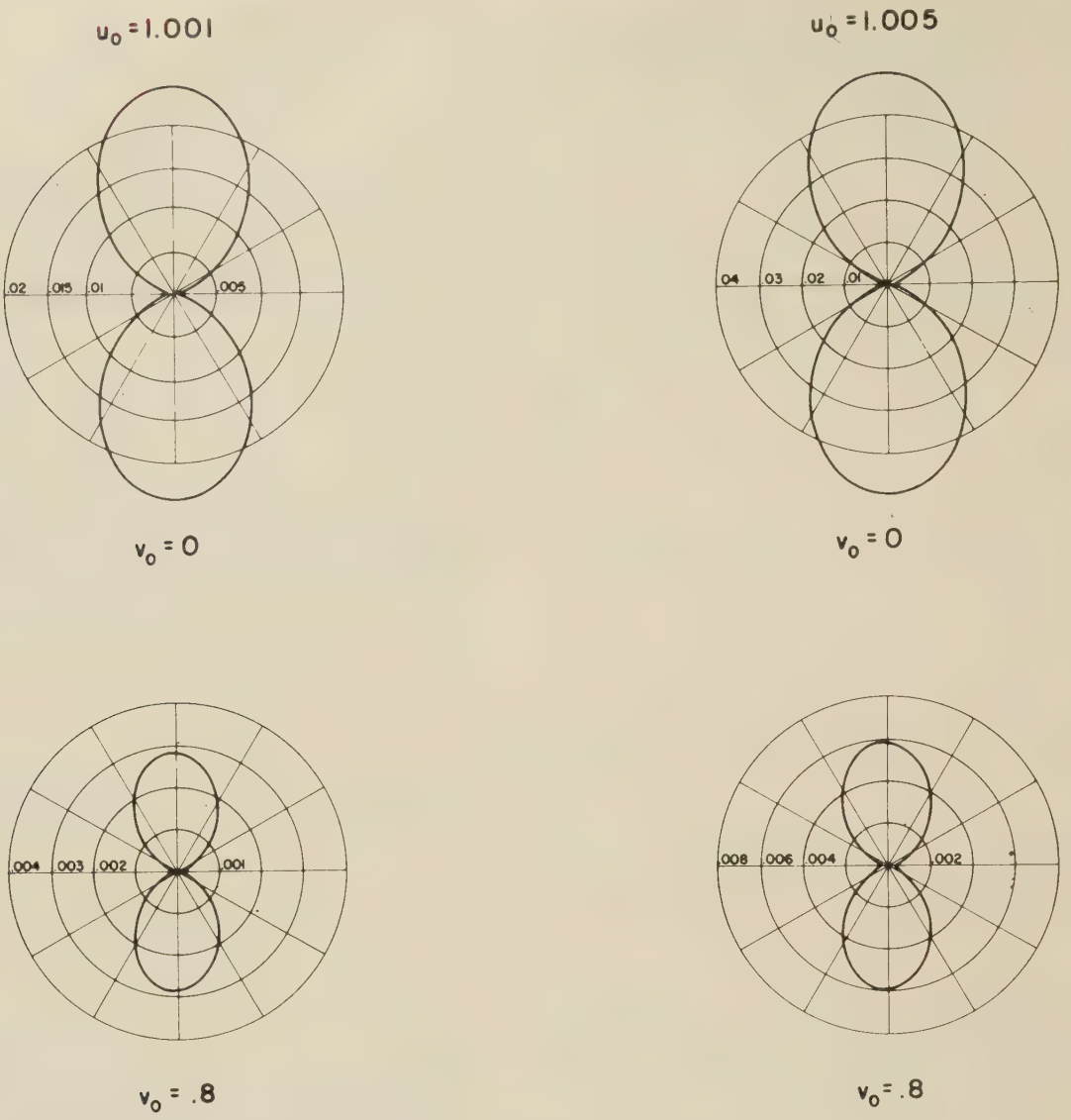

Fig. 4—Radiation patterns: $c = \beta L = 1 \left(2L = \frac{1}{\pi}\lambda\right)$.

Conclusions

The angular functions of the wave equation in prolate spheroidal coordinates were obtained in the form of a power series expanded about the origin. This form has the following advantages: 1) The angular functions have a simple recursion formula and are therefore easily computed. 2) The functions can be easily evaluated for any value of the variable, in contrast to angular functions that depend upon tables of associated Legendre polynomials. 3) If the applied field can be expressed in any of a number of simple closed forms, use of the orthogonality properties leads to an integral expression for the coefficients in the series expansion of the solution [the a_r of (6)] that can be evaluated by elementary methods. The disadvantage of the power series representation is that the norms are not as easily computed as they are by other methods.

The radial functions were obtained in the form of a Laurent series. This method is valuable in that it furnishes an independent check on the values of the radial functions obtained by other methods. In addition, there is a complete check at almost every step of the computations. A disadvantage is that, in its present form, it is not convenient for computation of radial functions for a large number of L/D ratios for the same c and ν values. However, usually only two or three different L/D ratios are required, and the computation of radial functions for extra L/D values would require only a small fraction of the time spent in computing the radial constants.

Radiation patterns have been obtained for antennas of three different lengths up to about one wavelength long, for length/thickness ratios of about 5/1, 10/1, 22/1, and 316/1, and for nine unsymmetrical gap loca-

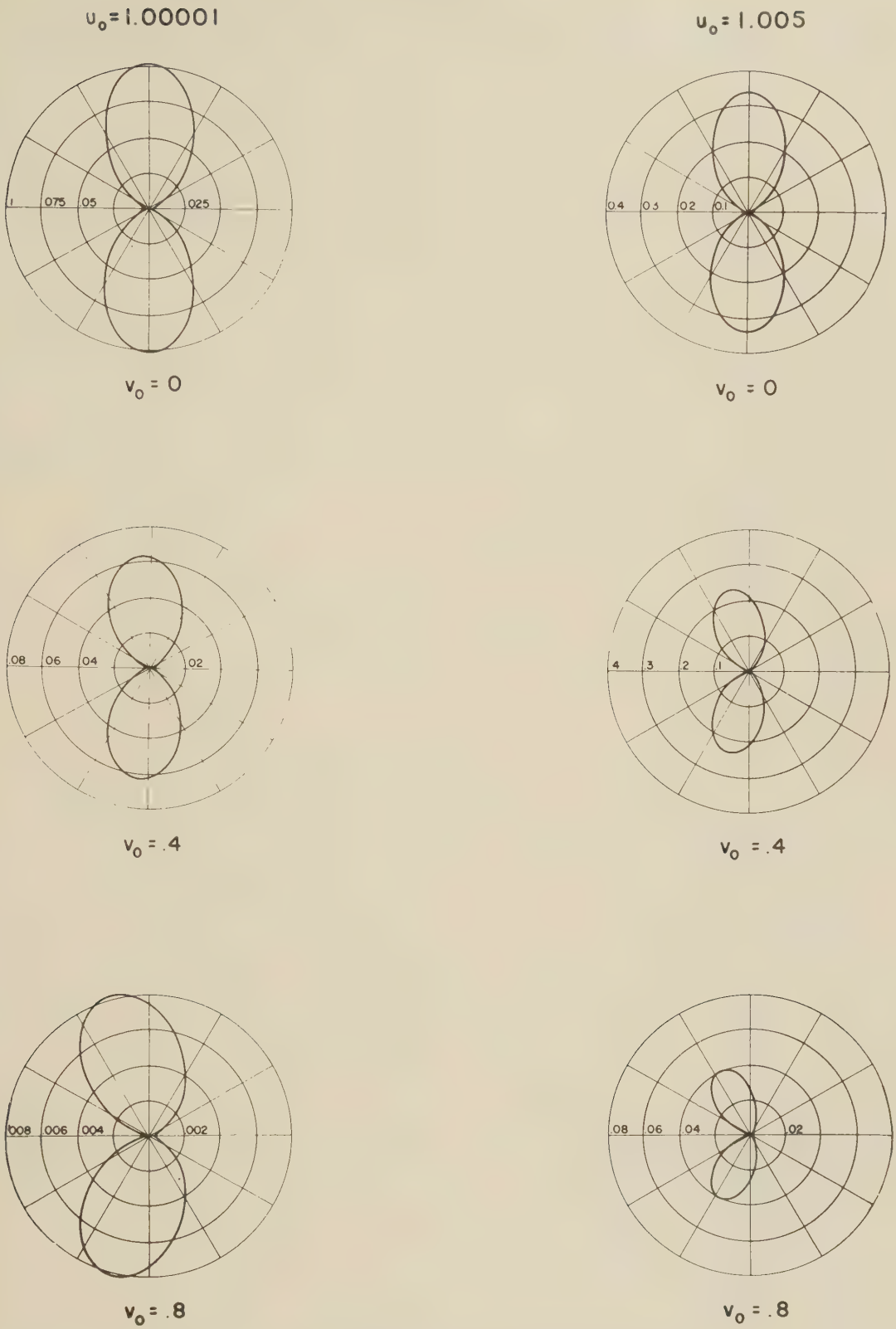

Fig. 5—Radiation patterns: $c = \beta L = 2\left(2L = \frac{2}{\pi}\lambda\right)$.

tions as well as for the symmetrically-fed cases. It was found that the radiation patterns depended primarily on the frequency of the source and the gap location. The tables for the angular and radial functions and their related constants will be included in a forthcoming report for the Office of Ordnance Research.

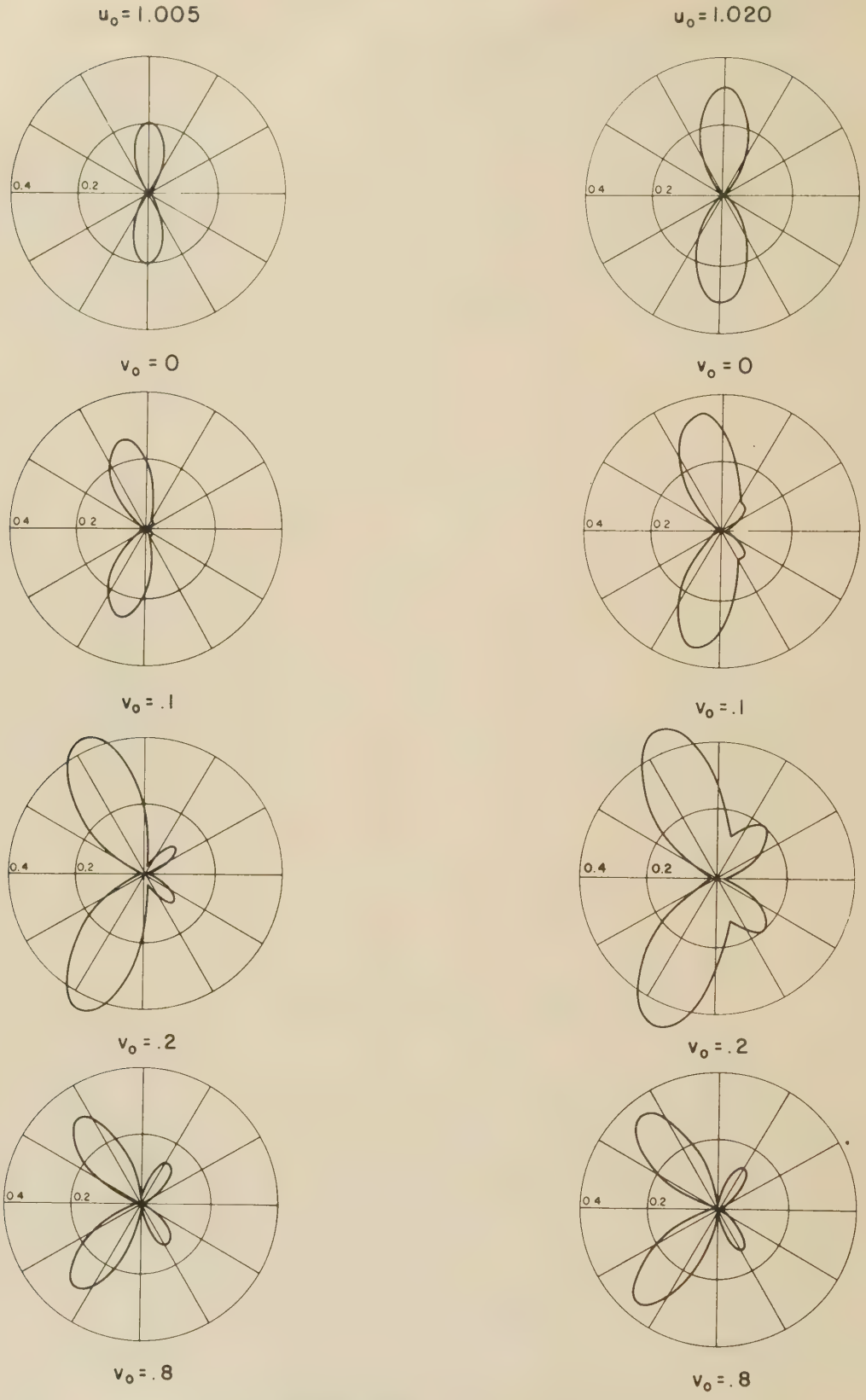

Fig. 6—Radiation patterns: $c = \beta L = 3\left(2L = \frac{3}{\pi}\lambda\right)$.

Acknowledgment

The author wishes to express his sincere thanks to Professor C. P. Wells of Michigan State College, East Lansing, Michigan, for his help and encouragement in the execution of this work, and to the Office of Ordnance Research for the financial support which made it possible to complete this investigation.

Optical Fresnel-Zone Gain of a Rectangular Aperture*

CHARLES POLK†

Summary—**An equation for the on-axis gain of a uniformly illuminated rectangular aperture is derived which is valid in the "Optical Fresnel Zone." This equation is formulated in terms of the ordinary radiation field gain multiplied by a correction factor which depends upon the aperture dimensions and the distance, R, from the aperture at which the gain is measured. A table of the function $[C^2(v)+S(v)]/v^2$ is given; $C(v)$ and $S(v)$ being the Fresnel integrals. The gain of a square aperture ($L\times L$ meters) in the Fresnel-zone region is compared with the gain of a circular aperture and it is shown that for apertures of equal area $G_{\text{square}}<G_{\text{circle}}$ when $(L^2/\lambda)<R\leq(2L^2/\lambda)$; it is also shown that G_{square} has minima, but not zeros at $R=L^2/7.30\lambda$, $R=L^2/15.24\lambda$. Furthermore it is shown that for $R\geq L^2/2\lambda$ the first order gain correction factor of a square aperture is equal to the gain correction factor of a circular aperture having a diameter equal to 1.208 times the sidelength of the square. An approximate formula for the Fresnel-zone gain of a long and narrow aperture is also given.**

Introduction

BASED UPON scalar diffraction theory the Fresnel-zone or "Quasi-Fraunhofer" gain of a uniformly illuminated circular aperture has been given by Silver[1]; his result has been extended to certain types of tapered illumination by Yang.[2] As far as the author knows, corresponding results have never been published for a rectangular aperture.

The problem is of importance when one desires to perform antenna gain measurements at distances, R, shorter than indicated by the usual far-field limit $R\geq 2L^2/\lambda$; L being the largest linear dimension of the aperture and λ the wavelength. The results are also applicable in certain radio interference problems where the field intensity in the Fresnel region is of interest.

The present paper considers only the uniformly illuminated aperture having zero phase-error. It will be shown that the Fresnel gain correction factor for such a rectangular aperture differs significantly from the corresponding simple $(\sin x/x)^2$ factor of a circular aperture even if the aperture is a square. This is particularly true at distances d such that the $(\sin x/x)^2$ factor would predict zero gain.

For reference and comparison with the result given in the next section, the Fresnel-zone gain of a circular aperture is quoted from Silver[1]

$$G = G_0\left(\frac{\sin x}{x}\right)^2 \tag{1}$$

where

G_0 = true Frauenhofer gain
$x = ka^2/4R$
$k = 2\pi/\lambda$
a = radius of circular aperture.

Mathematical Derivation

In terms of the symbols defined in Appendix II and on the basis of scalar diffraction theory the field at a point P, due to the aperture shown in Fig. 1, is given[3] by

$$U_p = \frac{1}{4\pi}\int_A P(\xi,\eta)\frac{e^{-jkr}}{r} \cdot \left\{\left(jk+\frac{1}{r}\right)\bar{\imath}_z\cdot\bar{r}_1 + jk\bar{\imath}_z\cdot\bar{s}\right\} d\xi d\eta. \tag{2}$$

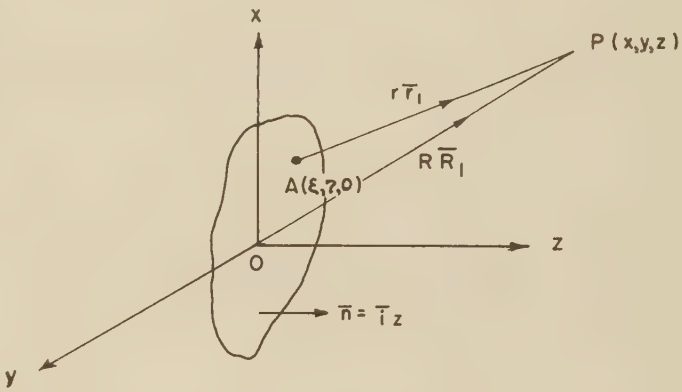

Fig. 1—Coordinate system.

The following approximations are made when the field in the optical-Fresnel zone is to be computed:

1) $(1/r)\ll k$.
2) The variation of $\bar{\imath}_z\cdot\bar{r}_1$ over the aperture is neglected, we use $\bar{\imath}_z\cdot\bar{r}_1\approx\bar{\imath}_z\cdot R_1$.
3) As different points on the aperture are considered the change in the value of $1/r$ outside the bracket in (2) is neglected. We let $(1/r)\approx(1/R)$.
4) In the phase term $\exp(-jkr)$ we note that

$$r = [(x-\xi)^2+(y-\eta)^2+z^2]^{1/2}$$

and for $z\gg|x-\xi|$, $|y-\eta|$ we write

$$r \approx z + \frac{(x-\xi)^2}{2z} + \frac{(y-\eta)^2}{2z} = z + r_a. \tag{3}$$

The approximation indicated by (3) differentiates the Fresnel field from the Fraunhofer field. In the analysis of the latter, one generally neglects all terms above the

* Manuscript received by the PGAP, July 30, 1955. This work has been made possible by the support of the U. S. Air Force's Air Research and Development Command, Rome Air Development Center, under Contract AF 30(602)-583.

† Moore School of Elec. Engrg. Univ. of Pennsylvania, Philadelphia, Pa.

[1] S. Silver, "Microwave antenna theory and design," M.I.T. Rad. Lab. Ser., vol. 12, McGraw-Hill Book Co., Inc., New York, N. Y., p. 199; 1949.

[2] R. F. H. Yang, "Quasi-Fraunhofer gain of parabolic antennas," Proc. I.R.E., vol. 43, p. 486; April, 1955.

[3] S. Silver, *op. cit.*, p. 170.

first order in ξ and η; thus, still employing rectangular coordinates, one would write for the Fraunhofer field.[4]

$$r \approx R - \left[\left(\frac{x}{R}\right)\xi + \left(\frac{y}{R}\right)\eta\right] \qquad (4)$$
$$R = [x^2 + y^2 + z^2]^{1/2}.$$

Eq. (2) reduces for the Fresnel region to

$$U_p = \frac{j}{2\lambda}\frac{e^{-jkz}}{R}\int_A F(\xi, \eta)e^{-jkr_a}(\cos\theta + \bar{i}_z\cdot\bar{s})d\xi d\eta. \qquad (5)$$

For uniform unit amplitude, $F(\xi, \eta) = 1$, and uniform phase, $\bar{i}_z\cdot\bar{s} = 1$, one obtains from (5)

$$U_p = \frac{j}{2\lambda}(\cos\theta + 1)\frac{e^{-jkz}}{R}\int_A e^{-jkr_a}d\xi d\eta. \qquad (6)$$

In particular, the expression for the field at a point P on the z axis is given, from (3) and (6), by

$$U_p = \frac{j}{\lambda}\frac{e^{-jkR}}{R}\int_{\xi=-L_1/2}^{\xi=L_1/2}\int_{\eta=-L_2/2}^{\eta=L_2/2} e^{-jk\xi^2/2R}e^{-jk\eta^2/2R}d\eta d\xi. \qquad (7)$$

Substituting $k = 2\pi/\lambda$ and $u = \xi\sqrt{\pi/R\lambda}$, $p = \eta\sqrt{\pi/R\lambda}$ and writing (7) as the product of two integrals, we obtain

$$U_p = \frac{j}{\pi}e^{-jkR}\int_{-u_0}^{u_0} e^{-ju^2}du\int_{-p_0}^{p_0} e^{-jp^2}dp. \qquad (8)$$

These integrals can be evaluated in terms of the Fresnel-integrals tabulated in Jahnke and Emde[5]; letting v and t be arbitrary variables, we write

$$C(v) = \int_0^v \cos\frac{\pi}{2}t^2dt \qquad (9)$$

$$S(v) = \int_0^v \sin\frac{\pi}{2}t^2dt. \qquad (10)$$

$C(v)$ and $S(v)$ are related to the integrals $\int \sin v^2dv$ and $\int \cos v^2dv$ by[6]

$$\int \cos v^2dv = \frac{\pi}{2}C\left(\sqrt{\frac{2}{\pi}}v\right) + \text{constant} \qquad (11)$$

$$\int \sin v^2dv = \frac{\pi}{2}S\left(\sqrt{\frac{2}{\pi}}v\right) + \text{constant}. \qquad (12)$$

We also note[7] that both $C(v)$ and $S(v)$ are odd functions: $C(-v) = -C(v)$. Thus

$$\int_{-v_0}^{+v_0}\cos v^2dv = \sqrt{2\pi}C\left(\sqrt{\frac{2}{\pi}}v_0\right) \qquad (13)$$

and similarly

$$\int_{-v_0}^{+v_0}\sin v^2dv = \sqrt{2\pi}S\left(\sqrt{\frac{2}{\pi}}v_0\right). \qquad (14)$$

Substituting (13) and (14) into (8) and defining $u_1 = u_0\sqrt{2/\pi} = L_1/\sqrt{2R\lambda}$ and $p_1 = L_2/\sqrt{2R\lambda}$ we obtain:

$$U_p = j2e^{-jkR}[C(u_1) - jS(u_1)][C(p_1) - jS(p_1)]. \qquad (15)$$

The square of the absolute value of U_p is

$$|U|^2 = 4[C^2(u_1) + S^2(u_1)][C^2(p_1) + S^2(p_1)]. \qquad (16)$$

This equation appears, in somewhat different notation, in Schelkunoff's "Electromagnetic Waves."[8]

The power transmitted per unit solid angle is given by

$$P = R^2|\bar{S}| \qquad (17)$$

where $\bar{S}$ is the Poynting vector. In free space and for steady-state sinusoidal time dependence

$$P = \sqrt{\frac{\epsilon}{\mu}}\frac{R^2}{2}|\bar{E}|^2. \qquad (18)$$

Consequently the power per unit solid angle on the z axis is given by (16) and (18) as

$$P_z = 2R^2\sqrt{\frac{\epsilon}{\mu}}[C^2(u_1) + S^2(u_1)][C^2(p_1) + S^2(p_1)]. \qquad (19)$$

The total power, W, radiated by the aperture is[9]

$$W = \frac{1}{2}\sqrt{\frac{\epsilon}{\mu}}A. \qquad (20)$$

The gain in the z direction is defined[10] as

$$G = \frac{4\pi P_z}{W}. \qquad (21)$$

Thus, for the rectangular aperture in the Fresnel-zone

$$G = \frac{16\pi R^2}{A}[C^2(u_1) + S^2(u_1)][C^2(p_1) + S^2(p_1)]. \qquad (22)$$

Noting that the gain in the Fraunhofer region is[11] $G_0 = 4\pi A/\lambda^2$, we divide (22) by $u_1^2p_1^2$ and obtain

$$G = G_0\frac{C^2(u_1) + S^2(u_1)}{u_1^2}\frac{C^2(p_1) + S^2(p_1)}{p_1^2} \qquad (23)$$

$$G = G_0M(u_1)M(p_1). \qquad (24)$$

The function $M(v) = [C^2(v) + S^2(v)]/v^2$ is plotted in Fig. 2 and given to four significant figures in Appendix I.

Approximation for $R \geq L^2/2\lambda$

Schelkunoff[7] gives the power-series expansions of the Fresnel-integrals $C(v)$ and $S(v)$. The first three terms of the two series are:

[4] Ming-Kuei Hu, "Study of near-zone fields of large aperture antennas," Interim rep. No. 1. October, 1954. Contract AF 30(602)–928. Syracuse Univ. Res. Inst., Elec. Engrg. Dept., Rep. No. EE282–55411, p. 6.

[5] E. Jahnke and F. Emde, "Tables of Functions with Formulae and Curves," Dover Publications, New York, Fourth Edition, p. 34; 1945.

[6] W. Grobner and N. Hofreiter, "Integraltafel, Erster Teil, Unbestimmte Integrale," Springer-Verlag, Vienna, p. 135; 1949.

[7] S. A. Schelkunoff, "Applied Mathematics for Engineers and Scientists," D. Van Nostrand Co., Inc., New York, p. 385; 1948.

[8] S. A. Schelkunoff, "Electromagnetic Waves," D. Van Nostrand Co., Inc., New York, p. 367; 1943.

[9] S. Silver, *op. cit.*, Eq. 17, pp. 177, 199.

[10] S. Silver, *ibid.*, p. 2.

[11] S. Silver, *ibid.*, p. 177.

$$C(v) = v - (\pi^2/40)v^5 + (\pi^4/3456)v^9 - \cdots \quad (25)$$

$$S(v) = (\pi/6)v^3 - (\pi^5/336)v^7 + (\pi^5/42240)v^{11} - \cdots . \quad (26)$$

If we take the square of first two terms of $C(v)$ and of first term of $S(v)$ and neglect all powers of v higher than v^6, we obtain following approximate expression

$$M(v) \approx 1 - 0.219v^4 + \cdots , \quad (27)$$

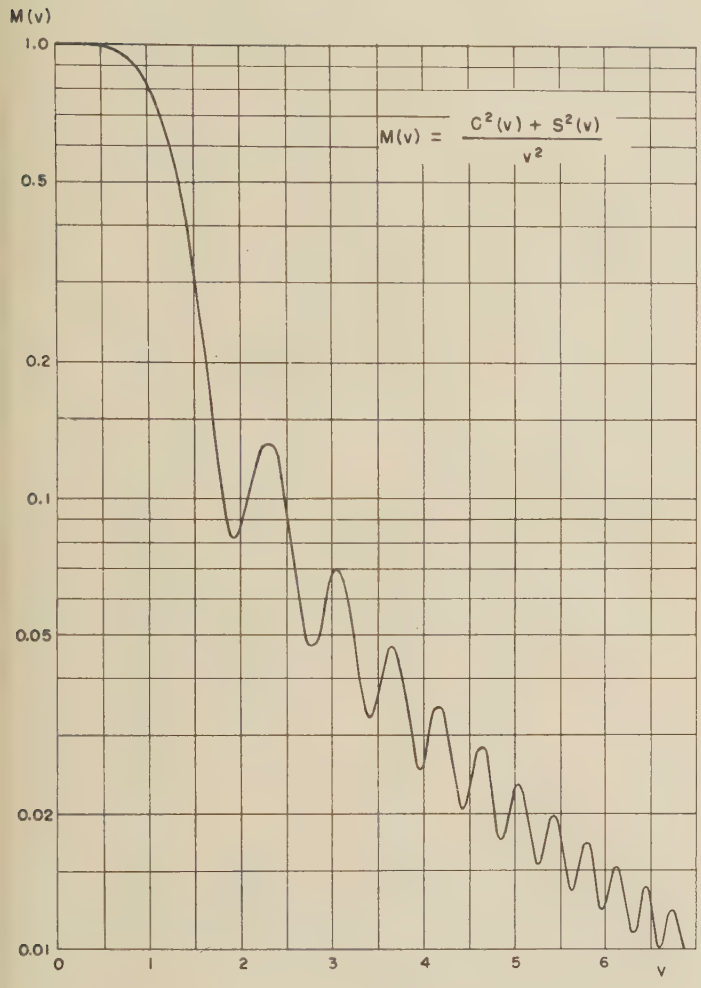

Fig. 2—The function $M(v) = \dfrac{C^2(v) + S^2(v)}{v^2}$.

Comparison with Table I shows that (27) represents a very good approximation of $M(v)$ for small v and gives $M(v)$ still to within 2.43 per cent when v is equal to 1.

It is interesting to note $v^2 = u_1^2 = p_1^2 = 1$ corresponds to a distance from aperture which is only one-fourth of usual far-zone field limit expressed by $R \geq 2L^2/\lambda$.

Comparison of Fresnel-Zone Gain of Square and Circular Apertures

For a square aperture $L_1 = L_2 = L$. Accordingly we let $u_1 = p_1 = v_1$ and (24) becomes

$$G_{sq} = G_0 M^2(v_1). \quad (28)$$

The corresponding equation for the circular aperture was

$$G_{cr} = G_0(\sin x/x)^2.$$

Comparing the gain correction factors for square and circular apertures having the same Fraunhofer gain, G_0, hence for apertures having the same area, we write

$$L^2 = \pi a^2$$

and substituting the value of a^2 thus determined into the expression for x given in the last paragraph of the introduction we obtain

$$x = \frac{L^2}{2R\lambda} . \quad (29)$$

For the square aperture

$$v_1^2 = \frac{L^2}{2R\lambda} . \quad (30)$$

Therefore the comparison of the gain-correction factors reduces to a comparison of $(\sin x/x)^2$ with $M^2(v_1)$. Both functions are plotted against $x = v_1^2$ in Fig. 3.

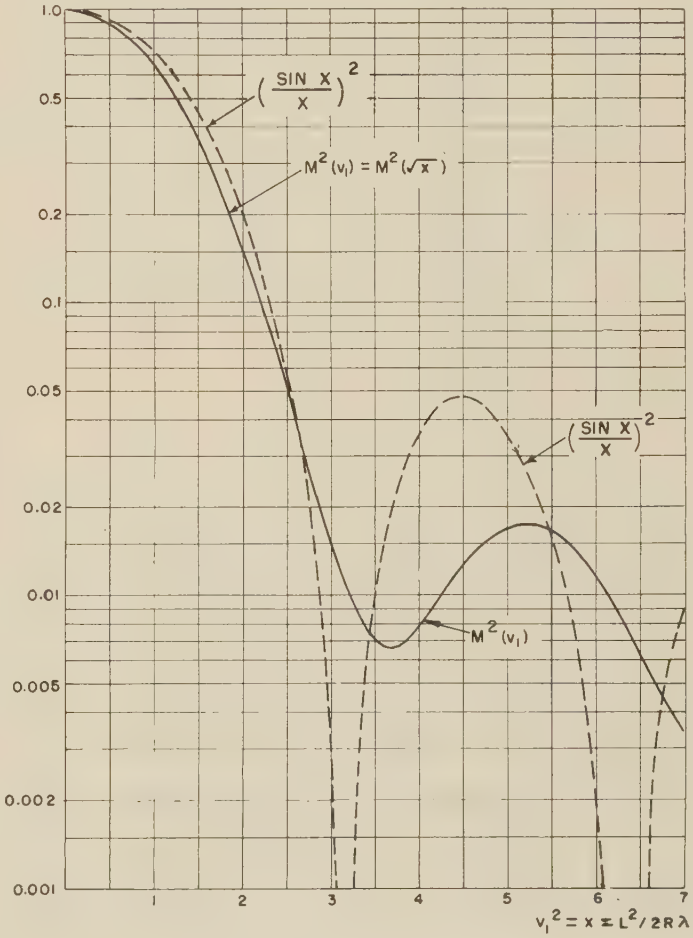

Fig. 3—Comparison of $\left(\dfrac{\sin x}{x}\right)^2$ with $M^2(\sqrt{x})$.

Two differences are immediately apparent:

1) Near the outer limit of the Fresnel-zone; *i.e.*, in the region $R > L^2/5.2\lambda$ or $x = v_1^2 < 2.6$ the correction for the square aperture leads to a smaller net gain than the correction for the circular aperture. This effect could have been predicted immediately by comparing the first two terms in the series for $M(v_1)$ and for $\sin x/x$:

$$v_1^2 = x \qquad M(v_1) \approx 1 - 0.219x^2 + \cdots \quad (31)$$

$$(\sin x/x) \approx 1 - 0.167x^2 + \cdots . \quad (32)$$

Using the exact values for the two functions from tables one obtains

$$v_1^2 = x \qquad M(v_1) \leqq (\sin x/x) \qquad x \leqq 2.6. \quad (33)$$

2) The gain correction factor for the circular aperture has zeros at $x = n\pi$ while the rectangular aperture has minima, but not zeros at $v_1^2 = x = 3.65, 7.62$.

The absence of sharp zeros in the Fresnel-zone field of a uniformly illuminated square or rectangular aperture can also be predicted by an approximate analysis of the problem employing the method of Fresnel zones[12] indicated by Fig. 4. It is well known that the field at a point P on z axis, due to a circular aperture, is given by

$$U_p = \tfrac{1}{2}(U_1 \pm U_n)$$

where U_1 and U_n are the contributions of the first and n'th Fresnel zones. Also

$$U_p = \tfrac{1}{2}(U_1 - U_n) \approx 0 \text{ for } n \text{ even.} \quad (35)$$

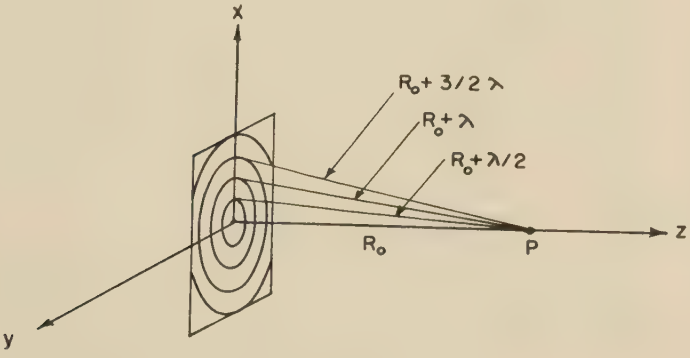

Fig. 4—Fresnel zones.

Examination of Fig. 4 shows that the n'th Fresnel zone in a rectangular or square aperture is necessarily incomplete. Therefore one obtains

$$U_1 \neq U_n \quad \text{and} \quad U_p > 0.$$

It is also interesting to find the relation between the diameter of a circle and the side of a square such that the first order gain corrections become exactly identical. For this purpose we substitute (30) into (27):

$$M(v_1) \approx 1 - \pi^2 L^4/45(4)R^2\lambda^2. \quad (36)$$

Further, when definition of x, in introduction, is substituted into series expansion for $\sin x/x$, one obtains

$$(\sin x/x) = 1 - \pi^2 a^4/24R^2\lambda^2. \quad (37)$$

If the correction terms are now equated the result is

$$D = 2a = L\sqrt[4]{32/15} = L(1.208). \quad (38)$$

This diameter is nearly equal to the arithmetic mean of the sidelength and the diagonal of the square:

$$D \approx L(1+\sqrt{2})/2.$$

[12] S. Silver, *ibid.*, p. 197.

Fresnel-Zone Gain of a Long and Narrow Aperture

We call an aperture long and narrow when $L_1 \gg L_2$ or $L_2 \gg L_1$. We note from (27) and the definition of p_1 that

$$0.98 < M(p_1) \leqq 1 \quad \text{when} \quad R \geqq 1.65L_2^2/\lambda. \quad (39)$$

Therefore, if $L_1 \gg L_2$ such that $R \geqq 1.65L_2^2/\lambda$ when $R \ll 2L_1^2/\lambda$ (24) for the gain in the optical Fresnel zone reduces to:

$$G = G_0 M(u_1). \quad (40)$$

The function $M(v)$ has been plotted already in Fig. 2.

Appendix I

TABLE I

TABLE OF $M(v)$ AND $M^2(v)$

$$M(v) = \frac{C^2(v) + S^2(v)}{v^2}$$

This table is based upon the values of $C(v)$ and $S(v)$ given by Jahnke and Emde.[5,13] In the antenna application of the present paper: $v = L/\sqrt{2R\lambda}$.

v	v^2	$M(v)$	$M^2(v)$	v	v^2	$M(v)$	$M^2(v)$
0	0	1.0000	1.0000	4.0	16.00	.0266	.0007
.1	.01	1.0000	1.0000	4.1	16.81	.0330	.0011
.2	.04	.9994	.9988	4.2	17.64	.0346	.0012
.3	.09	.9982	.9964	4.3	18.49	.0275	.0008
.4	.16	.9945	.9890	4.4	19.36	.0210	.0004
.5	.25	.9862	.9726	4.5	20.25	.0230	.0005
.6	.36	.9719	.9446	4.6	21.16	.0278	.0008
.7	.49	.9486	.8998	4.7	22.09	.0255	.0007
.8	.64	.9134	.8343	4.8	23.04	.0185	.0003
.9	.81	.8647	.7477	4.9	24.01	.0183	.0003
1.0	1.00	.8004	.6406	5.0	25.00	.0227	.0005
1.1	1.21	.7200	.5184	5.1	26.01	.0218	.0005
1.2	1.44	.6253	.3910	5.2	27.04	.0163	.0003
1.3	1.69	.5200	.2704	5.3	28.09	.0161	.0003
1.4	1.96	.4102	.1683	5.4	29.16	.0197	.0004
1.5	2.25	.3044	.0927	5.5	30.25	.0177	.0003
1.6	2.56	.2116	.0448	5.6	31.36	.0136	.0002
1.7	2.89	.1406	.0198	5.7	32.49	.0154	.0002
1.8	3.24	.0971	.0095	5.8	33.64	.0172	.0003
1.9	3.61	.0817	.0067	5.9	34.81	.0134	.0002
2.0	4.00	.0891	.0079	6.0	36.00	.0125	.0002
2.1	4.41	.1084	.0118	6.1	37.21	.0153	.0002
2.2	4.84	.1265	.0160	6.2	38.44	.0133	.0002
2.3	5.29	.1320	.0174	6.3	39.69	.0109	.0001
2.4	5.76	.1201	.0144	6.4	40.96	.0134	.0002
2.5	6.25	.0948	.0090	6.5	42.25	.0125	.0002
2.6	6.76	.0671	.0045	6.6	43.56	.0100	.0001
2.7	7.29	.0493	.0024	6.7	44.89	.0120	.0001
2.8	7.84	.0474	.0022	6.8	46.24	.0114	.0001
2.9	8.41	.0576	.0033	6.9	47.61	.0092	.0001
3.0	9.00	.0681	.0046	7.0	49.00	.0112	.0001
3.1	9.61	.0680	.0046	7.1	50.41	.0101	.0001
3.2	10.24	.0556	.0031	7.2	51.84	.0086	.0001
3.3	10.89	.0399	.0016	7.3	53.29	.0105	.0001
3.4	11.56	.0326	.0011	7.4	54.76	.0087	.0001
3.5	12.25	.0372	.0014	7.5	56.25	.0085	.0001
3.6	12.96	.0454	.0021	7.6	57.76	.0096	.0001
3.7	13.69	.0456	.0021	7.7	59.29	.0075	.0001
3.8	14.44	.0361	.0013	7.8	60.84	.0087	.0001
3.9	15.21	.0266	.0007	7.9	62.41	.0082	.0001

[13] The numerical computations were performed by Miss Rosemary Duffy.

TABLE I (*continued*)

v	v^2	$M(v)$	$M^2(v)$
8.0	64.00	.0072	.0001
8.1	65.61	.0085	.0001
8.2	67.24	.0067	.00004
8.3	68.89	.0077	.0001
8.4	70.56	.0070	.00005
8.5	72.25	.0067	.00004

Appendix II

Glossary of Mathematical Symbols

U_p = Diffraction field at a point $P(x, y, z)$ in space, see Fig. 1. U_p has amplitude and phase, but it is not a vector. The direction of the electric field $\overline{E}_p$, equal in magnitude to U_p, is determined by the direction of the electric field in the diffracting aperture.

$\overline{E}$, $\overline{H}$ = Electric and magnetic field vectors.

ξ, η = coordinates of a point A in the diffracting aperture.

$F(\xi, \eta)$ = field over the aperture.

r = distance from A to P.

$\bar{r}_1$ = unit vector in the direction from A to P.

R = distance from the origin of coordinates to P.

$\overline{R}_1$ = unit vector in the direction from the origin to P.

$\bar{i}_z$ = unit vector in the z direction.

$\bar{s}$ = unit vector in the direction of a ray at a given point on the aperture; $\bar{s}$ is normal to the wave front at the point.

θ = angle given by $\bar{i}_z \cdot R_1 = \cos\theta$.

L_1 = length of the aperture parallel to the x axis.

L_2 = length of the aperture parallel to the y axis.

$u = \xi\sqrt{\pi/R\lambda}$.

$p = \eta\sqrt{\pi/R\lambda}$.

$u_0 = (L_1/2)\sqrt{\pi/R\lambda}$.

$p_0 = (L_2/2)\sqrt{\pi/R\lambda}$.

$u_1 = L_1/\sqrt{2R\lambda}$.

$p_1 = L_2/\sqrt{2R\lambda}$.

v, t = arbitrary variables.

$C(v) = \int_0^v \sin(\pi/2)t^2 dt$, Fresnel integral.

$S(v) = \int_0^v \cos(\pi/2)t^2 dt$, Fresnel integral.

P_z = power per unit solid angle in the z direction.

ϵ = dielectric constant of free space.

μ = permeability of free space.

W = total power radiated by the aperture.

A = area of aperture $= L_1 \times L_2$.

$M(v) = [C^2(v) + S^2(v)]/v^2$.

Some Relationships between Total Scattered Power and the Scattered Field in the Shadow Zone*

J. T. BOLLJAHN† and W. S. LUCKE†

***Summary*—Equations are derived which relate the far-zone scattered field, as measured in the shadow zone of an electromagnetic scatterer, to the total energy scattered and absorbed by the scatterer. In the case of a perfectly conducting scatterer, the energy stored in the fields about the scatterer is also related to the far-zone scattered field in the shadow zone.**

Introduction

THIS NOTE serves to present several relationships which exist between the amplitude of a scattered electromagnetic wave and the energy which is scattered, absorbed, or stored by the scattering object. Although some of these relationships have been deduced by others,[1–5] it is felt that they are sufficiently obscure and useful to warrant more widespread publication. The relationship involving stored energy appears to have particular utility in the study of electromagnetic resonance behavior. It is hoped that it will

* Manuscript received by the PGAP, April 22, 1955; revised manuscript received September 15, 1955. Sponsored by AF Cambridge Res. Ctr, Contract AF 19(604)-266.

† Stanford Research Inst., Stanford, Calif.

[1] M. Lax, "On a well-known cross section theorem," *Phys. Rev.*, vol. 78, pp. 306–307; May 1, 1950.

[2] H. Levine and J. Schwinger, "On the theory of electromagnetic wave diffraction by an aperture in an infinite plane conducting screen," *Commun. on Pure and Appl. Math.*, vol. 3, pp. 355–391; December, 1950.

[3] C. J. Bouwkamp, "On the diffraction of electromagnetic waves by small circular disks and holes," *Phillips Res. Reps.*, vol. 5, pp. 401–422; December, 1950.

[4] W. S. Lucke, "Transmission through a rectangular aperture in an infinite screen," Tech. Rep. 25, Contract AF 199(122)78, Stanford Res. Inst., Menlo Park, Calif.; September, 1951.

[5] V. Twersky, "Certain transmission and reflection theorems," *J. Appl. Phys.*, vol. 25, pp. 859–862; July, 1954.

lead to an experimental procedure of sufficient simplicity and generality to possibly replace better known methods.

The analysis below shows that the sum of the scattered power and absorbed power due to an arbitrary scatterer in a plane wave may be determined by a measurement of the scattered field amplitude and phase at a single point in the shadow zone. In the case of a perfectly conducting scatterer, both the scattered power and the mean stored energy in the scattered field can be determined by such a measurement.

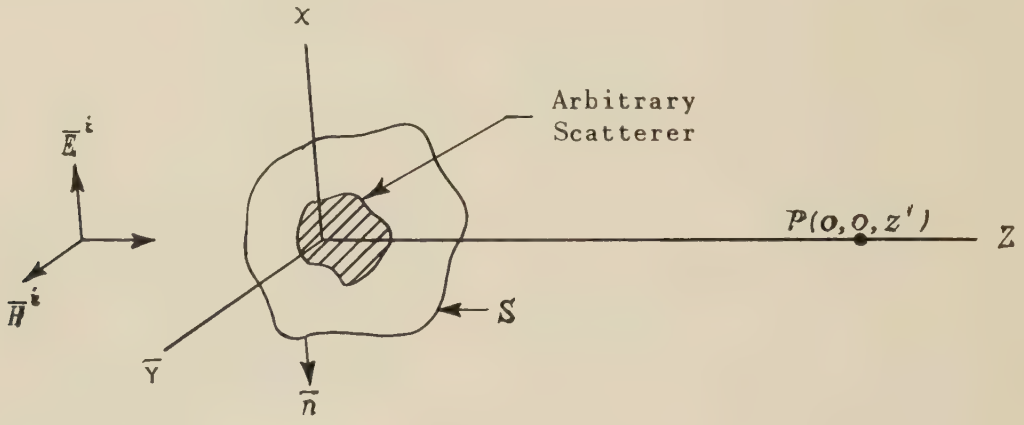

Fig. 1.

Analysis

Consider an arbitrary scattering object impinged upon by a plane wave, as shown in Fig. 1.

The incident field is given by

$$\left.\begin{aligned}\bar{E}^i &= \bar{a}_x E_0 e^{-jkz}\\ \bar{H}^i &= \bar{a}_y H_0 e^{-jkz}\end{aligned}\right\} \tag{1}$$

where

$$H_0 = \frac{E_0}{\eta}\cdot$$

And the total fields are given by

$$\left.\begin{aligned}\bar{E} &= \bar{E}^i + \bar{E}^s\\ \bar{H} &= \bar{H}^i + \bar{H}^s\end{aligned}\right\} \tag{2}$$

where $\bar{E}^s$ and $\bar{H}^s$ are the scattered fields. Define scattered power[6] as

$$P_s = Re \int_S \bar{E}^s \times \bar{H}^{s*}\cdot\bar{n}ds \tag{3}$$

where s is an arbitrary surface enclosing the scatterer, and substituting from (2),

$$\bar{E}^s = \bar{E} - \bar{E}^i \quad \text{and} \quad \bar{H}^s = \bar{H} - \bar{H}^i$$

results in the following relationship.

[6] For an extended discussion of the physical meaning of this type of definition, see L. Brillouin, "The scattering cross section of spheres for electromagnetic waves," *Jour. Appl. Phys.*, vol. 20, p. 1110; November, 1949.

$$P_s = \text{Re}\int_S \bar{E}\times\bar{H}^*\cdot\bar{n}ds + \text{Re}\int_S \bar{E}^i\times\bar{H}^{i*}\cdot\bar{n}ds$$
$$-\text{Re}\int_S (\bar{E}\times\bar{H}^{i*} + \bar{E}^i\times\bar{H}^*)\cdot\bar{n}ds. \tag{4}$$

The first integral involves total fields and is seen to be equal to minus the total power absorbed by the scatterer. The second integral is equal to the total power entering S due to the incident field alone and is hence equal to zero.

Thus,

$$P_s + P_A = -\text{Re}\int_S \bar{E}\times\bar{H}^{i*}\cdot\bar{n}ds$$
$$-\text{Re}\int_S \bar{E}^i\times\bar{H}^*\cdot\bar{n}ds \tag{5}$$

where P_A is the total power absorbed by the scatterer.

Applying (2) again to remaining integrals, and noting again there is no net power flow into S due to incident wave alone, (5) may be rewritten as follows

$$P_S + P_A = -\text{Re}\int_S \bar{E}^s\times\bar{H}^{i*}\cdot\bar{n}ds$$
$$-\text{Re}\int_S \bar{E}^i\times\bar{H}^{s*}\cdot\bar{n}ds. \tag{6}$$

Substituting now for $\bar{E}^i$ and $\bar{H}^i$ from (1), this expression reduces, after some manipulation of the vector quantities, to

$$P_S + P_A = -E_0\,\text{Re}\left[\frac{1}{\eta}\int_S e^{jkz}\overline{a_y}\cdot(\bar{n}\times\bar{E}^s)ds + \int_S e^{-jkz}\overline{a_x}\cdot(\bar{H}^{s*}\times\bar{n})ds\right]\cdot \tag{7}$$

Noting that only the real part of this expression is of interest, it is seen that the right member may be put into more symmetric form by replacing the second integral with its conjugate complex.

Thus

$$P_S + P_A = -E_0 \operatorname{Re}\left[\frac{1}{\eta}\int_S e^{jkz}\overline{a_y}\cdot(\bar{n}\times\overline{E}^s)ds + \int_S e^{jkz}\overline{a_x}\cdot(\overline{H}^s\times\bar{n})ds\right]. \quad (8)$$

It is now of interest to examine the expression for the far-zone scattered field at a point, P, which is directly in the shadow of the scatterer. The field component, $E_x{}^s$, is given by

$$E_x{}^s = \frac{-j\omega\mu e^{-jkz'}}{4\pi z'}\left[\frac{1}{\eta}\int_S e^{jkz}\overline{a_y}\cdot(\overline{E}^s\times\bar{n})ds + \int_S e^{jkz}\overline{a_x}\cdot(\bar{n}\times\overline{H}^s)ds\right]. \quad (9)$$

The term in brackets is seen to be just negative of the bracketed term in (8) and hence it is possible to eliminate this term by solving (8) and (9) simultaneously. Thus, from (9)

$$\operatorname{Re}\left[\frac{1}{\eta}\int_S e^{jkz}\overline{a_y}\cdot(\bar{n}\times\overline{E}^s)ds + \int_S e^{jkz}\overline{a_x}\cdot(\overline{H}^s\times\bar{n})ds\right] = \frac{4\pi z'}{\omega\mu}\operatorname{Re}(-je^{jkz'}E_x{}^s) = \frac{4\pi z'}{\omega\mu}\operatorname{Im}(e^{jkz'}E_x{}^s). \quad (10)$$

Substituting (10) into (8) gives

$$P_S + P_A = -\frac{4\pi z' E_0}{\omega\mu}\operatorname{Im}(e^{jkz'}E_x{}^s). \quad (11)$$

Defining, now, the scattering and absorption cross sections as

$$\sigma_s = \frac{\eta P_S}{E_0{}^2} \quad \text{and} \quad \sigma_A = \frac{\eta P_A}{E_0{}^2},$$

respectively, (11) may be rewritten after some further reduction as

$$\sigma_S + \sigma_A = -2z'\lambda \operatorname{Im}\left(\frac{E_x{}^s}{E^i}\right)_P \quad (12)$$

where $E^i = E_0 e^{-jkz'}$ is the value of the incident field at the observation point, P.

Thus, the sum of the scattering and absorption cross section of an arbitrary scatterer may be determined if the far-zone scattered field is known at just one point directly in the shadow of the scatterer.

It does not seem possible to deduce a relation similar to (12) from the imaginary part of (4) in the general case. However, the extension is possible in the case of perfectly conducting scatterers. Noting in this case that $P_A = 0$, and taking the surface, S, to be the surface of the scatterer, the steps preceding (6) may be retraced with both real and imaginary parts of expressions retained, and the following result is obtained.

$$P_S' = -\int_S \overline{E}^s\times\overline{H}^{i*}\cdot\bar{n}ds - \int_S \overline{E}^i\times\overline{H}^{s*}\cdot\bar{n}ds. \quad (13)$$

where $P_S' = P_S + j\omega Q_S$ and Q_S is the excess of the mean stored magnetic-field energy over electric-field energy in the scattered field.

The first integral may be shown to be equal to zero by substituting for $\overline{E}^s$ from (2) and noting again that $\int_S \overline{E}^i\times\overline{H}^{i*}\cdot\bar{n}ds = 0$ and also that

$$\int_S \overline{E}\times\overline{H}^{i*}\cdot\bar{n}ds = \int_S \bar{n}\times\overline{E}\cdot\overline{H}^{i*}ds = 0,$$

since $n\times\overline{E} = 0$ on S due to the condition that the scatterer is perfectly conducting.

Thus, (13) reduces to

$$P_S' = -\int_S \overline{E}^i\times\overline{H}^{s*}\cdot\bar{n}ds. \quad (14)$$

Introducing now expression for $\overline{E}^i$ from (1) results in

$$P_S' = -E_0\int_S e^{-jkz}\overline{a_x}\cdot(\overline{H}^{s*}\times\bar{n})ds. \quad (15)$$

The first integral in (9) also vanishes in the same manner for a perfectly conducting scatterer, so (9) reduces in this case to

$$E_x{}^s = \frac{-j\omega\mu e^{-jkz'}}{4\pi z'}\int_S e^{jkz}\overline{a_x}\cdot(\bar{n}\times\overline{H}^s)ds. \quad (16)$$

Proceeding as before, the following relationship is found between P_S' and $E_x{}^s$.

$$\sigma_S' = \frac{P_S'}{E_0{}^2} = -j2z'\lambda\left(\frac{E_x{}^s}{E^i}\right)_P. \quad (17)$$

Considering real and imaginary parts of (17), it is seen

$$\sigma_S = -2z\lambda \operatorname{Im}\left(\frac{E_x{}^s}{E^i}\right)_P, \quad (18)$$

in agreement with (12), and

$$\sigma_Q = -2z'\lambda \operatorname{Re}\left(\frac{E_x{}^s}{E^i}\right)_P. \quad (19)$$

The expression for σ_Q in (19) shows that a 90 degree phase relationship between $E_x{}^s$ and E^i at P indicates a condition of no net stored energy in the scattered fields. From (12) and (18) it is seen that since Σ_s and σ_A must be positive quantities, the scattered field, $E_s{}^x$, must lag the incident field at point P by an angle between 0 degrees and 180 degrees.

Acknowledgment

The authors wish to express their appreciation for the assistance of Dr. Carson Flammer in reviewing this presentation and providing some of the references.

Long Range Meteoric Echoes via F-Layer Reflections*

J. T. deBETTENCOURT† and W. A. WHITCRAFT, JR.‡

Summary—This note reports HF observations of meteoric backscatter echoes at ranges greatly exceeding radio line-of-sight. The observations were part of a program of measurements on backscatter using COZI equipment.

Examples are given of observations at South Dartmouth, Massachusetts in 1949 on 16 mc and of more recent observations in 1954 on 12 and 16 mc using improved equipment. Short duration echoes are observed in advance at ranges shorter than those of the ground backscatter. No such meteoric echoes are observed when the ground backscatter disappears. The meteoric echo ranges move with time of day just as the range to the ground backscatter moves. A plausible explanation for the observed meteoric echo ranges exceeding 1,000 miles is that they are due to backscatter from the trail, ionospherically propagated to and fro via the F region, just as the ground backscatter. Other possible ionospheric propagation modes are discussed.

Introduction

EXPERIMENTAL ionosphere propagation research started at Raytheon in 1948 under the sponsorship of Watson Laboratories, AMC, USAF after an intensive two year study program. During the second year of the study phase, relatively high powered pulse transmitters, conventional rhombics, Yagi antennas of various types and antennas for special purposes were constructed for the experiments to follow, and were installed at the South Dartmouth, Massachusetts, field station. Also developed was an MTI system, employing a Raytheon storage tube. Transponder beacons employing 20 kw peak pulse power transmitters were installed at White Sands, New Mexico and San Juan, Puerto Rico. Data recording equipments were developed to monitor continuously the amplitudes and time delays of beacon pulses arriving at South Dartmouth by various modes from the remote sites. Other equipments at South Dartmouth recorded polarization and angle of arrival of downcoming ionospherically propagated signals. Five 1 kw peak pulse power beacon transponders were constructed and installed at various places within the continental limits of the United States to assist further in mode identification, and another 1 kw beacon transponder was developed for installation in aircraft.

Conclusions reached in 1949–1950 were summarized in a report to the USAF in April 1951.[1] Some of these conclusions were as follows:

1) By use of the beacon technique[2,3] it was proved beyond reasonable doubt that, for frequencies greater than about 1.5 times the vertical incidence critical frequency, the leading edge of the long distance backscatter pattern is produced by ground scatter propagated by way of the ionosphere.

2) Measuring the apparent range to the leading edge of the backscatter pattern and the angle of arrival of backscatter (or the height of the reflecting layer at the control point) leads directly to determination of skip distance.[4]

3) Average seasonal ionospheric layer heights may be used without appreciable error in determining skip distances greater than about 600 miles.[4]

4) Accurate measurement of layer heights is afforded by the beacon technique.[2,3]

5) If skip distance is computed from oblique incidence soundings at frequency intervals of about 5 mc, interpolation acurately gives skip distances for other frequencies.[5] Extrapolation, however, may lead to extreme errors in prediction.

6) Usable backscatter is regularly obtained at HF with peak pulse powers as low as 150 watts if pulse widths greater than 500 μsec are employed.[1,5,6]

From the beginning of the experimental program, frequent echoes of relatively short time duration and of widths equal to that of the transmitter pulse were noted, both at short range (up to about 800 miles) and at long range (upwards of 1,500 to 2,000 miles). A long range and persistent echo lasting over five minutes with no change in range, is shown in Fig. 1 which was taken from continuous film records of April 11, 1949. From the nature of these echoes it was clear that meteor trails were being detected, although the means by which detection at the extreme ranges was possible was not fully understood at that time. More recent work at the South Dartmouth Field Station, employing improved equipment, has led to a theory which is advanced in this article.

* Manuscript received by the PGAP, September 15, 1955. Presented at the URSI-IRE Washington Meeting, May 4, 1955. Work performed under contracts with Rome Air Dev. Center and AF Cambridge Res. Center of the Air Res. and Dev. Command, USAF.

† Formerly at Lincoln Laboratory, M.I.T., now at Pickard and Burns, Needham, Mass.

‡ Raytheon Mfg. Co., Newton, Mass.

[1] Interim Report No. 7, Applied Propagation Studies at High Frequencies, Raytheon Manufacturing Company, prepared for Watson Laboratories, AMC, USAF, issued April 1, 1951.

[2] J. T. deBettencourt and H. Klemperer, "The beacon technique as applied to oblique incidence ionosphere propagation," PROC. IRE, vol. 38, pp. 791–792; July, 1950.

[3] W. G. Abel and L. C. Edwards, "The source of long distance backscatter," PROC. IRE, vol. 39, pp. 1538–1541, December, 1951.

[4] J. T. deBettencourt, "Instantaneous prediction of ionospheric transmission circuits by the communication zone indicator ("COZI")," TRANS. IRE, vol. 3-AP, pp. 202–209; August, 1952.

[5] W. G. Abel, L. C. Edwards, C. H. Hoeppner, and W. A. Whitcraft, Jr., "COZI," paper presented at 1952 Conference on Airborne Electronics, Dayton, Ohio, May 12–14, 1952, pp. 61–64 of published abstracts.

[6] L. C. Edwards, "COZI—communication zone indicator," *Electronics*, vol. 26, pp. 152–155; August, 1953.

Long Range Meteor Detection

Although the maximum height which has been reported for the beginning of a meteor trail is in the F region,[7] it is known that for most meteors the height of first appearance is confined to a region roughly from 80 to 120 km above the earth's surface.[7,8] As an extreme case, assume a meteor trail at 200 km height is detected

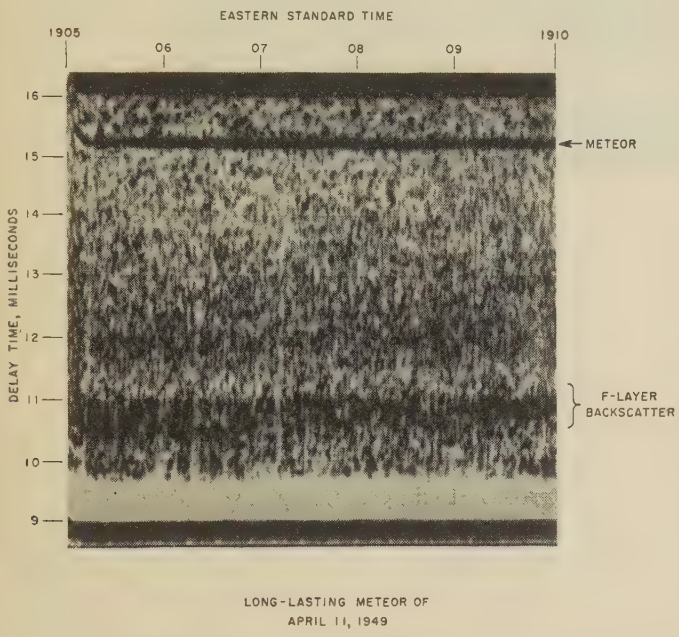

Fig. 1—Long-lasting meteor of April 11, 1949.

by a pulse sounding station T (Fig. 2) by a path M tangent to the earth. The path M will be approximately 1,955 km long, so that the trail will appear at a delay time of about 10.7 milliseconds on the receiving oscilloscope. The tangent ray is physically not attainable with practical antennas, so that a meteor trail detected by line-of-sight at a range corresponding to 10.7 milliseconds of delay time would in fact have to occur at a height substantially greater than 200 km.

A more realistic case would be for a trail at a height of 120 km for which the corresponding (tangent ray) echo delay time is about 8.3 milliseconds. By far the bulk of line-of-sight meteors detected in recent experiments at the South Dartmouth Field Station have been confined to delay times less than this figure.

Fig. 3 illustrates the possibility that meteor trails occurring in the vicinity of the E region but at ranges too great to be detected by a direct ray may in fact be detected by a reflection from the F region, as at the point C. If the broken line, TCD, represents the critical ray for a given frequency and time, meteor trails may

[7] S. K. Mitra, "The Upper Atmosphere," The Asiatic Society, Calcutta, India, Second edition, p. 82; 1952.

[8] W. L. Hartsfield, "Observations of distant meteor-trail echoes followed by ground scatter," Jour. of Geophysical Res., vol. 60, No. 1, pp. 53–56; March, 1955.

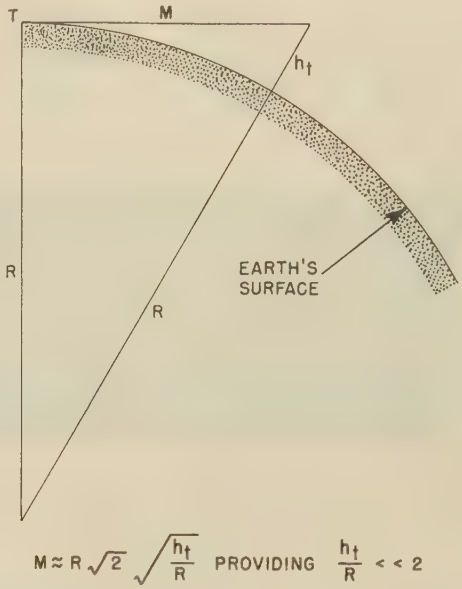

Fig. 2—Illustrating tangent-ray detection of meteor trail.

be detected at and to the right of the point B by such a reflection but cannot be detected by a direct ray since this region is below the line-of-sight (tangent) ray. If the mechanism of detection is correct as described, there should be a region AB in which meteor trails cannot be detected by either a direct or F-reflected ray, provided a high enough frequency is employed. A sample of the continuous film records from October 6,

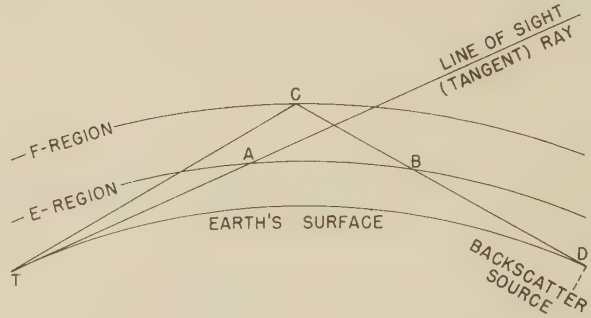

Fig. 3—Illustrating meteor-trail detection beyond line of sight.

1954 is shown as Fig. 4. During this series of tests, 20 kw of peak pulse power, with 200 μsec pulses at a rate of 20 per second, was employed with a rhombic antenna beamed south toward Puerto Rico. The frequency was 12.730 mc. Displayed in the record are three echoes identified as line-of-sight meteor trails, normal F backscatter in the vicinity of 11 milliseconds delay, and echoes in advance of the F backscatter, in the region beyond about 9.2 milliseconds. The blank zone evident between the short range and the long range echoes is believed to correspond to a region such as AB of Fig. 3.

The morning of October 6, 1954 was characterized by a good F layer but no regular E layer groundscatter on

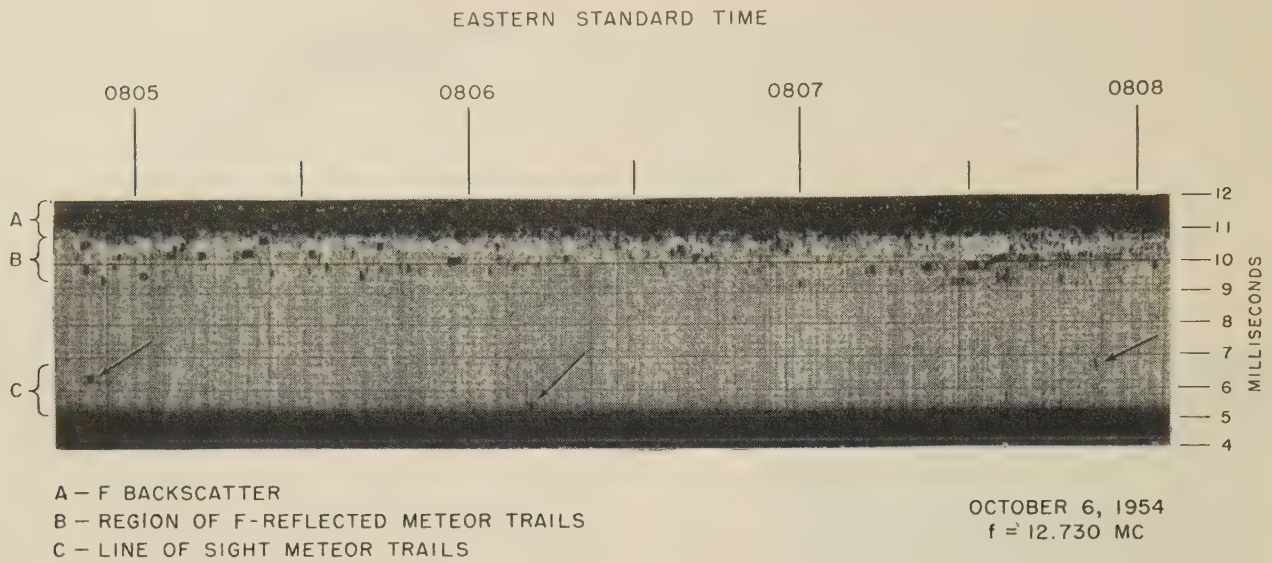

Fig. 4—Illustrating meteor-trail returns in advance of backscatter. October 6, 1954—$f = 12.730$ mc.

12.730 mc. Sporadic E became evident in the south after about 0815. Data taken from the film record (of which Fig. 4 is a sample) were used in preparing Fig. 5. Only 162 echoes, all having durations greater than 0.1 second, were selected from the long range group although many hundreds more were recorded, since very short duration echoes could be confused with random noise spikes or other interference. Of these 162 trails, one lasted six minutes and seven lasted as long as two minutes. Although the sample is statistically small, the dotted line in the figure would seem to indicate that the distribution of longer lasting trails is roughly the same as that for all F-reflected trails.

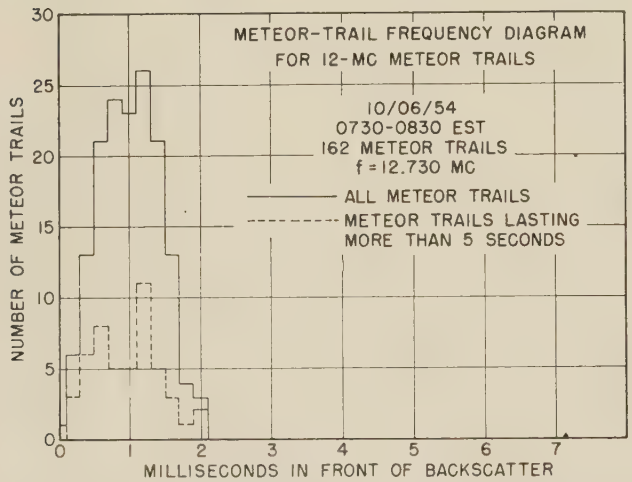

Fig. 5—Meteor-trail frequency diagram for 12-mc meteor trails.

The simple geometry shown in Fig. 6 indicates that for higher frequencies there should be an increase in the available space in front of the backscatter in which meteor trails (assumed to occur at E region heights) can be detected. On the morning of October 13, 1954, meteor trail data on 16 mc looking south were analyzed to prepare Fig. 7. A slight broadening of the zone in question, as compared with that of Fig. 6, is indeed noted, although the hourly incidence rate was much lower than that recorded on October 6. On October 13 F scatter first appeared at 0545 EST at 16 milliseconds delay time. In the three hour period from 0600 to 0900 there were 100 meteor trails just in advance of backscatter lasting more than 0.1 second, of which 19 lasted over 5 seconds and one lasted nearly 2 minutes.

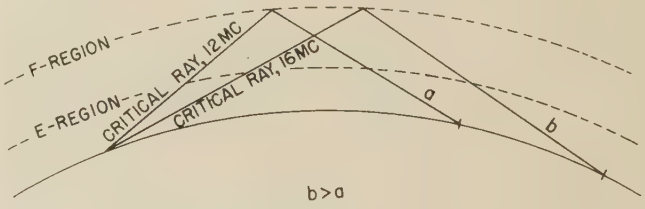

Fig. 6—Illustrating broadening of long range meteor-trail zones by increasing frequency.

It should be noted that the trails are readily detected in the backscatter pattern itself through their characteristic flutter. Trails could have been detected beyond the backscatter, as shown in Fig. 1, but oscilloscope sweep lengths available for the recent experiments would not permit such investigation. In the continuous film type of recording (Fig. 4), trails within the backscatter are lost because of film integration effects and system saturation. These complex fluctuations, having apparent frequency components up to a few cycles per second and characteristic of all meteor trails observed during the experiments are thought by some workers to be due to turbulence in the ionized trail.[9] Such fluctuations are not true Doppler flutter caused by the motion of the meteor body itself (forming the trail), for the flutter

[9] S. K. Mitra, *op. cit.*, p. 109.

rate corresponding to ordinary meteor radial velocities would go up to the kilocycle range. For trails in advance of the backscatter there is no apparent difference in the flutter rate whether these trails are line-of-sight or F-reflected. This has also been reported by other observers.[10]

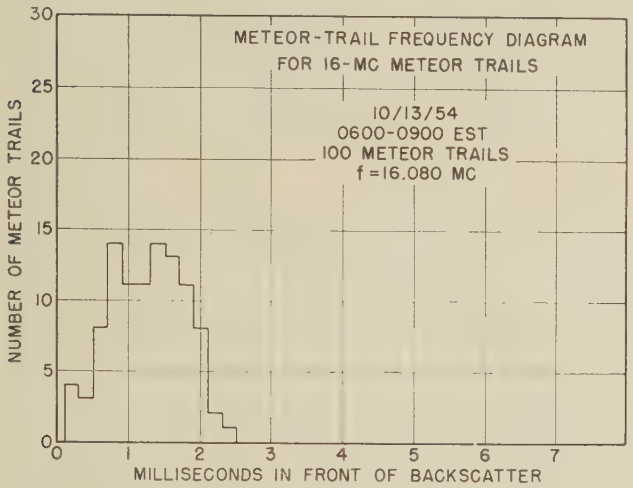

Fig. 7—Meteor-trail frequency diagram for 16 mc meteor trails.

It is of considerable interest to note that an approximate measure of the minimum height of the distant meteor trails is afforded by a knowledge of the three quantities F layer height (or departure angle for the critical ray), time delay to the meteor zone and time delay to the backscatter. Refer first to Fig. 8. Given the delay time to the F-reflected meteor zone we draw a line TM of length corresponding to that delay time and at the critical angle A appropriate for the frequency being used. A tangent to the circle representing the F region is drawn at the control point C, and the point M reflected geometrically in this tangent line as point M', giving a possible location of the observed meteor trail.

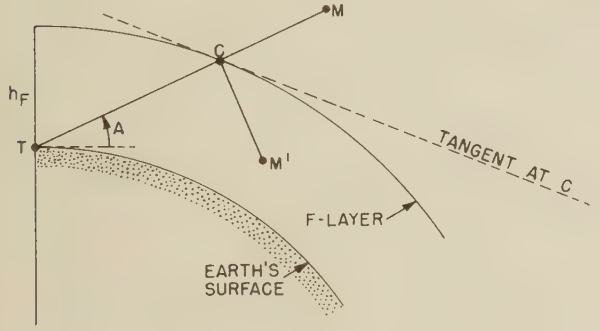

Fig. 8—Illustrating construction geometry (exaggerated scale).

Continuing this process for angles less than the critical angle A generates a locus of points, shown in Fig. 9 as $M'M''M'''$, equidistant (via F layer reflection) from the transmitter T. The minimum height is obtained from the following formula, readily derived from simple geometry:

$$h = R\left[\sqrt{\left(\frac{d}{R} + \sin A\right)^2 + \cos^2 A} - 1\right]$$

where

h = minimum height for trails associated with the critical angle A

R = earth's radius = 6,371 km

d = distance BD (from Fig. 4) derived from delay time records

A = critical angle for the frequency being used.

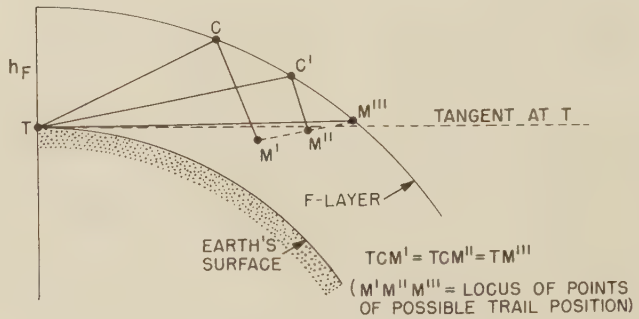

Fig. 9—Possible locations of trail at given delay time (exaggerated scale).

Selected portions of the continuous film records of the morning of October 6, 1954 were analyzed assuming an F layer height of 250 km, and Table I was prepared to show typical results.

TABLE I

Meteor Zone Delay Time, Milliseconds	Backscatter Delay Time, Milliseconds	d, in Kilometers	Skip Distance Kilometers	A, Degrees	Meteor Trail Minimum Height, Kilometers
9.6	12.1	374	1,707	12.0	76.5
9.3	11.9	388	1,675	12.5	95.5
9.2	11.3	314	1,585	13.5	87.8
9.1	11.2	314	1,570	13.9	82.9
9.0	11.3	344	1,585	13.5	89.2
9.0	11.2	329	1,570	13.9	86.0

If, as is believed, meteor trails occurred randomly with range during the experiments, a flat frequency distribution would be expected. That the antenna pattern by itself does not account for the shape of the meteor trail frequency diagrams, Figs. 5 and 7, may be seen from Figs. 10 and 11. These figures show the rhombic antenna measured patterns for 16.080 mc in horizontal and vertical planes, the former being for the best measured vertical angle. The deviation of the measured vertical pattern from that calculated using Harper's method[11] is small, and is attributed to the slope of the

[10] P. G. Gallagher and A. M. Peterson, "The contribution of meteors to long range backscatter," presented at URSI-IRE Washington meeting, May 4, 1955.

[11] A. E. Harper, "Rhombic Antenna Design," D. Van Nostrand Company, Inc., (1941).

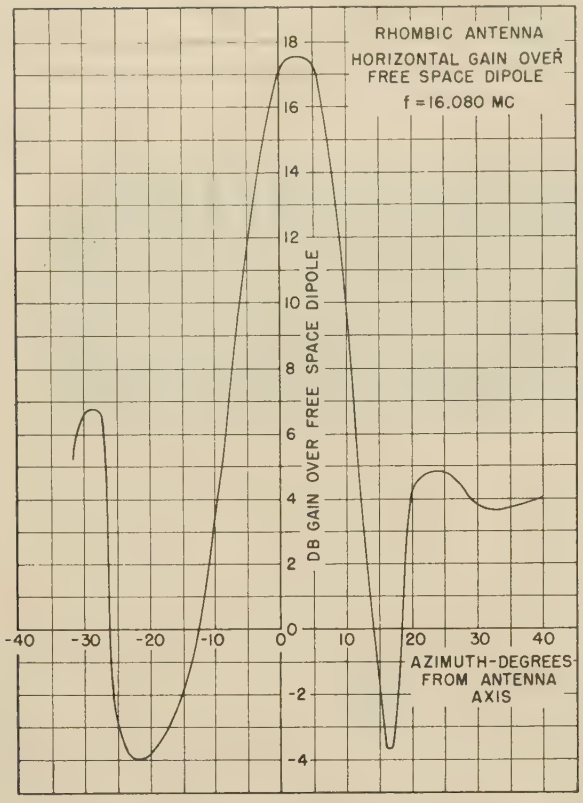

Fig. 10—Rhombic antenna horizontal gain over free space dipole—$f = 16.080$ mc.

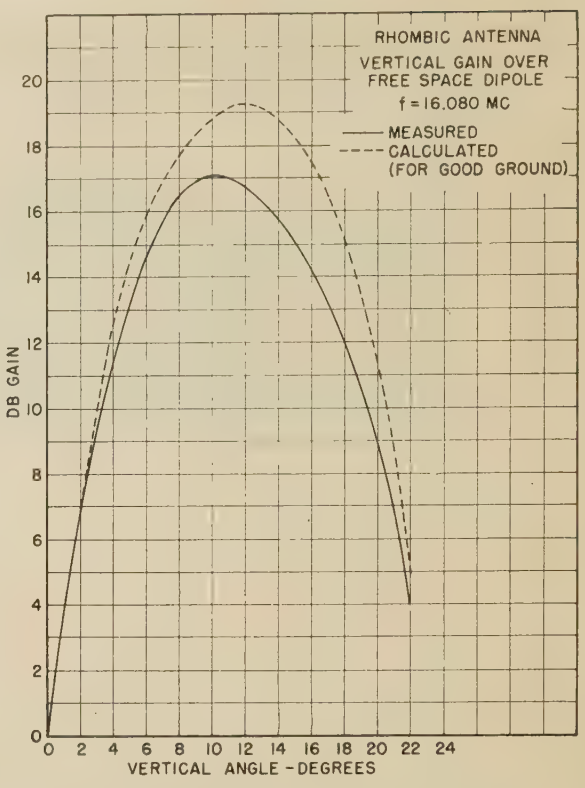

Fig. 11—Rhombic antenna vertical gain over free space dipole—$f = 16.080$ mc.

land surrounding the antenna and to the deviations of actual effective ground constants from those assumed. Calibration was accomplished with the aid of a government-furnished Navy helicopter during a six week period ending in November, 1949. Although the measured vertical pattern on 16 mc is characterized by a broad maximum, not greatly different from the pattern calculated for 12 mc, the ionosphere evidently created sufficient beam distortion to create the peaked shape of the meteor trail frequency diagrams.

Conclusions

Meteoric trail echoes can be observed at ranges greatly in excess of the radio line-of-sight by a reflection from the ionized F layer. An estimate of the minimum height of occurrence of trails associated with the critical ray is afforded by simultaneous measurement of delay time to the trail echo and delay time to the backscatter. The distribution of trail echoes with apparent range ahead of the backscatter is in all probability due to distortion of the transmitted beam by the F layer itself.

Acknowledgement

Thanks are due Raytheon engineers, D. A. Hedlund and L. C. Edwards, for their valuable comments and criticisms during the preparation of this article; J. Borden and J. J. Molla, of the Raytheon South Dartmouth Field Station for expert assistance in taking the data; and to Mr. G. M. Hamm, now at Hycon Eastern, who directed the antenna pattern measurements program at Raytheon in 1949. Special thanks are due to Mr. C. A. Strom, Jr., of Rome Air Development Center and to Dr. P. Newman, of Air Force Cambridge Research Center for their encouragement and assistance in making the data available for publication.

Correlation in VHF Propagation over Irregular Terrain*

R. S. KIRBY† AND F. M. CAPPS†

Summary—**A study has been made of the correlation in transmission loss observed over irregular-terrain paths. Simultaneous mobile measurements were made of two pairs of VHF broadcasting stations in the Washington, D. C.–Baltimore, Maryland area. The correlation coefficients derived from sample sets of transmission loss data indicate that when reception is from opposite directions, no significant correlation is evident, and when the paths of propagation are the same even though the frequencies are separated considerably, the correlation appears to be significantly high.**

Introduction

THE RELATIONSHIP between transmission loss and distance from the transmitter in the propagation of radio waves over a homogeneous smooth earth is well known.[1] However, over most transmission paths involved in VHF propagation, the intervening terrain is neither homogeneous nor smooth. Over such paths many variations from smooth-earth expected values can be observed. Within roughly fifty miles from the transmitter tropospheric effects are generally negligible, and the variations in observed transmission loss are almost entirely the result of constructive and destructive interference of several rays arriving at the receiving location over different irregular-terrain paths. The relative phase and amplitude of these rays depend on the relative lengths of the paths, the amount of reflection and refraction involved, etc.

The variations in field strength at these distances depend primarily on location, since only a negligible amount of variation with time is apparent at any given location. In making estimates of the interference ratios of the fields from two co-channel stations expected over VHF irregular terrain paths, a question arises as to whether or not the transmission losses at given receiving locations are correlated; that is, whether they tend to be high or low simultaneously. The distribution of values of each field can be characterized to a large extent by its mean and standard deviation which can be estimated from the data. In determining the interference effects of two such fields, the results would be entirely different, depending upon how the fields were correlated. For example, the nuisance value of an interfering station would tend to be uniform over a large number of receiving locations if the field strengths were positively correlated to a high degree. The ratios of desired to undesired field strengths would tend to be more widely distributed with less correlation, and the variance of this distribution would be greatest as the correlation coefficient approached minus one.

* Manuscript received by the PGAP March 28, 1955; revised manuscript received September 13, 1955.

† National Bureau of Standards, Central Radio Propagation Lab., Boulder, Colo.

[1] K. A. Norton, "The calculation of ground-wave field intensity over a finitely conducting spherical earth," PROC. IRE, vol. 29, pp. 623–639; December, 1941.

It is the purpose of this paper to present the results of a study of correlation in VHF irregular terrain propagation. Mobile field strength measurements have been made using the transmissions of three VHF broadcasting stations in the Washington, D. C.–Baltimore, Maryland area. These are WMCP-FM operating at 94.7 mc in Baltimore, WRC-FM at 93.9 mc and WNBW-TV (aural) at 71.75 mc both in Washington. The latter two transmissions emanate from a single antenna. The measurements were obtained in 1950 and originally reported on at the joint spring meeting of the International Scientific Radio Union and the Institute of Radio Engineers in Washington, D. C., in April, 1951.

Continuous measurements of transmission loss were made of two stations simultaneously while driving along selected routes. The first route was chosen to be a perpendicular bisector of the line between WRC-FM and WMCP-FM so as to cause the radio waves to arrive from essentially opposite directions. The second route was chosen to be circular around WRC-FM and WNBW-TV with a radius of approximately 37 miles, for which radio waves at the two frequencies arrived over exactly the same propagation path. Location of transmitters and routes followed are shown in Fig. 1.

Description of Measurements and Equipment

A van-type truck equipped with a 30-foot telescopic mast was used for continuous mobile recording. The recording antenna consisted of a horizontally polarized Alford Loop antenna which is omnidirectional in the horizontal plane. A trailer-mounted, five-kw gasoline generator supplied power for recording and operation of auxiliary equipment.

In operation the receiving antenna was connected to two receivers at the same time through suitable isolating preamplifiers, making it possible to record pairs of stations simultaneously. National Model 108R FM receivers suitably modified with recording circuits and to provide for logarithmic response were used for recording the FM broadcasting stations, and an RCA Model WX1A Field Intensity Meter was used to record the sound transmissions of the television broadcast station. Esterline Angus recording milliammeters connected to the odometer of the truck by a flexible shaft were employed for the actual recording function. The chart advance depended only on the distance traveled and was independent of speed or variations in speed of the truck. For practical purposes a chart drive ratio was employed such that $2\frac{3}{4}$ inches on the chart represented one mile of road. The chart drives of the two Esterline Angus meters were coupled mechanically and the chronometer pens connected in parallel so that the records could easily be matched for scaling and analysis.

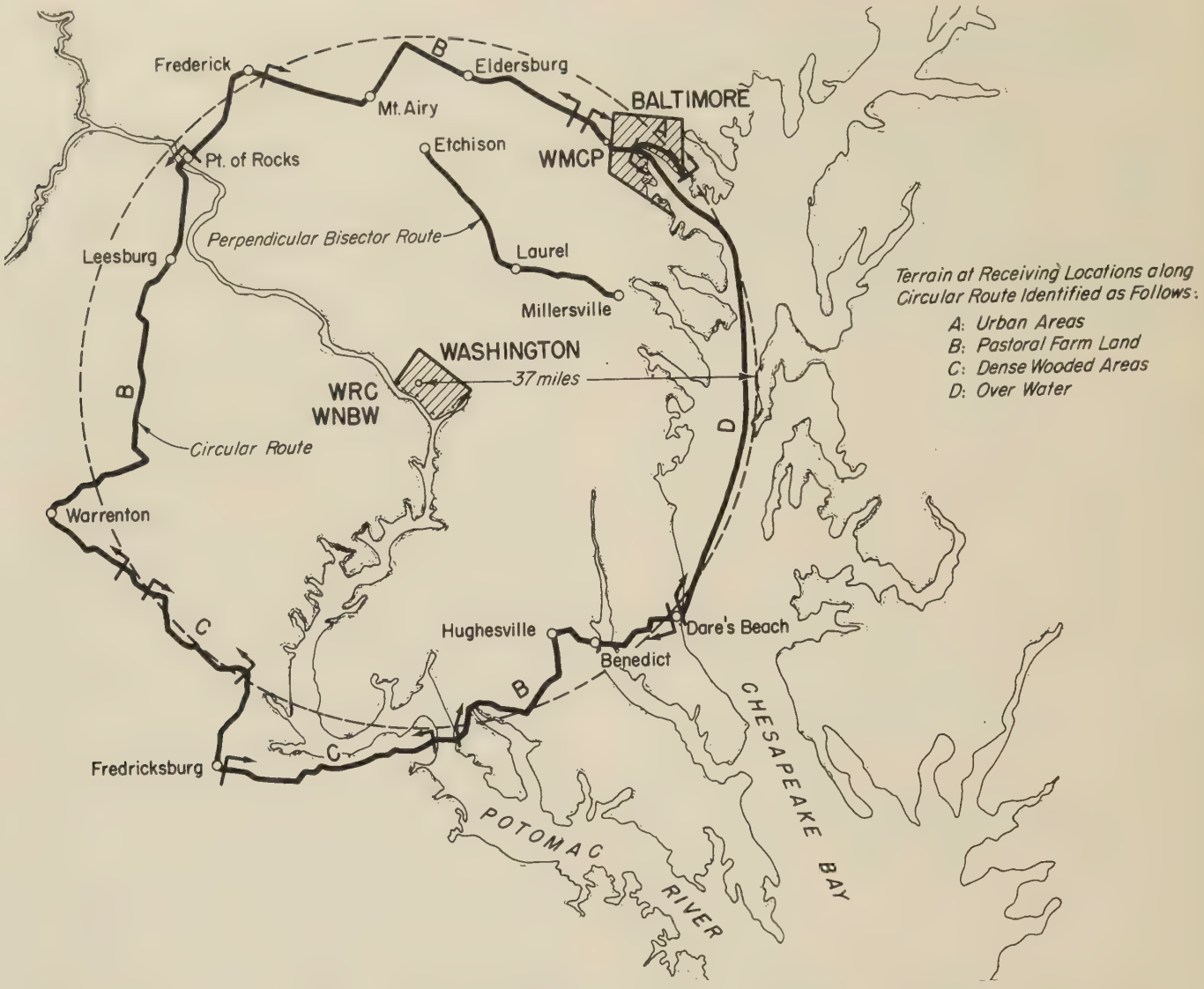

Fig. 1—Routes followed in making simultaneous mobile transmission loss measurements.

Calibration of all the recorders was made in terms of μv per meter at the receiving antenna. These were later converted to units of basic transmission loss, L_b, as defined by Norton.[2] The value of basic transmission loss corresponding to one μv per meter for each of the stations recorded is as follows: WRC-FM, 159.6 db; WMCP-FM, 159.8 db; and WNBW-TV, 157.3 db.

The recording route from Millersville to Etchison, Maryland, followed as closely as possible a perpendicular bisector of the line joining the transmitting antennas of WRC-FM in Washington and WMCP-FM in Baltimore 34.5 miles apart. The countryside along the route was rolling farm land with large stands of woods here and there. A large number of wires and tree limbs extended over the road making it impractical to record with antenna heights greater than fifteen feet, which is the height at which all measurements reported here were made.

A sample of the Esterline Angus recorder charts obtained simultaneously over this route is shown in Fig. 2. Scaggsville, Maryland, lies almost on the line drawn between the two transmitters. It can be seen from these records that many wide variations in observed transmission loss occur in very short space intervals. It is interesting to note in repeating the measurements on other days that the records were almost identical even to some of the finest detail, indicating the lack of any significant time variation.

Similar recordings were obtained over a circular route receiving WRC-FM at 93.9 mc and WNBW-TV at 71.75 mc simultaneously over exactly the same propagation path. This route was followed over land from Baltimore, Maryland, to Dares Beach, Maryland, and over water between the same two points in Chesapeake Bay at an average radius of approximately 37 miles from the WRC-WNBW transmitting tower.

Because of wide differences in the terrain at receiving locations along the circular route, the data were arbitrarily classified by terrain into four groups as follows:

A) Metropolitan Areas
B) Farm Land (Not Heavily Wooded)
C) Heavily-Wooded Areas
D) Over Water

Sample Esterline Angus charts obtained from this

[2] K. A. Norton, "Transmission loss in radio propagation," PROC. IRE, vol. 41, pp. 146–152; January, 1953.

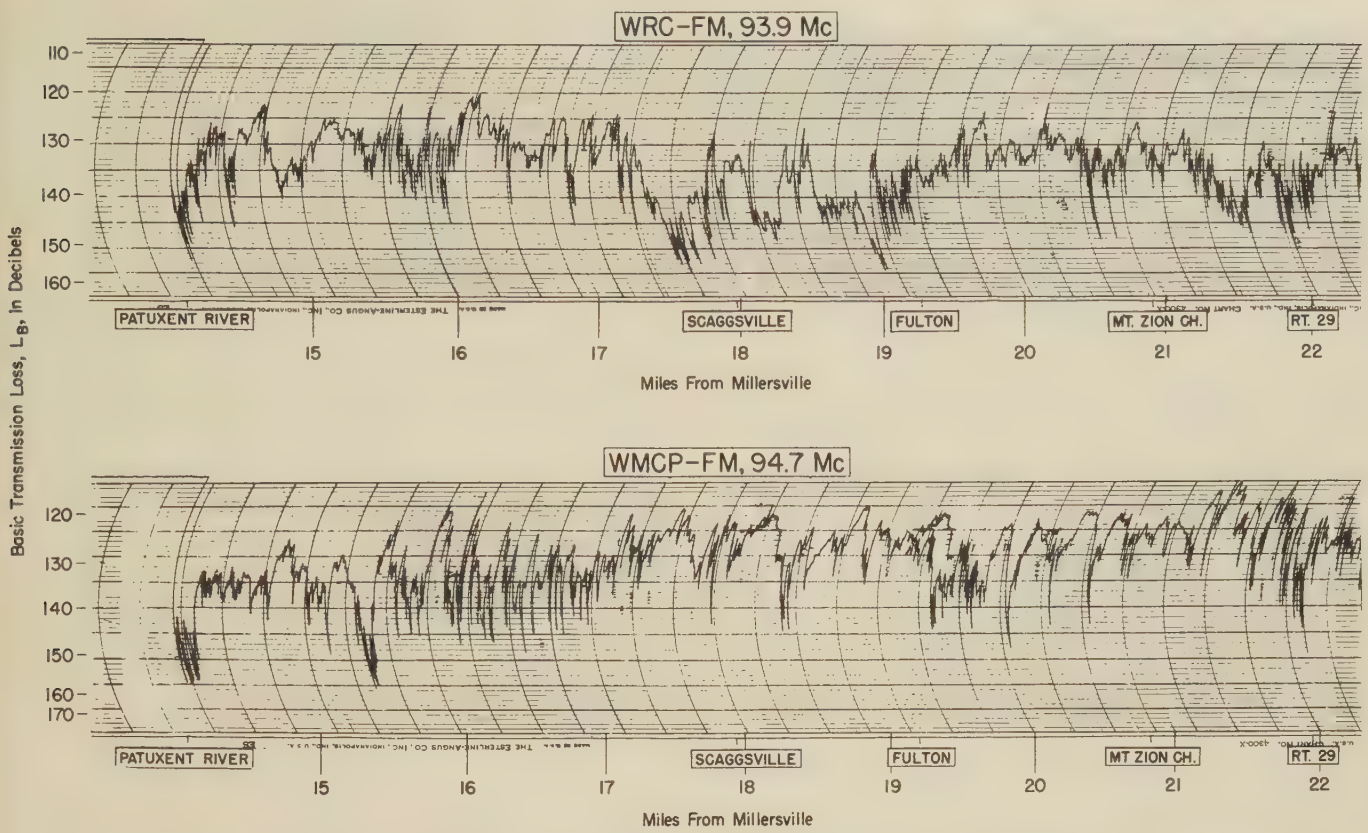

Fig. 2—Sample simultaneous mobile recording of WRC-FM and WMCP-FM-Recordings made along perpendicular bisector route—April 25, 1950—Receiving antenna height: 15 feet.

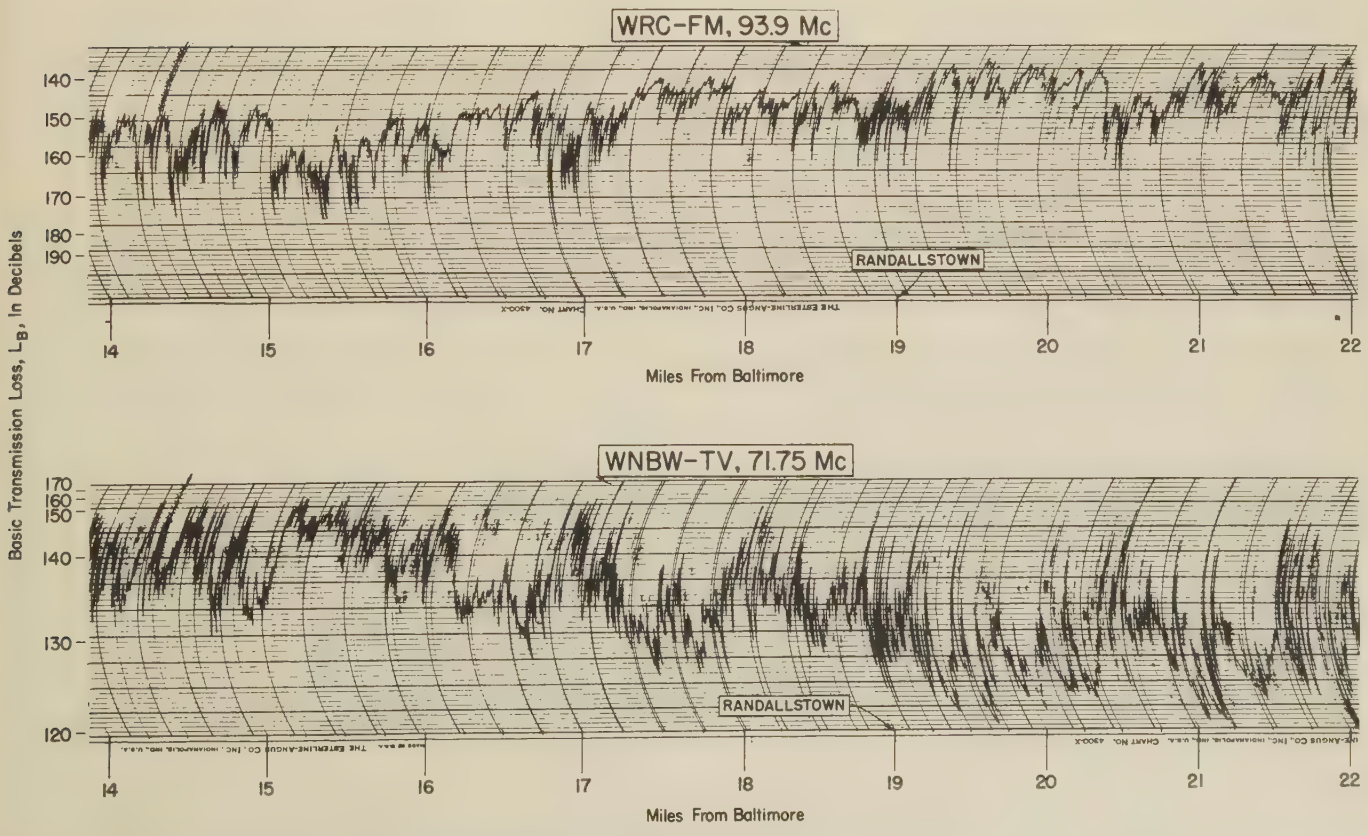

Fig. 3—Sample simultaneous mobile recording of WRC-FM and WNBW-TV-Recordings made along circular route—June 15, 1950—Receiving antenna height: 15 feet.

recording run are shown in Fig. 3. It should be noted that the recorded deflection for WNBW-TV was in the opposite direction from that for WRC-FM as indicated by the transmission loss scale at the left-hand end of the charts. With this in mind a cursory examination of the recordings shows that there is apparently a tendency for the observed transmission loss to be high or low simultaneously.

Correlations and Distributions of Perpendicular Bisector Measurements

The correlation of the data obtained along the perpendicular bisector route between WMCP-FM and WRC-FM will be considered first. If correlation between the two fields exists, it would perhaps be logical to assume that simultaneous sector medians would be more highly correlated than simultaneous discrete values since on the recordings there appears to be a random component producing variations with very short periods. These variations would be somewhat eliminated in taking sector median values of transmission loss. However, it might also be reasoned that these closely-spaced random variations might be the result of the effect of the terrain immediately adjacent to the receiving antennas, in which case it is conceivable that these instantaneous values could be more highly correlated than sector medians. Consequently, the data have been tabulated by two methods: first, by pairs of medians of quarter-mile sectors; and second, by sampling discrete pairs of observations every quarter of a mile. To remove systematic effects due to the variation in distance from each transmitter, the tabulated value of observed transmission loss is subtracted from an expected value of transmission loss which is the smooth-earth theoretical value corrected by the Ad Hoc terrain factor[3] to give a residual value expressed in decibels.

Fig. 4 shows in graphical form the observed quarter-mile sector median values of transmission loss for both WRC-FM and WMCP-FM as a function of mileage from Millersville, the starting point of the recording run. The Ad Hoc predicted value of transmission loss over irregular terrain is also shown. Several gaps in the data occur due to the necessity for lowering the antenna to clear overhanging obstacles over the road.

Cumulative distributions of the sector median residuals and the discrete residuals are shown plotted on normal probability paper in Fig. 5. The straight lines on Fig. 5 are the normal distributions about the means of each set of data and with variances as determined from the data. The distributions of the logarithmic residuals approach the normal distribution sufficiently close to permit the assumption that the data are drawn from normally distributed populations.

Before any statistical significance by ordinary means can be attached to a correlation coefficient determined from such data, it is necessary to take samples of the data in such a way that no significant serial correlation is present. This is accomplished by taking the data with sufficient lag between sectors so that the serial correlation is negligible. The appropriate lag determines the limiting number of observations which can be used in estimating correlation between sets of data. The serial correlation coefficients were determined in the circular manner described by Anderson[4] and checked by the noncircular method of Kendall[5] which is more appropriate but less tractable mathematically.

The serial correlation coefficients of the sector medians of WRC-FM and WMCP-FM for lags of one to ten quarter-mile sectors are shown as correlograms in Fig. 6. The 1 per cent and 5 per cent significance levels are also shown in Fig. 6 (below which 99 per cent and 95 per cent respectively of the estimates of the serial correlation coefficients would fall if there were no serial correlation present in the parent population). An exam-

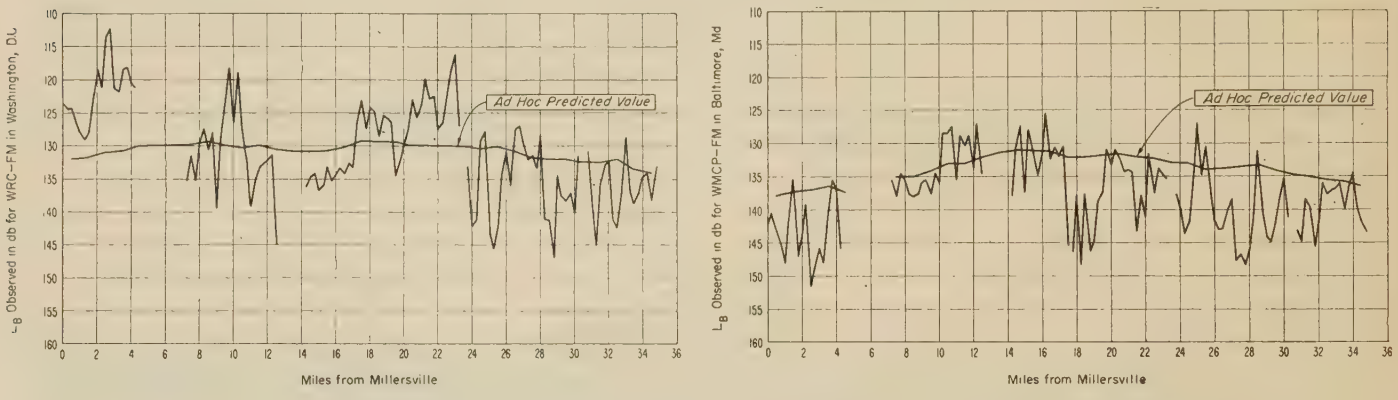

Fig. 4—Observed quarter-mile sector median values of basic transmission loss—Measurements made along perpendicular bisector route from Millersville to Etchison, Maryland.

[3] K. A. Norton, M. Schulkin, and R. S. Kirby, "Ground-wave propagation over irregular terrain at frequencies above 50 mc," Reference C to the report of the Ad Hoc Committee of the Federal Communications Commission for the evaluation of the radio propagation factors concerning the television and frequency modulation broadcasting services in the frequency range between 50 and 250 mc; June 6, 1949.

[4] R. L. Anderson, "Distribution of the serial correlation coefficient," *Annals of Math. Stat.*, vol. 13, pp. 1–13; March, 1942.

[5] M. G. Kendall, "The Advanced Theory of Statistics," Charles Griffin and Co. Ltd., London, vol. II, p. 402; 1946.

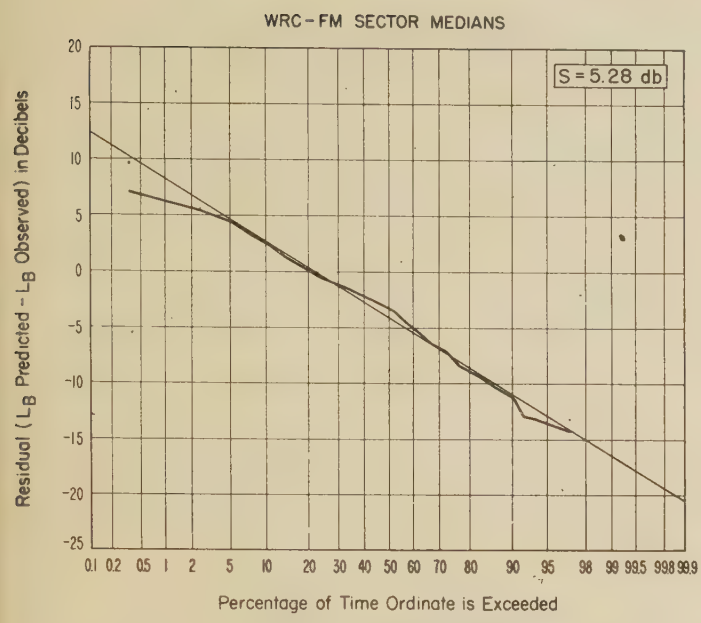

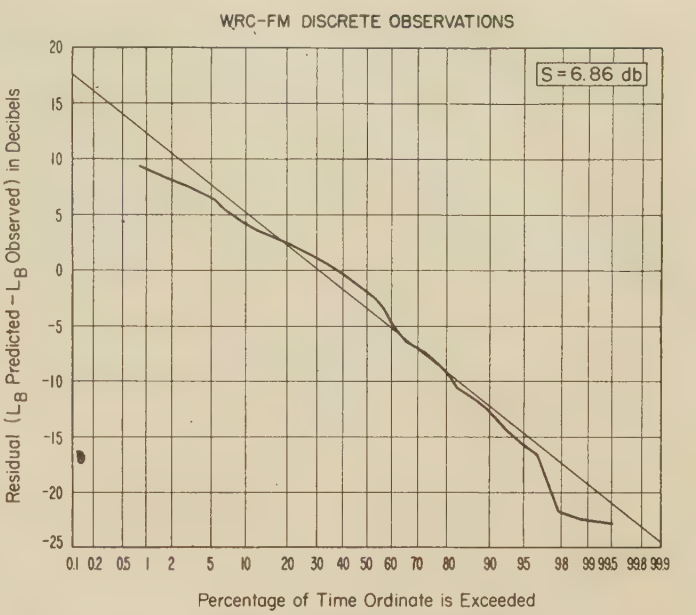

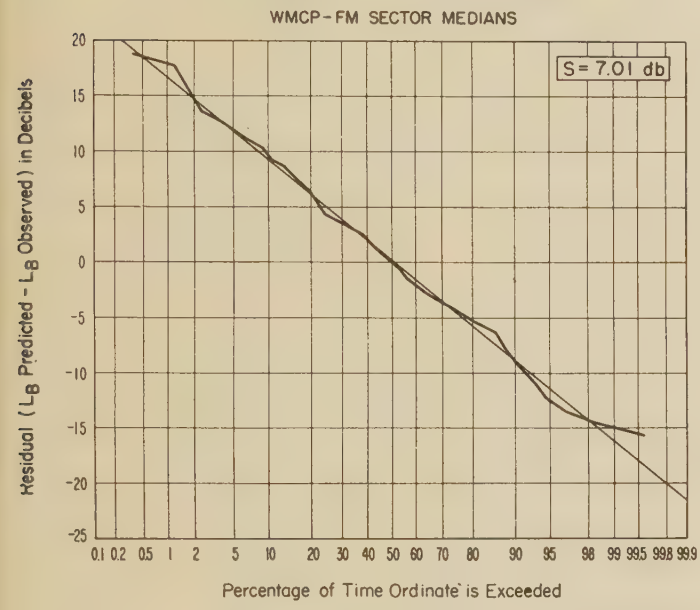

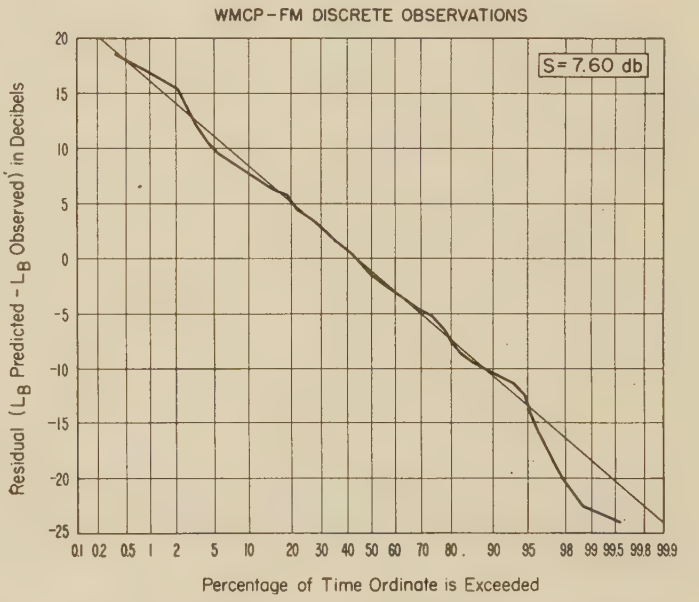

Fig. 5—Distributions of residual transmission loss recorded along perpendicular bisector route.

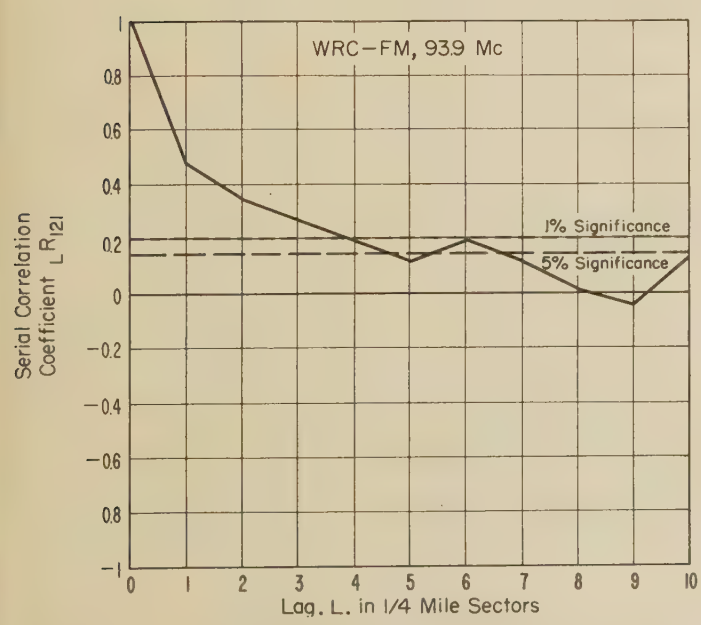

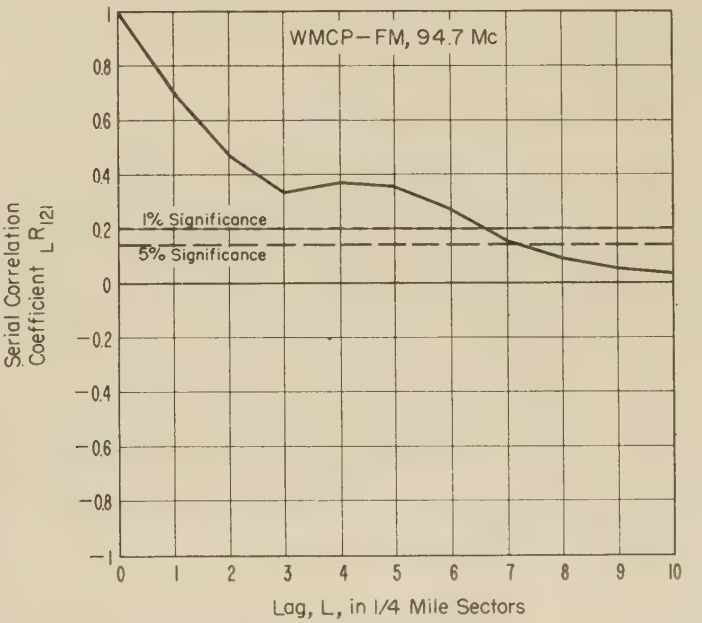

Fig. 6—Serial correlation as a function of lag between successive observations in sector medians of irregular terrain propagation data recorded along perpendicular bisector route, Millersville to Etchison.

ination of the correlograms in Fig. 6 indicates that if the data are taken with a lag of seven or eight sectors, the true serial correlation coefficient should be negligible. A lag of eight sectors (two miles) is taken for our purposes since it provides more assurance against having serial correlation in the data. It should be noted that, although use of data which are negligibly serially correlated as independent observations seems reasonable in case of normal distributions, method is merely an intuitive and approximate one. Hence even confidence intervals for correlation coefficients in Figs. 7 and 10 (which will be discussed below) are approximations (though intuitively reasonable ones).

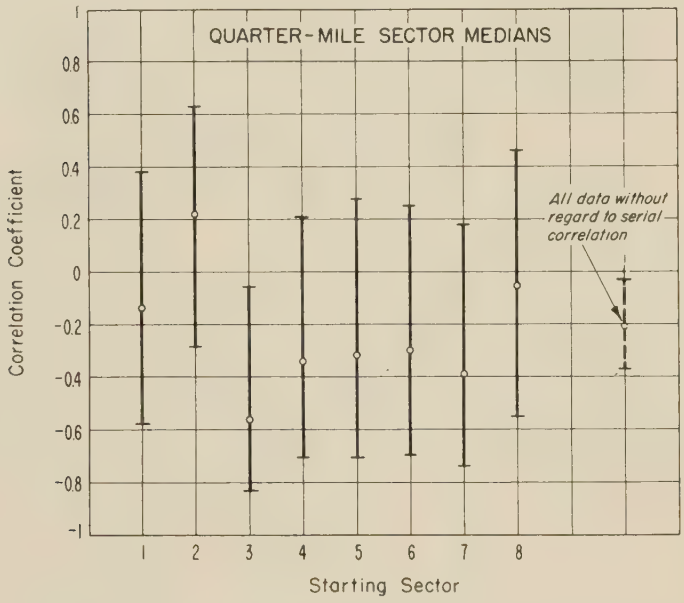

Fig. 7—Estimates of correlation coefficients with 95 per cent confidence interval for WRC-FM and WMCP-FM perpendicular bisector measurements—Eight dependent estimates made from eight starting points with separation of two miles between successive observations.

Having established a lag of eight sectors to be adequate for the purpose of correlation of the data, the sector medians are next taken in simultaneous pairs of sector medians for every eighth sector and the correlation coefficient determined between sector median residual values of transmission loss for WRC-FM and WMCP-FM. Eight estimates of the correlation coefficient are made using eight different sectors as starting points. Unfortunately, these estimates are not independent of each other since serial correlation is involved between estimates. Similar estimates are made using the sampled discrete values. The approximate 95 per cent confidence limits for the true correlation coefficient are determined from the charts prepared by F. N. David.[6] For comparison, a value of R_{XY} with the corresponding confidence limits is tabulated taking all the data into consideration without regard to the serial correlation.

The values for the sector median residuals are shown graphically in Fig. 7. Similar results were obtained using discrete residual values. With one exception all of the eight confidence intervals where a lag of two miles was used include the value zero at the 95 per cent confidence level. Consequently, it is assumed that for the amount of data available, no significant correlation between the fields from WRC-FM and WMCP-FM is apparent. The 95 per cent confidence interval about the correlation coefficient for all data does not include zero in one case, but no significance is attached to this inasmuch as the serial correlation was disregarded; however, this fact does point out the necessity of taking the serial correlation into account.

Correlations and Distributions of Circular Path Measurements

The measurements made along the circular route, where observations were made of the transmission losses of WRC-FM and WNBW-TV simultaneously, are treated in very much the same manner as the perpendicular bisector data of the previous section. However, the data have been classified into four groups in accordance with the type of terrain at the receiving location as noted previously.

Because of the length of the run and because the lag required to eliminate serial correlation is large, on the order of two miles, half-mile sector medians have been determined rather than quarter-mile values. Estimates of the correlation coefficients are made for groups A, B, and C. No estimates are made for the overwater case, since little variation from sector to sector is observed, and this type of data does not lend itself to this kind of analysis. Fig. 8 shows the sector medians plotted for each half-mile sector starting at the east side of Baltimore. The sector numbers are continuous even though measurements in some locations could not be obtained. To obtain the distance along the route from the starting point it is only necessary to divide the sector number by two. The Ad Hoc predicted values are shown on this figure for comparison with the measured values. As before it is the residual between the sector median of the measured values and the Ad Hoc predicted value that is used in estimating the correlation coefficient.

Cumulative distributions of residual values are shown in Fig. 9 (p. 84) for each of three overland terrain types. These distributions are determined from 26 observations in metropolitan areas, 215 in farm lands, and 98 in heavily-wooded areas. The straight line on each of the plots is the normal distribution about the mean of each set of data and with a standard deviation, S, as estimated from the data. It appears that the distribu-

[6] F. N. David, "Tables of correlation coefficient," Biometrika Office, London; 1938.

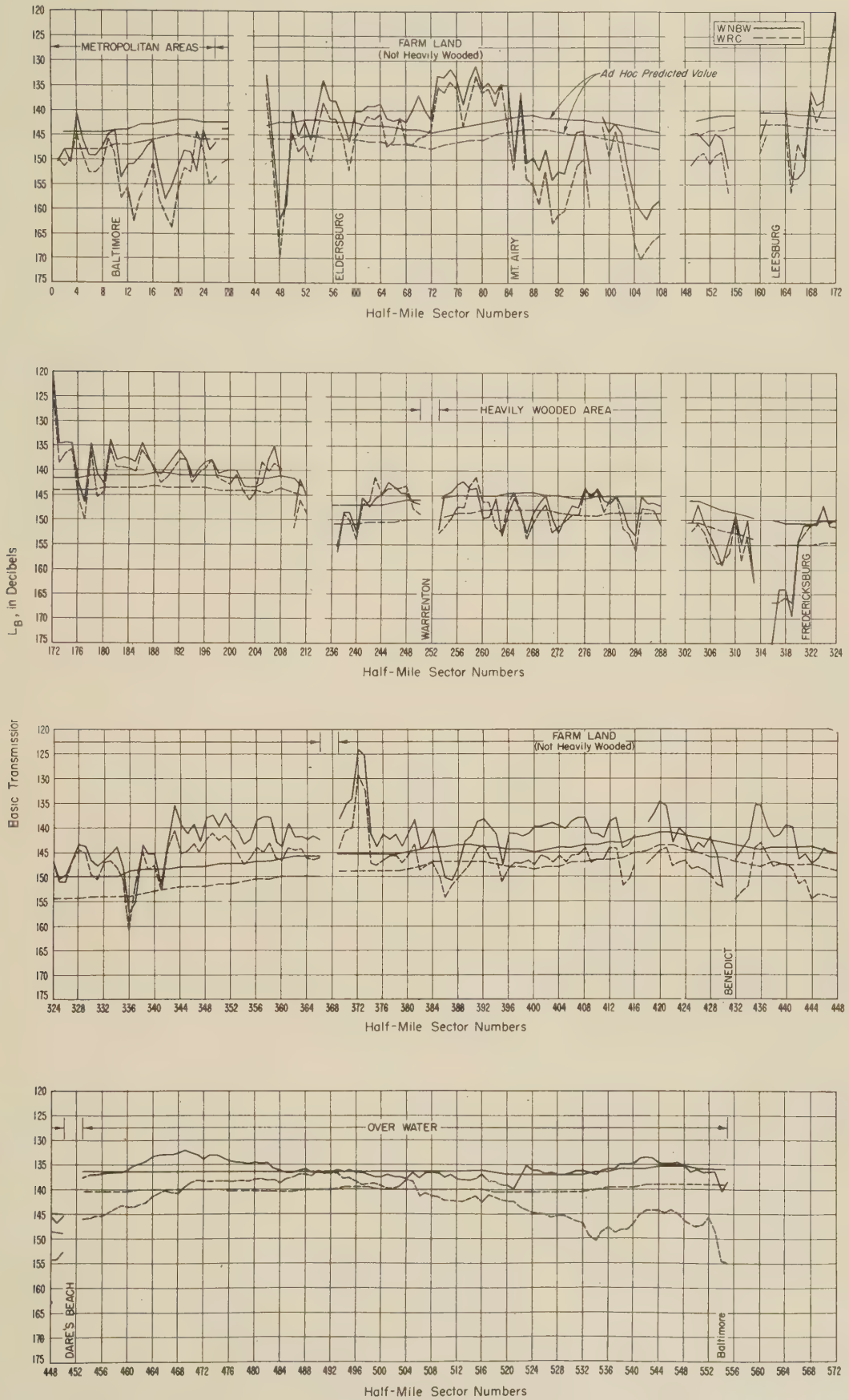

Fig. 8—Observed half-mile sector median values of basic transmission loss measurements made along circular route.

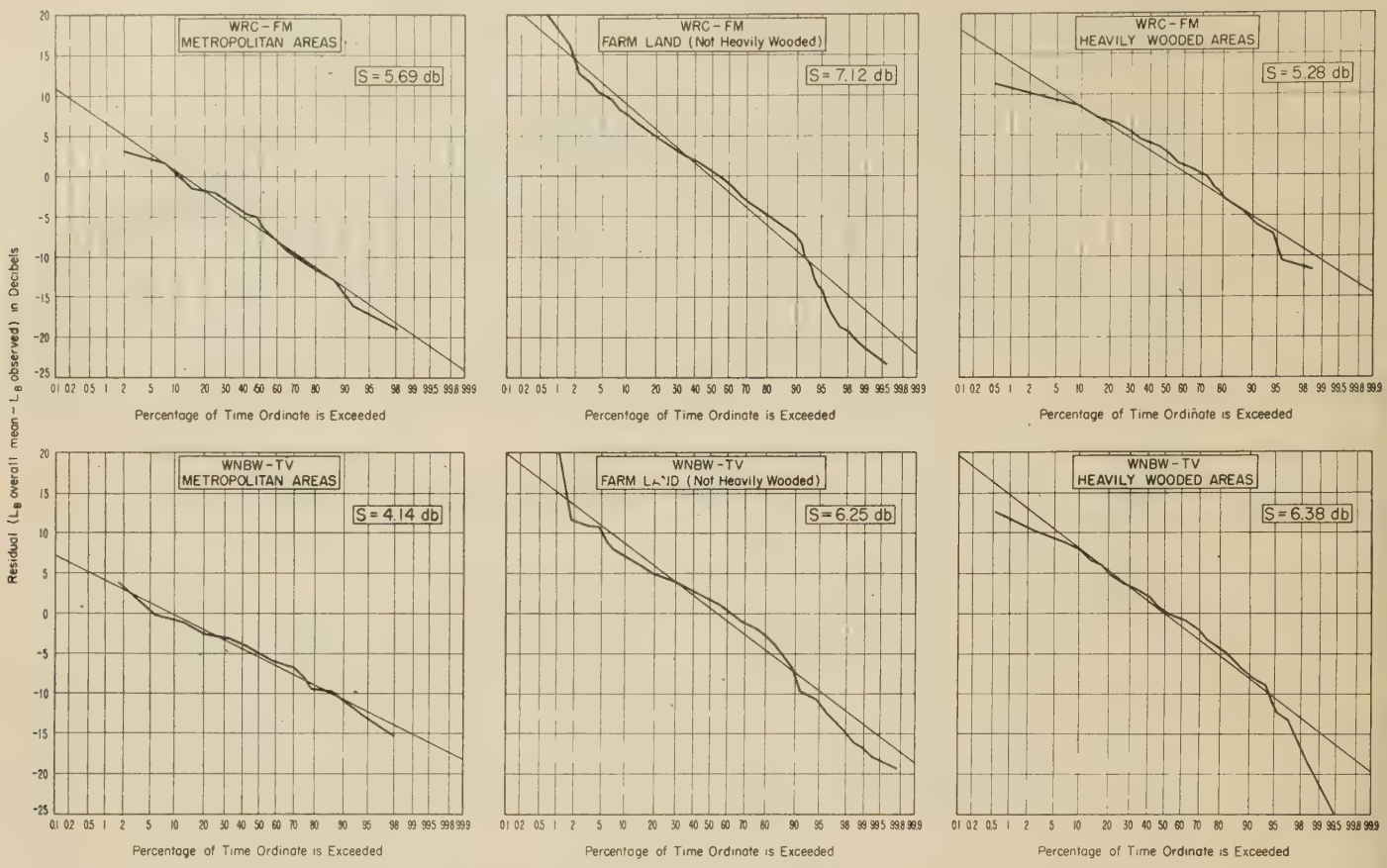

Fig. 9—Distributions of residuals of half-mile sector medians recorded along circular route.

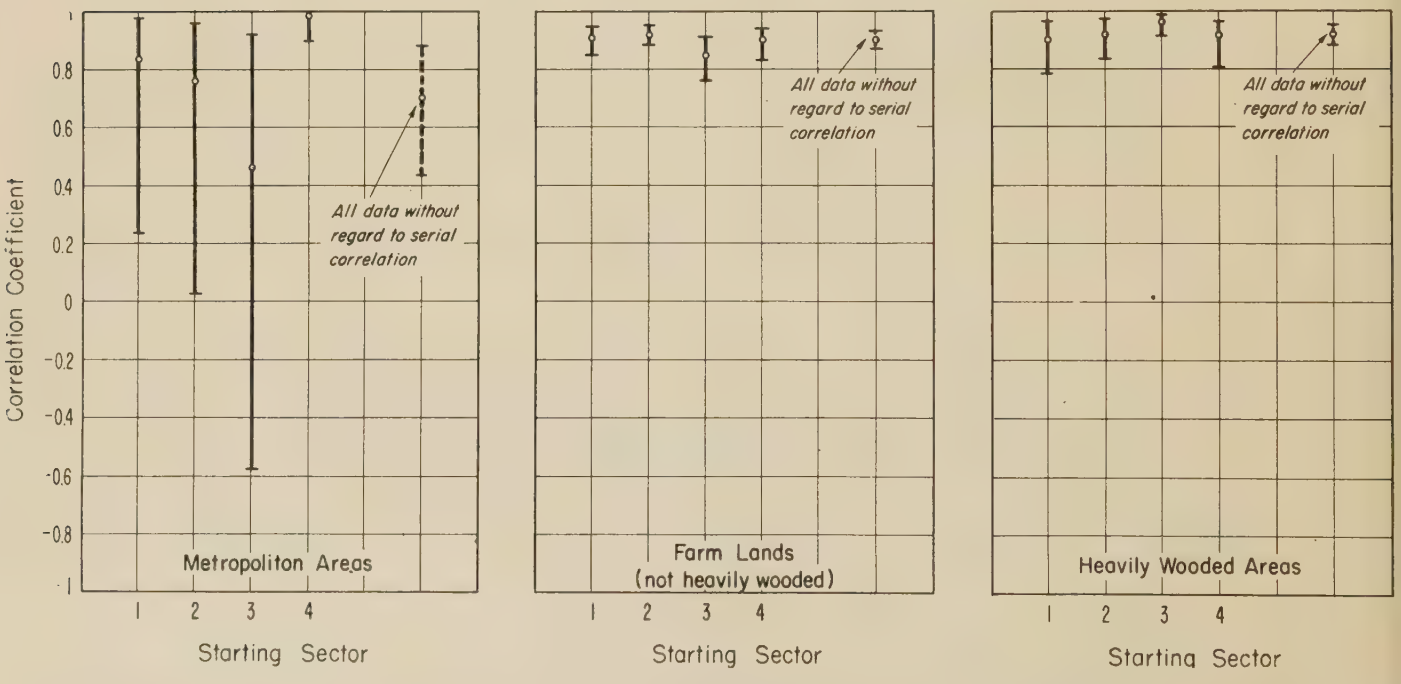

Fig. 10—Estimate of correlation coefficients with 95 per cent confidence interval for WRC-FM and WNBW-FM half-mile sector median residual data obtained on circular route—Four dependent estimates made from four starting points with separation of two miles between successive observations.

tion of sector residuals approaches the normal distribution sufficiently closely to permit the assumption that the data are drawn from normally distributed populations. These distributions show the departures observed from the average of all the values for each station.

The correlation coefficients for WRC-FM and WNBW-TV along the circular route were determined using a lag of two miles as before. In each estimate every fourth pair of residuals is taken, which gives rise to four different, although dependent, estimates of the correlation coefficient. For comparison an additional estimate is made disregarding the serial correlation.

These values are shown in graphical form in Fig. 10. A significantly high correlation in simultaneous sector medians of WRC-FM and WNBW-TV is apparent. There appears to be no applicable difference in the values obtained over farm lands and over wooded areas, and inasmuch as the distributions shown in Fig. 9 are very similar, there is probably no need to differentiate between them. The measurements obtained in the metropolitan area show considerably less correlation as might be expected.

Conclusions

A study has been made of the correlation in transmission loss observed over irregular terrain paths. Simultaneous mobile measurements were made of two pairs of VHF broadcasting stations in the Washington D.C.–Baltimore, Maryland area. For WRC-FM and WMCP-FM the frequencies were essentially the same, 93.9 mc and 94.7 mc respectively, and the paths of propagation were in opposite directions from the receiving point. For WRC-FM and WNBW-TV frequencies were widely separated, 93.9 and 71.75 mc respectively, and the paths were identical. Correlation coefficients derived from sample sets of transmission loss data indicate that when reception is from opposite directions, no correlation is evident. When paths of propagation are the same even though frequencies are separated considerably, as with WRC-FM and WNBW-TV, correlation appears to be significantly high.

communications

Control of Surface Currents by the Use of Channels*

W. K. SAUNDERS†

THE PRESENCE of radiation in the shadow zone of an antenna depends upon surface currents that flow away from the optically lighted region. Minimizing this shadow illumination requires control of these surface currents. For example, even with a large cylinder (circumference $=40\lambda$) excited by an infinite axial slot, the shadow zone of the theoretical pattern has maxima 90° from the slot which are down only 3 db, and others 180° away only 28 db below the power level at 0°. This paper is an experimental study of methods of controlling shadow zone illumination.

* Received by the PGAP, March 11, 1955; revised manuscript received September 19, 1955.

† Diamond Ordnance Fuze Labs., Washington 25, D. C.

In order to study the interruption of surface currents two parallel slots were made in a moderately large ground plane (Fig. 1). The one slot served as a transmitter and the second as a receiver. The equipment was arranged so that the receiving slot could be moved parallel to the direction of its long dimension. This was done so that the interruption of the surface current might be studied in directions other than directly perpendicular to the long dimensions of the slots. To see how the surface currents might be varied, a channel, separating the two slots, was cut in the ground plane. A large variety of lossless and lossy structures were placed therein. The experiment was limited, however,

to structures that did not extend above the ground plane.

The first choices of structures were lossy materials and the traditional one-quarter wave choke.[1] Neither had a perceptible influence on the surface currents. The

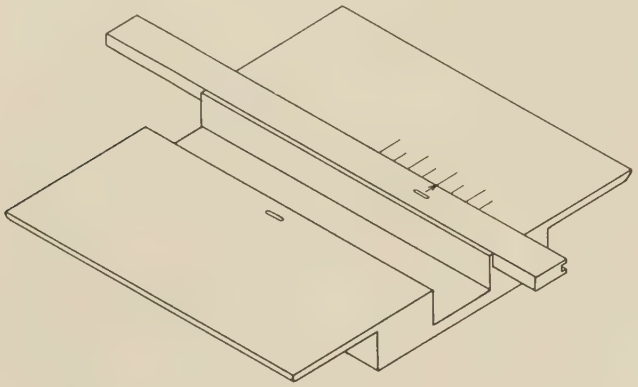

Fig. 1

explanation in the case of the lossy materials seems to be that the higher the dielectric constant, the less the penetration of the wave into the structure and hence the less effect of the material in the structure. The failure of the one-quarter wave choke is somewhat more baffling. In a previous problem, that of decoupling two horns with parallel axes (Fig. 2) a one-quarter wave

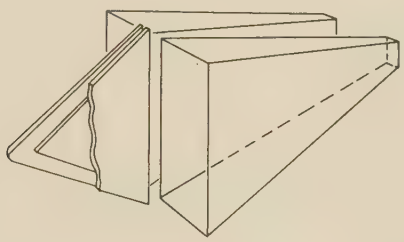

Fig. 2

choke cut in the edge of a plate placed between the horns had given 15 db of additional decoupling over that gotten with the plate alone. The problems, however, have this essential difference. With the horns the wave must reverse its direction of propagation to enter the second horn, and hence if the current around the edge of the plate is broken the wave tends to leave the plate and flow out into space. In the case of the ground plane part of the wave leaving the transmitting slot is headed toward the receiving slot. Any attempt to interrupt this flow causes the wave to bridge the structure and reform on the far side. In addition to the quarter-wave choke and lossy materials, many other structures were placed in the channel. None decoupled as successfully as the channel itself. By cut and try (see Figs. 3 and 4) a width of 2.42 cm and a depth of 1.11 cm was arrived at for a frequency of 9,375 megacycles. Such dimensions appear to be optimum when compared with the decoupling yielded by other dimensions in this range. A channel of this size gives a 9 db decrease in the

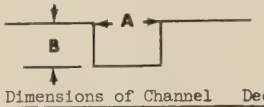

Dimensions of Channel		Decoupling of the Channel
A	B	
1/16"	3/10"	0 db.
1/16"	7/20"	-1.0
1/16"	4/10"	-2.0
1/16"	9/20"	-2.2
3/32"	9/20"	-2.0
1/8"	9/20"	-1.5
3/16"	9/20"	0.5
7/32"	9/20"	0.5
1/4"	9/20"	0.8
9/32"	9/20"	1.0
5/16"	9/20"	1.4
3/8"	9/20"	1.6
1/2"	9/20"	2.0
5/8"	9/20"	1.0
11/16"	9/20"	1.3
13/16"	9/20"	8.0
13/16"	1/2"	8.0
14/16"	1/2"	7.0
29/32"	1/2"	7.0

Fig. 3

power coupled into a receiving slot placed directly across the channel, or offset as much as an inch. Although the effectiveness of the channel decreases for offsets greater than an inch, the coupling between such slots drops sharply with offset, even in the uncut plane.

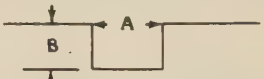

Dimensions		No Offset	1/2" Offset	1" Offset	1 1/2" Offset	2" Offset
A	B					
25/32	11/32	1.6 db.	0.9 db.	-0.3 db.	-1.5 db.	-2.5 db.
26/32	11/32	3.0	1.9	0.5	-1.4	-3.0
27/32	11/32	4.0	3.2	1.4	-1.2	-3.2
28/32	11/32	4.7	4.0	2.0	-0.7	-3.1
25/32	13/32	5.1	3.9	1.4	-1.1	-3.1
26/32	13/32	7.0	5.9	3.2	0.1	-2.7
27/32	13/32	7.5	6.9	4.7	1.5	-1.5
28/32	13/32	7.5	6.9	5.7	2.3	-0.5
25/32	15/32	9.0	8.7	6.0	1.4	-2.1
26/32	15/32	9.1	9.1	7.9	3.5	-0.5
27/32	15/32	9.1	9.1	8.8	5.0	1.2
28/32	15/32	9.2	9.1	9.3	6.9	3.0
25/32	1/2	9.1	9.2	7.8	3.8	-0.5
26/32	1/2	8.4	8.6	9.4	5.8	1.7
27/32	1/2	7.8	8.2	10.0	8.4	4.3
28/32	1/2	8.2	8.0	8.9	8.6	4.8

Fig. 4

This is not indicated in Fig. 4, since the figures shown there represent the increase in decoupling relative to the value obtained by using the uncut plane for each offset listed. No smaller channel gives the degree of decoupling obtained by optimum channel, but there may well be much larger channels or combinations of channels which

[1] J. R. Pierce, "Design procedure for disk choke couplings," Bell Tel. Labs. Memo MM-44-140-22; April 26, 1944.

are other (perhaps more favorable) optima.

The method goes over directly to the cylindrical antenna. In the measured pattern it is seen that the radiation in the shadow zone of the large cylinder is, within experimental error, reduced by 9 db placing two such channels in either side of the radiating slot (Fig. 5). In fact, the reduction takes the form of 1 db at 50° beyond the point chosen for the channel, 5 db at 50° beyond, and 9 db from 80° on, which is of interest in itself for the information it yields of the relationship between the surface current and the radiation pattern of such a cylinder. (See current literature on the creeping wave theory.)

A solution, exact or approximate, of Maxwell's equations for the four-corner structure represented by the channel unfortunately appears unobtainable. The size of the channel is not such as would be predicted by any type of quarter-wave line theory plus end correction, and in addition, both dimensions of the channel are critical. Some predictions can be perhaps arrived at by optical theory, but the theoretical justification of the short wave approximation is nowise apparent.

The author is indebted to H. M. Young for the measurements.

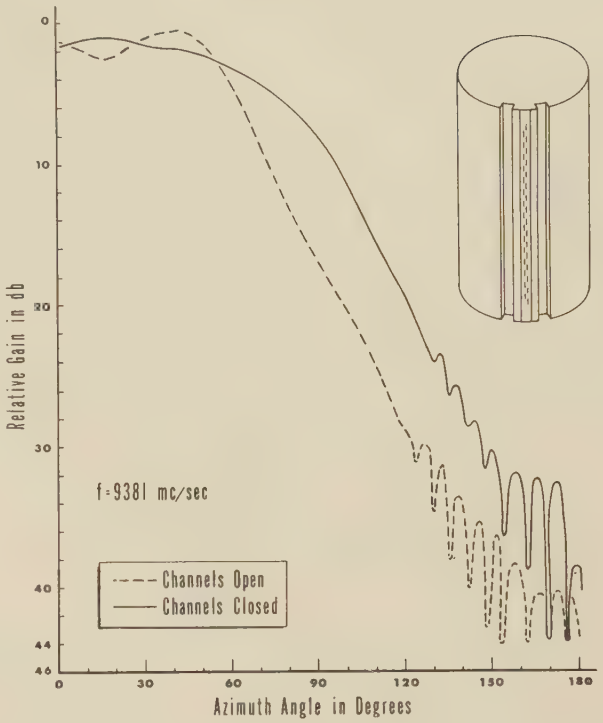

Fig. 5

The Impossibility of Certain Desirable Luneberg Lens Modifications*

A. F. KAY†

THE DIFFICULTY of rapid scanning over the outer surface of a Luneberg lens has led Gutman[1] to devise a lens in which the feed moves on a smaller radius. In Gutman's lens the feed horn points toward the center of the lens and the center section, which rotates during the scan, also serves as a focusing region. In some applications it would be desirable to point the feed horn outward and reserve this center section for rf components. The rotational torque required could also be reduced considerably thereby. We assume throughout that the lens must be radially symmetric to allow 360° of scan.

A priori, a number of types of ray systems suggest themselves (Figs. 1, 2, 3, and 4). All these lenses are shown to be impossible from general considerations, although simple arguments may dispose of some of them directly. For example, a point of radial tangency such as A in Fig. 1 is impossible, and this consideration alone rules out a lens of this type in which one of the focused rays coincides with the radial line through the focus. In the remaining cases, only a bundle of rays of included vertex angle at the focus somewhat less than 90° could possibly be focused. Assuming a certain directivity of the feed itself, this restriction need not be of practical importance in most cases.

If $n=n(r)$ is the refractive index with $n(r_0-)=n(r_1+)=1$, the differential equation for any ray is

$$\frac{d\theta}{dr}=\frac{r_0 \sin \psi_0}{r(n^2r^2-r_0^2 \sin^2 \psi_0)^{1/2}}, \tag{1}$$

where $\psi=\psi(r)$ is the directed angle from the radius vector to the ray, and $\psi_0=\psi(r_0-)$. This equation may readily be put in a form analogous to Snell's Law

* Received by the PGAP, August 26, 1955.
† Technical Research Group, New York, N. Y.
[1] A. S. Gutman, "Modified Luneberg lens," *J. Appl. Phys.*, vol. 25, pp. 855–859; July, 1954.

$$nr \sin \psi = \text{constant} = r_0 \sin \psi_0. \quad (2)$$

From (2) we see that since $\sin \psi \leq 1$,

$$nr \geq r_0 \sin \psi_0, \quad (3)$$

throughout $r_0 < r < r_1$ with equality holding only when $\psi = \pi/2$. If, for example, for some r_2 with $r_0 < r_2 < r_1$, the

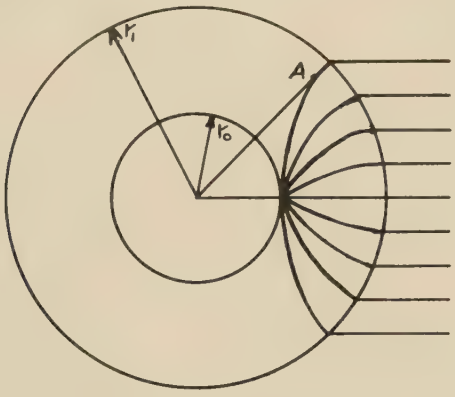

Fig. 1

inequality $r_2 n(r_2) < r_0 \sin \psi_0$ held, then the ray leaving the focus at an angle ψ_0 to the radius vector would not cross the circle $r = r_2$ and could never focus. If equality holds at all in (3), it will hold only for the largest ψ_0 in the entire bundle of rays to be focused. We drop this ray from consideration, and so are able to assume in view of (1) that 1) $|\psi| < \pi/2$ and 2) $d\theta/dr$ is a monotone function of r and hence

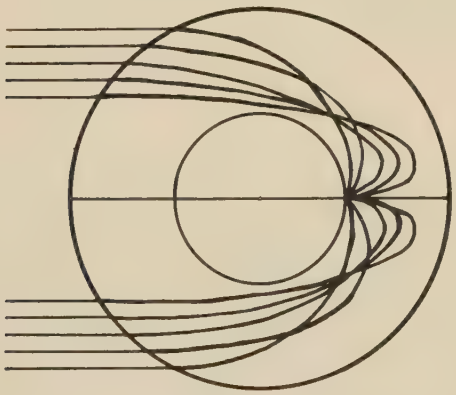

Fig. 2

$$\theta_1 = r_0 \sin \psi_0 \int_{r_0}^{r_1} \frac{dr}{r(n^2 r^2 - r_0^2 \sin^2 \psi_0)^{1/2}}, \quad (4)$$

where $\theta_1 = \theta(r_1)$. The condition for focus is seen from Fig. 3 to be

$$\theta_1 = \phi - \psi_1 \quad (5)$$

where ϕ is the direction of focus and independent of ψ_0.

From (2),

$$r_1 \sin \psi_1 = r_0 \sin \psi_0, \quad (6)$$

so that the condition for focusing becomes

$$r_0 \sin \psi_0 \int_{r_0}^{r_1} \frac{dr}{r(n^2 r^2 - r_0^2 \sin^2 \psi_0)^{1/2}} - \phi + \sin^{-1}\left(\frac{r_0 \sin \psi_0}{r_1}\right) = 0. \quad (7)$$

The branch of the inverse sine is determined as follows. As ψ_0 approaches zero, from (1), $\theta = \theta(r)$ approaches zero identically so that ψ_1 approaches zero.

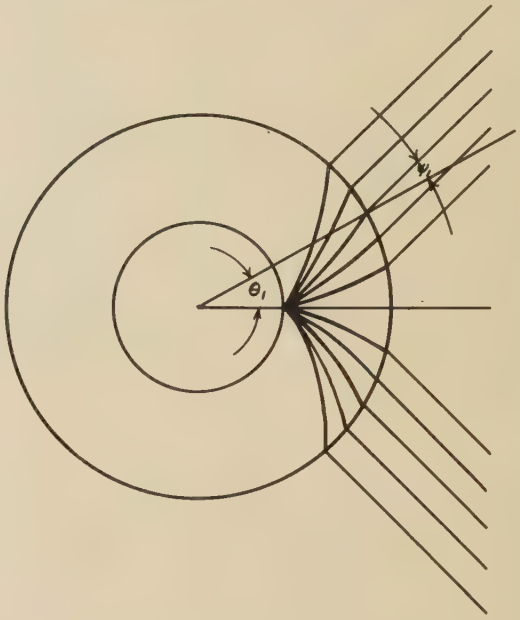

Fig. 3

Thus we are dealing with the principal value of the inverse sine. Left member of (7), however, from inspection is a strictly increasing function of ψ_0 in range $0 \leqq \psi_0 \leqq \pi/2$; (7) hence can hold only for a single ray.

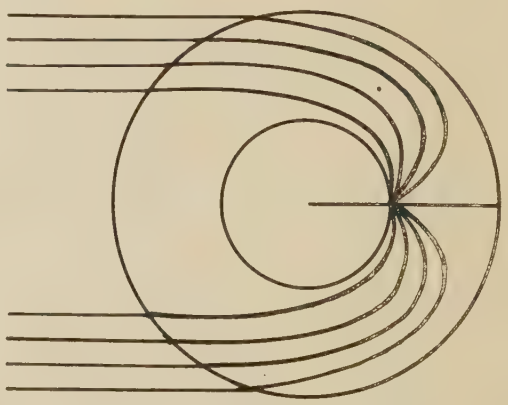

Fig. 4

In conclusion, we have shown that the following is impossible: a radially symmetric lens occupying an annular region, $r_0 < r < r_1$, which focuses perfectly any bundle of rays (no matter how small) emanating from a point source on $r = r_0$ into a parallel beam.

Discussion* on

"Fresnel Antenna Patterns"†

L. W. LECHTRECK‡

D. K. Cheno:[1] In a recent article, Lechtreck presented a number of radiation patterns for rectangular apertures with quadratic phase errors. I would like to make several comments about that article.

1) It does not appear to me that the square signs over the C and S Fresnel integrals and the $\pm$ signs in the radiation pattern expressions should be there. Mr. Lechtreck did not explain whether he used the $+$ or the $-$ signs when he computed the radiation patterns but it seems that all $\pm$ signs in his expressions should be just $-$ signs. Also, Mr. Lechtreck apparently defined his C and S integrals as

$$C + jS = \int_0^t \epsilon^{jx^2} dx, \tag{1}$$

instead of in the conventional way:

$$C + jS = \int_0^t \epsilon^{j(\pi/2)x^2} dx. \tag{2}$$

To my knowledge, all available C and S tabulations are based on the conventional definitions (2).

2) Mr. Lechtreck computed radiation patterns for values of b as large as 5 or 1.67π. There is some doubt as to the validity of the use of Fourier transform for obtaining radiation patterns for such large phase errors. The illumination at the aperture edge would already be in opposite phase to that at the center when $b = \pi$.

3) The location of the side lobes and the minima in the radiation pattern depends upon the extent of aperture phase error. Therefore, it does not seem right to fix the u-values on the curves of Figs. 3 and 4.

4) I wish to point out that the radiation patterns for rectangular apertures with phase errors of the linear, step, staircase, quadratic, and cubic types have been analyzed and computed[2] for uniform and $\cos^2(0.37^5\pi x)$ illuminations; the latter illumination was chosen because it gives -25.9 db first side lobes which is a desirable level. For each type of phase error, three cases were considered, namely: deviation on one side, anti-symmetrical deviation, and symmetrical deviation. Tables containing data on beam shift, maximum radiation amplitude, main-lobe beamwidth at -3 db and -10 db, first side-lobe levels, and gain factor are available. Similar analyses have also been done for the circular aperture.

L. W. Lechtreck: 1) The functions referred to in the article are those defined by Harry Bateman[3] in equations (4) and (5):

$$C(x) = \sqrt{\frac{2}{\pi}} \int_0^x \cos(t^2) dt$$

$$S(x) = \sqrt{\frac{2}{\pi}} \int_0^x \sin(t^2) dt.$$

These functions have been tabulated by Eugene Jahnke and Fritz Emde in "Tables of Functions . . . ," p. 35, published by Dover Publications, 1945; G. N. Watson, in "A Treatise on the Theory of Bessel Functions," pp. 744–745, published by Cambridge, 1944; and in "Report of British Association for the Advancement of Science," pp. 274–275, published by Oxford, 1926. When defined in this manner, the square and $\pm$ signs are necessary as shown in the complete derivation. The minus sign is used when the limit of integration is positive; the plus sign when this limit is negative.

2) The curves in this article are applicable only to antennas for which the radiation pattern can be represented as a simple, separable, scalar, Fourier integral. The large phase error curves are useful in predicting the far-field radiation pattern of a large aperture in the angular region near the aperture normal. Under these conditions the phase front normal is parallel to the aperture normal and Silver's equation[4] is not violated. The problem of securing a rapidly converging series approximation for large values of B and U was avoided through the use of tables of Fresnel integrals.

3) In Figs. 3 and 4, the labels designating the locations of the nulls and peaks are in error. The numbers given are those of the zero phase error curves and the angular location of the radiation nulls and peaks do move slightly with changes in b. This results in errors in calculated pattern magnitudes at true peaks and nulls, of about ± 0.2 db for range of b shown in these figures.

4) I am sorry not to have known about the reports of Dr. Cheng, however, it seems that both of our studies were predated by a paper[5] presented at the "Conference

* Received by the PGAP, August 18, 1955.
† Trans. IRE, vol. AP-3, pp. 138–140; July, 1955.
‡ Emerson Electric Mfg. Co., St. Louis, Mo.
[1] Electrical Engrg. Dept., L. C. Smith College of Engrg., Syracuse University, Syracuse, N. Y.
[2] D. K. Cheng, "Phase-Error Effects in Microwave Antennas," Interim Reports on Contract Nos. AF30(120)-425-E.E.4 and AF30 (602)-300 Syracuse University Research Institute; April, 1952 and September, 1953.
[3] Bateman Project Staff, "Higher Transcendental Functions," Vol. II, McGraw-Hill Book Co., Inc., New York, N. Y., p. 149; 1953.
[4] S. Silver, "Microwave Antenna Theory and Design," M.I.T. Rad. Lab. Ser., McGraw-Hill Book Co., Inc., New York, N. Y., vol. 12, p. 172; 1949.
[5] K. Milne, "The Effects of Phase Errors on Simple Aperture Illuminations," Her Majesty's Stationery Office. (Thanks to W. C. Jakes of Bell Telephone Labs.)

on Centimetric Aerials for Marine Navigation Radar" held in London in June 1950. In that paper Mr. Milne numerically described the radiation patterns from rectangular apertures with linear, cosine, and cosine squared illumination for phase errors quadratic through quintic.

D. K. Cheng: 1) The definitions of the Fresnel integrals C and S that appear in Bateman's "Higher Transcendental Functions," vol. II, to which Mr. Lechtreck referred, are identical with those used in Jahnke and Emde's "Tables of Functions" and Watson's "Theory of Bessel Functions." (The upper limit in Mr. Lechtreck's expressions should be $\sqrt{x}$ instead of x.) They are based on eq. (2) of my original comments. If Mr. Lechtreck had used these definitions, he would not have obtained the radiation-pattern functions as given in his paper.

For an aperture illumination

$$f_1(x) = 1\epsilon^{jbx^2}, \qquad -1 \le x \le +1,$$

the radiation-pattern function would be

$$g_1(u) = \int_{-1}^{1} \epsilon^{jbx^2}\epsilon^{jux}dx$$

$$= \sqrt{\frac{\pi}{2b}}\,\epsilon^{-ju^2/4b}\left\{C(U_2)-C(U_1)+jS(U_2)-jS(U_1)\right\}$$

where

$$U_1 = \sqrt{\frac{2b}{\pi}}\left(\frac{u}{2b}-1\right) \quad \text{and} \quad U_2 = \sqrt{\frac{2b}{\pi}}\left(\frac{u}{2b}+1\right).$$

For the aperture illumination

$$f_2(x) = \cos\left(\frac{\pi}{2}x\right)\epsilon^{jbx^2}, \qquad -1 \le x \le +1,$$

the radiation-pattern function would be

$$g_2(u) = \int_{-1}^{1} \cos\left(\frac{\pi}{2}x\right)\epsilon^{jbx^2}\epsilon^{jux}dx$$

$$= \frac{1}{2}\left[g_1\left(u+\frac{\pi}{2}\right)+g_1\left(u-\frac{\pi}{2}\right)\right].$$

If Mr. Lechtreck used the tables in either Jahnke and Emde or in Watson, his results would be in error.

2) The validity of the use of Fourier integral for obtaining radiation patterns for b as large as 5 is questionable even in the angular region near the aperture normal because of the fact that the term $i_{z\cdot s}$ appears in the integrand[4] which has to be integrated over the entire aperture surface. Curves given by Mr. Lechtreck extend to values of u as large as 15.

3) I have not been aware of Milne's work in England. However, curves in my reports were for both rectangular and circular apertures with various types of phase errors that appear in the outer half of the aperture; there is probably little duplication of effort.

Summary of Normal Mode Theory Symposium

A SYMPOSIUM on Normal Mode Theory was convened, under the chairmanship of Dr. S. A. Schelkunoff, at the Navy Electronics Laboratory on July 5, 6, and 7, 1955. This symposium consisted of an informal trip to Palomar Mountain on July 5 and a round-table discussion on July 6–7 for the purpose of exchanging ideas about the present state of theoretical knowledge of wave propagation through stratified media, the known methods of attack, and the outstanding unanswered questions. Although the emphasis was on normal mode theory, the possibility of extending the ray theory of physical optics was explored. The following list of topics was on the agenda:

1. Ray Theory: what it is, the extent of its proved usefulness, and its limitations.
2. Huygens' Principle; what it is, the extent of its usefulness, its limitations, and possible extensions.
3. Mode Theory: what it is, and its relation to the Ray Theory.
4. The contrast between the Mode and Ray Theories, when both yield exact results.
5. The interaction of experiment and the Mode Theory in the radio history of long waves, ionospheric waves, and tropospheric waves.
6. Effect of small perturbations in the index of refraction on mode series.
7. Effect of discontinuities in the index of refraction or its derivatives on mode series; interpretation of this effect.
8. Convergence of mode series.

9. Methods of computing the individual terms of mode series.
10. Methods of summing mode series.
11. Effect of ground constants on modes.
12. Surface roughness and its representation in analysis.
13. Absorbing boundaries and their representation in analysis.
14. Boundary conditions in general.
15. Curved earth.
16. Natural oscillations of the earth.
17. Calculation of fields in the visible region.
18. Calculation of fields near the horizon.
19. Calculation of fields beyond the horizon.
20. Other topics that may be suggested before or during the conference.

Ray Theory

The first topic dealing with ray theory was introduced by Dr. Smyth. Historically, ray theory embraces all that is derivable from Fermat's principle, *i.e.*, Snell's Law. More recently, investigators consider ray theory everything that is contained in the asymptotic solution to the wave equation for the limiting case of the wavelength approaching zero. Some suggest that correction terms in regions of caustics should be included as an integral part of ray theory. Hadamard defined rays as the normals to the discontinuity surface associated with a pulse disturbance. Rays have also been defined as the stream lines of energy flow. Another definition considers rays as the contributions to the observed signal which have distinct arrival times. This definition appears to be identical to one definition of mode given later. It was pointed out that the rays derived from the asymptotic solution to the wave equation and from Hadamard's definition are identical for Maxwell's equations but not identical for Schrodinger's equation. It was generally agreed that the most useful definition of ray theory is contained in the asymptotic solution to the wave equation. The corpuscular concepts basic to geometrical optics are being replaced by mathematical procedures and this branch of physics is becoming a special case of wave theory.[1]

In practice the basic law of Snell is used to determine the ray path and in addition it is tacitly assumed that these rays are the stream lines of energy flow. The wave nature of the radiation is called upon at this point to take the phase relationship of the rays into account. The familiar interference patterns in acoustic and radio fields associated with multipath transmissions have been described in this manner. Ray theory has not enjoyed much success in describing diffraction effects, including fields near caustics.

[1] Cf. R. K. Luneberg, "Mathematical Theory of Optics Lectures in Advanced Mechanics," Brown University; 1944.

Huygens' Principle

Dr. Bouwkamp opened the discussion of Huygens' principle. He began with some historical remarks, pointing out that Huygens introduced his principle to explain the laws of rectilinear propagation, reflection, and refraction. However, its extremely important application to diffraction was unknown to Huygens, as was diffraction itself. According to Huygens, each wavefront was to be considered as an envelope of secondary sources, but he did not explain why there was no backward radiation. This problem was eventually solved by Kirchhoff. Kirchhoff's formula is a representation theorem for solutions of the wave equation in terms of boundary values on a closed surface. But since the monochromatic wave equation is of elliptic type one cannot prescribe arbitrarily both the wave function and its normal derivative on the boundary. Hence this formulation is limited in its application. In this connection Dr. Bouwkamp also brought up the divergence of opinion as to the precise meaning of Huygens' principle. He differs with the views put forward by Volterra, Hadamard, and M. Riesz, whose attempts at a precise mathematical formulation may be found in the book "Huygens' Principle" by Baker and Copson.

There followed a discussion of the use of the representation theorem in diffraction problems wherein one assumes a field distribution in the aperture although one actually does not know this field. It was pointed out that iteration does not work here.

Dr. Bouwkamp, however, brought up the fact that one may consider the problem as a *saltus* problem, and instead of prescribing (approximately) the field in the aperture, one prescribes the discontinuities of the field across the boundary. Then the Kirchoff formulation yields an exact solution of the saltus problem. He also stressed that, from the physicist's point of view, no formulation which permits backward radiation can be considered as a mathematical representation of Huygens' principle.

An example in which the use of the Kirchhoff-Huygens theory in far zone backscatter gave good agreement with experiment was also mentioned.

Normal Mode Theory

Dr. Bremmer began the discussion on this subject. According to his view, the essential point of mode theory is that one starts from the boundary conditions, leaving the sources out of consideration, in determining the modes. The sources are then taken into account by linear superposition of mode solutions. He discussed in some detail the problem of a plane earth with an inhomogeneous but horizontally stratified atmosphere, separated from the earth by a homogeneous layer.

Dr. Friedman gave the following as a possible definition of mode: for the wave equation in a separable

coordinate system any solution of the equation which satisfies the boundary conditions for all except one of the coordinates is a mode; any distribution of sources being expressible as a linear combination of modes.

The question of physical meaning of a mode was discussed; *i.e.*, is a mode simply a term in a mathematical formula or does it have some definite physical meaning. In this connection the problem of the unbounded medium and the accompanying continuous spectrum of modes was brought forth. It was pointed out that modes of a continuous spectrum could hardly be assigned any physical meaning since the path of integration could be altered. This point of view was, however, disputed on the ground that the basic representation was unique and that other representations were merely means of calculation.

In the problem of propagation of explosive sound between two parallel perfectly reflecting planes it has been possible to interpret each mode physically as being associated with a given angle of reflection from the bounding surfaces.

Regarding series expansions of a field quantity in some cases one finds that one can attach specific physical ideas to each term. For example, each term can exist by itself, each carrying a finite amount of power. In other cases, notably including the continuous spectrum case, the term cannot exist independently and each may have infinite energy content. The question is then: should any series expansion be considered a mode expansion, or should one restrict the latter label to the case where each term has some accompanying physical idea. The members of the panel did not seem to be agreed on this point, some wishing to restrict the term "mode" to the case of finite energy content, while others would use the term in any formal (but convergent) series expansion.

Sommerfeld Surface Wave

This topic was introduced by Prof. Baños. Historically, the subject is based upon the 1909 paper of Sommerfeld.[2] The statements which Baños made were a result of his joint research[3] over the last several years. The main problem is a mathematical one and arises from the solution of the problem of an electric dipole placed in the interface between two conducting media. The solution to this is represented as an integral in the complex plane. By the use of contour integration a further representation is obtained consisting, in general, of three terms. Of these, two are integrals along certain branch cuts while the third is the residue arising from a certain pole in the complex plane. It is this residue term which Sommerfeld called the "surface wave" and which Baños calls the "Sommerfeld surface wave." The main point of Baños' introduction was that at some intermediate range (which is a well-defined function of the parameters of the problem) the residue or surface-wave term has a $r^{-1/2}$ dependence and hence is the dominant part of the solution. However, for large r the branch cut integrals asymptotically cancel the residue term. Baños referred to this as the "swallowing-up" of the surface wave at infinity.

The first point of the rather lively discussion that followed was an objection by Dr. Schelkunoff. He read a lengthy quotation from Zenneck[4] which stated, in effect, that the surface wave behaved essentially as $r^{-1/2}$ for all r and therefore became dominant with infinite range. This was in obvious disagreement with Baños' statement concerning the "swallowing-up" of the surface wave at infinity. Schelkunoff agreed that his disagreement with Baños might be a semantical one and that instead of the term "Sommerfeld surface wave" we should use the term "contribution arising from the residue at the pole."

Following this, several other members of the panel entered into a fairly detailed discussion of the mathematical difficulties of the problem, which are not inconsiderable. Of the points which were discussed the most important seemed to be that brought out by Dr. Bouwkamp. This concerned the application of the classic (Sommerfeld) radiation condition in the presence of a plane interface. He said that this is a crucial point in problems of this type and that much work needs to be done along this line. Since Sommerfeld's original paper in 1909, about fifty papers have appeared on the subject. Most of these contain differences and some, mistakes. In fact, Sommerfeld himself had made contradictory statements as late as 1947. One alternative radiation condition was suggested to Bouwkamp and it was not immediately obvious that it was equivalent to Sommerfeld's. Various members of the panel suggested ways of determining the physical existence of surface waves (!), and debated whether or not surface waves would exist (either mathematically or physically) if neither medium were allowed to have conductivity. The session was closed by Dr. Bremmer who summarized a recent (unpublished) paper by van der Pol concerning the existence of a transient surface wave.

Propagation Beyond the Horizon

The subject was introduced with a brief summary by Dr. Carroll of the history of the problem and of the work on it in which he has been engaged. He pointed out that the original "line-of-sight" hypothesis was inadequate to explain the observed phenomena and

[2] Sommerfeld, "Über die ausbreitung der wellen in der drahtlosen telegraphie," *Ann. Phys.*, vol. 28, pp. 665–737; 1909.

[3] Baños and Wesley, "The horizontal electric dipole in a conducting half-space," Parts I and II, *SIO*, vol. 53, p. 33; September, 1953; and *SIO*, vol. 54, p. 31; August, 1954.

[4] A. E. Seelig, "Lehrbuch der drahtlosen Telegraphie," McGraw-Hill Book Co., Inc., New York, N. Y., sec. 139; 1915.

that the classical theory was vulnerable to criticism on two counts: 1) the use of an "effective" radius of the earth, taken as four-thirds the actual radius, to compensate for the presence of the inhomogeneous atmosphere in ray-theoretical calculations; and 2) the fact that the gradient only and not the absolute value of the index of refraction makes its appearance in the theory.

As an alternative to the classical approach, Dr. Carroll offered a solution based on Furry's theory of bilinear gradients. In the particular model which Carroll used, the index of refraction decreases linearly with increasing distance above the earth to the value unity at a certain height, and then remains equal to one as the height continues to increase. Otherwise no special assumptions about the atmosphere are made. The eigenfunction expansion obtained on the basis of this model gives results which are consistent with the observed dependence of energy upon distance from the source, namely, the lobe structure within the horizon, the sharp drop-off at the horizon, and the gradual decrease beyond the horizon.[5]

An added feature of the theory is that the results are virtually independent of frequency over a wide range; this led to the conjecture that the theory was applicable over the entire electromagnetic spectrum. In confirmation it was noted that the duration and attenuation of twilight, an optical phenomenon known from the earliest times but as yet unexplained, came within the scope of the theory and was successfully accounted for by it. The term "twilight zone" has consequently been suggested for the region just beyond the horizon.

Carroll's presentation was followed by a lively discussion, in which the Booker-Gordon theory, a prominent rival solution to the problem, played an offstage role. The latter explains propagation beyond the horizon in terms of refraction by zones of turbulence, or "blobs of inhomogeneity," in the atmosphere. It was suggested that since Carroll's modal theory hardly takes notice of the physical properties of the atmosphere, it is incapable of dealing with such phenomena as signal fluctuation, the angular spectrum of the received signal, and the information bandwidth; further that incoherent scattering, which predominates outside the zone of the direct field, cannot be explained solely by adopting an index of refraction. Carroll answered that insofar as these phenomena were caused by thermal effects or by molecular scattering as distinguished from turbulent scattering, they could at length be fitted into the theory. He in turn criticized the turbulence theory on the grounds that the large number of parameters at one's disposal tended to make each particular case of the theory an *ad hoc* creation, whereas the modal theory was derived on a minimum number of assumptions.

[5] These results are written up in detail by T. J. Carroll and R. M. Ring, "Normal tropospheric propagation of short radio waves well beyond the horizon," M.I.T. Lincoln Lab. Tech. Report 38; February 12, 1954.

Several speakers were interested in the influence on the final results of the "kink," or corner, in the bilinear gradient profile. Carroll's own position was that the bilinear model was taken as it was in order to lead to tractable formulas, that the discontinuity in the first derivative could be avoided by joining the two segments with a suitable arc, that this process resulted in no important change in the calculations (*i.e.*, of the field beyond the horizon), hence that the presence of the corner was not a decisive feature of the theory. The opposite view was expressed by Prof. Friedman, who presented an argument based upon the location of the eigenvalues associated with the bilinear profile. Friedman's conclusion was that the greater the difference in slope between the two segments of the gradient the smaller the attenuation of the field a great distance beyond the horizon, but that there was a significant difference in the attenuation between the cases of a perfectly straight angle and a very nearly straight angle between the segments.[6] Other speakers pointed out that the question was ultimately relative to the wavelength and the accuracy with which one could measure a change in refractive index over a measurable fraction of a wavelength in the vertical direction. These said that it was nonsense to criticize a mathematical model on physical grounds within a range where physical measurements could not be made. Others maintained that, on the contrary, the details of the profile were of major imprtance, owing to the energy levels used and the high order of the modes necessary to get the results. They found in the high accuracy required in Carroll's solution a possible breeding ground for errors and an obstacle to an understanding of the physical processes involved.

The question about the kink in the gradient profile in the mode theory had its counterpart in a discussion over the cusp at the origin in the autocorrelation for the turbulence theory. This function, which characterizes the inhomogeneity distribution, has usually been assumed to be exponential, and the exponential function has a cusp. The belief was expressed that the cusp assumption is necessary to achieve agreement with experiment, but the presence of the cusp implies that the refractive index changes discontinuously at the boundary of a blob. L. Liebermann's[7] work on scattering by temperature inhomogeneities in the ocean was cited.

After the Symposium proper Dr. Carroll submitted a list of unresolved problems, which may well be made part of the record. These questions together with his own ideas of the answers follow, together with a few additional remarks of his concerning the course of future investigations on the problem.

[6] Dr. Friedman's summary of his position is contained in Appendix. His detailed calculations are contained in two reports, which may be obtained from Technical Research Group, 56 W. 45th Street, New York 36, New York.

[7] L. Lieberman.

Questions Unanswered Due to Lack of Time

Although the crucial issues were well brought out, it was an inevitable consequence of time pressure that many of the questions raised by the audience and the round-table members were not dealt with, even though they could have been in the present state of knowledge. Chief of the questions may be listed as follows, along with a suggestion (in parentheses) of the gist of the answers which should have been given if time had permitted: 1) Mode theory explanation of twilight region fading (a combination of variation of index profile with time, and the effects of thermal motions of the scattering molecules as yet not considered in mode theory); 2) "Gain loss" and observed pattern broadening on beam swinging experiments with antennas of many wavelengths aperture (phase variation of the wave functions must be small over the vertical aperture of the antenna for the usual antenna gain relations to hold; in twilight region antenna pattern measurements, the effective source is not a point, but rather the illuminated air over the middle of the path, which subtends at the receiver an appreciable angle and causes beam broadening, as do radio stars which are not "points" as viewed by a narrow-beamed radio receiving antenna); 3) Comparison of polarization effects on the two theories (experiments have been performed and seem to me to favor the idea of scatterers very small compared to a wavelength such as the molecular scatterers of mode theory); 4) Small frequency dependence of twilight fields (a consequence in mode theory of the frequency independence of the index of refraction in the radio region, and obtainable in turbulence theory only by assumption of sharp sided blobs); 5) Limited pulse lengthening in experiments (due in mode theory to the limited range of phase velocity of the modes which contribute importantly to the twilight field); 6) physical basis of mode theory (coherent scattering in the air, combined with a careful treatment of the outgoing radiation condition at great heights); 7) Coalescence of the bilinear modes to unusual airless earth modes in the limiting case of no air (mode summing must be carried out to see how the bilinear model calculated fields go over to the airless earth case deeper into the shadow as the air layer is gradually removed).

While it was regrettable that time pressure prevented discussion of these and other questions at the Symposium, future expositors of mode theory will profit tremendously from knowing in advance the questions which have arisen to retard its acceptance.

An Important Task Immediately Ahead

It is clear the mode theory needs a much more complete explanation and physical interpretation than has yet appeared. This is necessary so that all workers in the field (theoristis and experimenters alike) shall see through the purely formal complications which are unfortunately inherent in any wave propagation theory without ray-type approximations, and may thus come to have confidence in the twilight region calculated fields which come merely from introducing the absolute value of the index of refraction properly into the calculation, and vacuum propagation conditions at great heights. Furry's original treatment of the bilinear model is based on a treatment derived from similar potential well problems in wave mechanics, and this in itself introduces an element of unfamiliarity to classical radio propagation theorists. In addition, the radio problem has peculiarities of its own, such as the complex eigenvalues and the large ratio of earth radius and air layer thickness to the wavelength. Of course, the optical theory of propagation in inhomogeneous media underlies both the radio and the quantum mechanical problems. There is the difference that in optics the inhomogeneous medium problem can usually be simplified to the one of piecewise homogeneous media. This cannot be done in radio wave propagation through the inhomogeneous atmosphere where the complication of a smoothly varying index of refraction must be handled correctly and without oversimplification, when highly accurate results are desired.

Reflections on Recent History of Propagation Theory

To the partisan believer in mode theory, the conference brought a sense of relief that the omnipresent air layer itself, kept there by gravity, is very soon to have proper but belated consideration as the cause of omnipresent and useful radio twilight propagation. Optical twilight is its analog, both theoretically and observationally. The essential ingredients in this puzzle were known ten years ago: Furry's bilinear moded theory had been developed, and the experimental discrepancies well beyond the horizon had begun to show up. It has nevertheless taken years to fit the pieces of nature's puzzle properly together, and to view interesting bypaths, such as the turbulence hypothesis, in proper perspective.

The importance of verifying theory by experiment and *vice versa* is surely a lesson retaught by this recent history of tropospheric propagation. Marconi's 1901 experiment upset the dogmatic "line of sighters" of that day, but only beginning in 1918 did the theory catch up sufficiently to incite the experimental discovery of the ionosphere in 1925, and the usefulness of short waves which had been long mistakenly relegated to the amateurs as too short to be useful. The curved earth diffraction theory for vhf and microwave propagation around an airless earth became understood only in the late 1930's, only to suffer the fate of being too firmly believed in. In effect, it restored the line of sight limitation into experimenter's thinking, so that the interpretation of the radio twilight phenomenon has been delayed to the present time despite Marconi's anticipation of the phenomenon in 1932.

Contributors

L. L. Bailin (SM'53) was born in Chicago, Ill., on May 28, 1922. He received the B.A. degree in physics from U.C.L.A. in 1943. After a year as a teaching assistant in physics at U.C.L.A., he joined the technical staff of the Naval Ordnance Laboratory in Washington, D. C. He returned to U.C.L.A. in 1945 for graduate study in physics, and received the M.A. degree in 1946 and the Ph.D. in 1949.

L. L. Bailin

In 1948 Dr. Bailin was employed as a mathematician by the Institute for Numerical Analysis of the National Bureau of Standards. From 1949 to 1955, he was engaged in microwave propagation and antenna studies as a member of the technical staff of the Hughes Aircraft Co. Since 1953, he has been with the Department of Electrical Engineering of the University of Southern California as an associate professor.

Dr. Bailin is a member of the American Physical Society, Sigma Xi, RESA, Pi Mu Epsilon, and Eta Kappa Nu.

❖

D. G. Berntsen (S'48–A'50) was born in Tacoma, Wash. on May 9, 1925. He served in the U. S. Navy from 1943 to 1946 as a radio technician. He attended the California State Polytechnic College and received the B.S.E.E. degree in 1949.

D. G. Berntsen

Mr. Berntsen has been employed by the Boeing Airplane Co. since 1949 where, as a research engineer with the physical research staff, he is engaged in the design and development of antenna systems for high speed aircraft.

❖

J. T. Bolljahn (A'43–SM'53) was born in Oakland, Calif., in 1918. He received the B.S. and Ph.D. degrees from the University of California in 1941 and 1950, respectively. From August, 1941, until January, 1946, he was employed by the Naval Research Laboratory in Washington, D. C. His work in this position was concerned with the development of aircraft and shipboard antennas. From February, 1946, to September, 1949, he was with the University of California Antenna Laboratory.

J. T. Bolljahn

Dr. Bolljahn joined Stanford Research Institute in September, 1949, and is now manager of the Antenna Systems Laboratory.

He is a member of Sigma Xi, Tau Beta Pi, and Eta Kappa Nu.

❖

E. H. Braun was born in New York, N. Y., on March 27, 1925. He majored in physics at Columbia University, receiving his bachelor s degree in 1948 and master's degree in 1950. Previous to this he served in the U. S. Army.

E. H. Braun

He is currently engaged in research and development work on microwave antennas and related components as a member of Antenna Research Branch at the Naval Research Laboratory in Washington.

❖

Albin Bystrom, Jr. (A'51) was born in Seattle, Wash. on November 9, 1924. He served in the U. S. Navy from 1943 to 1946 as a radio technician, maintaining radio, radar, and sonar equipment. In 1946, he entered the University of Washington and received the B.S.E.E. in 1950.

A. Bystrom, Jr.

Since then he has been at Boeing Airplane Co. as a research engineer assigned to the antenna group of the Physical Research Staff. He took part in the development of uhf and shf cavity type helical antennas and has a patent pending dealing with a cavity type helical antenna.

He is a member of Tau Beta Pi and Sigma Xi.

❖

F. M. Capps was born in Great Bend, Kan. on May 18, 1918. He served as flight engineer with the Air Force in the China, Burma, India theater from 1942 through 1946. He received his B.A. degree from the University of Colorado in 1950 and did graduate work at Texas Christian University. Since 1951 he has been engaged in research on irregular terrain propagation with the Tropospheric Propagation Research Section of the National Bureau of Standards in Boulder, Colorado.

F. M. Capps

He is a member of Phi Delta Kappa.

❖

S. B. Cohn (S'41–A'44–M'46–SM'51) was born in Stamford, Conn. in 1920. He received the B.E. degree in electrical engineering from Yale University in 1942; the M.S. degree in communication engineering in 1946, and the Ph.D. degree in engineering sciences and applied physics in 1948, both from Harvard University. From 1942 to 1945, he was employed as a special research associate by the Radio Research Laboratory of Harvard University, also representing that Laboratory as a technical observer with the U. S. Army Air Force in the Mediterranean Theater of Operations. Dr. Cohn worked at Sperry Gyroscope Co. from 1948 to 1953, where he held the position of research engineer in the Microwave Instruments and Components Department.

S. B. Cohn

Since February, 1953, he has been with the Stanford Research Institute, as head of the Microwave Group of the Antenna Systems Laboratory.

He is a member of Tau Beta Pi and Sigma Xi.

❖

J. T. deBettencourt (A'50) was born in Washington, D. C., on June 9, 1912. He received the B.E.E. degree in 1932 and the M.S. degree in physics in 1934 both from the Catholic University of America. He received the M.S. degree in 1937 and the Sc.D. degree in 1949 both in communication engineering at Harvard University.

deBettencourt

From October, 1941 to June, 1946, Dr. deBettencourt served with the Bureau of Ships, during the latter period as head of the Airborne Radar Design Section. After the war, he joined the Raytheon Manufacturing Co. as part-time engineer while finishing his Doctorate as research associate at Harvard. Until 1951 he was section head and section manager in the Engineering Division. In January, 1951, he joined the Research Laboratory of Electronics at M.I.T. He joined the staff of Pickard and Burns as vice-president of research in August, 1955.

L. B. Felsen (S'47–A'53–M'54) was born in Munich, Germany, on May 7, 1924. He entered the United States in 1941, and during World War II was concerned with work on electronic ballistic calibration devices. He received the B.E.E., M.E.E., and D.E.E. degrees from the Polytechnic Institute of Brooklyn in 1948, 1949, and 1952, respectively.

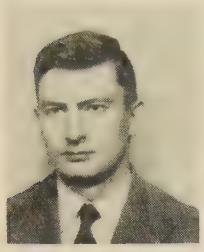

L. B. Felsen

Since 1948, he has been employed at the Microwave Research Institute of the Polytechnic Institute of Brooklyn and presently holds the position of research assistant professor. His work has been concerned chiefly with electromagnetic diffraction problems, and microwave circuit and measurement techniques.

Dr. Felsen is a member of Eta Kappa Nu, Tau Beta Pi, and Sigma Xi.

❖

R. C. Honey (S'48–A'53) was born in Portland, Ore., on March 9, 1924. He received the B.S. degree in physics from the California Institute of Technology in 1945, and the E.E. and Ph.D. degrees in electrical engineering from Stanford University in 1950 and 1953 respectively.

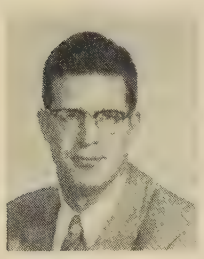

R. C. Honey

He served as a radio technician in the U. S. Navy until 1946 and was a member of the local oscillator microwave project at Stanford University Electronics Research Laboratory from 1948 to 1952. Since 1952, he has been with the Microwave Group of Stanford Research Institute.

❖

E. M. T. Jones (S'46–A'50–SM'56) was born in Topeka, Kan., on August 19, 1924. He received the B.S. degree in electrical engineering from Swarthmore College in 1944 and the M.S. and Ph.D. degrees in electrical engineering from Stanford University in 1948 and 1950 respectively.

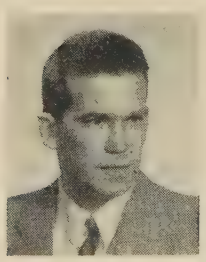

E. M. T. Jones

From 1944 to 1946, Dr. Jones was a radar maintenance officer in the U. S. Navy. While at Stanford, he was a research associate working on the microwave local oscillator project. Dr. Jones joined the staff of the Stanford Research Institute in 1950 where he is a senior research engineer.

He is a member of Sigma Tau and RESA.

R. S. Kirby (M'50) was born in Lawrence, Kan., on July 31, 1920. He received the B.S. degree in engineering in 1943 from the U. S. Naval Academy. He served as an officer on Pacific Fleet destroyers from 1943 until 1946, his duties including those of communications officer, navigator, and executive-officer afloat.

R. S. Kirby

In 1947 Mr. Kirby joined the staff of the National Bureau of Standards, and has been engaged in propagation studies at the Central Radio Propagation Laboratory. In 1948 he acted in an advisory capacity on propagation tests of air-to-ground communications conducted at the Naval Air Test Center, Patuxent River, Md. Since 1951 he has been working with the Laboratory in Boulder, Colo.

He is a member of study group V, International Radio Consultative Committee.

❖

W. S. Lucke was born in Knoxville, Tenn. in 1921. He received the B.S. degree in 1943, the M.A. and M.E.S. degrees in 1947, and the Ph.D. degree in physics in 1949, all from Harvard University.

W. S. Lucke

He was a member of the technical staff at Bell Telephone Laboratories from 1943 to 1946, and a research associate at Cruft Laboratory, Harvard University, from 1948 to 1949.

Dr. Lucke joined Stanford Research Institute in May, 1949. He has devoted a major portion of his time to the problems of the Radio Systems Laboratory.

He is a member of Sigma Xi, RESA, and SIAM.

❖

P. N. Mathur was born in Delhi, India, and received the B.Sc. and M.Sc. degrees in physics from the University of Delhi. He entered the United States in 1947, and thereafter received the M.S. degree in aeronautical engineering, and later, M.S. and Ph.D. degrees in theoretical and applied mechanics, all from the University of Illinois.

P. N. Mathur

During his residence at the University of Illinois, he worked on various projects as research assistant in the College of Engineering, and at the Meteorology Radar Laboratory of the Illinois State Water Survey for the State Department of Education. He is presently employed in the Gas Turbine Department of the Scientific Laboratory at Ford Motor Co.

He is a member of Sigma Xi and the American Society for Mechanical Engineers.

❖

Tetsu Morita (S'44–A'49–SM'54) was born in Seattle, Wash., in 1923. He received the B.S. degree in electrical engineering from the University of Nebraska in 1944, and the Ph.D. degree in engineering sciences from Harvard University in 1949.

Tetsu Morita

From 1949 to 1953, he was a research fellow and head of the antenna research group at Harvard University. From 1951 to 1953, he was a consultant on microwave antennas for Trans-Sonics Inc., and in 1953, for Sylvania Electric Co.

Dr. Morita joined the staff of Stanford Research Institute in October, 1953.

He is a member of the American Physical Society, Sigma Xi, and RESA.

❖

E. A. Mueller was born on May 3, 1927 in Belleville, Ill. He received the B.S. degree in electrical engineering from the University of Illinois in 1951, and the M.S. degree in electrical engineering in 1952 from the same university.

E. A. Mueller

For four years, he served in the Navy as an instructor in the Aviation Electronics school. In 1952, he joined the staff of the Illinois State Water Survey as a research engineer.

Mr. Mueller is a member of Eta Kappa Nu, Tau Beta Pi, and Pi Mu Epsilon.

❖

H. A. Myers (S'51–A'54) was born in Lansing, Mich. on July 11, 1925. He received the B.S. degree in electrical engineering from the University of Oklahoma in 1946, and the M.S. degree in electrical engineering in 1950, and Ph.D. in applied mathematics in 1954, both from Michigan State College.

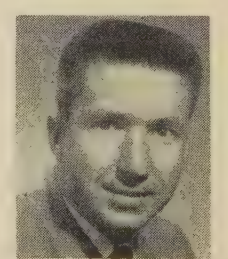

H. A. Myers

He joined International Telephone and Telegraph as an engineer in 1946. Dur-

ing 1950–51 he was a graduate assistant in electrical engineering, and from 1953 to 1954 held the same position in the mathematics department of Michigan State College. Since 1954, he has been an associate engineer with the RAND Corp.

Dr. Myers is a member of Tau Beta Pi, Phi Kappa Phi, Pi Mu Epsilon, Eta Kappa Nu, Sigma Tau, and Sigma Pi Sigma, and an associate member of Sigma Xi.

❖

M. A. O'Grady was born in Ottawa, Canada, in 1934. She received her secondary education in Ottawa and then attended St. Patrick's College of Ottawa University. Her major was mathematics and she received the B.S. degree in June, 1954. For one year, she was employed by the Defense Research Board in research work at the Radio Physics Laboratory.

M. A. O'Grady

At present, Miss O'Grady is taking graduate courses toward a teaching degree at the Ontario College of Education. She hopes to teach mathematics and Latin on a secondary level.

❖

Charles Polk (A'52) was born on January 15, 1920 in Vienna, Austria. He came to this country in 1940. From 1943 to 1946 he served in the U. S. Army, part of this time as an instructor in a service school concerned with electro-medical equipment. He received the B.S. degree in electrical engineering from Washington University in 1948 and the M.S. degree in physics from the University of Pennsylvania in Philadelphia in 1953.

Charles Polk

From 1948 to September, 1952, Mr. Polk was employed by Radio Corporation of America working mostly on problems related to uhf television transmitting antennas. Since that time, he has been at the Moore School of Electrical Engineering of the University of Pennsylvania where he has been engaged in research, teaching, and study for the Ph.D. degree in electrical engineering.

E. W. Seeley (S'50–A'55) was born in Miles City, Mont., on February 24, 1926. He received the B.S. degree in electronic engineering from California State Polytechnic College in 1952, and the M.S. degree from Stanford University in 1953.

E. W. Seeley

In 1953, Mr. Seeley joined the fuze division of the National Bureau of Standards in Corona, Calif., and remained with that laboratory when it was transferred to naval ordnance. Presently he is working in the antenna group which is concerned with miniaturizing antennas and antenna systems.

❖

Samuel Silver (M'46–SM'50–F'54) was born on February 25, 1915, in Philadelphia, Pa. He received the A.B. in physics in 1935, and the M.A. in physics in 1937, both from Temple University. In 1940, he received the Ph.D. degree from Massachusetts Institute of Technology.

Samuel Silver

He was a research assistant in physics at Ohio State University from 1940 to 1941, and an instructor and assistant professor at the University of Oklahoma from 1941 to 1943. His research work during this time was on molecular structure and vibrational spectra.

From 1943 to 1946, Dr. Silver was a staff member of the Radiation Laboratory at M.I.T. and the following year worked as a physicist in the antenna research section of Naval Research Laboratory. Since 1947, he has been with the department of electrical engineering of the University of California where he is now a professor of engineering science. Applied electromagnetic theory, antennas, and microwave optics have been his major fields of research since 1943.

Dr. Silver is a fellow of the American Physical Society, a member of Sigma Xi, and the American Association for the Advancement of Science, and the co-chairman of the Technical Program Committee of Wescon for 1955. He was awarded a Guggenheim Research Fellowship in 1953, and in 1954 began a three-year term as President of the Commission on Radio Waves and Circuits of the International Scientific Radio Union.

J. R. Wait was born in Ottawa, Canada, in January, 1924. He attended McGill University for a brief period before enlisting in the Canadian Army in 1942. By the end of the war he was a foreman in a radar workshop at Kingston, Ontario.

J. R. Wait

He received the B.A.Sc. and M.A.Sc. degrees in engineering physics from the University of Toronto in 1948 and 1949 respectively. At this time he was employed as a junior research engineer at the Hydro Electric Power Commission of Ontario where he assisted in the development of an infra-red bolometer. Returning for further graduate work to the University of Toronto, he obtained a Ph.D. degree in electromagnetic theory in 1951.

From 1949 to 1952 Dr. Wait was associated with Newmont Exploration Ltd. of Jerome, Ariz. where he conducted theoretical and experimental research in electrical prospecting. From 1952 to 1955 he was a section leader in the Defence Research Telecommunications Establishment in Ottawa where he was mainly concerned with theoretical problems in radiation. He is now a theoretical physicist with the Central Radio Propagation Laboratory of the National Bureau of Standards in Boulder, Colorado.

He is a member of the Research Society of America, the Society of Exploration Physicists, the Professional Engineers of Ontario, and the Canadian Association of Physicists.

❖

W. A. Whitcraft, Jr. (S'47–A'48–M'51–SM'55) was born on April 2, 1917, in Cambridge, Ohio. He received the A.B. degree in music from Harvard College in 1939 and M.S. in communications engineering from Harvard University in 1947.

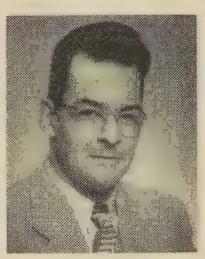

W. Whitcraft, Jr.

From 1941 to 1946 he served in the armed forces, spending two years in the South and Southwest Pacific as a Ground Radar Officer and later as IFF Officer and Assistant Air Radar Officer of 13th Air Force Headquarters.

Since June, 1947, Mr. Whitcraft has been with the Raytheon Manufacturing Co. of Waltham, Mass., engaged in engineering research and development activities on various government contracts. This work has included pulse handling circuit techniques, antennas, and problems of wave propagation in the high-frequency band.

IRE Transactions on Antennas and Propagation

Index to Volume AP-3—1955

Contents

Index to Authors

Numbers refer to index numbers in contents listing.

Index to Technical Subjects

Nontechnical Index

INSTITUTIONAL LISTINGS

The IRE Professional Group on Antennas and Propagation is grateful for the assistance given by the firms listed below, and invites application for Institutional Listing from other firms interested in the field of Antennas and Propagation.

COLLINS RADIO COMPANY, Cedar Rapids, Iowa
Antenna Design and Propagation Research Related for Airborne and Ground Communication Systems.

DEVELOPMENTAL ENGINEERING CORP., Washington, D. C. and Leesburg, Va.
Antenna Systems Research, Design, and Evaluation

DORNE AND MARGOLIN, INC., 30 Sylvester Street, Westbury, L. I., New York
Antenna Research and Development—Radiation Pattern Measuring Services.

D. S. KENNEDY & CO., Cohasset, Mass.
Microwave Antennas, Reflectors, Lenses, Radomes and Accessories. Design, Development and Production.

THE GABRIEL LABORATORIES, Div. of the Gabriel Co., 135 Crescent Road, Needham Heights 94, Mass
Research and Development of Antenna Equipment for Government and Industry.

HUGHES AIRCRAFT COMPANY, Culver City, California
Research, Development, Mfr.: Radar, Missiles, Antennas, Radomes, Tubes, Solid State Physics, Computers.

I-T-E CIRCUIT BREAKER CO., Special Products Div., 601 E. Erie Ave., Philadelphia 34, Pa.
Design, Development and Manufacture of Antennas, and Related Equipment.

JANSKY & BAILEY, INC., 1339 Wisconsin Ave. N.W., Washington 7, D.C.
Radio & Electronic Engineering; Antenna Research & Propagation Measurements; Systems Design & Evaluation.

MARYLAND ELECTRONIC MANUFACTURING CORPORATION, College Park, Md.
Antenna and System Development and Production for Civil and Military Requirements.

RADIO ENGINEERING LABS., INC., 36-40 37th St., Long Island City 1, N. Y.
Equipment for Communication and Propagation Test Beyond the Horizon UHF Systems.

WEINSCHEL ENGINEERING CO., INC., Kensington, Md.
Attenuation Standards, Coaxial Attenuators and Insertion Loss Test Sets.

WHEELER LABORATORIES, INC., 122 Cutter Mill Road, Great Neck, New York
Consulting Services, Research and Development, Microwave Antennas and Waveguide Components.

The charge for an Institutional Listing is $25.00 per issue or $75.00 for four consecutive issues. Application may be made to the Technical Secretary, The Institute of Radio Engineers, 1 East 79th Street, New York 21, N.Y.